Technical University of Denmark

DTU

Improved radiotherapy for locally advanced Non-Small Cell Lung Carcinoma (NSCLC) patients

Ottosson, Wiviann; Andersen, Claus E.; Behrens, Claus F.

Link back to DTU Orbit

DTU Library
Technical Information Center of Denmark

![DTU]

Improved radiotherapy for locally advanced Non-Small Cell Lung Carcinoma (NSCLC) patients

Wiviann Ottosson

March 23, 2015

DTU Nutech
Center for Nuclear Technologies
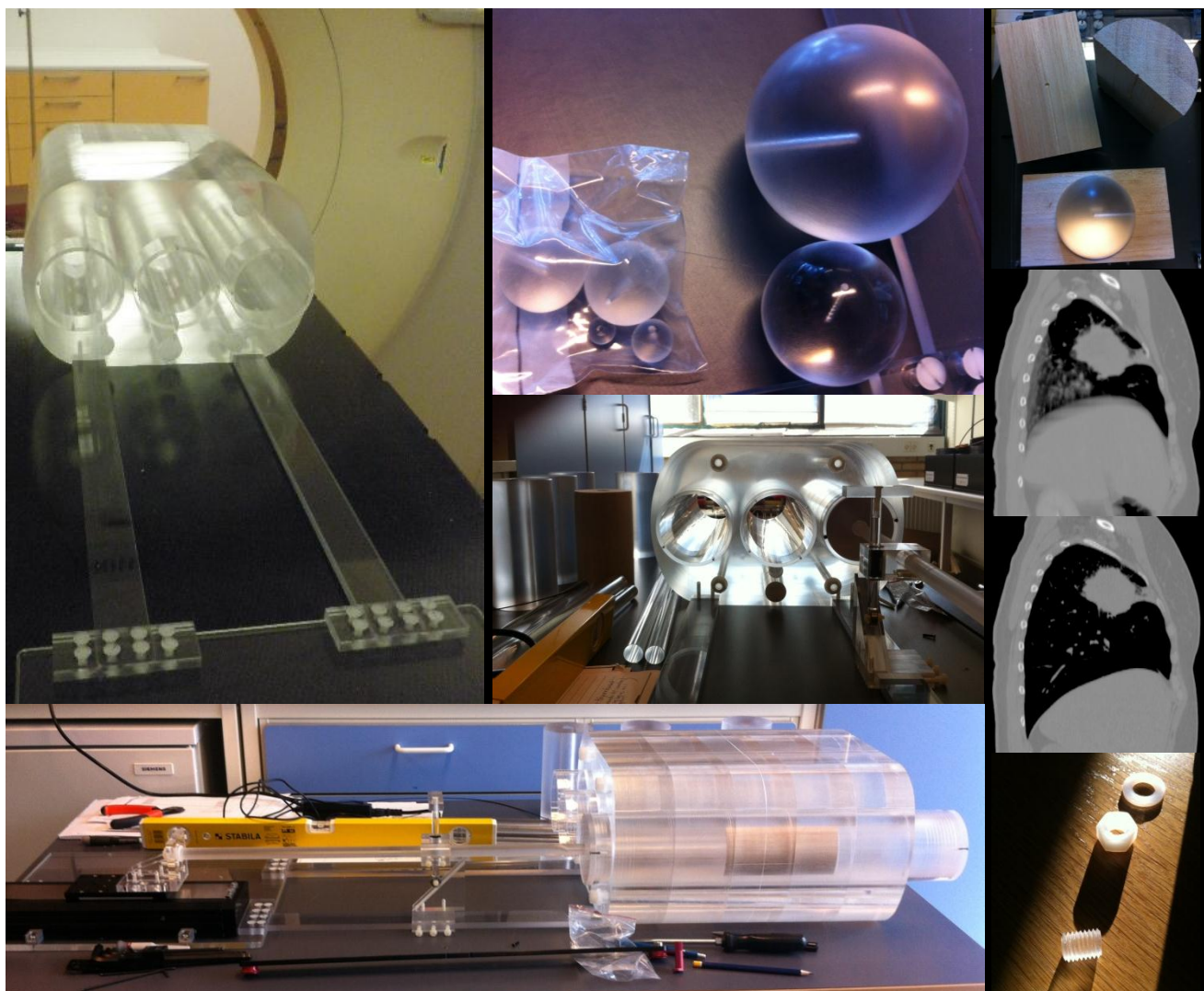
Preface

This PhD project was carried out as a collaboration between the Center for Nuclear Technologies (Nutech), the Radiation Physics Division, at the Technical University of Denmark (DTU), where I was employed, and the Department of Oncology at Herlev Hospital, University of Copenhagen. The work was partly carried out within the EMRP: "Metrology for radiotherapy using complex radiation fields" (HLT09). The EMRP is jointly funded by the EMRP participating countries within EURAMET and the European Union. A travel grant was received from "Novartis Healthcare A/S, travel and educational support in clinical oncology and hematology 2013" to participate in the ICCR2013 conference 6-9 May in Melbourne, Australia. The clinical protocol and clinically relevant treatment planning and dose measurements were carried out at the Department of Oncology at Herlev Hospital. Phantom construction was carried out by the Nutech workshop. The project was supervised by the senior scientist Claus E. Andersen at DTU Nutech and the lead senior scientist Claus F. Behrens at the Radiotherapy Research Unit at Herlev Hospital.

Abstract

Lung cancer is worldwide one of the most common cancer diseases with a high mortality rate. There is thus an urgent need for improving radiotherapy for these patients. Radiotherapy for lung cancer patients is challenging because the tumor and organs at risk (OARs) move with the breathing motion. Deep-Inspiration-Breath-Hold (DIBH) is a technique that potentially can improve the treatment for these patients. DIBH is frequently and routinely used for breast cancer treatments. However, it is still an experimental method for lung cancer patients e.g. due to preconceptions about their incapability to comply with the DIBH technique. For DIBH, the patients are guided to hold their breath almost at their maximum inspiration level during imaging and treatment. This leads to reduction of the breathing motion which decreases the movement of the tumor and OARs. It also expands the lung tissue which is beneficial with respect to sparing the healthy lung from radiation. In order to ensure that the tumor is receiving the prescribed dose, safety margins are added to the gross tumor volume (GTV). The size of the margins depends on the uncertainties related to the patient setup, target delineation, respiration, other internal motion, etc. These extra margins result in larger irradiated volumes, increasing the risk of radiation-induced side effects. By reducing the uncertainties and thereby the margins, the healthy tissue can be spared from unnecessary radiation. The respiratory uncertainties can potentially be reduced by the DIBH method for the lung cancer patients.

The overall aim of the clinical part of this thesis was to clarify the potential benefit of offering DIBH gating, compared to free-breathing (FB), for lung cancer patients. Particularly, the benefits for locally advanced non-small cell lung cancer (NSCLC) patients were explored. For the dosimetric part of the thesis, the dosimetric aspects of correct dose calculations in heterogeneous patient-like geometries were studied.

The clinical aspects of DIBH were evaluated in three different studies, where planning and setup verification images acquired in both FB and DIBH were evaluated.

In adaptive radiotherapy (ART) the treatment plan is adapted to geometrical changes of the patient over the course of treatment. However, defining anatomical structures for treatment planning is a time consuming process prone to large uncertainties. In order to save time and to reduce the uncertainties during ART, image registrations between the planning computed tomography (CT) and the subsequently acquired images may facilitate the delineation process. *Study I* investigated the uncertainties related to automatic deform image registrations between the planning CT and the setup images acquired at the accelerator, and the extra CTs acquired over the course of treatment. The studied algorithm was found not to be adequate enough to correct for image artifacts and large anatomical deformations present in the images. Furthermore, no difference between DIBH and FB was observed.

Study II investigated different image based setup verification protocols. The goal was to minimize the applied setup margins. It was found that soft-tissue registration on the tumor volume resulted in the smallest planning target volume (PTV), irrespectively of FB and DIBH. Setup uncertainties were however introduced during DIBH, but the resulting PTV in DIBH was nevertheless smaller compared to FB. We speculate the increased uncertainty

was due to some patients tended to arch with their back to compensate for their insufficient compliance to reach the breath-hold amplitude level.

Study III investigated the clinical dosimetric benefit of DIBH treatments, planned using a commercial Anisotropic-Analytical-Algorithm (AAA) dose calculation algorithm. Detailed Monte Carlo (MC) simulations were carried out for this purpose. DIBH resulted in better dose sparing of the OARs, compared to FB. However, the MC simulations revealed similar inferior target dose coverage between MC and AAA irrespectively of FB and DIBH treatment plans. This observation is therefore related to the treatment planning dose calculation algorithm rather than the breathing adapted treatment technique.

The dosimetric aspects of complex dosimetry in heterogeneous patient-like geometries were explored in two different studies in the thesis. In order to investigate known calculation issues in the thorax region, a thoracic-like phantom was designed and constructed to obtain detailed dosimetry information in heterogeneous clinically relevant geometries. The lungs of the phantom were constructed in low-density balsa wood, the body in Poly(methyl methacrylate) (PMMA), and the bone in high-density delrin.

Study IV investigated the performance of AAA, using a plastic scintillator detector system and the well-defined heterogeneous phantom. The treatment planning system (TPS) calculated doses agreed for the least complex cases, while for the more complex cases dose deviations $\geq$ 4% were observed. The dosimetric challenges in TPS calculations for clinically relevant geometries were underpinned.

For lung cancer treatments, tumor volume changes during radiotherapy are well known. Due to incorrect scatter calculations by the TPS, the dosimetric challenges increase when tumor and field sizes decrease. The philosophy of radiotherapy is to deliver the same prescribed dose to the tumor volume, irrespective of the size of the tumor.

Study V investigated the dosimetric challenges for the TPS in the heterogeneous thoracic-like geometry and its dependence on tumor size. Thus, a change of tumor size and resulting plan adaption over the course of a treatment was simulated. For this purpose, tumor inserts of different sizes (ranging from 1-8 cm in diameter) was used in the phantom. Severe dose deviations were observed, especially for small tumor sizes $\leq$ 2 cm in diameter. Our results imply that there exist severe tumor-size dependency, which potentially could have implications on the radiotherapy treatment planning of lung cancer.

This thesis concludes that the clinical gain of DIBH is not always beneficial over FB treatments. There were additionally identified severe tumor-size dependent dose deviations that were large enough to potentially have implications for lung cancer radiotherapy treatment planning. The scintillator system and the heterogeneous phantom provide a promising tool for critical evaluation of complex radiotherapy calculations and dose delivery.

Resumé (in Danish)

Lungecancer er den næst-hyppigste kræftsygdom i Danmark, med ca. 4500 nye tilfælde i 2012, hvor ca. 18% af patienterne med lungecancer blev henvist til strålebehandling. Dødeligheden blandt patienter med lungecancer er højere end ved de fleste andre former for cancer, og 5 års overlevelsen er kun 12%. Der er derfor et presserende behov for forbedring af strålebehandling til patienter med lungekræft. Strålebehandling af lungetumorer er vanskelig, fordi tumoren bevæger sig med vejrtrækningen. Deep-Inspiration-Breath-Hold (DIBH) gating er en teknik, som potentielt kan forbedre strålebehandlingen af patientgruppen. DIBH bruges rutinemæssigt til brystcancer-patienter, men det er stadigt en eksperimentel metode til lungecancer-patienter. Ved DIBH gating vejledes patienterne i at holde vejret tæt på deres maksimale inspiration i den tid (15-30 sekunder) strålebehandling og billeddannelse varer. Dette fører bland andet til en dæmpning af tumorens bevægelse og en udvidelse af lungevævet, hvilket er en fordel med hensyn til at skåne det rask lunge væv. Ved planlægning af stråleterapi appliceres margener omkring tumoren for at sikre at den planlagte dosis levereres til tumorvolumen og, at der tages højde for de usikkerheder der er under planlægning og behandling (for eksempel på grund af respiration, andre organ bevægelser, lejringsusikkerheder af patienten etc.). De ekstra margener resulterer i at et større område omkring tumoren bestråles, hvilket øger risikoen for toksicitet i tilstødende normalt væv. Ved at bruge DIBH gated stråleterapi kan det bestrålede volumen omkring tumoren potentielt reduceres, og derved kan rask lungevæv og omkringliggende risiko-organer bedre skånes for stråling. Dette kan gøre det muligt at øge stråledosis til kræftvævet uden at give for meget dosis til risikoorganerne.

Formålet med den kliniske del i denne afhandling var at afklare den mulige kliniske gevinst ved at tilbyde DIBH gating til patienter med lokalt-avanceret lungecancer. Tre forskellige studier er udført hvor planlægnings- og opstillingsbilleder optaget i DIBH og frit åndedræt (free-breathing, FB) er evalueret.

Under behandlingsforløbet over flere uger kan det ske at anatomien i patienterne ændrer sig, og det kan derfor være nødvendigt at adaptere planen undervejs. At definere det anatomiske volumen til planlægning af strålebehandling er en vigtig og tidskrævende proces som tillige indeholder store usikkerheder. For at spare tid og mindske usikkerhederne forbundet med anatomidefinition, kan planlægnings-CT billedet registreres med den nye CT-skanning, eller de daglige setup verifikationsbillederne taget på acceleratoren. Efterfølgende kan de oprindelige strukturer propageres til de nye billeder. I *Studie I* undersøges usikkerheder relateret til automatisk deform billederegistrering brugt til det formål at propagere anatomiske strukturer. Vi fandt at den deforme registrerings-algoritme ikke var tilstrækkelig god til at korrigere for billedartefakter, som forstyrrede billedet eller store anatomiske forandringer. Endvidere fandt vi ikke nogen forskel mellem DIBH og FB.

I *Studie II* undersøges forskellige daglige setup verifikationsprotokoller med det formål at mindske de applicerede margener. Ved mindre margener kan det friske omkringliggende væv bedre skånes for stråledosis, hvilket giver en bedre behandling for patienterne. Vi fandt at den billedbaserede opstillingsprotokol, der resulterede i det mindste planlagte

bestrålingsvolumen (planning target volume, PTV) var baseret på bløddelsmatch på tumoren, uanset FB eller DIBH. Vi fandt også at DIBH introducerede større afvigelser i længderetningen i forhold til frit åndedræt. Dette mener vi har at gøre med at patienterne kompenserer sin dybe indånding med at bue ryggen for at opnå det vejrtrækningsniveau, der var forudbestemt i planlægningsstadiet. Dog var det resulterende DIBH PTV imidlertid mindre i forhold til det i FB.

I *Studie III* undersøges den kliniske dosimetriske gevinst med DIBH i forhold til FB. Udover almindelige dosberegninger udførtes også mere detaljerede Monte Carlo simuleringer for at opnå mere korrekte dosisberegninger i heterogene geometrier. Vi fandt at DIBH resulterede i bedre beskyttelse af risikoorganer fra unødvendig bestråling end FB. Dog viste Monte Carlo simuleringerne at dosisdækningen af tumorvolumen ikke modsvarede den dosis, der var planlagt, hvor der var lige så dårlig dosisdækning for FB som for DIBH. Dette problem med dosisdækningen af tumorvolumen er derfor relateret til dosberegningsalgoritmens begrænsninger og ikke til den vejrtrækningsteknik, der var brugt.

Formålet med den tekniske del i denne afhandling var at udvikle og anvende et målefantom for klinisk relevant dosimetri i heterogene geometrier. Det er velkendt at de fleste kommercielle dosisberegningssystemer ikke kan udføre korrekte beregninger af hvordan stråling spredes og absorberes i kroppen, når der forekommer store forskelle mellem densiteter og atomnummer. De største unøjagtigheder er i overgangen mellem forskellige materialer. Et målefantom, der simulerer en lungecancer-patient, er derfor udviklet med formålet at udføre uafhængige dosiskontroller af kliniske strålebehandlings-planer i veldefinerede heterogene og homogene geometrier. Lungerne simuleres af balsatræ med lav densitet, kroppen af plexiglas, og knogle af delrin med høj densitet. Arbejdet med at udvikle dette fantom er en del af det europæiske fælles forskningsprojekt "Metrology for radiotherapy using complex radiation field" som er finansieret i fællesskæb af landene indenfor EMRP (European Metrology Research Programme) indenfor EURAMET og EU. Udviklingen af et menneskelignende fantom til at evaluere dosisberegningssystemer indgår i arbejdspakke 6 "Methods for verification of treatment planning systems in anthropomorphic phantoms".

I *Studie IV* undersøges et kommercielt dosisberegningssystem ved brug af scintillationsdosimetri og det heterogene menneskelignende målefantom. Forskellige fantomkonfigurationer og behandlingsplaner med varieret kompleksitet evalueredes. Vi fandt god overensstemmelse med de mindst komplekse geometrier, mens der var dosisafvigelser over 4% i de mere komplekse tilfælde. Vores resultater understreger, at der er dosimetriske udfordringer i det kommercielle dosisplanlægningssystem. Scintillations-systemet sammen med den særlige phantom er et lovende redskab til evaluering af levering af komplekse og klinisk relevante strålebehandlingsplaner.

Udfordringen med at beregne korrekt dosis er størst for små felter, og for geometrier med store inhomogeniteter på grund af ukorrekt beregning af spredt stråling. Det er kendt, at tumorer mindskes eller øges i størrelse over behandlingsforløbet. Formålet med strålebehandling er at levere den samme ordinerede dosis til tumorvolumen, uanset størrelsen af tumoren, og uanset hvilken patient det er. I *Studie V* undersøges derfor dosimetrien ved forskellige tumorstørrelser i målefantomet. Lungetumorer med størrelser

mellem 1-8 cm i diameter var positioneret i center i fantomet, og omgivet af balsatræ med lav densitet. Vi fandt alvorlige dosisberegningsproblemer, specielt for små tumorer ≤ 2 cm i størrelse. Vores resultater indikerer derfor at der er en alvorlig tumor-størrelse afhængighed, der potentielt kunne påvirke planlægningen af strålebehandlingen af lungepatienter.

Denne afhandling konkluderer, at den kliniske gevinst ved at behandle med DIBH ikke altid er bedre end at give behandlingen i FB. Der blev endvidere identificeret alvorlige tumor-størrelse afhængige dosisafvigelser, der potentielt kunne påvirke planlægningen af strålebehandlingen af lungepatienter. Det udviklede målefantom og scintillator viser et stort potentiale til at evaluere dosisberegninger i heterogene geometrier bestrålede med både simple og komplekse klinisk relevante behandlingsplaner.

Acknowledgement

Publications and presentations

The thesis is based on the following five manuscripts (hereafter referred to by their roman numerals). The manuscripts are described in an order relevant for the thesis, not in the order of publication. Paper I-IV have all been submitted for publication in peer-reviewed international journals and presented as oral presentations and posters at international conferences. This section lists the various contributions. The papers are presented in the thesis with a text identical to the original manuscripts. All references are gathered in the bibliography list at the end of the thesis to increase the readability. Likewise, numbers of sections will refer to the chapter of the thesis.

I.   W. Ottosson, J.A. Lykkegaard Andersen, S. Borissova, A. Mellemgaard, and C.F. Behrens, **"Deformable image registration for geometrical evaluation of DIBH radiotherapy treatment of lung cancer patients"**, J. Phys. Conf. Ser. 489, 012077 (2014).

II.   W. Ottosson, F. Rahma, D. Sjöström, C.F. Behrens, and P. Sibolt, **"The advantage of Deep-Inspiration Breath-Hold and soft-tissue auto-match for cone-beam CT setup methods in locally advanced lung cancer radiotherapy"**, Submitted.

III.   W. Ottosson, P. Sibolt, C. Larsen, J.A. Lykkegaard Andersen, S. Borissova, A. Mellemgaard, and C.F. Behrens, **"Monte Carlo calculations support organ sparing in Deep-Inspiration Breath-Hold intensity-modulated radiotherapy for locally advanced lung cancer"**, Submitted.

IV.   W. Ottosson, C.F. Behrens, and C.E. Andersen, **"Dose verification of radiotherapy for lung cancer by using plastic scintillator dosimetry and a heterogeneous phantom"**, J. Phys. Conf. Ser. 573, 012022 (2015).

V.   W. Ottosson, P. Sibolt, C.F. Behrens, and C.E. Andersen, **"Organic scintillator dosimetry reveals tumor-size dependency in a heterogeneous lung cancer setup for radiotherapy with 6MV photon beams"**, Manuscript.

Publications and presentations

Co-authorship not covered in this thesis:

i. M. Baker, S. Vallentin, K. Andersen, <u>W. Ottosson</u>, and D. Sjöström. **"Evaluation of cardiopulmonary and ladca dose in left-sided breast cancer patients by utilizing the deep inspiration breath holding technique"**, in Perspectives on Kurdistan's economy and society in transition, vol.2, Almas Heshmati, Alan Dilani and Serwan M. J. Baban, Eds., Newcastle upon Tyne, UK: Cambridge Scholars Publishing, 2013, pp. 154-168.

Oral presentations made at international conference:

a. <u>W. Ottosson</u>, C.F. Behrens, and C.E. Andersen, **"Dose verification of radiotherapy for lung cancer by using plastic scintillator dosimetry and a heterogeneous phantom"**, presented at IC3DDose 2014 in Ystad, Sweden, 4-7 September, 2014.
b. <u>W. Ottosson</u>, **Oral review presentation of my PhD work**, presented at the 2nd Øresund meeting on radiotherapy in Helsingborg, Sweden, 24-25 February, 2014.
c. <u>W. Ottosson</u>, **Oral review presentation of my PhD work**, presented at the 1st Øresund meeting on radiotherapy in Malmö, Sweden, 24 January, 2013.

Poster presentations at national and international conferences:

A. F. Rahma, <u>W. Ottosson</u>, C.F. Behrens, D. Sjöström, P. Sibolt. **"Soft-tissue matching methods for lung cancer radiotherapy - benefits, limitations and margin determination"**, Presented as a poster at the 8th European Conference on Medical Physics (ECMP) in Athens, Greece, 11-13 September, 2014. Abstract is available in Phys Medica 2014;30:e93–e94.

B. <u>W. Ottosson</u>, C.F. Behrens, and C.E. Andersen. **"Commissioning of a novel heterogeneity phantom for fiber-coupled organic scintillator dosimetry"**, Radiother Oncol 2014; Volume 111, Suppl 1: S567, abstr. 1462. Presented as an electronic poster at ESTRO33 2014 in Vienna, Austria, April 4-8, 2014. The abstract is available at: http://www.estro.org/binaries/content/assets/pdf-files-and-documents/pdf-events-2013/estro33_abstractbook_webpart2.3.pdf.

C. <u>W. Ottosson</u>, C. Larsen, J.A. Lykkegaard Andersen, S. Borissova, A. Mellemgaard, C.F. Behrens. **"Potential clinical benefit of Deep-Inspiration-Breath-Hold (DIBH) for locally advanced NSCLC lung cancer patients"**, presented as an oral poster at BIGART2013 in Aarhus, Denmark, 11 - 13 June, 2013.

D. <u>W. Ottosson</u>, J.A. Lykkegaard Andersen, S. Borissova, A. Mellemgaard, C.E. Andersen, C.F. Behrens. **"Deformable image registration for geometrical evaluation of DIBH treatment of lung cancer patients"**. Presented as a poster at the ICCR2013 in Melbourne, Australia, 6 - 9 May, 2013.

E. <u>W. Ottosson</u>, J.A. Lykkegaard Andersen, S. Borissova, A. Mellemgaard, S. Lind, H. Klitgaard Mortensen, C.F. Behrens. **"Deform image registration of lung tumour variations over the course of treatment: DIBH vs. normal breathing"**. Radiother Oncol 2013; Volume 106, Suppl 2: S 259, abstr. 1271. Presented as an electronic poster at the 2nd ESTRO Forum 2013 in Geneva, Switzerland, April 19 - 23, 2013.

F. <u>W. Ottosson</u>, S. Buranurak, G. Kertzscher, R. Cronholm, A. Beierholm, L. Lindvold, J. Helt-Hansen, and C.E. Andersen. **"Dosimetry developments at DTU"**, presented as a poster at the DSMF Symposium 2012 at Nyborg strand, Denmark, 17 April, 2012.

Acronyms

2D DRR	2-dimensional Digital Reconstructed Radiograph
3DCT	3-dimensional conventional CT
4DCT	4-dimensional respiratory correlated CT
AAA	Anisotropic-Analytical-Algorithm
ART	Adaptive radiotherapy
AVG	Average image reconstruction
BART	Breathing Adapted Radiotherapy
CBCT	Cone Beam CT
CI	Conformity Index
CLR	Cerenkov Light Ratio
COPD	Chronic Obstructive Pulmonary Disease
CPE	Charged Particle Equilibrium
CSD	Continuous Slowing Down Approximations
CT	Computed Tomography
CTV	Clinical Target Volume
dCT	Deformed CT image
DIBH	Deep-Inspiration-Breath-Hold
DIR	Deform Image Registration
D_m	Dose-to-medium
d_{max}	Depth of dose maximum
dMLC	Dynamic multi leaf collimator
DSC	Dice Similarity Coefficient
DVF	Deformation Vector Field
DVH	Dose Volume Histogram
D_w	Dose-to-water
EMRP	European Metrology Research Programme
EPID	Electronic Portal Imaging Device
EURAMET	European Association of National Metrology Institutes
FB	Free-Breathing
fCT	Final CT
FN	False Negative
FP	False Positive
fx	Fractions
GM	Group Mean
GTV	Gross Tumor Volume
Gy	SI derived unit of absorbed dose
H	Height
HU	Hounsfield Unit
ICRU	International Commission on Radiation Units and Measurements
IMRT	Intensity-Modulated-Radiation Therapy
IRB	Institutional Review Board
ITV	Internal Target Volume
IV	Intravenous contrast

Acronyms

K_{Col}	Collision KERMA
KERMA	Kinetic Energy Released in Matter
kV	kilovoltage
L	Length
LAT	Lateral
LCF	Lesion-Coverage-Fraction
LCNEC	Large Cell Neuroendocrine Carcinoma
LNG	Longitudinal
LuCaRa	Lung Cancer Radiotherapy clinical protocol
MC	Monte Carlo
mCT	Midterm CT
μ_{en}	Energy absorption coefficient
MIP	Maximum-Intensity-Projection
MLC	Multi Leaf Collimator
MRI	Magnetic Resonance Imaging
MU	Monitor Units
MV	Megavoltage
NaN	Not-a-Number
NSCLC	Non-Small Cell Lung Cancer
NTOF	Normal-Tissue-Overdosage-Fraction
OBI	On-Board Imager
OAR	Organs-at-Risk
pCT	Planning CT
PET	Positron Emission Tomography
PMMA	Poly(methyl methacrylate), Perspex, Plexiglas, Acrylite, Lucite
POM-C	Polyoxymethylene, Delrin, Acetal, Polyformaldehyde
PRV	Planning-Risk-Volume
PSD	Plastic scintillator detector
PTV	Planning-Target-Volume
RA	Rapid Arc
ROC	Receiver-Operator-Curve
RPM	Real-time Position Management System
RT	Radiotherapy
RTT	Radiotherapist
Σ	Systematic error component
σ	Random error component
SBRT	Stereotactic Body Radiotherapy
SCLC	Small Cell Lung Cancer
S_{Col}	Collision stopping power
SD	Standard deviation
SI	International System of Units
SPR	Stopping Power Ratio
TN	True Negative
TNM-staging	Tumor-Node-Metastasis classification
TP	True Positive
TPS	Treatment Planning System

XVI

V_{DEF}	Deformed registered structure volume
VMAT	Volumetric Modulated Arc
VOI	Volume-of-Interest
V_{REF}	Reference structure volume
V_{RIG}	Rigidly registered structure volume
VRT	Vertical
W	Width

Content

Content

Content

XXII

Content

1   Thesis objectives and outline

Radiotherapy for lung cancer patients is a challenging task. Breathing motion moves the target and the organs at risk during treatment, increasing the positional uncertainty that affects the treatment outcome negatively. The patient geometry is heterogeneous, with large density variations between lung-tissue, soft-tissue, and bone-tissue in the thorax region. Large density variations result in known dose calculation issues for most commercial treatment planning systems. The absorbed dose delivered to lung cancer patients is therefore of special interest since their soft-tissue tumors frequently are embedded in low-density material that affect the dose calculations.

Lung cancer patients are normally treated while breathing freely, known as the Free-Breathing (FB) method. Deep-Inspiration-Breath-Hold (DIBH) is a gating method routinely used for breast cancer patients to mitigate the breathing motion. This reduces the positional uncertainties related to the breathing motion. DIBH is however still an experimental method for lung cancer patients and needs to be further investigated for this group of patients. The planning of radiotherapy is regularized by target dose coverage and the dose constraints of the radiosensitive organs at risk (OARs) closely located to the tumor volume. Thus it is imperative that the absorbed dose can be accurately predicted in the heterogeneous region of the lung tumor. One of the most widespread dose calculation algorithm used for treatment planning is the Anisotropic-Analytical-Algorithm (AAA). This algorithm is therefore investigated in the current work. There are however, known calculation issues of AAA in heterogeneous geometries. Monte Carlo (MC) is one method utilized in this thesis that has the potential to accurately calculate the dose in heterogeneous geometries. Another method employed in this thesis, is detailed dosimetry by a well-defined in-house designed phantom and scintillator detector system. For lung cancer treatments, tumor volume changes occur frequently and rapidly over the course of treatment. However, known incorrect scatter calculations are carried out by AAA, where the dosimetric challenges are increased when the tumor and field sizes decrease. The goal with radiotherapy is to deliver the same prescribed dose to the tumor, irrespective of the size of the tumor. In order to investigate this further, tumor inserts embedded in low-density medium was used in the phantom to simulate different tumor sizes.

The overall aim of this thesis was to address the following topics related to irradiation of heterogeneous lung cancer geometries, represented by enrolled lung cancer patients or a specially designed phantom mimicking heterogeneous lung cancer setups, with varying tumor sizes. The influence of breathing motion was additionally evaluated for the clinical cases.

1. Study the performance of a deform image registration software based on a modified Demon's algorithm for contour propagation on both FB and DIBH CT and Cone-beam CT (CBCT) images.

2. Investigate the influence of DIBH versus FB on different pre-treatment image-based setup verification protocols and assess the impact on the resulting planning target volumes (PTVs).

3. Determine the dosimetric impact of DIBH compared to FB for complex treatment plans, and benchmark the impact against detailed MC simulations.

4. Develop a well-defined thoracic-like phantom enabling detailed scintillator dosimetry measurements in heterogeneous and homogeneous setups simulating clinical relevant lung cancer geometries.

5. Assess calculation issues present in a commercial treatment planning system for heterogeneous geometries relevant for lung cancer radiotherapy. For this purpose, an in-house developed scintillator detector system and the well-defined thoracic-like phantom were used.

The main parts of the thesis consist of background chapters, followed by discussion, perspectives and conclusion, related publications, bibliography, and technical phantom details and clinical protocol details in the appendices.

Chapter 2 gives an introduction to lung cancer, describes the most relevant aspects of radiotherapy, and how to account for breathing motion and daily patient variations.

Chapter 3 describes theory of image registrations for medical physics applications, where focus is on deformable image registration in radiotherapy. Common validation measures are stated.

Chapter 4 deals with the theoretical aspects of absorbed dose calculations, simulations, and measurements. Interaction processes of ionizing radiation with matter, inhomogeneity calculation corrections, the calibration method and stem-effect removal method for scintillator dosimetry are described.

Chapter 5 explains the clinical methods carried out in more detail. A pre-clinical DIBH study is presented, and the respiratory coaching and treatment workflow is described in more detail.

Chapter 6 describes the design of a thoracic-like phantom, analogous to a lung cancer patient for fiber-coupled organic plastic scintillator dosimetry.

Chapter 7 serves as the conclusion of this thesis, summarizing the main conclusions and findings of the project.

Chapter 8 is a paper presented at the XVII International Conference on the Use of Computers in Radiation Therapy 2013 (ICCR2013). The work is published in the Journal of Physics: Conference Series. The performance of a deformable image registration software based on a modified Demon's algorithm for contour propagation was investigated for three lung cancer cases. Analyzed CT and CBCT images were acquired during both FB and DIBH breathing.

Chapter 9 is a paper submitted for Radiotherapy & Oncology. The influences of DIBH versus FB on three different pre-treatment CBCT image-based setup verification protocols were investigated, in terms of obtaining the smallest PTV.

Chapter 10 is a paper submitted for Radiotherapy & Oncology. The dosimetry of complex treatments for locally advanced non-small cell lung cancer patients treated in FB

or DIBH was investigated. Detailed MC simulations were carried out and compared against, less accurate, dose calculations carried out by a commercial dose calculation algorithm.

Chapter 11 is a paper presented at the 8th International Conference on 3D Radiation Dosimetry (IC3DDose). The work is published in the Journal of Physics: Conference Series. The specially designed thorax phantom was used for scintillator dosimetry in homogeneous and heterogeneous setups, mimicking a lung cancer patient. Clinical relevant treatment plans of different complexities were measured and compared to calculations.

Chapter 12 is an unpublished study describing dosimetry issues for small tumor sizes in a heterogeneous setup. Tumor-size dependency was explored for different treatment techniques. For this purpose, scintillator dosimetry was carried out in the thoracic-like phantom, mimicking a lung cancer patient with lung tumors of different tumor sizes. Clinical relevant treatment plans of different complexities were measured and compared to calculations.

2   Lung cancer

Lung cancer is worldwide one of the most common cancer diseases with a high mortality rate (Figure 1). Compared to other Nordic countries, the rate of lung cancer incidence is the highest in Denmark, where approximately 4500 persons were diagnosed in 2012 [1]. This is likely due to the fact that smoking prevalence is more common in Denmark, especially for women. The incidence rate for women in Denmark the last 10 years has increased by 1%/year, while it has decreased about 1%/year for men, approaching an equal state between the sexes (Figure 2). This tendency is due to the fact that the smoking habits nowadays are equal between the sexes [2]. Half of the lung cancer patient population is older than 69 years, and 5% are older than 85 years (Figure 2). Co-morbidities are thus complicated influential factors affecting the treatment outcome.

(a.) Incidence

1,824,701 (13.0%)
1,671,149 (11.9%)
1,360,602 (9.7%)
1,094,916 (7.8%)
951,594 (6.8%)
782,451 (5.6%)
527,624 (3.8%)
455,784 (3.2%)
429,793 (3.1%)
4,969,280 (35.3%)

(b.) Mortality

1,589,925 (19.4%)
521,907 (6.4%)
693,933 (8.5%)
307,481 (3.7%)
723,073 (8.8%)
745,533 (9.1%)
265,672 (3.2%)
400,169 (4.9%)
165,084 (2.0%)
2,788,798 (34.0%)

Lung   Prostate   Cervix uteri
Breast   Stomach   Oesophagus
Colorectum Liver   Bladder
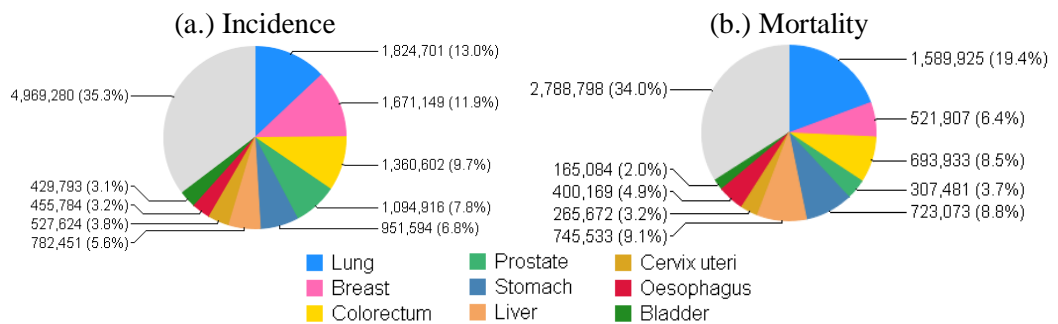
Figure 1. World cancer incidence and mortality in 2012. Source: GLOBOCAN 2012 [3].
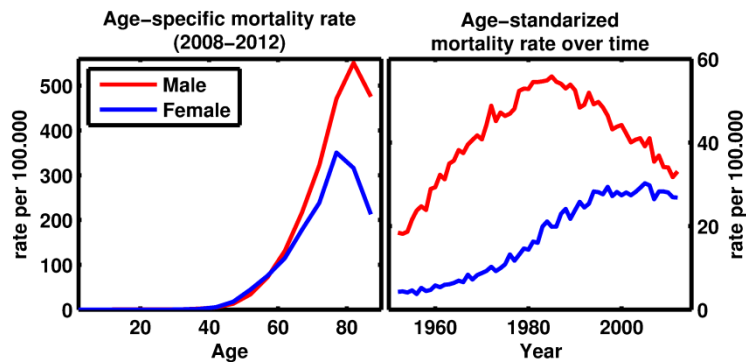
Figure 2. Age-specific and age-standardized lung cancer mortality in Denmark. Values for men and women are separated. The figures are based on data from the NORDCAN database [1,4].

In Denmark, about 18% of the lung cancer patients are referred to radiotherapy [5]. The mortality rate is higher than for most other types of cancer, and the 5-year-survival in 2012 was only 12%. Hence, there is an urgent need for improving radiotherapy for lung cancer patients.

2.1 Treatments

The tumors are classified according to the TNM-classification (staging of primary Tumor, nearby lymph Nodes, and distant Metastasis), where stage I-II represent local disease, stage III locally advanced, and stage IV advanced disease [6]. Lung cancer can be stratified into two groups: Small Cell Lung Cancer (SCLC) and Non-Small Cell Lung Cancer (NSCLC).

2.1.1 SCLC

SCLC is an aggressive disease with highly proliferating cells, which accounts for about 15% of all the lung cancer cases [5]. These patients are often treated with radiotherapy and chemotherapy with quick and good response. However, relapse is very common for these patients, and the overall survival is low.

2.1.2 NSCLC

NSCLC accounts for about 78% of all the lung cancer cases. The choice of treatment depends on the tumor size, location, and whether there is involvement of lymph nodes. Surgery, radiotherapy, chemotherapy and targeted treatments, alone or in combination, are used to treat NSCLC. Most stage I-II tumors are treated with surgery where the lobe or a section of the lobe is removed. The survival rate is increased if postoperative chemotherapy is administrated, known as "adjuvant chemotherapy". NSCLC patients with stage III tumors that cannot be operated are typically treated with chemotherapy in combination with radiotherapy in concomitant or sequential regimes. Stage IV patient are treated with radiotherapy to mitigate their pain, known as "palliative care". Chemotherapy is often delivered to the patients prior to surgery or radiotherapy, in order to shrink the tumor size before the other treatment starts. This form of treatment is known as "neoadjuvant treatment". The tumor shrinkage makes it easier to remove the tumor during surgery, or increase the effectiveness of radiation, since healthy radiosensitive organs at risk (OARs) closely situated to the tumor can be saved from unnecessary radiation. Patients with advanced lung cancer with certain molecular biomarkers may receive treatment with a targeted drug alone or in combination with chemotherapy.

2.2 Radiotherapy of locally advanced NSCLC

It is beneficial to treat lung cancer with high doses of radiotherapy [7,8]. However, high doses can lead to severe radiation-induced side effects, mainly lung toxicity [9,10]. NSCLC patients with peripheral local disease which cannot be operated due to their general condition can be treated with stereotactic radiotherapy, where a high radiation dose in few fractions (hypofractionation) is delivered. Also alternative fractionation schedules such as delivering radiotherapy twice daily (hyperfractionation) has been evaluated with good results, but it is not very commonly carried out due to the logistical challenge in the clinics and the increased hassle for the patients. If the stage I-II tumors are centrally located or the patient has locally advanced disease involving lymph nodes (stage III), their treatment cannot be hypofractionated due to the risk of inducing acute side effects. To avoid this, these patients are currently only treated with 2 Gy / fraction in 30-33 fractions, resulting in a total dose of 60-66 Gy [11].

2.3 Aspects of radiotherapy treatment planning

The goal of radiotherapy is to obtain local tumor control, without radiation-induced side effects. In the early days, lung tumors were treated with simple anterior-posterior treatment fields, or an open-field box technique to achieve acceptable target dose coverage. The major problem with these techniques was the unnecessary radiation dose delivered in tissue other than the tumor volume, which increased the risk of radiation-induced side effects. The treatment was then restrained by the toxicity, rather than the local tumor control. The treatment techniques have become more advanced, where conformal patient-specific dose distributions minimizing the dose delivered to the adjacent OARs is achievable by Intensity-Modulated-Radiation-Therapy (IMRT) and Volumetric-Modulated-Arc-Therapy (VMAT).

2.3.1 Target definition

Three dimensional (3D) Computed Tomography (CT) and Positron Emission Tomography (PET) are nowadays standard imaging devices utilized to visualize the anatomy, the tumor and the functional processes within the body in 3D. Modern treatment planning is utilizing this 3D anatomical information to design patient-specific treatment plans. The target delineation is an estimate of the true Gross Tumor Volume (GTV), and is much affected by image artifacts present during the delineation process [12,13].

In order to ensure that the tumor is receiving the prescribed dose, safety margins are added to the GTV. To account for the extension of clinical microscopic disease a Clinical Target Volume (CTV) is created by adding a margin to the GTV. This margin is based on experience from histological examinations. Clinical practice at Herlev Hospital is to add an isotropic margin of 5 mm. The Planning Target Volume (PTV) is a geometrical concept introduced by the International Commission on Radiation Units and Measurements (ICRU) for treatment planning and evaluation [14]. With this margin, the absorbed dose distribution can be shaped to ensure that the prescribed absorbed dose is delivered to the CTV with a clinically acceptable probability, despite geometrical uncertainties such as organ motion and setup variations, etc. In a similar way, ICRU recommend to apply planning risk volumes (PRVs) to the OARs to ensure that they do not get overdosed during treatment.

2.3.2 Error definitions and margin calculations

Errors in radiotherapy can occur both during the planning process and the treatment delivery process. Anatomical misalignments can be expressed in terms of the overall group mean (GM), systematic (Σ) and random (σ) errors, according to van Herk [15]. In the absence of significant biases, the GM will be close to zero. The systematic error is a measure of the reproducibility of the setup among patients. It is introduced in the planning process, and is present during each treatment fraction. The systematic error is defined as the standard deviation of the GM of the patient population. The random error is due to day-to-day variations and is a measure for the reproducibility of setups between treatment fractions. It is defined as the root mean square of the standard deviations of intra-patient shifts. Treatment execution (random) variations lead to a blurring of the dose distribution,

while treatment preparation (systematic) deviations lead to a displacement of the dose distribution with respect to the CTV [16].

The most common margin concept to use is population based CTV to PTV margins to account for all the present uncertainties over the course of treatment [15,16]. The margin formulas suggested by van Herk (the CTV to PTV margin, eq. 2.1) and McKenzie (the PRV margin, eq. 2.2) are based on the systematic, Σ, and random, σ, error components, measureable over the course of treatment for a patient population.

$$\text{Margin}_{\text{PTV}} = 2.5 \cdot \Sigma + \beta \cdot \sqrt{\sigma^2 + \sigma_p^2} - \beta \cdot \sigma_p \qquad (2.1)$$

where σ_p is the penumbra factor, and the parameter β=1.64 assures delivery of 95% of the prescribed dose to 90% of the patient population [17].

Current practice at Herlev Hospital is to apply a PRV margin to the spinal cord, since this organ is one of the most radiosensitive organs in the body. Since the spinal cord is a serial OAR, and the treatments in this work were delivered as three dimensional IMRT or RA plans, the PRV margins for the spinal cord were calculated according to the McKenzie's formula [18]:

$$\text{Margin}_{\text{OAR}} = 2.5 \cdot \Sigma + 0.5 \cdot \sigma \qquad (2.2)$$

To take into account the intra-fractional motion in the margin calculations, all the systematic and all random components were added in quadrature, according to [15,16]:

$$\Sigma = \sqrt{\Sigma_{\text{Inter}}^2 + \Sigma_{\text{Intra}}^2} \qquad (2.3)$$

$$\sigma = \sqrt{\sigma_{\text{Inter}}^2 + \sigma_{\text{Intra}}^2} \qquad (2.4)$$

Some uncertainties affecting the size of the applied CTV to PTV margin if not corrected for are; the respiratory motion (baseline shifts and daily variations) [19,20], other internal organ motion, setup uncertainties [21–27], anatomical deformations (weight loss, tumor growth/shrinkage, anatomical changes such as atelectasis, pneumonitis, and pleural effusion) [26], and target definitions (inter- and intra-observer variations, and image artifacts) [12,28]. Identifying and minimizing these uncertainties can permit shrinkage of the CTV to PTV margin. This will in turn minimize the irradiated volume and reduce the irradiation of OARs, decreasing the risk of radiation-induced side effects during radiotherapy. A smaller PTV will also allow for higher target dosage.

2.3.3 Treatment toxicity

To avoid radiation toxicity, radiation dose constraints of the adjacent OARs, such as the spinal cord, the heart, the healthy lung, the esophagus, and the plexus brachialis are applied during the treatment planning process (Table 1).

Table 1. Current dose constraints for NSCLC patients at the Department of Oncology at Herlev Hospital.

Priority	DVH constraints	V$_{5\,Gy}$	V$_{20\,Gy}$	V$_{45\,Gy}$	V$_{50\,Gy}$	V$_{55\,Gy}$	V$_{66\,Gy}$	< D >
1	Spinal cord			= 0%				
1	PRV Spinal cord				= 0%			
2	Total lung	≤ 60% [a]	≤ 35%					≤ 20 Gy
2	Healthy lung	≤ 40%						
3	Heart				≤ 20%			≤ 46 Gy
3	Esophagus					≤ 30% [a]	= 0% [b]	≤ 34 Gy [a]
4	Plexus brachialis						= 0%	

DVH, dose volume histogram; PRV, planning risk volume; <D>, mean dose; V5Gy, V20Gy, V45Gy, V50Gy, V55Gy, V66Gy percentage of an organ volume receiving at least 5 Gy, 20 Gy, 45 Gy, 50 Gy, 55 Gy, respectively. [a] Aimed for, but it is not the primarily goal. [b] Absorbed doses up to 70 Gy are allowed in small volumes (< 1 cm^3).

2.4 Breathing adapted radiotherapy

The respiratory motion is an important challenge for lung cancer patients, influencing both imaging and treatment delivery. The breathing motion is required to be considered during both the treatment planning process and the treatment delivery [29,30].

2.4.1 4DCT imaging

A tool to measure the breathing motion is four-dimensional (4D) respiratory correlated CT imaging (4DCT) [31,32]. The respiratory signal is recorded during the scanning procedure by either an external or internal marker, flow or temperature differences of the breath [33]. The breathing signal is retrospectively co-registered with the individual time stamped CT images, resulting in a 4DCT image set. The 4DCT data can be binned either according to the amplitude or the phase of the breathing signal [32,34,35]. Bad correlation between the external marker and the internal organ motions results in image artifacts. However, 4DCT images are still advantageous over 3DCT in terms of erroneous imaging during breathing [13].

2.4.2 Respiratory motion management

There are several approaches to account for the breathing motion within radiotherapy [33,36]; motion-encompassing methods, free-breathing respiratory gated techniques, breath-hold techniques, respiratory synchronized techniques. A summary of the breathing adapted treatment techniques are listed below. The current work is based on the deep-inspiration-breath-hold (DIBH) gating technique, which is further described in detail in Chapter *5.2. DIBH - LuCaRa protocol*.

2.4.2.1 Motion encompassing methods

Tumor motion during free-breathing treatment delivery can be accounted for already in the treatment planning process. For the motion encompassing method, the treatment is planned to ensure target dose coverage of the full tumor motion encompassing volume. There are different concepts to obtain this volume by using free-breathing 4DCT imaging.

One approach, which is the current practice at Herlev Hospital, is to utilize the Maximum Intensity Projection (MIP) concept [37–40]. The GTV is delineated based on the MIP reconstruction, which includes the internal tumor motion at the time of 4DCT imaging. In the MIP image set, the maximum CT number in a given voxel is found over all respiratory phases in the 4DCT image set. It is recommended to visually check the MIP delineated GTV in each breathing phase of the 4DCT data set, especially in those cases where the tumor is closely situated to the diaphragm or mediastinal area where there is a risk of CT number overlap [37,41]. The tumor motion encompassing GTV can alternatively be delineated in each individual image set, and then combined into a union of GTVs [41].

Another approach is to single out one breathing phase representing the phase where the tumor position is close to its time-average position, known as the Mid-ventilation concept [42]. This approach results in smaller total GTV volumes, compared to the MIP concept. However, CTV to PTV margins are required to include the measured breathing motion in the 4DCT data set.

2.4.2.2 Respiratory gating

Irradiation of the patient (during both imaging and treatment delivery) can be carried out in a specific phase of the breathing cycle, known as respiratory gating [33]. Compared to free-breathing conventional radiotherapy, imaging and treatment times are pro-longed. The advantage with gating is the decrease of the uncertainties related to the breathing motion.

Free-breathing gating can either be carried out as expiration- or inspiration-gating [33,43,44]. Since the patient is longer time in the expiration phase compared to the inspiration phase, expiration-gating will be a faster method (with a higher duty-cycle) during imaging and treatment delivery. However, the larger resulting lung volume during inspiration-gating is more advantageous in terms of sparing dose to the healthy lung. DIBH is a breath-hold gating method where the patients hold their breath at a level close to their maximum inspiration level, and thereby increases the time in the advantageous inspiration phase. In addition to the increased lung volume, the diaphragm pulls the heart posteriorly and inferiorly away, which also may reduce the cardiac toxicity depending on the position of the lung tumor.

The breathing reproducibility during treatment delivery and each treatment fraction is a major challenge that needs to be taken into account during radiotherapy planning and treatment delivery. There are several methods to approach reproducible breathing [44–46]. The patients can either be guided by audio- or visual-guidance, or a combination of both (audio-video-guidance). Alternatively, their breath can be controlled by a spirometric device, known as active breath control (ABC) [47]. Nevertheless, although the breathing pattern is optimized, there are known issues of baseline shifts [19,20,48]. Both the internal and external breathing pattern vary on a day-to-day basis, where the internal tumor and organ motions may correlate badly to the motion of the external tumor surrogate (e.g. a marker-box on the thorax surface) or the internal tumor surrogate (e.g. implanted gold markers, used to visualize the tumor in X-ray images) [19,20,24]. Respiratory correlated image guidance for patient setup prior to treatment delivery is therefore necessary to minimize the tumor position uncertainties [20,46].

An alternative to the breath-hold approach that mitigates the breathing motion is the use of an abdominal compression devise [49]. A plate is pressed against the abdomen that reduces the diaphragmatic motion. This method is primarily used for liver patients and lung cancer patients with tumors situated close to the diaphragm with large tumor displacement during breathing. However, it is not all patients that benefit from the abdominal compression. In some cases the compression induce unwanted effects, such as displacement of tumor, or induces irregular breathing motion due to discomfort or anxiety [49,50].

2.4.2.3   Real-time tumor tracking

For a more efficient treatment, with a duty cycle of 100%, real-time tumor tracking is an alternative to gating. The radiation beams dynamically follow the tumor position which compensate for the tumor motion [51]. This approach is more complex than the gating procedures described earlier. Compared to DIBH, the advantage of increased lung volume is omitted. For real-time tumor tracking, detection of the tumor position is the most important challenge. Available systems are based on different techniques [33]; (1.) Direct tumor imaging using radiographic/fluoroscopic images during treatment. (2.) Tracking on internal implanted tumor surrogate fiducial markers. (3.) Tumor position prediction based on tracking of external breathing markers. The tracking techniques are not commercially available for conventional linear accelerators. However, there are other treatment units specially designed to carry out real-time tumor tracking, such as the Vero SBRT system [52,53] and CyberKnife [54]. Research has been carried out on a linear accelerator system, using the dynamic multi leaf collimator (dMLC) to track the tumor motion [55–59].

In real-time tumor tracking there is a need for tumor position prediction to account for latency in the system. Better target localization and tracking latency would improve the synchronization of the dMLC tracking with the tumor motion [56,57]. Real-time tumor tracking has the potential to decrease the tumor position uncertainties during both imaging and treatment and still deliver an efficient treatment. Efficiency of IMRT delivery has found to be dependent on if the tumor motion was tracked in the direction of the MLC leaf travel or perpendicular to the leaf travel [58]. Implantation of fiducial markers as an internal tumor surrogate can lead to pneumothorax, limiting the clinical feasibility of real-time internal tumor tracking. Markerless soft-tissue tracking is a solution for this. This feature is currently not clinically available, but thorough investigations are carried out [60,61].

2.5   Image guided pre-treatment verification

In order to account for external and internal daily variations pre-treatment image guided verification is required [20,46,62]. Setup uncertainties can be minimized if patient fixation equipment are used, e.g. a standard fixation board or a patient specific vacuum cushion [23]. Pre-treatment verification can be carried out by registering the planning CT with a corresponding setup image. 2-dimensional (2D) digitally reconstructed radiographs (DRR) from the planning CT can be registered either by 2D orthogonal kilovoltage (kV) X-ray images acquired by a CBCT system, or 2D megavoltage (MV) image acquired by an electronic portal image device (EPID) system, both attached at the treatment unit. A major disadvantage with DRRs, 2D kV, and MV images is that they only provide bony anatomy

positional information. 3D CBCT imaging provides additional soft-tissue visualization with anatomical positional information of tumor and OARs, as well as anatomical changes in the thorax area, such as atelectasis (collapse or closure of the lung), pneumonitis (inflammation of lung tissue), and pleural effusion (water in lungs) [26]. Direct match on the lung tumor itself (i.e. soft-tissue tumor registration) compared to bony match on the spine has the potential to minimize the required setup margins in the thorax area [21,63,64]. The CBCT images are either manually or automatically registered to the reference CT images. Manual registration is a complex and time consuming task and can be subject to inter-observer variability, contrary to automatic registration [65,66].

Differences between three types of automatic CBCT image–based setup protocols in combination with FB and DIBH are described in Paper II (Chapter 9), where the primary objective was to identify which automatic CBCT match method that resulted in the smallest PTV. The study provides clinical guidance on what automatic CBCT match protocol to use for DIBH or FB setup verification, and it specifically addresses how match results depend on the breathing techniques. The three investigated automatic CBCT match methods focused on: (1.) the bony anatomy of the spine, (2.) the soft-tissue of the primary gross tumor volume (GTV-T), and (3.) the soft-tissue of the total tumor volume (GTV-Total), including malignant lymph nodes (GTV-N).

2.6   Interfractional adapted radiotherapy

As described in Chapter *2.5. Image guided pre-treatment verification*, daily pre-treatment imaging can be carried out to correct for day-to-day variations. However, major anatomical changes such as change of tumor size as a response to the treatment, or creation or ablation of atelectasis, pneumonitis or pleural effusion over the course of treatment are hard to correct for without affecting the target dose coverage or the spearing of dose to the OARs. In adaptive radiotherapy (ART), the treatment plan is adjusted during the course of treatment to minimize the divergence from the planned treatment. ART is a modern, workload heavy approach to end up with the most optimal treatment, that has the potential to account for major anatomical changes not accounted for by applied margins or daily setup verification [36,67]. To adapt a treatment plan, the patient is re-CT scanned and re-planned, where new anatomical structure delineations are required on each new image set. The delineation process is a time consuming task for clinicians, and a major contributor of systematic errors in radiotherapy [28,68]. To save time on the delineation process and to streamline the outcome, deformable image registration (DIR) is a promising tool in assisting with the delineation process. DIR deforms the reference contours from the planning CT into the anatomy of a re-CT or CBCT image. The deformed structure set on the new image set is subsequently visually checked by a clinician and modified until satisfaction before the start of the treatment planning process. More detailed information about image deformations are described in the next section, Chapter *3. Image registrations and deformations*.
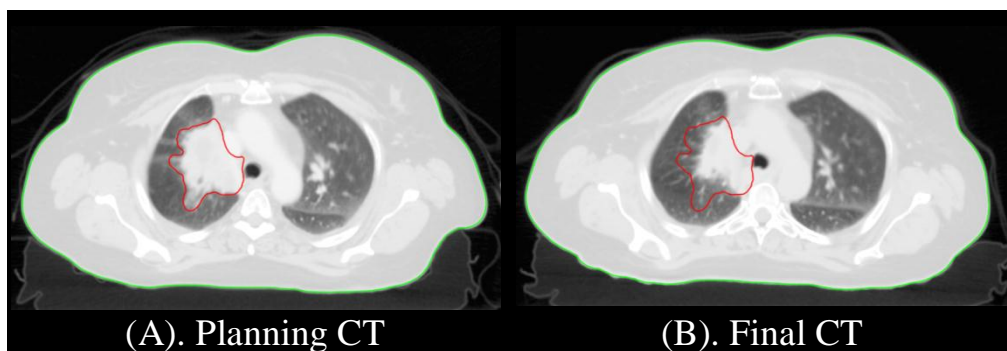
Figure 3. Example of tumor shrinkage observed between the planning CT (A) and the CT acquired at the last treatment session (B). The GTV and the body contour is colored red and green, respectively.

3 Image registrations and deformations

3.1 Introduction

Image registration is the process of determining the geometrical transformation that aligns the points of an image with corresponding points in a reference coordinate frame, i.e. a reference image. When a shape of an object is changed non-rigidly, either temporarily or permanent, it is deformed. To correlate the anatomical information from the various images, deformed image registration is a valuable tool.

Image registration adds values to medical images by enabling:

- Monitoring anatomical motion or changes of an individual patient (intra-patient variations).
- Registration of information from different imaging modalities (like CT, PET, Magnetic Resonance Imaging (MRI), etc.).
- Comparing one patient anatomy with others (inter-patient variation, atlas-based segmentation [69]).
- Comparing a groups' anatomy with others, in order to quantify the biological variability for population studies.

Within the field of modern radiotherapy, image registrations and segmentations are important parts of the treatment. Firstly, in order to diagnose cancer diseases and to make accurate medical statements, the patients are imaged by a combination of various imaging modalities. Since there is not only one imaging device able to perform all imaging techniques at once, it is necessary to fuse (register) the acquired 3D images with each other to correlate the anatomical information in the various sets of images. Unless the image acquisitions are done with the same resolution, within a short period of time or using the same setup, anatomical changes such as baseline shifts, volume change, and change of breathing patterns, etc. may affect the image correlations. Thus, image registrations are required. Secondly, to ensure a god treatment reproducibility during the course of radiotherapy, everyday-pre-treatment imaging is acquired and registered to the planning CT image used for treatment planning. Furthermore, during an ART approach (described earlier in Chapter *2.6. Interfractional adapted radiotherapy*), anatomical structure de-lineations are required for the image sets acquired over the course of treatment to be able to adapt the treatment plan. Manual delineation of the target and OARs is a time consuming process prone to intra- and inter-observer variations [28,68]. DIR and automated segmentation methods are promising tools in reducing the delineation workload and streamline the delineation outcome, minimizing the delineation uncertainties [70]. However, the transformed delineations are still required to be reviewed and modified by a clinician subsequently.

Original   Re-CT   Difference image
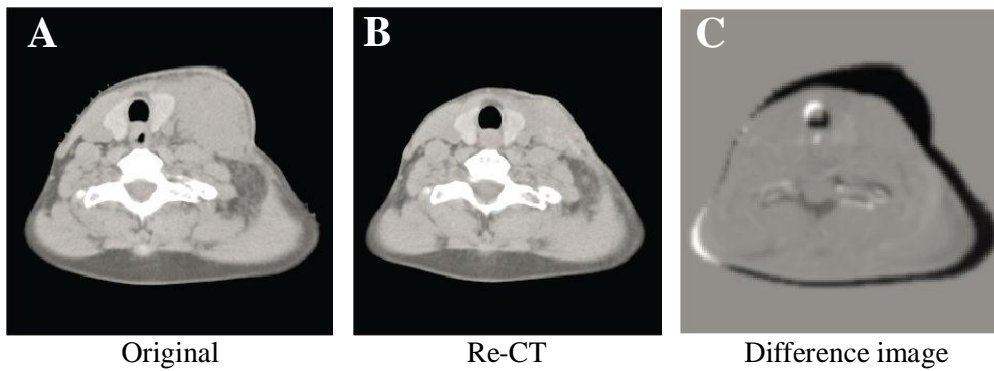
Figure 4. An example of anatomy change in a neck nodal region during radiotherapy. (A) The transversal slice of the original CT image. (B) The same slice of the re-CT image acquired 37 days after the start of radiotherapy. (C) The difference image of (A) and (B). There is clearly a visible shrinkage of the anatomy. Source: Wang et al. [71].

3.2 Elements of image registration

The basic idea of image registration is to find a transformed version of the image that becomes similar to the reference image. There are four elements essential in the image registration process [72]: (1.) 'The geometrical transformation' that rigidly or deformable transforms the image. (2.) 'The similarity measure' that describes the goodness of the registration. (3.) 'The optimization algorithm' that determines the parameters used to maximize the similarity measure. (4.) 'The regularization term' that secures that only reasonable transformations are carried out.

For pre-treatment verification using a standard treatment couch it is sufficient to consider translational differences to correlate the patient position to the planned treatment. However, if using a six degree-of-freedom (DOF) treatment couch, rotations could be included in the correlation.

3.3 Deformable image registration algorithms

Deformable (non-rigid) image registration algorithms can be categorized into either 'feature-based' or 'grayscale based' classes [70,71].

3.3.1 Feature based

Feature-based algorithms match contours, fiducial markers, or anatomical landmark points or lines in the image with the corresponding features of the reference image. These features needs to be defined prior to registration for the algorithm to work, which can be a time consuming process, especially if it is delineated manually.

3.3.2 Grayscale based

In contrast, grayscale-based algorithms use the intensities in the images to register the images, voxel-by-voxel. Due to the consistency in CT pixel intensities it is often advantageous to use a grayscale image-based algorithm for radiotherapy applications, although these often work slower [71]. Mutual information is a commonly used similarity

measure used for grayscale feature based image registrations [70]. Non-linear registrations are frequently based on B-spline or Demon based registrations. A modified Demon's algorithm is used in the current work (Paper I, Chapter 8), therefore are the basics of this algorithm described in more details below.

3.3.2.1 *Demon's algorithm*

Demon's algorithm is one of the most acknowledged image deformation algorithm used clinically [70,71,73–75]. The first version of the algorithm was completely grayscale based, and was originally introduced by Thirion [74,75]. Initially it used the gradient information in the images for registration. Demons algorithm is based on a diffusion model, letting one image diffuse through the interfaces of the other images. The diffusion is steered by demons, hence the name, which are local forces guiding the voxels of the image to be registered to the reference image, i.e. the "static" image. An important parameter of the algorithm, describing the extremity of the deformation, is the ratio of the external to internal force strength, and the regularization of it. The external forces search for similar features in the images to register and the internal forces regulate the resulting transformation. The optical flow formula (eq. 3.1.) can be used to estimate the demons forces. The estimated displacement $\vec{u}$ in three dimensions (u_x, u_y, u_z) required for a given point P in a static image S, with intensity s, to match the corresponding point in the deformed image M, with intensity m, is given by:

$$\vec{u} = \frac{(m-s)\vec{\nabla} s}{\left|\vec{\nabla} s\right|^2 + (m-s)^2} \tag{3.1}$$

$\vec{\nabla}s$ is the gradient of the static image, i.e. the derivate. The *(m-s)* term is the external force of the interaction between the static and the deformed image. The deformation field is regularized by a Gaussian filter with a normal distribution.

The Demon's algorithm has been modified and further developed to be a faster and more accurate image registration algorithm [70,71,73].

There are two major restrictions of the Demon's algorithm [74]. Firstly, the original positioning of the two objects to be registered is crucial for the success of the method. Secondly, the intensities of the two images must be similar. A general solution to this for inter-modality registrations is to make the intensities of the two images similar prior to registration, by for an example atlas-based segmentation.

Original CT scan, with manually delineated structures.

Re-CT scan, with manually delineated structures.

Deformed image (re-CT registered to the original CT scan), including the DVF (light grey lines) and the propagated deformed structures overlaid on the original structures.
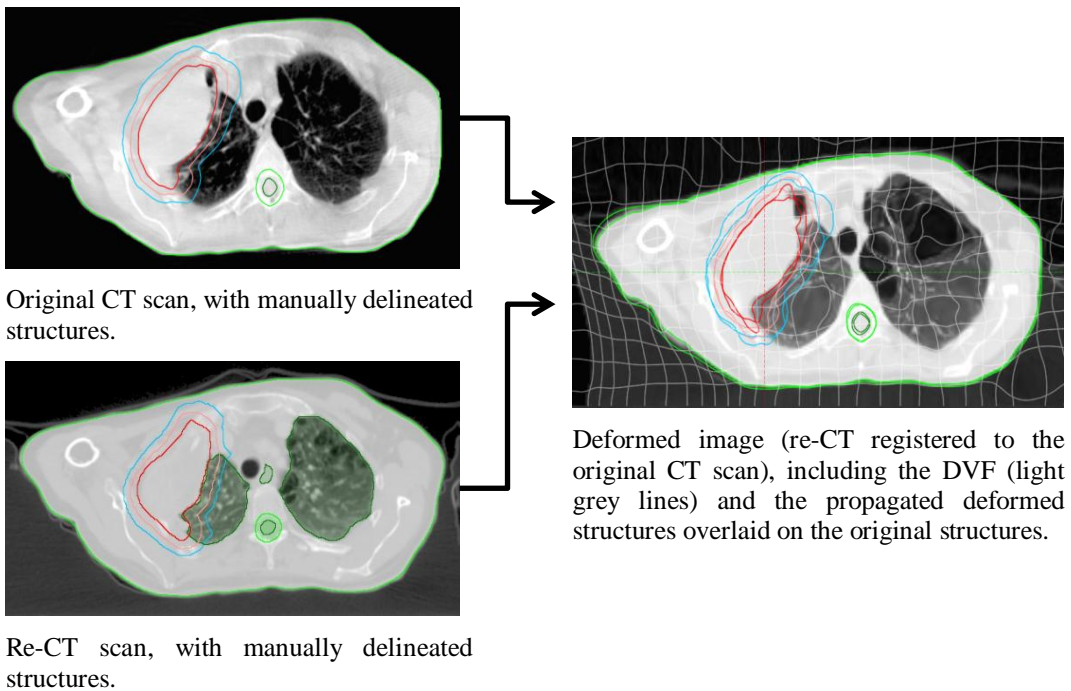
Figure 5. Creation of a deformed image and corresponding deformed structures of a thorax region. The propagated deformed structures are produced by applying the deformation vector field (DVF) (illustrated by the light gray lines in the right figure) to the manually delineated structures on the re-CT scan. GTV, CTV, and PTV are colored red, pink and blue, respectively.

3.4 Validation measures

An important aspect of developing medical image analysis algorithms is demonstrating that the algorithms actually work. This is done by comparing the transformed image with a pre-defined ground truth image. One approach is demonstrated in Figure 5, where the manually delineated structures regarded as "the ground truth" were created by an experienced radiation oncologist. The transformed image can alternatively be compared with an estimate of a population-based ground truth image.

Image transformations can be evaluated for accuracy, efficiency, or reliability by various methods. Simple volume analysis is the most widely reported method [76]. Other common volume analysis methods are listed below.

3.4.1 Center of Mass

Center of Mass (COM) is a measure for describing the displacement of the center position of the segmented volume investigated [70,76]. The COM analysis is effective to use for small spherical volumes, but can be limited for larger complexly shaped volumes, as it is possible for two volumes under comparison to have identical COM, but a very different volume measurement (Figure 6).
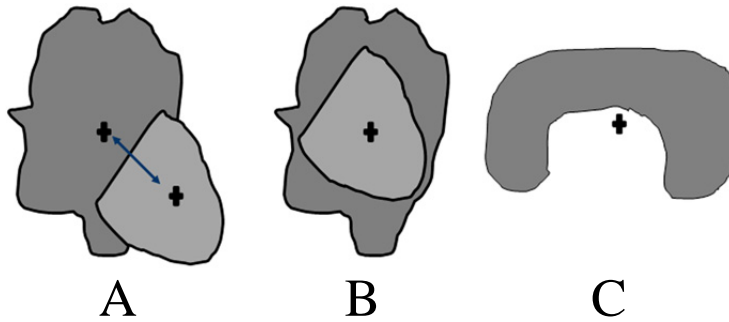
Figure 6. COM examples. (A.) The two volumes of different size and shape have clear COM displacement. (B.) The same two volumes, but now with identical COM. (C.) A single curved shaped volume with the COM located outside of the volume. Source: Hanna et al. [76].

3.4.2 *Overlap methods*

Overlap methods are a bit more complex than just simple volume analysis, and are popular metrics for evaluating transformations of larger complexly shaped volumes. The percentage of overlap of two volumes as a fraction of their total volume is estimated [70,76]. The most common quantitative measures used for comparison of two samples are the 'Conformity Index' (CI) (also known as the Jaccard coefficient, or Minkowski Index) and the 'Dice Similarity Coefficient' (DSC). CI is the ratio of intersection of two volumes and the union of the two volumes (eq. 3.2). The DSC is closely related to CI, and will give a slightly different value compared to the CI for the same volume comparisons (eq. 3.3) [72,76,77].

Overlapping evaluation methods can also be used for applications other than for image analysis. In the current work (Paper III, Chapter 10) new overlapping concepts according to Van Esch et al. [78] were applied in order to evaluate the quality of the treatment plans in terms of target dose coverage and spread of high dose to OARs. The CI_{95}, the 'lesion coverage fraction' (LCF), and the 'normal tissue overdosage fraction' (NTOF) were calculated for the 95% isodose. In brief, the CI_{95} was defined as the 95% isodose volume relative to the size of PTV. The LCF_{95} was defined as the fraction of PTV that was covered by the 95% isodose volume, i.e. it is a measure for target underdosage. The $NTOF_{95}$ was defined in a similar way as the fraction of the 95% isodose volume that was outside the PTV. Thus, NTOF is a method to quantify the relative amount of high dose (i.e. in our case dose over 95% of the prescribed dose) delivered outside of the PTV. CI_{95} assesses only the relative size of the isodose volume without respect to target location. The LCF and NTOF allows for more detailed quality quantification.

Ideal overlap is characterized by a CI, DSC, and LCF close to unity, and a NTOF approaching zero.
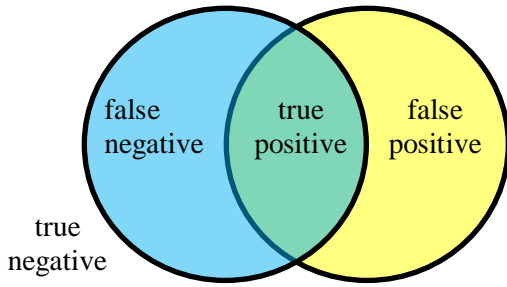
Figure 7. Graphical representation of the concepts of true (T) and false (F) positives (P) and negatives (N). The "ground truth" manually delineated structure is colored blue, and the propagated to-be-evaluated volume is yellow.

$$CI = \frac{\text{Blue} \cap \text{Yellow}}{\text{Blue} \cup \text{Yellow}} = \frac{\text{TP}}{(\text{TP} + \text{FN} + \text{FP})} \tag{3.2}$$

$$DSC = 2 \cdot \frac{\text{Blue} \cap \text{Yellow}}{\text{Blue} + \text{Yellow}} = 2 \cdot \frac{TP}{((FN + TP) + (FP + TP))} =$$
$$= \frac{2\text{TP}}{(2\text{TP} + \text{FN} + \text{FP})} \tag{3.3}$$

3.4.3   Sensitivity and specificity

ROC-analysis is an additional method to evaluate image registrations [72]. All pixels in the 3D image can be classified according to Figure 7, where the background is classified as the true negative (TN) values. False negative (FN) and false positive (FP) refer to registration errors made by the automated algorithm compared to the ground truth image. By using information from the TP, true negative (TN), FP, and FN, a Receiver Operator Curve (ROC) plot can be made where the true positive rate (sensitivity) is plotted against the false positive rate (specificity). The sensitivity is defined by (TP/[TP+FN]), and the specificity by (TN/[TN+FP]). If the registration corresponds perfectly with the ground truth, they will both have the maximum value of 1. The area under the curve of the ROC plot should be as close to 1 as possible to have a good registration result. ROC curves can be very practical to use if transformation results from various image registration algorithms shall be analyzed against each other.
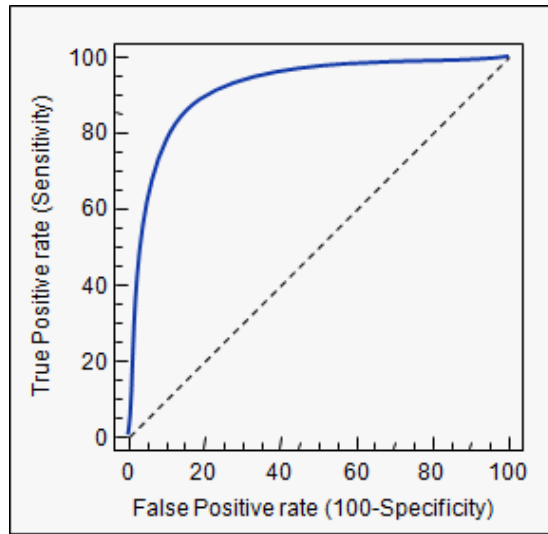
Figure 8. ROC curve. Source: MedCalc Software [79].

3.5 Summarization

Image deformations can be a very handy tool within the field of medical physics. The image quality of moving objects such as the heart, lung tumors, prostate, cervix, bladder, liver etc., can be improved by utilizing image deformations for motion corrections in 4D imaging [73]. Moreover, image deformation techniques enables fast structure propagation of delineated structures from a reference image to images acquired at a later time, or at another imaging modality. This feature can save a lot of time in the delineation process for the clinicians. By utilizing automatic structure propagation, the inter-observer variability is minimized. Furthermore, there is ongoing research on DIR based ART workflows [80]. DVFs obtained between the planning CT and the daily CBCT images, acquired for pre-treatment setup verification, are utilized to propagate the CT Hounsfield unit (HU) values onto the CBCT images, allowing for calculating the "dose of the day" on the CBCT image. These calculations can subsequently be re-mapped onto the planning CT to eventually evaluate the actually delivered dose to the patient compared to the planned treatment. DVFs can additionally be utilized to adapt the MLC aperture to account for tumor deformations in real-time [81].

New and improved deformation algorithms, both rigid and non-rigid, are constantly developed. Image registrations are however very sensitive for image artifacts. Special notice should therefore be taken to image artifacts in the images prior to image registrations. Figure 9 demonstrates two patient examples of image registrations where the resulted deformed registration is incorrect due to image artifacts in the registered images.
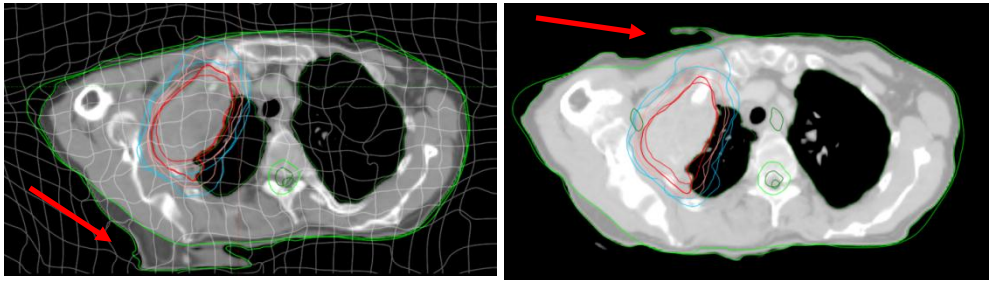
Figure 9. Two examples of erroneous CBCT image registrations (red arrows) due to image artifacts in the registered images (not presented, see example in Paper I, Chapter 8). The DVF is presented as light gray lines in the left figure.

Investigation of the performance of a DIR software based on a modified Demon's algorithm for contour propagation is described in Paper I (Chapter 8). DIR was carried out between the planning CT and the re-CTs and daily CBCTs acquired over the course of treatment to obtain the DVFs used for contour propagation. The images were acquired for both FB and DIBH for three lung cancer patients.

4 Dosimetry

4.1 Interactions of ionizing radiation with matter

To measure absorbed dose in a point, an infinitesimal volume, *dv*, is considered. The SI unit for absorbed dose is Gy (J/kg), which is defined as the energy imparted, *dε*, by ionizing radiation in an infinitesimal volume, where, *dm*, is the mass in the volume (eq. 4.1) [82].

$$D = \frac{d\varepsilon}{dm} \qquad (4.1)$$

The fluence of the primary photon beam, N_0, passing through a media of a certain thickness, *x*, is attenuated exponentially through indirect interactions with certain probability (μ) (eq. 4.2).

$$N(x) = N_0 \cdot e^{-\mu \cdot x} \qquad (4.2)$$

The dose is not deposited by the photon radiation directly, but indirectly by the secondary charged particles generated by photon interactions in the media. The energy deposition in tissue from photon irradiation occurs thereby in two steps [82,83]:

- The kinetic energy of the primary photon radiation is transferred to charged particles in the media. The photons interact with the media through three processes yielding secondary charged particles by 'Photoelectric absorption', 'Compton scattering', and 'Pair-production'. For the megavoltage photon beams used in radiotherapy, Compton scattering is the predominant process. The amount of kinetic energy per unit mass transferred to electrons is defined as the KERMA.

- The secondary charged particles deposit their energy in the media through ionization and excitation along their particle track by elastic and inelastic scattering processes. The most likely scattering process is with small angles and small energy transfers, due to the Rutherford scattering cross section ($d\sigma/d\Omega \sim 1/(\sin^4(\theta/2))$) and the energy transfer cross section ($d\sigma/dT \sim 1/T^2$). Since the incident charged particles only transfer a fraction of their kinetic energy, it is convenient to think of it as the particle loses its energy gradually, known as the Continuous Slowing Down Approximation (CSDA). The CSDA range is very close to the average path length of the charged particle for low-Z materials. The mass stopping power, $dT/\rho dx$, is a measure for the energy loss per unit path length, *dx*, by a charged particle of certain energy, *T*, in a media of mass density, *ρ*. The mass stopping power consists of two parts, the mass collision and radiative stopping power. Since the radiative contribution is not deposited locally, only the collision part (S_{Col}) is considered for the absorbed dose in the infinitesimal volume. The amount of kinetic energy released locally is known as collision KERMA (K_{Col}).

The kinetic energy transferred from the photon beam to the secondary charged particles in the media does not lead to full energy absorption at the same location. This is due to the relatively long range of the secondary electrons generated in the media. Just below the surface of the media, there exists no charged particle equilibrium (CPE). Therefore, the absorbed dose starts to build up through the depth (Figure 10). As the depth increases, CPE is eventually reached, approximately at the depth equal to the maximum range of the secondary electrons (CPE condition is described in Figure 11). Due to the convergence of the beam and the photon fluence attenuation in the media, the production of secondary electrons decreases accordingly, resulting in transient CPE in the region where the absorbed dose, D, is proportional to K_{Col}. The dose curve reaches a maximum (d_{max}) at the depth where the rising slope due to buildup of charged particles is balanced by the descending slope due to attenuation of the indirectly ionizing radiation [82].
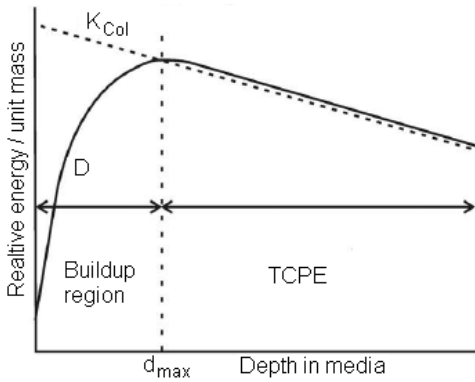
Figure 10. Collision KERMA and absorbed dose as a function of depth in a medium irradiated by a high energy photon beam. Redesigned illustration from Podgorsak [84].
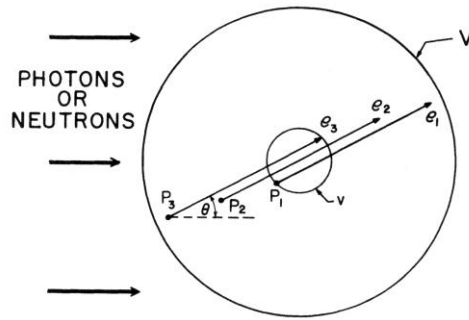
Figure 11. CPE condition for an external source. If the minimum distance separating the boundaries of the larger volume (V) and the smaller internal volume (v) is greater than the maximum range of charged particles present, CPE exist in v. Source: Attix [82].

For mono-energetic photons with the energy, E, the absorbed dose is related to K_{Col} under CPE condition in the media for external beams according to:

$$D = \frac{d\varepsilon}{dm} \overset{\text{CPE}}{=} K_{\text{Col}} = \Psi\left(\frac{\mu_{\text{en}}}{\rho}\right) = \left(\frac{\mu_{\text{en}}}{\rho}\right) E\Phi^{\text{Photons}} \qquad (4.3)$$

Where Ψ is the photon energy fluence, (μ_{en}/ρ) is the mass-energy absorption coefficient of the media, and $\Phi^{Photons}$ is the photon fluence. Correspondingly, during equilibrium in terms of secondary electrons, the dose is given according to:

$$D \overset{\delta\text{-eq}}{=} \left(\frac{S_{\text{Col}}}{\rho}\right)\Phi^{e^-} \qquad (4.4)$$

Where (S_{Col}/ρ) is the unrestricted mass collision stopping power and Φ^{e^-} is the electron fluence in the media.

For shallower depths $<$ d_{max} the transport of charged particles must be explicitly taken into account. Lateral CPE is additionally dependent on if the field size is large enough to establish CPE in all directions. This is an issue for narrow field sizes less than the range of the secondary charged particles. Since the change of density affects the range of the secondary charged particle, this will be a greater issue for low density lung-tissue, where the range of electrons is approximately four times greater than in water. Additionally, this effect increases the penumbra width in low density media.

4.2   Inhomogeneity corrections

Input data for the treatment planning systems (TPSs) are obtained in water [85,86]. However the human body is heterogeneous and consists of various materials and cavities of different radiological properties, such as soft-tissue, lung-tissue, bone-tissue, air cavities, metal prosthesis, etc. (Figure 12). Due to the dependence of interaction probabilities in the media, the presence of heterogeneities influences the dose deposition in the patient. Thus, inhomogeneity corrections are required for more correct dose calculations in heterogeneous geometries.
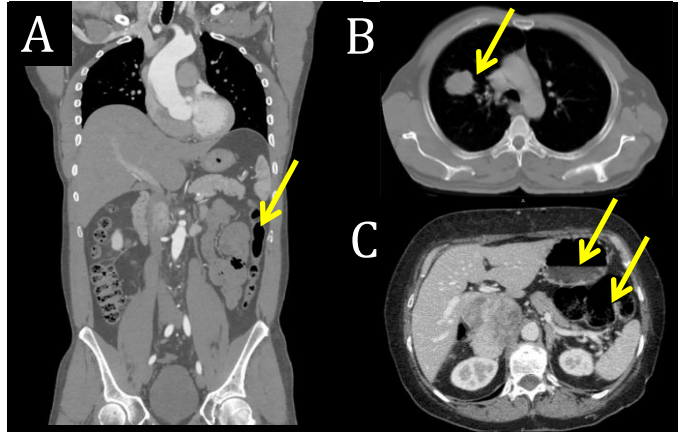
Figure 12. Examples of heterogeneous patient anatomies containing soft-tissue, lung-tissue, bone-tissue, air cavities, and fluid. (A) A coronal slice of the middle part of the body. The arrow indicates air in the intestine. (B) A transversal slice of the thorax. The arrow indicates a lung tumor located in center of the patient's right lung. (C) A transversal slice of the abdomen. The upper arrow indicates fluid in the stomach. The fluid is illustrated by the straight surface since the patient is lying down during imaging. The lower arrow indicates air in the colon.

Different inhomogeneity correction methods differ mainly in the way how they account for the scattered photon contribution, primary electrons, and in the sampling of anatomical 3D density information (Table 2) [83,87]. MC algorithms that use photon interaction probabilities and model the electron scatter in heterogeneous geometries belong to a calculation approach explicitly accounting for density inhomogeneities and correctly calculates absorbed dose in regions with non-existing CPE conditions (Table 2). Other methods are often based on approximations to account for density related fluence and

particle range changes in order to save calculation time. For correct inhomogeneity corrections in patients, all assumptions are required to be accounted for, where both changes in density and atomic number composition need to be considered.

Table 2. Categorization of different inhomogeneity correction algorithms according to the level of anatomy sampled (1D or 3D) and the inclusion or exclusion of electron transport. Source: Papanikolaou [83].

	Local energy deposition	**Non-local energy deposition**
	Category 1	**Category 3**
1 D	1. Linear attenuation 2. Effective attenuation 3. Ratio of TAR (RTAR) 4. Power law (Batho) 5. Equivalent path length (EPL)	1. Convolution (pencil beam, PB) 2. Fast Fourier Techniques (FFT)
	Category 2	**Category 4**
3D	1. Equivalent TAR (ETAR) 2. Differential SAR (DSAR) 3. Delta volume (DVOL) 4. Beam subtraction method	1. Superposition / Convolution (Collapsed Cone Convolution, CCC) 2. Monte Carlo (MC) 3. Differential TAR (dTAR)

4.3   Modern TPS algorithms

Modern commercial TPSs are based on advanced algorithms that decompose the radiation beam into primary and scatter components and calculate them independently. Superposition and convolution principles are used to calculate the dose distribution based on MC simulated dose spread kernels and the energy deposited at each point in the volume. Hence, they account for changes in scattering, caused by variations in beam shape, intensity, patient geometry and tissue inhomogeneities. However, approximations are employed, not comparable to MC simulations.

Throughout this thesis the Varian Eclipse (Varian Medical systems, Palo Alto, CA, USA) TPS was used for treatment planning, where the AAA was utilized [88]. Additional MC simulations were carried out in Paper III (Chapter 10). The superposition AAA dose calculation algorithm and the basics of MC simulations are therefore described in more details below.

4.3.1   Anisotropic-Analytical-Algorithm

The AAA algorithm has previously been described extensively [88–92]. The AAA algorithm is a three source pencil-beam convolution-superposition model, where the primary and secondary photons and the contamination electrons are individually calculated for each beamlet. The dose contributions from all sources are subsequently superpositioned to the final dose distribution, where the heterogeneity correction only is carried out during the superposition phase by a modified Batho heterogeneity correction [88]. The most important approximation of AAA is that the energy deposition is divided into two components, the first component models the photon interactions along the fanline, and the second component models the scatter perpendicular to the fanline as a sum of six radial exponential functions for a discrete number of angular sectors [88–90]. Thus, the two component approximation does not take the divergent scatter of heterogeneities from upper

levels correctly into account. The depth and lateral components are anisotropically scaled independently according to the electron density distribution of the medium. Additionally, the approximation of using a discrete number of angular sections for the radial exponential functions cause smoothing of the calculated dose distribution near heterogeneous interfaces [88,89].

4.3.2   *Monte Carlo simulations*

The initial MC simulation of the photon generating process in the accelerator head is an advantage over other dose calculation algorithms. Each photon history is subsequently simulated until the kinetic energy of the generated secondary charged particles is released, typically down to a cut-off energy of about 10 keV. For sufficient statistics, a large number of photon interactions are required to be simulated due to the long mean free path length of photons resulting in few interactions in the patient body. This results in long calculation times, which is the major reason why MC simulations are not frequently used in clinical environments. However, increased computer powers and variance reduction techniques may speed up the MC calculation processes enough to make them clinically acceptable for routine use [83]. More detailed information about the MC simulations carried out in this thesis is described in Paper III, *10.2.6, Monte Carlo simulations*.

4.3.2.1   *Dose-to-water conversion*

Generally for most TPSs, the calculated absorbed dose is reported as dose-to-water (Dw) [93]. MC simulations report the absorbed dose as dose-to-medium (Dm), where the patient-specific electron density information obtained from each patient's CT image set, and media dependent interaction cross sections are used to calculate the absorbed dose. In order to compare MC doses with TPS computed dose distributions, Dm needs to be converted into Dw. The conversion procedure is described by Siebers et al. [94]. In short, they propose an analytical method based on Bragg-Gray cavity theory, in which they use the Spencer-Attix mass restricted collision stopping power ratios (SPRs) as conversion factors. They calculated the ratio of tabulated stopping power for water and the investigated medium for a nominal energy. A better approach is to use MC computed SPRs for the beam in question. The dose-to-water conversion method employed in Paper III is a conversion approach in between, where MC computed SPRs for a reference beam of the linear accelerator in question is used according to eq. 4.5.

$$D_w = D_m \times SPR_m^w(Q,m)$$

(4.5)

Where Q is the beam quality, and m is the medium.

4.4   **Scintillator dosimetry**

The dosimetry in this thesis is carried out with fiber-coupled organic plastic scintillators (PSDs). The advantages of using PSD for complex and dynamic radiotherapy dosimetry in megavoltage photon beams have previously been presented in studies based on homogeneous setups in either water or solid water phantoms [95–98]. Benchmarking against MC simulations have shown good agreement with measurements [97]. Additionally, a recent study by Francescon et al. even concluded the Exradin W1 PSD (Standard Imaging, Middleton, WI, USA) to be the only detector of those investigated that

could reproduce the Monte Carlo simulated data in water with high accuracy [99]. PSDs are particularly well suited for complex dose verifications due to their water-equivalency, and small size for high spatial resolution and minimum perturbation of the radiation fields. Alanine and thermoluminescent dosimeters (TLDs) are also highly water equivalent, but they do not provide real-time output, which is a significant drawback in studies involving many treatments and complex phantom setups.

4.4.1 Calibration procedure

One drawback with PSD dosimetry is the fact that the signal is affected by produced Cerenkov light, and fluorescence light in the fiber during irradiation, known as the stem-effect. The amount of stem-effect is due to how much of the fiber that is irradiated. This needs to be corrected for during the calibration process. The obtained signal is therefore required to be corrected in order to acquire the absorbed dose delivered in the scintillator. The study by Guillot et al. [100] describes several different methods to remove the stem-effect. The stem-effect removal approach used in this thesis is referred to as the Method C, in their study. The essential of the method is described in more detail in this section. Chromatic removal of the unwanted signal is possible since the spectra of the Cerenkov and fluorescence light is different from the scintillator signal. The calibration procedure was conducted in a Solid Water (Gammex Inc., Middletron, WI, USA) calibration phantom according to Figure 13.

Configuration 1
$$D_1 = a \cdot A_1 + b \cdot B_1$$

Configuration 2
$$D_2 = a \cdot A_2 + b \cdot B_2$$
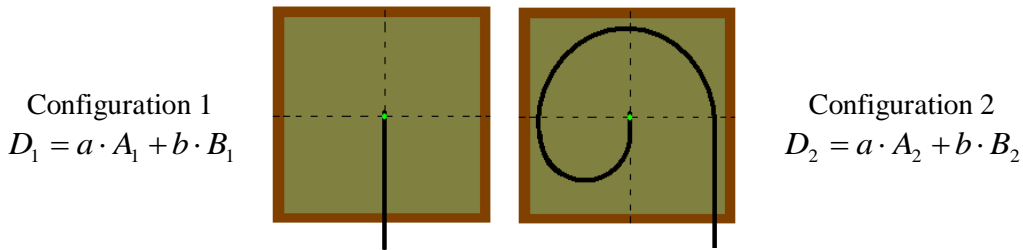
Figure 13. Schematic illustration of the calibration phantom used for chromatic removal calibration.

A is the signal in the green channel and *B* is the signal in the blue channel. The absorbed dose *D* in the scintillator would be given by the relation $D = a \cdot A + b \cdot B$. The unknown constants *a* and *b* are calculated by calibrating the scintillator at known delivered dose for two different irradiation conditions: (i) an irradiation with a small amount of the fiber in the radiation field (Configuration 1, left in Figure 13), to minimize the generation of Cerenkov light and fiber fluorescence; (ii) an irradiation involving as much fiber in the radiation field as possible to maximize the stem effect (Configuration 2, right in Figure 13). *a* is defined as the gain factor. The ratio $-b/a$ is defined as the Cerenkov Light Ratio (CLR), or stem-signal ratio.

4.4.1.1 Specific calibration procedure

The reference dose (100 MU, 10x10 cm^2 field at a source-surface distance of 90 cm, and depth of 11.5 cm) was measured by a Farmer ionization chamber, type 30011 (PTW, Freiburg, Germany) in the Solid Water phantom, at configuration 1. The depth of 11.5 cm agreed with the center position in the Poly(methyl methacrylate) (PMMA) phantom used

for scintillator dosimetry in heterogeneous setups (described in Chapter *6, Phantom details*). Irradiation was delivered by a Varian Clinac iX 2300 linear accelerator (Varian Medical Systems), with a beam energy of 6 MV at a dose rate of 600 MU/min. The calibration dose was normalized to the corresponding calculated dose in Eclipse to eliminate the daily output variation of the linear accelerator. To determine the dosimetric correction factor between the Solid Water phantom and the in-house developed PMMA phantom, corresponding measurements were carried out in the PMMA phantom (using the most homogeneous setup, where all body cylinders were filled with PMMA). The mean and one standard deviation (1 SD) of the dosimetric correction factor between the solid water calibration phantom and the PMMA phantom measured with the ionization chamber was 0.9983 (0.0013).

5 Clinical methods

This section gives an overall description on the methods used in the clinical studies not described in the papers. More detailed method descriptions are presented in each manuscript (Paper I-III).

5.1 Pre-clinical DIBH pilot study

Before initialization of the clinical DIBH-LuCaRa (Lung Cancer Radiotherapy) protocol, there existed preconceptions about the impracticability to perform DIBH for locally advanced lung cancer patients due to their comorbidities, such as chronic obstructive pulmonary disease (COPD) or poor pulmonary functionality, etc. For that reason a pre-clinical pilot study was carried out for locally advanced lung cancer patients to assess how long time these patients could hold their breath (Figure 14). Forty-eight patients planned for curative radiotherapy at Herlev Hospital in 2011 were enrolled in the pilot study.
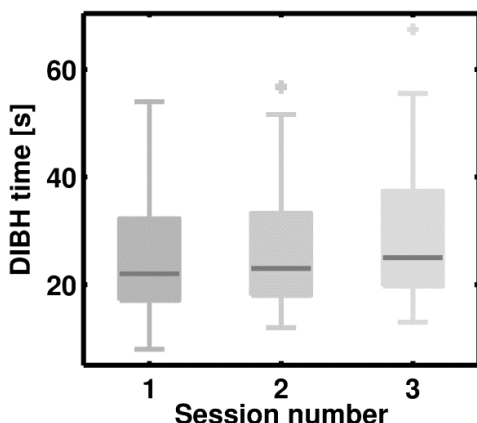
Figure 14. Duration of breath-hold times for 48 locally advanced lung cancer patients, reproduced in 3 breath-hold sessions for each patient. On each box, the central dark gray mark represents the median value. The edges of each box are the 25th and the 75th percentiles, the whiskers correspond to approximately $\pm$ 2.7 SD of the data, and outliers are plotted as crosses individually.

It was found that the patients in median could hold their breath for longer than 20 seconds. Breath-hold during 20 seconds is the required time frame for breast cancer patients to be offered DIBH treatment at Herlev Hospital [101]. Thus, the same requirement was applied for the locally advanced lung cancer patients enrolled in the clinical DIBH-LuCaRa study.

5.2 DIBH - LuCaRa protocol

A total of 23 locally advanced lung cancer patients were enrolled to the IRB approved DIBH-LuCaRa protocol by the Department of Oncology at Herlev Hospital between December 2012 and July 2014. The patient characteristics are summarized in Table 3. Every patient received verbal and detailed written information about the DIBH-LuCaRa protocol, and gave informed consent to the work before inclusion. For more details about the clinical protocol see *Appendix C: Clinical protocol (in Danish)*.

Table 3. Patient characteristics

	Age	Sex	PS	TNM	Tumor Loc.	Lymph nodes	Mediastinal involvement, Tumor	Mediastinal involvement, Lymph nodes	Tumor site	Differentiating	Comments
P1	74	M	0	T4N0M0	LUL	NaN	N	NaN	Central	Planocellular	
P2	68	M	0	T3N3M0	LUL, LLL	LUL, LLL, 7	Y	Y	Central	SCLC	Dropped before start of treatment
P3	59	M	1	T3N1M0	RUL	4R	Y	Y	Chest wall	Planocellular	
P4	53	F	0	T4N2M0	LUL	4L, 5, 7	Y	Y	Central	Adenocarcinoma	Dropped at fx 2
P5	57	M	0	T2aN2M0	RUL	4R, 11R, 12R	Y	Y	Central	Planocellular	
P6	68	M	0	T4N0M0	LUL	NaN	Y	NaN	Central	Planocellular	
P7	48	F	0	T4N2M0	RUL	2R, 4R, 7	Y	Y	Central	Adenocarcinoma	
P8	70	F	0	T4N0M0	LUL	Hilus left	Y	Y	Central, Chest wall	Adenocarcinoma	
P9	61	M	0	T2aN2M0	RUL	4R, 12R	Y	Y	Central	Adenocarcinoma	
P10	65	M	0	T2aN2M0	RLL	2R, 4R, 12R	N	Y	Chest wall	Planocellular	
P11	72	M	0	T1aN2M0	LUL	4L, 5, 7	N	Y	Peripheral	Adenocarcinoma	
P12	63	M	0	T3N2M0	RUL	2R, 4R, 10R	N	Y	Peripheral	Adenocarcinoma	Dropped at fx 12
P13	75	M	0	T2aN2M0	LUL	4L, 5	N	Y	Central	Adenocarcinoma	
P14	63	M	0	T3N2M0	LLL	4L	Y	Y	Chest wall	Adenocarcinoma	
P15	56	M	0	T4N3M0	RUL	2R, 4R, 4L, 7, 10R	Y	Y	Central	LCNEC	Dropped at fx 2
P16	53	M	1	T4N3M0	RML	4R, 5, 7	N	Y	Central, Peripheral	Adenocarcinoma	Changed to palliative
P17	56	F	0	T3N2M0	RUL	4R, 11R	N	Y	Central, Peripheral	Adenocarcinoma	
P18	56	F	0	T3N1M0	RUL, RML	11R	Y	Y	Central, Chest wall	Adenocarcinoma	Dropped at fx 1
P19	65	M	0	T3N3M0	RUL	4L, 4R	N	Y	Peripheral	Planocellular	
P20	54	M	0	T4N1M0	LLL	11L	N	N	Chest wall	Planocellular	
P21	57	M	0	T3N2M0	RLL	4R, 11R	Y	Y	Central	Adenocarcinoma	
P22	68	M	0	T3N3M0	RUL	2, 4L, 4R, 7, 10R, 11R	Y	Y	Chest wall	Adenocarcinoma	
P23	62	F	0	T1bN3M0	LLL	4R, 4L, 5, 7, 10L, 1L	Y	Y	Central	Adenocarcinoma	

PS, Performance Status; TNM, Tumor-Node-Metastasis staging; Loc., Location; M, Male; F, Female; L/R-UL, Left/Right-Upper Lobe; L/R-LL, Left/Right-Lower Lobe; RML, Right Middle Lobe; Y, Yes; N, No; NaN, Not-a-Number; SCLC, Small Cell Lung Cancer; LCNEC, Large-Cell Neuroendocrine Carcinoma; fx, fraction.

5.3   Respiratory coaching

Prior to imaging for treatment planning, all patients were introduced during a 30 minute training session to the DIBH procedure by a radiotherapist (RTT). The Varian real-time position management (RPM) system, version 1.7 (Varian Medical Systems), integrated with the CT and CBCT imaging systems, and the linear accelerator, was utilized to monitor the patients' respiration [32]. Infrared cameras were fixed at the end of the CT-couch and on the wall in the treatment room, facing the treatment-couch (Figure 15F). These were used for tracking the respiratory motion by the vertical displacement of a marker box with infrared reflective markers placed at the lower chest or upper abdomen of the patients (Figure 15 (B, D, E)).
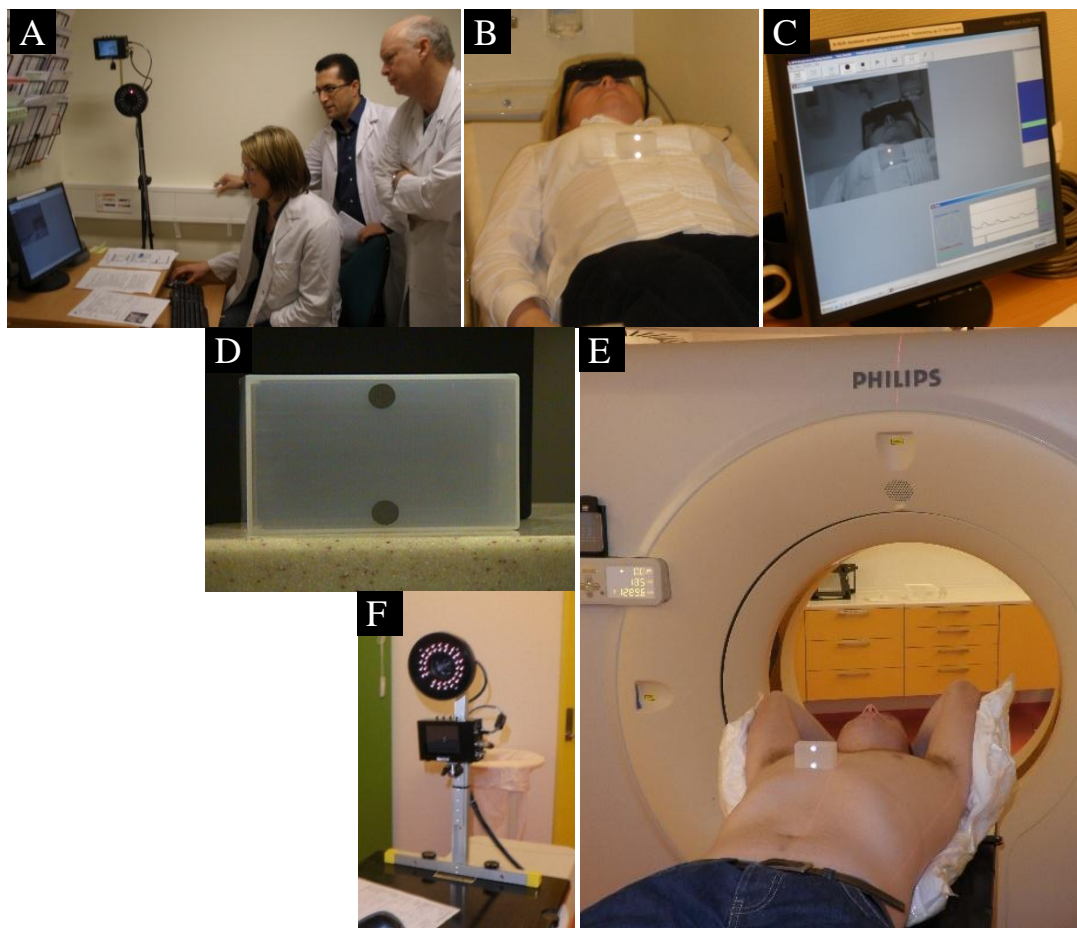
Figure 15. (A.) Operator during the training session. (B.) Computer goggles are used for visual guidance. The marker box is positioned on the thorax. (C.) The view of the operator. (D.) The marker box. (E.) Patient setup in an individualized fixation at the CT scanner, with the marker box positioned on the thorax. (F.) The RPM camera located at the end of the CT couch.

The goal with the training session was to establish stable reproducible breathing amplitude and to evaluate the patients' breath-hold capacity. The intended gating window

(i.e. the upper and lower gating thresholds) and the patients' amplitude level were individually decided for each patient. During the training sessions, the patients were verbally guided by the operator when to hold the breath (Figure 15 (A, C)). To achieve a reproducible inspiration level, they were additionally visually guided by using video goggles (Figure 15B) [101]. The patients were required to hold their breath at least 20 seconds at a reproducible patient-specific amplitude level and a gating window of 2-3 mm width to be enrolled in the DIBH-LuCaRa protocol. The operator guided the patients explicitly to fall down to their baseline between the deep breath-holds, since otherwise the relative breath-hold level was affected (For examples of baseline shifts see the section below).

5.3.1 Example of breathing curves

Four patient examples illustrate the importance of correct patient guidance to achieve an optimal DIBH treatment.
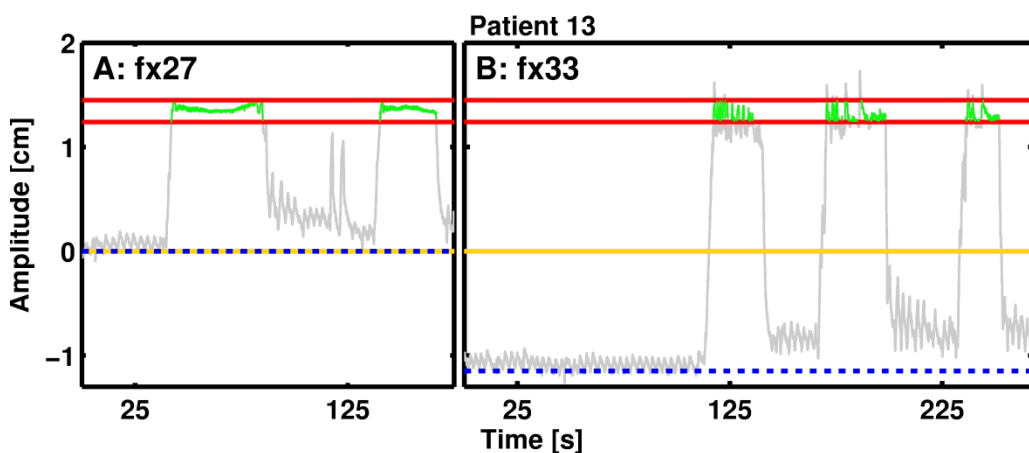
Figure 16. Two different examples of breathing curves for patient 13 to acquire a CBCT image. Yellow line is the initial baseline. The blue dashed line illustrates the baseline shift relative to the initial baseline (yellow line). The red lines define the gating window. The green color illustrate when the beam-on for image acquisition was active. (A.) A correctly carried out session with 2 breath-holds required to acquire the image at fraction (fx) 27. (B.) An example of severe baseline shift (increasing the amplitude by 12 mm, i.e. 95% amplitude increment). This was not accounted for by a re-initialization of the tracking software by the operator. Additionally, there were clearly observed increased fluctuations within the gating window compared to (A.) (even going below the gating window).
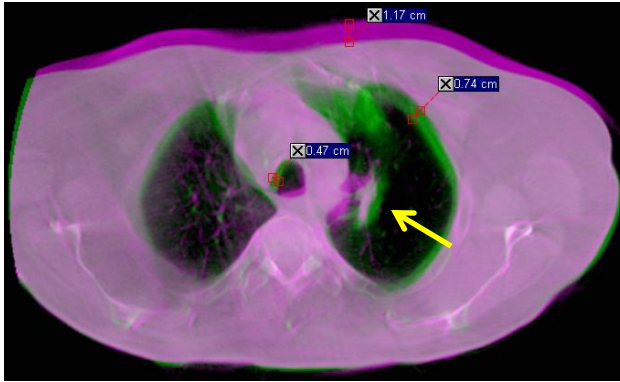
Figure 17. A correctly (green) and erroneously (violet, Figure 16B) acquired DIBH CBCT image for patient 13 at fx 33 overlaid on each other. The arrow indicates the tumor location. The color shifts are measures on how much the anatomy is shifted in the patient. The anterior surface shift (violet) corresponds to the baseline shift in Figure 16B.
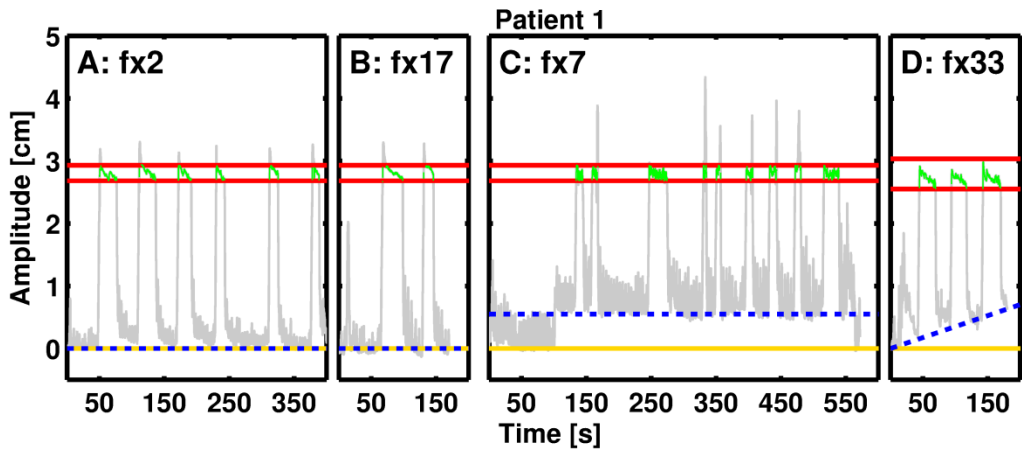
Figure 18. Four different examples of breathing curves for patient 1 to acquire a CBCT image. Additional figure explanations are described in Figure 16. (A.) A correctly carried out session with 6 small breath-holds (about 20-25 seconds long) were required to acquire the image at fx 2. (B.) At fx 17, only 2 longer breath-holds (about 30 seconds long) were required. (C.) At fx 7, the tracking was not re-initialized after moving the couch for patient positioning. The couch displacement affected the baseline, which decreased the breathing amplitude by about 5 mm. (D.) The operator forgot to guide the patient to fall down to the initial baseline after each deep breath-hold. Thus, the baseline was changed and the amplitude was decreased after each breath-hold. Observe that the gating window at fx 33 is wider (4.8 mm) than for the other fractions (2.5 mm) in this figure. This is due to a plan adaption with a re-CT scan at fx 22, where a new reference breathing curve was obtained which was more comfortable for the patient. Please note that this patient had a tendency to peak before falling into the gating window. This tendency was reduced after adjusting to a wider gating window (D).
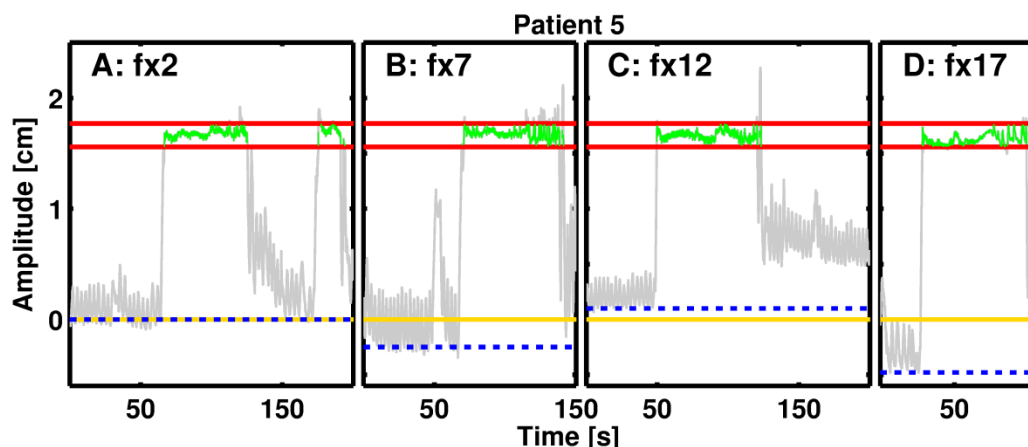
Figure 19. Four different examples of breathing curves for patient 5 to acquire a CBCT image. Additional figure explanations are described in Figure 16. Compared to Patient 1 and similar to patient 6, this patient was able to hold the breath approximately 60-70 sec, resulting in fewer times of breath-hold per image acquisition and faster total image acquisition time. (A.) A correctly carried out session with 2 breath-holds required to acquire the image at fx 2. (B.) At fx 7, only 1 long breath-hold (about 70 seconds) was required. The operator missed however to re-initiate the tracking before imaging, resulting in a baseline shift and increased amplitude of 2.5 mm. The fluctuation increased at the end of the breath-hold (even going above the gating window). This may be due to difficulties for the patient to hold the breath such long time (C.) At fx 12, although the patient was able to hold the breath during the whole image acquisition, there was observed some difficulties to fall down to the baseline subsequently after the long breath-hold. (D.) Similar to fx 7, the baseline was shifted, resulting in increased amplitude of 5 mm at fx 17.
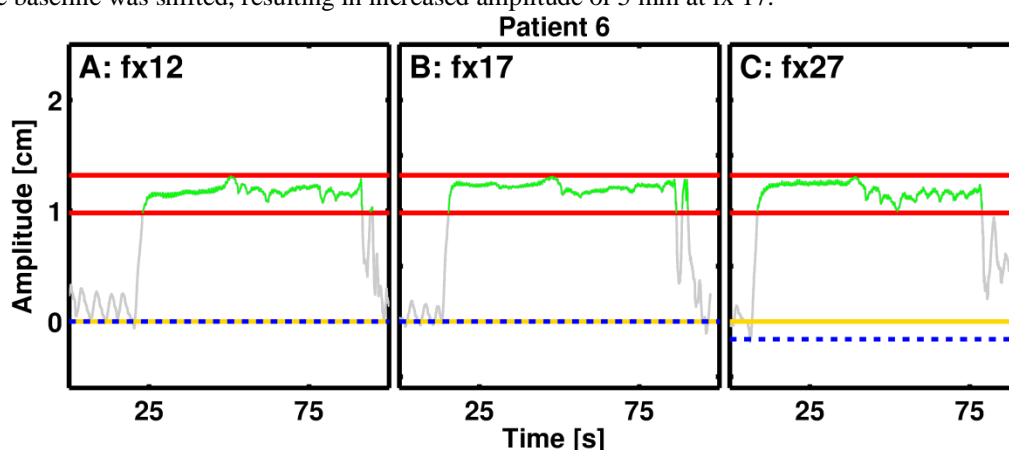
Figure 20. Three different examples of breathing curves for patient 6 to acquire a CBCT image. Additional figure explanations are described in Figure 16. The patient was able to hold the breath long enough to acquire a CBCT image during only 1 breath-hold. After approximately 30 seconds of the breath-hold, these three examples clearly illustrate patient induced compensations for insufficient capacity to hold the breath stable within the gating window.

5.4   Treatment

5.4.1   Imaging

Dual-CT scanning was carried out using a 16 slice Philips Brilliance CT Big Bore scanner, version 3.5.17001 (Philips Medical Systems, Cleveland, OH, USA). A 4-dimensional CT (4DCT) was acquired in FB and a normal CT in DIBH. The patients were positioned in treatment position by a patient-specific fixation used throughout the course of treatment for good patient position reproducibility. Intra-venous (IV) contrast was administrated during both 4DCT and DIBH CT imaging, for better contrast of nodal anatomy in the mediastinum. Information about the administration of the IV contrast is described in Paper II, *9.8.3. Details about the IV contrast administration*. Each image set included the entire lung volume, starting from the top of the sixth cervical vertebrae. From the FB 4DCT an un-tagged image reconstruction and a maximum intensity projection (MIP) image set were obtained. The un-tagged 4DCT reconstruction was routinely utilized for free-breathing treatment planning, due to its more correct HU representation, compared to the MIP reconstruction.

PET CT imaging was routinely carried out for all patients using a GEMINI TF 16 slice Big Bore PET/CT, version 2.3 (Philips Medical Systems) in order to diminish the delineation uncertainties. The patients were positioned in treatment position.

5.4.2   Delineation

Delineations of anatomical structures were performed according to standard protocol by only one experienced oncologist on all image sets for that patient [21]. Contouring of the GTVs were performed in collaboration with an experienced radiologist using information from the co-registered MIP and PET/CT images. The delineated GTV was subsequently verified and corrected in all breathing phases. Residual structures such as the CTV, PTV, spine, heart, esophagus, lung, healthy lung (subtracting the GTV from the total lung volume) were additionally delineated solely by the oncologist, whereas CT radiographers semi-automatically delineated the body contour.

5.4.3   Treatment planning

All treatment plans were created using the AAA dose calculation algorithm in Eclipse by one treatment planner experienced in lung cancer, in order to avoid inter-observer variability in the treatment planning process. All treatment plans were designed and optimized for PTV dose coverage and dose reduction to the OARs according to an established dose constraint protocol (Table 1). Only 6 MV photon beams were considered, since higher energy photon beams can compromise target coverage due to more pronounced lateral charged particle disequilibrium [83,102–104]. The treatment planner aimed to construct clinical acceptable VMAT plans for all image sets in FB and DIBH. For the cases where this was not achievable, comparative IMRT plans in terms of target dose coverage and preservation of the dose constraints were produced. The VMAT treatment plans were created by partial dual-arcs avoiding initial entrance dose through the healthy lung, medulla and the heart. The IMRT treatment plans were designed in a similar way, consisting of a 5- or 6-field beam arrangement. The beam and arc arrangements between FB and DIBH were for the most parts the same for the same patient. However, some

adjustments of beam angle, field weights and apertures were made to achieve clinically acceptable plans.

5.4.4   Treatment delivery

Daily pre-treatment setup verification was carried out by 2D kV orthogonal x-ray images, and weekly 3D CBCT images. The patients were routinely treated in free-breathing where the setup was based on bony match. According to the DIBH-LuCaRa protocol, each patient was weekly additionally CBCT imaged in DIBH pre- and post-treatment. The patients were furthermore CT imaged in FB and DIBH in the middle of their course of treatment and at their last treatment day (Figure 21).
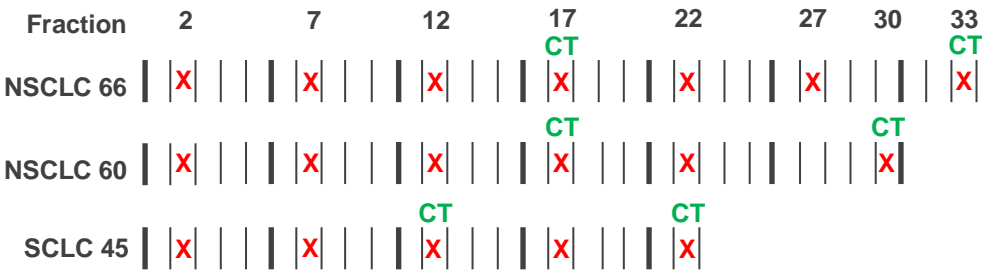
Figure 21. Schematic illustration over when extra CBCT images pre- and post-treatment (red cross) and re-CTs (green CT) acquired according to the DIBH-LuCaRa protocol over the course of treatment.

6 Phantom details

Within the field of radiotherapy, it is important to assure the prescribed dose is delivered to the treatment volume to achieve optimal clinical output. In order to do so, firstly, the output of the accelerator output needs to be thoroughly quality assured on a regular basis. Secondly, the dosimetry is required to be ensured in the patients. The major concern with treatment planning is the dose calculation issues present due to lack of CPE and incorrect scatter calculations [88–91,93]. In order to have control on what absorbed dose that is delivered, systematic dosimetry is required in heterogeneous patient-like geometries. For this reason, a thoracic-like PMMA phantom was designed. Phantom inserts of various materials were able to be located at different positions in the phantom in order to simulate various homogeneous and heterogeneous setups (Figure 22).
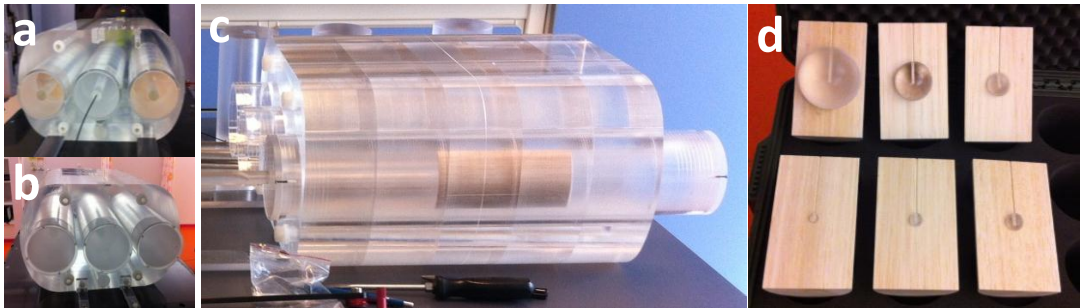
Figure 22. (a) A heterogeneous setup where the two lateral body cylinders are filled with balsa wood inserts. (b) A homogeneous setup, where the whole phantom are filled with PMMA inserts. (c) The heterogeneous setup described in (a) viewed from the side, where the lateral body cylinder containing the lung insert is longitudinal shifted from the central position in the phantom. (d) Balsa wood lung insert with associated tumors, ranging from 1-8 cm in diameter.

For lung cancer treatments, tumor volume changes during radiotherapy are well known [27,36,105–107]. The dosimetric challenges increase when tumor and field sizes decrease. The philosophy of radiotherapy is to deliver the same prescribed dose to the tumor volume, irrespective of the size of the tumor. In order to investigate this further, tumor inserts embedded in low-density medium was used in the phantom to simulate different tumor sizes. All tumor inserts were designed to suit BCF-60 scintillators from Saint-Gobain (Ceramics & Plastics Inc.) with an outer diameter of 2.2 mm and scintillator length of 2 mm, described by Beierholm et al. [97].

6.1 Design

The phantom design is illustrated in *Appendix A: Phantom design*. In short, the essential parts are the following: The body of the phantom is 34 cm in width, 23 cm in height, and 40 cm in length, mimicking the size of a thorax, containing three hollow cylinders with the length of 50 cm, and an outer diameter of 10 cm. These cylinders, with an inner diameter of 9 cm, can be filled with different inserts of various materials to simulate different homogeneous and heterogeneous geometries. The various inserts were made of delrin, balsa wood, and PMMA representing bone, lung and soft tissue, respectively. The lung

inserts were 15 cm long and with a diameter of 9 cm, mimicking a human lung in size. PMMA spheres of various sizes (1, 1.5, 2, 3, 5, 8 cm in diameter) embedded in low-density balsa wood were available to simulate tumors in lung (Figure 22d). In the lower part of the body, two smaller cylindrical holes, of a diameter of 2 cm and 3 cm (which also can be altered to 2 cm), are positioned at different distances from the phantom center, i.e. 6.5 cm and 9.5 cm, respectively. These holes can, one at a time, be filled with a delrin rod to simulate the spinal column at different diameters and position from the center of the phantom. Paper IV found good agreement between human tissue and the phantom materials in terms of Hounsfield unit representation of the various materials [108].

6.1.1   Motion simulation

The phantom can be equipped with an optional motorized linear stage moving one of the body cylinders in a one dimensional movement. In order to track the motion of the body cylinder, a motion measurement device can be attached to the phantom setup (For more phantom details about the linear stage and the motion measurement device see section *14.5* and *14.6* in *Appendix A: Phantom design*). The linear stage is the A-LST0250B with a built-in controller from Zaber Technologies Inc. (Vancouver, Canada). The linear stage can either be programmed in a simple mode in the freely available Zaber Console software, or more advanced programmed in LabView (National Instruments, Austin, TX, USA), using a freely available Zaber add-on. The linear stage has a moving range of 254 mm, controlled by a 2-phase stepper motor with unidirectional accuracy of 63 μm. The maximum force the linear stage exerts in the direction of travel is 350 N for the lowest speed (0.0047 mm/s), which is adequate to move the body cylinders accurately. Motion simulations were not carried out in the current thesis. However, the thoracic-like phantom was designed in order to enable future investigations on the dosimetric impact of breathing induced tumor motion.

6.2   Chemical composition analyses

In order to perform MC simulations of the dosimetry in the phantom, it is essential to know the chemical composition of the materials. The balsa wood and delrin materials were therefore analyzed for their chemical composition by BELAB AB (Norrköping, Sweden) and ALS Scandinavia AB (Luleå Sweden). The results and uncertainty data are presented in *Appendix B: Chemical analysis*. They are shortly presented in this section. It should be kept in mind that the uncertainty of the chemical analysis could be quite high for some of the analyses. For further analytical uncertainty details see Chapter *15.5 CHNO analysis, uncertainty data*.

In order to correlate the HU with the electron density of the image, the electron density relative to water is required, where the electron density of water is $3.343 \cdot 10^{23}$ e⁻/cm³ = $0.555 \cdot N_A$ e⁻/cm³, where N_A is the Avogadro's constant. The electron density, ρ_e, of a medium can be calculated according to (eq. 6.1).

$$\rho_e = \rho_m \cdot \sum_i w_i \cdot \frac{Z_i}{A_i} \qquad (6.1)$$

Where ρ_m is the medium density and w_i is the fraction by weight of the chemical element i in a compound or mixture, and $(Z/A)_i$ is the corresponding atomic number to atomic weight ratio of the chemical element i.

6.2.1 Balsa wood

The mass density of balsa wood was 0.1 g / cm^3. The chemical composition of balsa wood was found to be complex, including 5.4% humidity, and different trace elements ($\leq$ 1%), such as nitrogen, calcium, potassium, and magnesium, etc. The rest (94.6%), consisted of carbon (46.6%), hydrogen (5.7%), and oxygen (41.4%). About 1.7% of the balsa sample was ash, which was not analyzed. If excluding the ash and the humidity, the relative electron density of balsa wood was 0.095. If including the 5.4% humidity as water (H_2O), the relative electron density of balsa wood was 0.100.

6.2.2 Delrin

The mass density of delrin was 1.4 g /cm^3. The chemical composition of delrin was found to be similar to the nominal chemical formulation of the copolymer Polyoxymethylene (POM-C), $(CH_2O)_n$, where n is the amount of monomers in the molecular chain. According to the chemical analyze, the delrin material consisted of carbon (40.7%), hydrogen (6.9%), oxygen (52.3%), and nitrogen (< 0.1%). The relative electron density of the nominal POM-C composition was 1.362, while it was 1.347 for the chemical delrin composition analyzed.

6.2.3 PMMA

The mass density of PMMA was 1.18 g/cm^3. The nominal chemical composition of PMMA is $(C_5O_2H_8)_n$, resulting in a relative electron density of 1.147.

6.2.4 Solid Water

The calibration phantom used for finding stem-effect coefficients for the scintillator measurements was carried out in a Solid Water phantom (Gammex Inc.). The mass density of Solid Water is 1.02 g/cm^3. The chemical composition was carbon (67.2%), hydrogen (8.1%), nitrogen (2.4%), oxygen (19.9%), calcium (2.3%), and chloride (0.1%). This chemical composition resulted in a relative electron density of 1.014.

7 Conclusions

7.1 Summary

The manuscripts in the current thesis addresses some of the uncertainties present during radiotherapy of lung cancer patients. Breathing motion and the heterogeneity of the patient geometry in the thorax region are two major contributors to uncertainties affecting the treatment outcome for this group of patients. Twenty-three lung cancer patients were enrolled in a clinical protocol to investigate the clinical benefit to treat them in DIBH, compare to FB. Furthermore, a specially designed thoracic-like phantom was utilized for scintillator dosimetry to assess known calculation issues in heterogeneous and homogeneous setups relevant for lung cancer radiotherapy.

The findings, and their implications within the field of radiotherapy of lung cancer, are further discussed in the following sections.

7.1.1 Deformable image registration and structure propagations

Paper I specifically investigates the performance of a deformable image registration software based on a modified Demon's algorithm for contour propagation on both FB and DIBH CT and CBCT images acquired over the course of treatment for three lung cancer cases. Geometrical similarities were found between the propagated structures and the manually delineated structures, considered as the ground truth, with a slightly favor of FB imaging. This result was somewhat surprising as it is commonly believed that the image registration would be better for DIBH images since the image artifact are removed and the positional displacement of the anatomy is mitigated by gating. The study illustrates the difficulties of deformable image registration for large anatomical changes over time, apparent image artifacts, and low tissue contrast in the images, irrespectively of FB and DIBH. Unrealistic deformation vector fields were sometimes created during deformable image registration. Care should thus be taken if applying the deformation vector fields for any application, such as structure propagation, dose accumulation, or 4D reconstructions, since this could result in erroneous interpretations.

7.1.2 CBCT image-based setup verifications and resulting PTV sizes

Paper II provides clinically relevant guidance on what automatic CBCT setup verification protocol to use in combination with DIBH and FB for locally advanced NSCLC patients to achieve the smallest PTV. Three different match methods were evaluated; match on the soft-tissue of the GTV-T, or GTV-Total, or bony match on the spine. Both intra- and interfractional motion data were evaluated and used for CTV to PTV margin calculations. DIBH was found to be superior over FB regarding the size of PTV and lung sparing, where match on the GTV-T was the most optimal and feasible method. The study was based on weekly acquired CBCT images. Daily imaging would yield an even better and more thorough investigation on interfractional variations. Due to the extra dose this would yield to the patients, this was not an option in the current study. However, since the study was a population based study, enough residual information was extracted to draw our conclusions. Not all patients were able to comply with the DIBH technique throughout

their course of treatment. For that reason, it is recommended to have a FB backup treatment plan if implementing DIBH as a routine treatment. Large positional uncertainties in the longitudinal direction for the DIBH images, compared to the FB images, were found during matching on the bony structure. These are likely related to the fact that some patients tended to arch their back to compensate for their insufficient capacity to hold their breath within the patient-specific pre-defined gating window. This study indicates that precautions are required to minimize this arching issue. In clinical practice, it should be noted that the presented margin of the spine in the longitudinal direction is not clinically relevant to apply in the treatment planning process since the spinal cord runs in that direction. The magnitude of the margin presented was used as a quantitative measure including both the systematic and random error components, to evaluate the match method. In order to evaluate anatomical changes over time, weekly CBCT imaging could be used. However, to be able to assess at what occasion the anatomical change has occurred daily CBCT imaging is required. This anatomical information would not be available if only 2D orthogonal x-ray images for daily positioning and weekly CBCT images for soft-tissue verification was acquired. Nevertheless, the major reason to implement a daily image protocol is the online correction of the soft-tissue tumor position prior to treatment, i.e. to reduce baseline shifts related to tumor shift relative to the spine and/or external markers. This is especially important for DIBH treatments since external and internal motion are not correctly correlated. In many clinics it is common that it is the clinicians and physicists that review each setup image post treatment. A daily CBCT image based setup protocol would then be a very workload heavy process in the clinic. One approach to deal with this is to let the radiation therapists become more involved in the evaluation process of the images. If they find a systematic anatomical change affecting the treatment, then the clinicians and/or physicists are contacted to decide how to deal with that information. The extra cost for the clinic needs to be weighted against the clinical benefit for the patient, prior implementation of a daily image setup verification protocol.

7.1.3   *Dosimetric clinical impact of DIBH*

Paper III specifically addressed target dose coverage and organ sparing in DIBH, compared to FB, by using detailed MC simulations for locally advanced NSCLC patients treated with complex IMRT and VMAT treatment plans. Many commercial dose calculation algorithms have issues to correctly account for changes of lateral electron scatter, especially in heterogeneous situations. The largest inaccuracies are usually noticed in the transition between materials of different densities. Lateral charged particle disequilibrium will be emphasized during DIBH, since the lung density decreases. The range of secondary electrons will increase resulting in larger volume of disequilibrium and a broader penumbra at field boundaries, affecting the treatment calculation. MC simulations, on the other hand, are able to accurately predict the delivered dose in heterogeneous patient geometries. Although the treatment planning was carried out using AAA, the MC simulations supported organ sparing in DIBH, where DIBH was advantageous over FB. Additionally, MC simulations resulted in inferior target dose coverage compared to AAA, with similar deviations between MC and AAA for both FB and DIBH. The unsatisfactory target dose coverage was therefore concluded to be related to the treatment planning algorithm, rather than the treatment technique. Compared to FB

treatment, DIBH is a more resource intensive treatment technique. It would therefore be advantageous if it was possible to identify those patients with potential benefit from DIBH-based treatment. If implementing DIBH as a routine treatment, it is however recommended to carry out dual-treatment planning, in both FB and DIBH, as a treatment backup if the patients' health gets worse during the course of treatment, where they can no longer proceed with DIBH. The treatment planning may be improved if using a fully integrated MC optimization and dose calculation system. Care should however then be taken if clinically implemented, because all clinical radiation response data are based on old, less accurate dose calculation algorithms.

7.1.4 Dose calculation issues in heterogeneous setups

Paper IV and Paper V assess dose calculation issues of a commercial AAA dose calculation algorithm in heterogeneous patient-relevant geometries. In order to obtain accurate measurements of absorbed dose, a well-defined thoracic-like phantom was designed for point dose dosimetry by fiber-coupled organic PSDs. PSDs are well suited for complex dose verification in megavoltage photon beams due to their water-equivalency, and small size for high spatial resolution and minimum perturbation of the radiation fields. Previous studies have found good agreement with high accuracy between PSD measurements and MC simulations in homogeneous water setups. Due to these features, and the provided real-time output, PSDs were used for the heterogeneous dosimetry to assess potential dose calculation issues in heterogeneous setups, relevant for lung cancer radiotherapy. Clinical relevant treatment plans of different complexities were measured and compared to AAA calculations. In the simplest homogeneous setups, dose similarities were found between TPS calculations and measurements. Nevertheless, for more complex cases, large dose deviations were observed. A systematic tumor-size dependency was identified, where the largest dose deviations were observed for the smallest tumor sizes, independently of treatment technique. Additionally, conventional field techniques resulted in higher dose deviations compared to more complex treatment techniques, such as IMRT and VMAT. These observations could potentially be related to the fact that the more complex treatment plans (IMRT and VMAT) have several beam entries around the body of the phantom, and not just directly through the low-density material of the phantom, like the simple conventional beam configurations investigated. Thus, the larger dose deviation for the simplest field techniques could potentially be due to lack of sufficient spread of lateral radiation, required in order to obtain charged particle equilibrium. The observed dose deviations, and considerable tumor-size dependency may originate from imperfections in the AAA algorithm in heterogeneous setups. The effect is large enough to have implications for lung cancer treatment planning. Consolidating MC simulations will be of great value for further establishment of the observed dose deviations.

7.2 Main conclusions

This thesis concludes that the clinical gain of DIBH is not always beneficial over FB treatments, in terms of better image deformation for structure propagation, and reducing setup uncertainties. DIBH was however advantageous, in terms of reducing the dose to OARs during treatment planning, and reducing the resulting size of PTV-Total. There were identified severe tumor-size dependent dose deviations that were large enough to

potentially have implications for lung cancer radiotherapy treatment planning. The constructed thoracic-like phantom and the in-house scintillator system provide a promising tool for evaluation of dose calculations in heterogeneous geometries irradiated by clinically relevant treatment plans.

1. Geometrical similarities were found between propagated and manually delineated structures, with a slightly favor of FB imaging. There were identified difficulties to perform deformable image registration for large anatomical changes over time, apparent image artifacts, and low tissue contrast in the images, irrespectively of FB and DIBH. Care should therefore be taken if applying the resulting deformation vector fields for any application.

2. Compared to FB, larger setup uncertainties were introduced during DIBH, especially in the longitudinal direction. Precautions must therefore be applied during DIBH for the patients that tend to arch their back to compensate for their insufficient breath-hold level. DIBH was, however, found to be superior to FB for all match methods investigated in terms of smallest resulting PTV-Totals. Overall, soft-tissue auto-match was superior to bony registration, independently of FB and DIBH. The soft-tissue match on PTV-Total was more feasible than the match on PTV-T and PTV-N separately. For the soft-tissue match on PTV-Total, the resulting PTV-Total volume was in average reduced by approximately 13% for DIBH, compared to FB. The corresponding reduction for bony registrations was about 8%. If including the intra-fractional motion in the margin calculations, the PTV reductions were decreased.

3. Although the treatment plans were carried out by a simplified dose calculation algorithm (AAA), MC simulations confirmed that DIBH was advantageous over FB, in terms of reducing undesired dose to the OARs, and maintaining the target dose coverage between FB and DIBH. The lung volume increased in median by 86.8% in DIBH, while the size of GTV decreased by 14.8%. However, MC simulations additionally revealed severe under- and over-dosage of the target dose coverage, irrespectively of FB or DIBH treatment plans. This issue was therefore concluded to be related to the treatment planning algorithm, rather than the treatment technique.

4. A well-defined thoracic-like phantom was designed for scintillator dosimetry. Several homogeneous and heterogeneous setups relevant for lung cancer radio-therapy could be applied. The phantom made of PMMA can be filled with inserts of different materials, including simulated lung tumors made of PMMA spheres (ranging from 1-8 cm in diameter) embedded in low-density balsa wood to simulate lung-tissue. Delrin was used to simulate bone-tissue. PMMA, balsawood, and delrin were found to be HU-equivalent to human tissue. Chemical analyses were carried out to establish the anatomical composition of the phantom materials to enable MC simulation.

5. Calculation issues were identified with the thoracic-like phantom. Conventional field techniques resulted in higher dose deviations compared to more complex treatment techniques, such as IMRT and VMAT. A systematic tumor-size depen-

dency was found, which was emphasized for small tumors ≤ 2 cm in diameter. The identified tumor-size effect was large enough to potentially have implications for lung cancer radiotherapy treatment planning. The scintillator system and the heterogeneous phantom provide a promising tool for critical evaluation of complex radiotherapy calculations and dose delivery.

7.3 Future perspectives

The trend within modern radiotherapy is to make the treatments more individualized to increase the clinical outcome (Paper I, Paper II, and Paper III). With individualized margins and treatment plans the hope is to increase the chance of local tumor control, while minimizing the treatment toxicity. There are several aspects of uncertainties that contribute to the clinical output, such as target definition, setup verification, and treatment planning. When implementing a new treatment, such as DIBH, it is imperative to have a thorough clinical follow-up. This is the only way to assure that the risk of relapse or radiation-induced toxicity is not increased by individualizing the treatment. It would be of great interest to investigate the clinical impact of treating in FB and DIBH over the course of treatment. Assessment of implications for an adaptive approach, due to anatomical shifts and deformations, and changes of breathing pattern can then be evaluated for the two breathing methods. It would also be of interest to investigate the clinical feasibility of other image deformation algorithms in order to assess their clinical use for lung cancer radiotherapy applications.

As evident from the phantom studies (Paper IV and Paper V), no MC simulations have been conducted to benchmark our dosimetric findings. Detailed MC simulations together with independent dose measurements by other studies should be carried out to establish the implications for treatment planning of lung cancer. Other phantom inserts could be developed, for other types of dosimetry, such as alanine, gel, and film, etc. In the current thesis, measurements were carried out in static setups, without any movement of the target. It would be of great interest to carry out dosimetry in setups where breathing motion is simulated, in order to correlate the dynamic treatment output of the accelerator to the dynamic internal motions of the patients. For this purpose, the phantom is equipped with an optional motorized linear stage which could be programmed to simulate patient-like breathing motion in one dimension. It would additionally be interesting to incorporate the breathing motion into the MC simulations, in order to accurately assess the dosimetric impact of motion.

Manuscripts

8 Paper I

Deformable image registration for geometrical evaluation of DIBH radiotherapy treatment of lung cancer patients

Paper I was presented at the XVII International Conference on the Use of Computers in Radiation Therapy 2013 (ICCR2013), 6-9 May, 2013 in Melbourne, Australia. The work is published in the Journal of Physics: Conference Series **489** (2014) 012077. A commercial deformable image registration algorithm is investigated for three lung cancer cases. Analyzed images were acquired during both FB and DIBH breathing.

Deformable image registration for geometrical evaluation of DIBH radiotherapy treatment of lung cancer patients

W Ottosson[1,2], JA Lykkegaard Andersen[2], S Borissova[2], A Mellemgaard[2], and CF Behrens[2]

[1]Center for Nuclear Technologies, Technical University of Denmark, DTU Risø Campus, DK-4000 Roskilde, Denmark
[2]Department of Oncology, Radiotherapy Research Unit, Herlev Hospital, University of Copenhagen, DK-2730 Herlev, Denmark

E-mail: wiot@dtu.dk

Abstract.

Background and Purpose: Respiration and anatomical variation during radiotherapy (RT) of lung cancer yield dosimetric uncertainties of the delivered dose, possibly affecting the clinical outcome if not corrected for. Adaptive radiotherapy (ART), based on deformable image registration (DIR) and Deep-Inspiration-Breath-Hold (DIBH) gating can potentially improve the accuracy of RT. The objective was to investigate the performance of contour propagation on repeated CT and Cone Beam CT (CBCT) images in DIBH compared to images acquired in free-breathing (FB), using a recently released DIR software.

Material and Methods: Three locally advanced non-small cell lung cancer patients were included, each with a planning-, midterm- and final CT (pCT, mCT, fCT) and 7 CBCTs acquired weekly and on the same day as the mCT and fCT. All imaging were performed in both FB and DIBH, using Varian RPM system for respiratory tracking. Delineations of anatomical structures were performed on each image set. The CT images were retrospective rigidly and deformable registered to all obtained images using the Varian Smart Adapt v. 11.0. The registered images were analysed for volume change and Dice Similarity Coefficient (DSC).

Results: Geometrical similarities were found between propagated and manually delineated structures, with a slightly favour of FB imaging. Special notice should be taken to registrations where image artifacts or low tissue contrast are present.

Conclusions: This study does not support the hypothesis that DIBH images perform better image registration than FB images. However DIR is a feasible tool for ART of lung cancer.

8.1 Introduction

Anatomical changes and variations due to respiration influence the accuracy of imaging, treatment planning and treatment delivery, and may affect the outcome of the planned treatment if not corrected for [62]. In ART, the treatment plan is adjusted during the course of treatment to minimize the divergence from the planned treatment, in terms of target dose coverage and spearing of dose to adjacent healthy organs at risk. Thus, ART has the potential to account for major anatomical changes not accounted for by applied margins [36]. Conventionally, lung cancer patients are treated in FB. However, breathing adapted radiotherapy (BART) by means of DIBH may suppress the geometric and dosimetric uncertainties related to respiration. Furthermore BART makes it possible to safely reduce the margins to the targets, yielding a reduction of irradiated volume [109,110]. The advantages of BART and ART illustrates that more individualized treatments are called for to improve the quality of RT. ART is, however, a time consuming process since anatomical structure delineations are needed on each new image set. DIR may be a promising tool in assisting with the delineation process, by deforming the reference contours from the planning CT into the anatomy of a second CT or CBCT. Our hypothesis is that image registrations performed based on DIBH images will result in improved image registrations, with enhanced correlation of volumes and higher scoring of DSC, since they often have visually better image quality compared to images in FB. The objective of this study was to investigate the performance of contour propagation on repeated CT and CBCT images of the thorax over the course of lung cancer treatment, imaged in DIBH, compared to conventional FB, using a recently released DIR software, based on a modified demons algorithm [71].

8.2 Material and methods

8.2.1 Patient data

Three locally advanced non-small cell lung cancer patients treated in 33 fractions (fx) using volumetric modulated arc therapy with a prescribed dose of 66 Gy (2 Gy/fx, 5 fx/week) at Herlev Hospital, between December 2012 and May 2013, were included in this study. They were treated on Varian Clinac iX 2300 linear accelerators [21,85] (Varian Medical Systems, Palo Alto, CA) equipped with On-Board Imagers (OBI) capable of performing FB and DIBH CBCT, using version 1.4 of the OBI software.

8.2.2 Image acquisition

Each patient was dual-CT scanned (acquiring a 4DCT in FB and a DIBH CT) before the start of, in the middle of, and after completion of the course of treatment, (pCT, mCT, fCT, respectively). All imaging were performed in treatment position [21]. They were scanned in a 16 slice Philips Brilliance CT Big Bore, version 3.5.17001 (Philips Medical Systems, Cleveland, OH) integrated with a Varian real-time position management (RPM) system, version 1.7 (Varian Medical Systems), for monitoring the patients' respiration during CT scanning. Intra venous (IV) contrast was administered to the patients during both 4DCT and DIBH imaging, for better contrast of nodal anatomy in the mediastinum. During DIBH imaging, the patients were audio-visually guided to hold their breath within a predefined amplitude level and gating window of 2-3 mm width. Additionally, all patients had 6-7

dual-CBCTs (in FB and DIBH) acquired on the treatment unit using the OBI. The CBCTs were acquired weekly and on the same day as the mCT and fCT. The Varian RPM system was once more used for monitoring the respiration to acquire DIBH gated imaging.

8.2.3   Definition of target and organs at risk

Delineations of anatomical structures for each patient were performed according to standard protocol by only one experienced oncologist (JLA or SB) on all image sets for that patient [21]. Delineations were carried out in the treatment planning system Eclipse v. 10 (Varian Medical Systems). Contouring of FB and DIBH Gross Tumor Volumes (GTVs) were performed by the oncologist in collaboration with an experienced radiologist. Residual FB and DIBH structures such as Clinical Target Volume (CTV), Planning Target Volume (PTV), medulla, heart, esophagus, lung and body were additionally delineated by the oncologist. The heart, esophagus, and lung were not delineated in the CBCT images, since they extended the CBCT scanning range.

8.2.4   Deformable registration and contour propagation

All CT images were retrospective pre-aligned by semi-automatic rigid registration and subsequently automatic deformed registered to all obtained images (both CBCT and secondary CT images) using Smart Adapt v. 11.0 (Varian Medical Systems). This resulted in 54 rigid and 54 deformable registrations per patient (corresponding numbers were 48 for the one patient with only 6 CBCT scans), which in total resulted in 312 registrations for all patients. The rigid pre-alignment increased the accuracy of the subsequent DIR, and prevented large unrealistic deformations [71]. The initial rigid registrations were based on the bony anatomy of the columna (50-3000 Hounsfield units), where the rest of the settings were predefined from the manufacturer. The rigid registration was done in three steps, each step with a higher image resolution, which improved the efficiency of the algorithm. The default DIR algorithm used in Smart Adapt was derived from a modified demons algorithm [71] based on a diffusion model. In the algorithm additional interaction forces (demons) are added to the original demons algorithm [75] and the voxel resolution of the images gradually increases during the optimization process. The floating image is warped to form a deformed image that match the reference image as closely as possible voxel-by-voxel [71,75]. The driving forces are based on the intensity differences between the two images, as well as the gradient of the image object. A symmetric force is also built into the solver to fulfill the consistency requirement for DIR, i.e. the transformation that maps the reference image to the floating image should be consistent with the inverse transformation that maps the floating image to the reference image. The DIR in this study was restricted to the field of view of the smallest image (typically the CBCT scan), resulting in a volume of interest (VOI) which was further analyzed. All structures extending the VOI (typically the heart, esophagus, medulla, and body) were cropped to be comprised by the VOI, such that a common ground for comparison was created. For each DIR, the contours on the floating CT image were propagated onto the resulting deformed image (dCT) using the obtained image transformation.

8.2.5   Geometrical comparison

Rigidly and deformed registered structure volumes ($V_{RIG,DIR}$) were analyzed relative to the corresponding structure volumes (V_{REF}) on the reference image for volume change and DSC, where DSC was calculated according to eq. 8.1 [77].

$$DSC = 2 \cdot \frac{V_{RIG,DIR} \cap V_{REF}}{V_{RIG,DIR} + V_{REF}} \qquad (8.1)$$

For statistical analysis MATLAB Statistics Toolbox version 8.3 (R2013b) (The MathWorks, Natick, MA) was used. Paired t-tests to evaluate the median DSC measures of the various structures were performed, where differences were considered significant for $p < 0.05$.

8.3   Results/Discussion

Figure 23 (open triangles) illustrates that the manually delineated reference CT and CBCT GTVs overall are decreasing over the course of treatment. The DIBH volumes (upward pointing triangles) are in general smaller compared to FB (downward pointing triangles) which may be due to the lesser image artifacts (e.g. motion blurring) in the DIBH images resulting in smaller targets. The dCT GTVs do not correlate well with the manually delineated reference CBCT (Figure 23 (a)) or CT (Figure 23 (b)) volumes. If a perfect volume correlation was achieved between the dCT structures and the reference volumes, the filled triangles (Figure 23) would follow the corresponding curves with open markers (Figure 23 (a)) or be the same volume as the open markers (Figure 23 (b)). The dCTs of the pCT at fx 2 and 7 of patient 1 correlate well with the reference CBCTs, but for the remaining fractions the dCT of the mCT and fCT have better correlation with the reference CBCTs. This illustrates the difficulty to perform DIR registration when the anatomy changes over time. In this case, the patient would benefit from ART. It is clearly seen in Figure 23 (a), at fx 15-20 for patient 2, that appearing image ring artifacts (figure 2) in the reference CBCT image affect the DIR process, and thus the propagation of structures. The effect was equally seen for DIBH and FB images, and for all CT-CBCT registrations at fx 15-20 for patient 2. The CT-CBCT and CT-CT registrations of patient 3 (Figure 23) systematically underestimate the GTVs, both for FB and DIBH images. This may be due to DIR issues in regions with low level of tissue contrast (since the demons algorithm uses intensity values for registration) as the tumor for this patient was closely situated to the mediastinum.
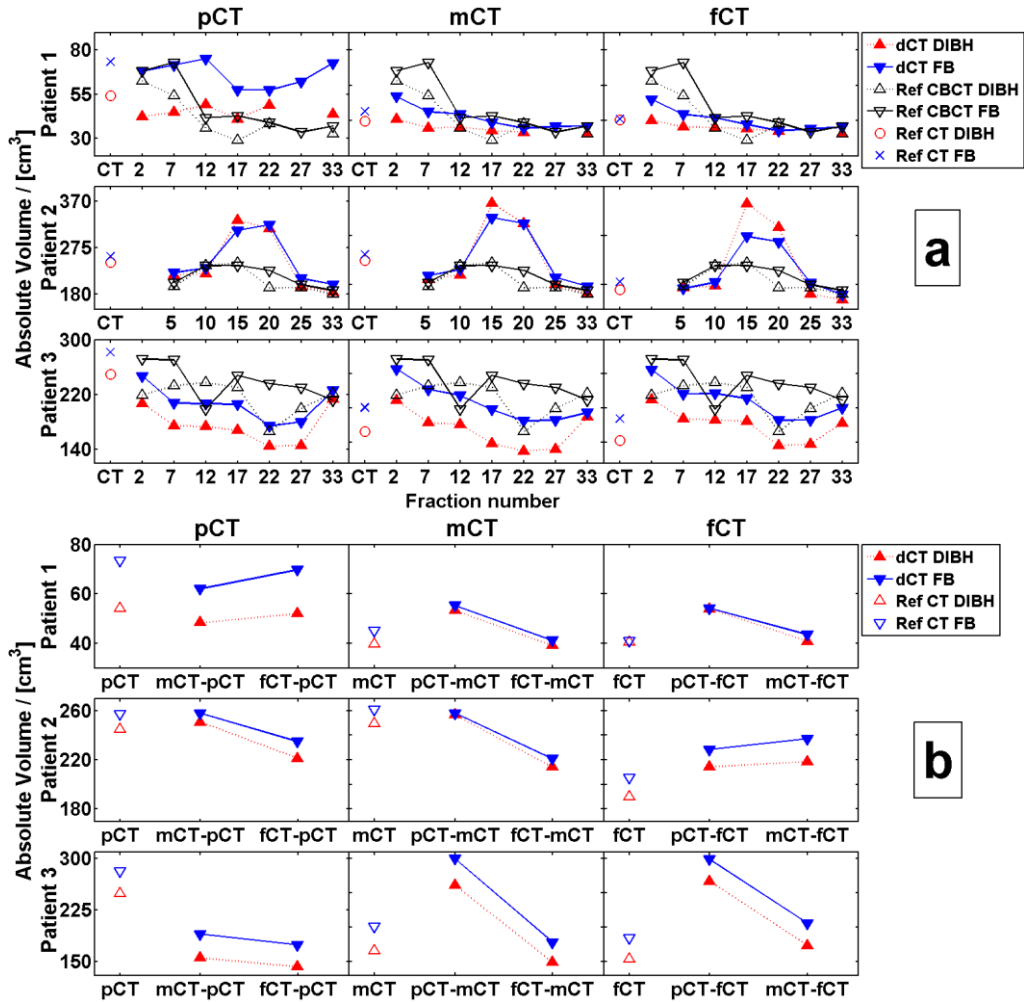
Figure 23. (a) Absolute volume per each fraction of the dCT GTVs (filled triangles) in relation to the manually delineated reference CBCT GTVs (open triangles) along with the manually delineated GTVs of pCT, mCT and fCT (x and circles) utilized when performing CT-CBCT DIR. Upward pointing triangles correspond to DIBH, and downward pointing triangles represent FB. In the pCT column it is the pCT that is deformed to match the CBCTs and similar for the columns labeled mCT and fCT. (b) Corresponding absolute volume of dCT GTVs (filled triangles) in relation to manually delineated reference CT GTVs (open triangles) when performing CT-CT DIR between the pCT, mCT and fCT. In the pCT column it is the mCT and fCT that is deformed to match the pCT and similar for the columns labeled mCT and fCT.
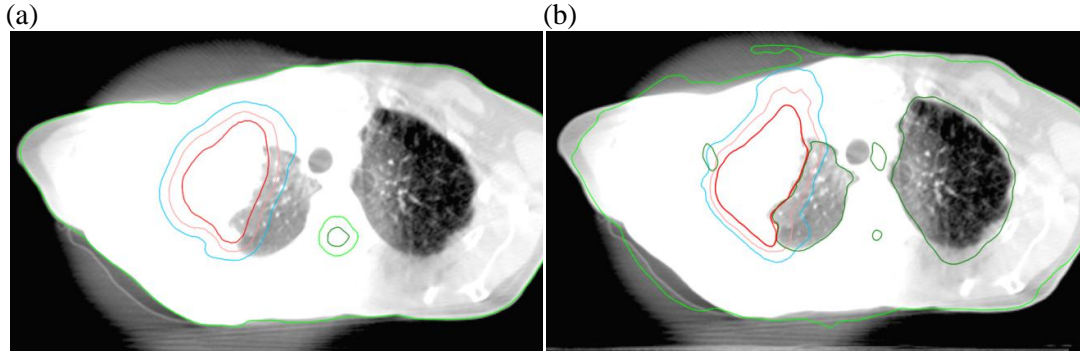
Figure 24. (a) The reference CBCT (fx 15) of patient 2 with manually delineated CBCT structures. (b) The same CBCT (fx 15) overlaid with the dCT structures, i.e. the propagated deformed pCT structures. The red, pink, blue and the outer light green delineations represent GTV, CTV, PTV and body contour, respectively. Colors are available in the online version.

No significant difference among DSC measures of the various structures were observed between DIBH and FB CT-CBCT and CT-CT image registrations over the course of treatment (Table 4). However, the FB images had slightly higher DSC median value compared to DIBH images (both for CT-CBCT registrations and CT-CT registrations). This observation conflicts with our hypothesis that DIBH imaging resulting in visually less image artifacts compared to FB imaging, yielding better image registration. The applied DIR improved the median DSC measure, compared to rigid registrations, except for some CT-CBCT registrations (indicated by bold font), though still within one standard deviation, and no significant difference was observed.

Table 4. Median DSC measures (one standard deviation) of the propagated deformed structures and rigidly registered structures for all patients during CT-CBCT and CT-CT registration. Bold values indicate that rigidly registered structures have a higher DSC score compared to the propagated structures of the dCT.

| Structures | CT-CBCT | | | | CT-CT | | | |
| | FB | | DIBH | | FB | | DIBH | |
	RIG[a]	DIR[b]	RIG[a]	DIR[b]	RIG[a]	DIR[b]	RIG[a]	DIR[b]
GTV	0.74(0.10)	0.78(0.13)	0.73(0.13)	0.74(0.15)	0.76(0.13)	0.84(0.16)	0.75(0.13)	0.83(0.20)
CTV	0.80(0.07)	0.81(0.09)	**0.79(0.10)**	0.78(0.11)	0.82(0.09)	0.88(0.12)	0.79(0.11)	0.86(0.17)
PTV	0.83(0.07)	0.84(0.07)	**0.82(0.08)**	0.81(0.08)	0.86(0.07)	0.89(0.09)	0.83(0.10)	0.87(0.14)
Body	0.98(0.01)	0.98(0.01)	0.97(0.01)	0.98(0.04)	0.97(0.01)	0.99(0.01)	0.97(0.01)	0.99(0.01)
Medulla	**0.75(0.10)**	0.72(0.13)	**0.77(0.05)**	0.74(0.14)	0.74(0.05)	0.76(0.05)	0.75(0.08)	0.78(0.07)
Esophagus	NaN[c]	NaN[c]	NaN[c]	NaN[c]	0.58(0.10)	0.73(0.08)	0.59(0.09)	0.70(0.08)
Heart	NaN[c]	NaN[c]	NaN[c]	NaN[c]	0.85(0.05)	0.90(0.06)	0.87(0.13)	0.93(0.08)
Total lung	NaN[c]	NaN[c]	NaN[c]	NaN[c]	0.89(0.01)	0.95(0.01)	0.93(0.04)	0.97(0.02)

[a.] Rigid image registration
[b.] Deformable image registration
[c.] Not available number

8.4 Conclusion

This study does not support the hypothesis that DIBH images result in better image registrations (both rigid and deformed) when using a modified demons type algorithm for deformable image registration. Large variation was observed for organs without sharp

contrast boundaries (including tumors close to mediastinum, atelectasis and thorax wall). Notice should also be taken to image artifacts and bad image quality that can affect the outcome of DIR (e.g. fx 15-20 for patient 2, Figure 24). Our observations indicate that ART planning may be necessary during the course of treatment for optimal lung cancer RT, since the pCT not always can be registered correctly to subsequent CBCT and CT images over the course of treatment due to large and rapid volume changes (e.g. fx 12 for patient 1, Figure 23 (a)). Based on this small patient dataset, it turned out that DIR sometime resulted in a worse median DSC measure compared to conventional rigid registration, though still within one standard deviation. The median DSC of the DIR for these three patients was however mostly higher compared to rigid registrations. Unrealistic deformation vector fields were also sometimes created during DIR. These unrealistic deformation vector fields should carefully be employed if used for other applications, e.g. such as dose deformation. DIR analysis provides a feasible and promising tool for indicating if adaptive re-planning is necessary based on geometrical variations throughout the course of lung cancer treatment, with slightly better correlation for FB than DIBH imaging.

Acknowledgment

9   Paper II

The advantage of Deep-Inspiration Breath-Hold and soft-tissue auto-match for cone-beam CT setup methods in locally advanced lung cancer radiotherapy

Paper II is submitted to the scientific journal Radiotherapy & Oncology, and is under review process at the moment. Three different automatic CBCT setup methods in combination with DIBH and FB were investigated, in terms of obtaining the smallest PTV.

Paper II

The advantage of Deep-Inspiration Breath-Hold and soft-tissue auto-match for cone-beam CT setup methods in locally advanced lung cancer radiotherapy

Wiviann Ottosson[1,2], Fatma Rahma[2], David Sjöström[2], Claus F Behrens[2], and Patrik Sibolt[2]

[1]Center for Nuclear Technologies, Technical University of Denmark, DTU Risø Campus, DK-4000 Roskilde, Denmark
[2]Department of Oncology, Radiotherapy Research Unit, Herlev Hospital, University of Copenhagen, DK-2730 Herlev, Denmark

E-mail: wiot@dtu.dk

Abstract

Background and Purpose: Three automatic cone-beam computed tomography (CBCT) match methods in combination with deep-inspiration breath-hold (DIBH) and free-breathing (FB) were investigated, in terms of obtaining the smallest planning target volume (PTV).

Material and Methods: CBCT images were acquired pre- and post-treatment in FB and DIBH, for 17 locally advanced lung cancer patients. Bony match on the spine, and soft-tissue matches on the primary gross tumor volume (GTV-T), and the total tumor volume (GTV-Total), including malignant lymph nodes (GTV-N), were retrospectively analyzed. All automatic matches were compared with manual ground truth matches. Translational residuals of GTV-T, GTV-N and spine were assessed and setup margins and resulting PTVs were calculated.

Results: For the soft-tissue matches PTV-Total was in average reduced by approximately 13% for DIBH compared to FB. The corresponding reduction for bony registrations was about 8%. The smallest residual misalignments of the spine were observed for FB, independently of match method.

Conclusions: Although DIBH was superior to FB for all match methods in terms of smallest PTV-Totals, more setup uncertainties were introduced. Soft-tissue auto-match was superior to bony registration, independently of FB and DIBH. Precautions must be applied during DIBH for the patients that tend to arch their back to compensate for their insufficient breath-hold level.

9.1 Introduction

In radiotherapy, margins are traditionally applied to the clinical target volume (CTV) and the organs at risk (OAR)s to account for different systematic and random sources of errors related to organ motion, patient positioning and target delineation [16]. Large margins limit the deliverable dose to the planning target volume (PTV) due to the dose constraints of the adjacent OARs. Smaller PTVs will spare the adjacent healthy tissue from unnecessary dose, and/or enable delivery of a higher dose to the target yielding a positive effect on the treatment outcome. There are two major aspects that affect the size of the PTV: Inter-fractional motion, and patient instability (intra-fractional motion). Pre-treatment verification by means of image guidance is a way to quantify and correct for setup errors [62–64]. Three dimensional (3D) cone-beam computed tomography (CBCT) is suitable for soft-tissue visualization and registration [62]. This image modality provides information about anatomical positions of tumor and OARs, as well as anatomical changes in the thorax area, such as atelectasis (collapse or closure of the lung), pneumonitis (inflammation of lung tissue), and pleural effusion (water in lungs) [26]. Direct match on the lung tumor itself (i.e. soft-tissue tumor registration) compared to bony match on the spine has the potential to minimize the required setup margins in the thorax area [21,63,64]. The CBCT images are either manually or automatically registered to the reference CT images. Manual registration is a complex and time consuming task and can be subject to inter-observer variability, contrary to automatic registration [65,66]. Respiratory motion is a challenge, influencing both imaging and treatment delivery [29,30]. Breathing adapted radiotherapy by means of deep-inspiration breath-hold (DIBH) may suppress the influence of respiration on geometric and dosimetric uncertainties, leading to reduced internal target motion and smaller PTVs [29,109–111].

This work studies CBCT setup verification of locally advanced lung cancer patients performing free-breathing (FB) and DIBH breathing techniques, with the primary objective to identify which automatic CBCT match method that results in the smallest PTV. The study provides clinical guidance on what automatic CBCT match protocol to use for DIBH or FB setup verification, and it specifically addresses how match results depend on the breathing techniques. The three investigated automatic CBCT match methods focused on: (a.) the bony anatomy of the spine, (b.) the soft-tissue of the primary gross tumor volume (GTV-T), and (c.) the soft-tissue of the total tumor volume (GTV-Total), including malignant lymph nodes (GTV-N).

9.2 Material and methods

Technical study details are provided in the supplementary material to this paper.

9.2.1 Patient data

Seventeen locally advanced non-small-cell lung cancer (NSCLC) patients scheduled for curative radiotherapy at Herlev Hospital, between December 2012 and July 2014, were enrolled (supplementary Table 10). The patients were treated with volumetric modulated arc therapy (VMAT) or intensity-modulated radiotherapy (IMRT) in 30-33 fractions (fx), receiving a total dose of 60-66 Gy (2 Gy/fx, 5 fx/week).

9.2.2   Image acquisition

All images were acquired in treatment position. Weekly CBCT images in FB and DIBH was acquired, both pre- and post-treatment, resulting in four CBCTs per weekly image session. Furthermore each patient was dual-CT scanned in a 16 slice Philips Brilliance CT Big Bore scanner, version 3.5.17001 (Philips Medical Systems, Cleveland, OH) (acquiring a 4DCT in FB and a normal CT in DIBH) before the start of, in the middle of, and after completion of the course of treatment. Intra-venous contrast was administered to the patients during both 4DCT and DIBH CT imaging, for better contrast of nodal anatomy in the mediastinum. Each patient was additionally scanned in a GEMINI TF 16 slice Big Bore PET/CT, version 2.3 (Philips Medical Systems) before the start of the course of treatment in order to diminish the delineation uncertainties in the planning CT. Delineation details can be found elsewhere [21,112].

The CT and CBCT systems were integrated with the Varian real-time position management (RPM) system, version 1.7 (Varian Medical Systems), for monitoring the patients' respiration during imaging. The patients were audio-visually guided during DIBH imaging using video goggles, where the patients held their breath within a patient-specific predefined amplitude level and a gating window of 2-3 mm width. All FB and DIBH CBCTs were acquired during the same treatment session.

9.2.3   Image registrations and residual setup deviations

All CBCT images were retrospectively registered to reference CTs in Offline Review v. 10 (Varian Medical Systems) by one observer solely (FR) to avoid inter-observer variations. The un-tagged reconstruction of a 4DCT scan in FB was used as reference CT for the FB CBCTs [21] and a DIBH CT scan was used as reference CT for the DIBH CBCTs. Only translational corrections were allowed in the vertical (VRT), longitudinal (LNG) and lateral (LAT) directions. Most of the automatic match settings were predefined by Varian [65].

Three match volumes of interest (VOIs) were used: (a.) The bony anatomy of the spine, where the planning risk volume (PRV) of the spinal cord plus an isotropic margin of 2.5 cm operated as the matching VOI for the bony match method. The PRV of the spinal cord was defined as an 0.5 cm isotropic expansion of the spinal cord. The Hounsfield unit (HU) interval within the VOI was set to [50; 3000] HU. (b.) The soft-tissue of the GTV-T (or GTV-T/IM for the FB imaging, which included the internal margin (IM) from the 4DCT reference scan according to the Maximum Intensity Projection (MIP) concept [21] plus an isotropic margin of 1 cm operated as the matching VOI for the primary tumor soft-tissue match method. The HU-interval was set to [-150; 150] HU. (c.) The soft-tissue of the GTV-Total, including the malignant lymph nodes, plus 1 cm isotropic margin operated as the matching VOI for the total tumor soft-tissue match method. The HU-interval was the same as in method (b.). All match VOIs are depicted in Figure 25.

The CBCTs were firstly aligned by automatic rigid registrations to the reference CT images. Each match was subsequently manually verified and readjusted to the best possible alignment, which were considered as the ground truth. Hereby the inter-fractional residual setup deviation of the bony anatomy of the spine, the primary tumor and the malignant lymph nodes were assessed as the differences between the automatic and manual regi-

strations. The patient stability (intra-fractional motion) was similarly quantified by the geometrical shifts between the manual matches of the pre- and post-treatment CBCTs for the spine, the primary tumor and the malignant lymph nodes.

The residual misalignments of the spine and GTV-T were obtained for all the automatic CBCTs registrations. The residual misalignments of GTV-N were, however, only obtained for the 7 patients with separately delineated GTV-Ns. Since the lymph nodes are not easily visible in the CBCTs, the main bronchi area was used as a lymph node match surrogate to get an estimation of the GTV-N residual misalignments. The main bronchi area, (including the trachea, carina and the bronchus) is a stable anatomical surrogate structure closely situated to the involved lymph node stations which were centrally positioned in this study (supplementary Table 10). To quantify the overall magnitudes of the translational shifts, the 3D-vectors of the residual deviations were calculated. Statistical tests were considered significant for $p \leq 0.05$.

9.2.4 *Error definition and margin calculations*

The anatomical misalignments for the different automatic match methods investigated were expressed in terms of the overall group mean (GM), and systematic (Σ) and random (σ) errors [15]. CTV to PTV margins were calculated according to the Van Herk formalism [15,16], and the PRV margins of the spine were calculated according to the McKenzie's formalism [18].

Since most tumors were located close to the mediastinum (Figure 25, supplementary Table 10), margins were calculated using two different penumbra factors (σ_P) in order to quantify the effect of different penumbra widths on the CTV to PTV margin. $\sigma_P = 0.64$ cm describes the width of the penumbra in lung tissue, and $\sigma_P = 0.32$ cm in water, i.e. soft-tissue, modeled by a cumulative Gaussian [17]. Margins were calculated both including and excluding the intra-fractional motion.

The calculated CTV to PTV margins for the tumor and lymph nodes were applied to each patient's CTV-T and CTV-N in the treatment planning system (TPS) Eclipse v. 10 (Varian Medical Systems). The sizes of the CTVs and PTVs in FB and DIBH were extracted from the TPS for evaluation.

9.3 Results

Details for intra- and inter-fractional misalignments, GMs, systematic and random error components are found in the supplementary Table 11.

9.3.1 *Analysis of intra-fractional motion*

For the intra-fractional motion, FB was found to be in favor over DIBH for all anatomical structures (Table 6, supplementary Figure 26). The significant differences in SDs between FB and DIBH were most noticeable in the LNG direction (supplementary Table 11). Compared with the GTV-T and GTV-N, larger maximum intra-fractional 3D-vectors were observed for the spine, which for DIBH, mainly was due to the misalignments in the LNG direction (Table 7, supplementary Table 11).

9.3.2 Analysis of inter-fractional motion

As expected, the smallest residual misalignments ($\leq$ 2 mm) and the smallest 3D-vector of the spine were observed in FB after automatic bony registration (Table 5, supplementary Figure 26 - Figure 29). Largest inter-fractional misalignments of the spine were observed during DIBH independently of match method, especially in the LNG direction.

For the lymph nodes, the smallest 3D-vectors were found for soft-tissue auto-match on the GTV-Total, regardless of FB or DIBH. No significant difference between the FB and DIBH 3D-vectors was observed for lymph nodes.

For the primary tumor, DIBH 3D-vector was superior to FB for the both automatic soft-tissue registrations, especially in the LNG direction (supplementary Table 11). The soft-tissue match on the GTV-T was favorable over match on GTV-Total, irrespectively of FB or DIBH. The largest 3D-vectors of GTV-T and GTV-N were found for the bony registration on the spine, regardless of FB or DIBH, where FB was favorable over DIBH.

No significant differences of the residual misalignments were found for any of the investigated structures if performing soft-tissue match on GTV-T or GTV-Total.

9.3.3 Analysis of CTV to PTV margins

Only minor, non-significant differences in the calculated CTV to PTV margins were found using the penumbra factor for lung tissue (σ_p = 0.64 cm) instead of using the penumbra factor for water (σ_p = 0.32 cm). CTV to PTV margins (Table 6) and PTVs (Table 9) are therefore only presented for lung tissue.

All margins increased when including the intra-fractional motions in the margin calculations (Table 6). The largest margin increases (1.1-2.2) mm were observed in the LNG direction during DIBH. Corresponding margin increments in FB were smaller (0.2-1.3 mm).

Compared to soft-tissue GTV-T registration, the disadvantage of the bony registration method were the larger misalignments of the tumor (especially in the LNG direction, and in DIBH), resulting in (when including the intra-fractional motion) an extra margin of 1.6-2.8 mm in FB and 2.0-3.4 mm in DIBH (Table 6). The margin differences for the GTV-N, if performing bony registration or soft-tissue registration on GTV-Total were not that large, ranging between -0.3-0.7 mm (FB) and -0.3-1.4 mm (DIBH), where the largest differences were observed in the LNG and LAT direction during DIBH. Bony registration yielded the smallest margin for the spine, compared to any soft-tissue registration method.

Although DIBH resulted in the overall largest margins, the resulting PTV-Total sizes were for most cases found to be smaller for DIBH compared to FB, regardless of what match method carried out (Table 9). The CTVs for DIBH were on average 14.2%, 9.0%, and 13.1% smaller than the corresponding values for FB, respectively (Table 8). These differences are mainly due to the two different treatment planning concepts applied (using the MIP concept for the 4DCT image). The largest reduction of PTV-Total were detected for both soft-tissue auto-match methods (about a 13% overall volume reduction if excluding intra-fractional motion and about 9% reduction if including it) (Table 9). The

equivalent numbers for bony auto-match on the spine were an 8% overall volume reduction if excluding the intra-fractional motion and about 7% reduction if included.

9.4   Discussion

The margins in Table 6 should be considered as a lower limit for safe radiotherapy since they exclude rotational errors, shape variations, and delineation uncertainties [16]. The potential registration biases due to repeated breath-holds during DIBH are expected to be small since no significant image artifacts during DIBH CBCT imaging were observed. The observed misalignments on GTV-T and GTV-N after bony registration are mainly in the VRT and LNG direction (Table 7), and may be due to the moving pattern of the tumor relative to the bony structure of the spine. Consequently, this relative tumor motion may also be the reason why the 3D-vectors of the spine are the largest after soft-tissue auto-match on the GTV-T.

9.4.1   Comparison with other studies

In the present study, 88% of the patients had mediastinal involvement. Several studies on patients with small primary tumors detached from the mediastinal areas referred to lung stereotactic body radiotherapy (SBRT), have demonstrated the advantage of soft-tissue registrations [63,66]. The current study suggests that also locally advanced lung cancer patients with mediastinal involvement benefit from soft-tissue registration on the tumor, regardless of FB or DIBH. This conclusion is supported by investigations of setup verifications in conventionally fractionated FB lung radiotherapy [22,64,65].

In the present study, the mean 3D-vector of the primary tumor after automatic bony registration was 3.2 mm ± 1.6 mm (1 SD) in FB and 4.1 mm ± 2.5 mm (1SD) in DIBH (Table 5). The result for FB is comparable with the study by Grams et al. [65] which reported a mean difference in the corresponding 3D-vector of 3.5 mm ± 1.8 mm (1 SD). They used a similar match VOI as in our study. However, only 2 patients out of 11 had mediastinal involvements. Other studies, where the patient populations did not include any [63,66] or very few [64] patients with mediastinal involvement, larger corresponding 3D-vectors were reported. This difference is likely due to the fact that the locally advanced tumors are more attached to the mediastinal area and close to the spine, and therefore less influenced by irregular breathing patterns. Yeung et al. [64] stated they could reduce the setup margin of the primary tumor by more than 1 cm by using tumor match instead of bony match. This is however not supported by our study, where only a reduction of 1.6-3.4 mm was found for the GTV-T. This may be because their patient population only included 3 patients out of 13 with mediastinal involvement. In accordance with [22,63–66], we found that it is not advisable to use the bony anatomy structure as a target surrogate. The PRV margins of the spinal cord during soft-tissue registrations in FB (about 3-5 mm (Table 6)) were comparable with spinal cord margins reported in [18,22,113]. Moreover, the residual GTV-N deviations and associated 3D-vector in FB and DIBH were found to be similar for the bony and soft-tissue match methods (Table 5), which agrees with [22]. In agreement of the results of Rahma et al. [22,113], the CTV to PTV margins of GTV-T were reduced regardless of what soft-tissue auto-match methods carried out, in comparison to bony registration on the spine.

9.4.2   *Compensation of insufficient breath-hold level*

Shallower breath-holds during DIBH, may result in patients arching with their back to compensate for their insufficient compliance to reach the breath-hold amplitude level. This was in some extent observed in the current study, since larger intra-fractional SDs and misalignments (> 5 mm) for the spine were observed in the LNG direction during DIBH, compared to FB (Table 7 and supplementary Table 11). The intra-fractional motions of GTV-T and GTV-N were, however, not affected that much by this, where maximum residual shifts of 5 mm in the LNG direction were observed for GTV-T, and 4 mm for GTV-N (supplementary Table 11). Since the DIBH CBCT imaging often extends over several deep-inspiration breath-holds. This may cause tiredness of the patients, yielding even more arching of their backs.

9.5   **Conclusion**

This study demonstrates the advantage of combining DIBH with soft-tissue CBCT auto-match setup verifications for locally advanced lung cancer patients to obtain the smallest treatment volumes. DIBH in combination with a soft-tissue auto-match procedure reduced the size of the total PTV between 9-13% on average compared to FB, depending on whether the intra-fractional motion was included or not. When included, the gain of DIBH was reduced. Bony registration resulted in about 1-5% on average larger PTV-Totals, compared to the soft-tissue registrations. Soft-tissue auto-match on GTV-T was found to be clinically most practical, since the target verification procedure is faster (compared to verification of GTV-Total), and more accurate (compared to bony registration). We advise against performing soft-tissue registration on GTV-Total if the GTV-T and GTV-N are not closely located within an image slice. If there exists several involved lymph nodes, and they are located far away from each other, there may be difficulties to verify the correct lymph node positions, and there is a risk that they may change their relative localization during DIBH. Thus, decision should be taken already at the stage of treatment planning, as to which part of the tumor volume to prioritize during verification, and thereby what setup margins to apply on the targets and OARs.

Although DIBH yields the smallest PTVs for all match methods investigated, the treatment technique introduces more setup uncertainties (especially in the LNG direction), resulting in larger CTV to PTV margins compared to FB. We believe this is because some patients tend to arch with their back to compensate for their insufficient compliance to reach the breath-hold amplitude level. Our recommendations are therefore not to push the patients to hold their breath at their maximum amplitude peak of breath-hold.

Conflict of interest statement

The authors declare no conflict of interest.

editing. Patients were enrolled by the radiation oncologists Jon A. Lykkegaard Andersen, Svetlana Borissova, and Anders Mellemgaard.

9.6   Figures
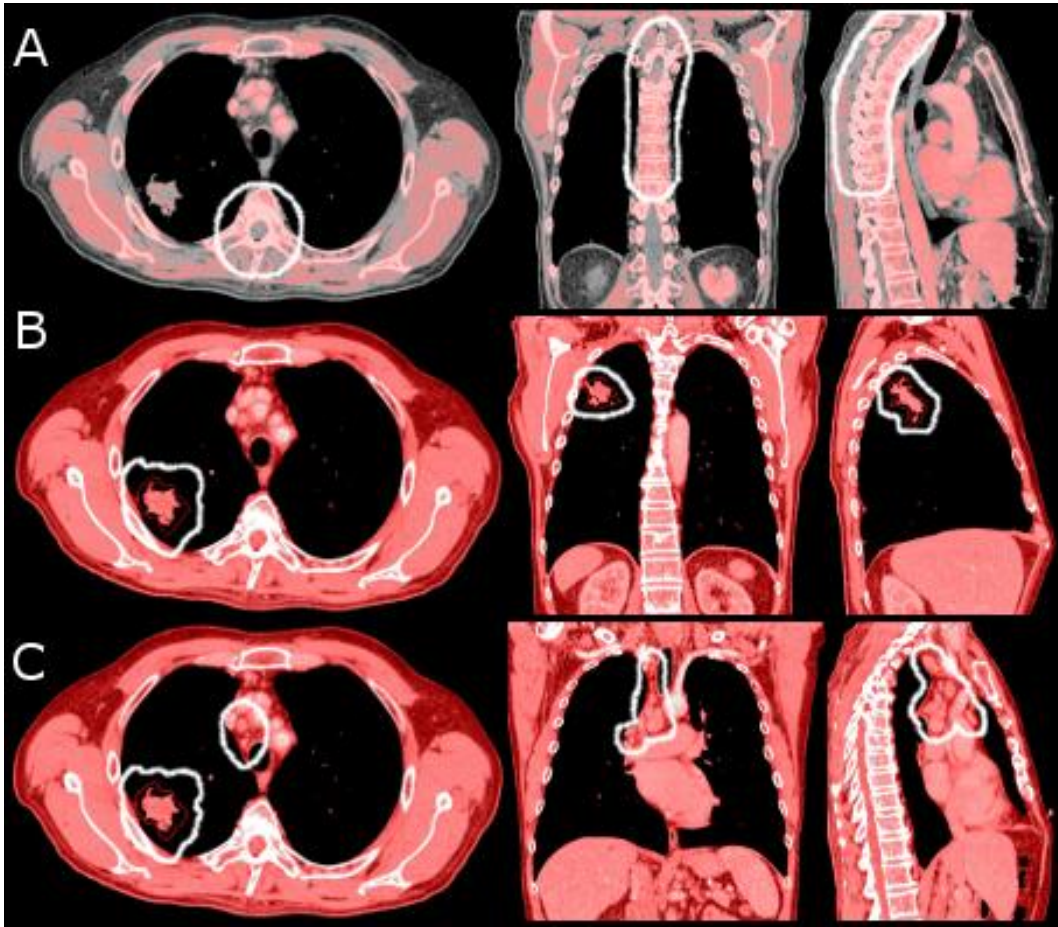
Figure 25. The different match VOIs presented on the DIBH CT image of patient 12. The white lines represent the match VOIs when performing (A) automatic bony match on the spine, (B) automatic soft-tissue match on GTV-T, and (C) automatic soft-tissue match on GTV-Total. The volume within the VOIs utilized for the registrations are colored red (i.e. pixels with an intensity range of [50; 3000] HU for bony match (A), and [-150; 150] HU for soft-tissue match (B and C)). Color version of figure is available online.

9.7 Tables

Table 5. Median and maximum residual 3D-vectors for the three different match methods investigated for the spine, GTVT-T and GTV-N in FB and DIBH. Italic style indicates that one breathing technique is statistically significant (p ≤ 0.05) superior to the other breathing technique in terms of the smallest mean. Corresponding significance in median value and variance for the 3D-vectors are indicated by underline and bold styles, respectively. P-values are presented in the supplementary Figure 26 - Figure 29. (See the supplementary Table 11 for more detailed data on the intra- and inter-fractional motion in each direction).

	Manual match on Spine [mm]		Manual match on GTV-T[mm]		Manual match on GTV-N [mm]	
	Intra-fractional motion					
	FB	DIBH	FB	DIBH	FB	DIBH
Manual match on Spine, GTV-T, and GTV-N, respectively						
3D-vector (SD)	_**1.4 (1.0)**_	1.7 (2.3)	_**1.9 (1.0)**_	2.8 (1.3)	_**2.0 (0.8)**_	2.8 (1.3)
|Max 3D-shift|	7.1	12.9	5.4	5.7	4.5	6.0
	Inter-fractional motion					
	FB	DIBH	FB	DIBH	FB	DIBH
Auto-match on Spine						
3D-vector (SD)	_**1.0 (0.7)**_	1.0 (2.2)	_**3.2 (1.6)**_	4.1 (2.5)	3.0 (1.9)	3.4 (2.4)
|Max 3D-shift|	2.2	9.3	8.5	16.2	10.3	14.4
Auto-match on GTV-T						
3D-vector (SD)	_**2.8 (1.7)**_	4.1 (2.2)	1.4 (1.2)	**1.4 (0.9)**	2.8 (1.2)	3.0 (1.2)
|Max 3D-shift|	7.4	9.9	8.2	3.6	5.4	6.2
Auto-match on GTV-Total						
3D-vector (SD)	_**2.5 (1.4)**_	3.5 (2.1)	1.9 (0.9)	1.6 (0.7)	2.5 (1.1)	2.5 (1.1)
|Max 3D-shift|	7.3	10.1	5.4	3.2	5.1	6.0

FB, free-breathing; DIBH, deep-inspiration breath-hold; SD, standard deviation.

Table 6. Margins (including or excluding the intra-fractional motion) for the three different match methods investigated for the spine, GTVT-T and GTV-N in FB and DIBH. (See the supplementary Table 11 for more detailed data on the overall group means (GMs), the systematic (Σ) and the random (σ) error components used for the margin calculations).

	Margin of Spine [mm]						Margin of GTV-T[mm]						Margin of GTV-N [mm]					
	FB			DIBH			FB			DIBH			FB			DIBH		
	VRT	LNG	LAT	VRT	LNG	LAT	VRT	LNG	LAT	VRT	LNG	LAT	VRT	LNG	LAT	VRT	LNG	LAT
Auto-match on Spine																		
Margin[a]	1.5	1.1	1.4	1.5	5.2	1.4	7.8	10.9	8.3	8.9	10.3	7.7	6.6	7.5	7.0	7.0	9.0	7.1
Total margin[b]	2.7	1.9	2.1	2.9	7.2	2.5	8.3	11.7	8.6	9.7	11.4	8.3	7.1	8.3	7.8	7.8	10.7	7.7
Auto-match on GTV-T																		
Margin[a]	4.3	4.9	5.2	5.5	7.4	5.4	6.0	7.8	6.2	6.3	6.2	5.1	7.5	6.3	7.5	8.0	8.1	6.6
Total margin[b]	4.8	5.2	5.5	6.1	8.9	5.9	6.7	8.9	6.6	7.5	8.0	6.3	7.9	7.3	8.1	8.6	9.9	7.3
Auto-match on GTV-Total																		
Margin[a]	3.3	4.8	4.0	4.0	5.6	4.2	6.6	7.3	5.9	5.4	6.3	5.3	6.4	7.9	6.1	7.4	7.1	5.8
Total margin[b]	4.0	5.0	4.3	4.7	7.5	4.8	7.3	8.6	6.4	6.9	8.1	6.4	6.9	8.6	7.1	8.1	9.3	6.6

FB, free-breathing; DIBH, deep-inspiration breath-hold; VRT, vertical; LNG, longitudinal; LAT, lateral. [a] The calculated margins excluding the intra-fractional motion. The PRV margin of the spine is calculated according to [18], and the CTV to PTV margins for GTV-T and GTV-N are calculated according to [15,16], using the penumbra factor $\sigma_p = 0.64$ cm. [b] The calculated margins including the contribution from intra-fractional motion.

Table 7. The number of shift events (n) including shifts of 0 mm and the overall relative percentage of residual misalignments greater than 3, 5 or 10 mm for FB and DIBH in the VRT, LNG and LAT direction for the intra- and inter-fractional match methods investigated on the spine, GTV-T and GTV-N.

	Manual match on Spine								Manual match on GTV-T								Manual match on GTV-N							
	FB				DIBH				FB				DIBH				FB				DIBH			
	VRT	LNG	LAT	[%]	VRT	LNG	LAT	[%]	VRT	LNG	LAT	[%]	VRT	LNG	LAT	[%]	VRT	LNG	LAT	[%]	VRT	LNG	LAT	[%]
Intra-fractional motion – Manual match on Spine, GTV-T, GTV-N, respectively																								
n	82	82	82		82	82	82		80	80	80		80	80	80		35	35	35		35	35	35	
n > 3 mm	1	0	0	0.4	3	8	1	4.9	3	3	0	2.5	2	8	2	5.0	1	0	0	0.9	1	6	1	7.4
n > 5 mm	1	0	0	0.4	1	4	0	2.0	0	0	0	0.0	0	0	0	0.0	0	0	0	0.0	0	0	0	0.0
n > 10 mm	0	0	0	0.0	0	0	1	0.4	0	0	0	0.0	0	0	0	0.0	0	0	0	0.0	0	0	0	0.0
Inter-fractional motion – Manual match on Spine																								
n	83	83	83		83	83	83		81	81	81		81	81	81		36	36	36		36	36	36	
n > 3 mm	0	0	0	0.0	0	11	0	4.4	3	9	3	6.2	14	28	7	20.2	3	7	1	10.2	5	5	1	10.2
n > 5 mm	0	0	0	0.0	0	0	7	2.8	0	3	1	1.6	0	11	0	6.6	0	1	0	1.9	1	1	0	3.7
n > 10 mm	0	0	0	0.0	0	0	0	0.0	0	0	0	0.0	0	1	0	0.4	0	0	0	0.0	0	1	0	0.9
Inter-fractional motion – Auto-match on Spine																								
n	81	81	81		83	83	83		80	80	80		81	81	81		36	36	36		36	36	36	
n > 3 mm	5	12	8	10.3	11	24	11	19.3	3	3	0		14	28	7		3	7	1		5	5	1	7.4
n > 5 mm	0	2	1	1.2	7	0	10	6.2	0	1	0		0	0	0		0	2	0		1	2	0	0.0
Inter-fractional motion – Auto-match on GTV-T																								
n	81	81	81		81	81	81		81	81	81		81	81	81		36	36	36		36	36	36	
n > 3 mm	12	8	1	19.3	24	11	0		0	0	0	0.0	0	0	0	0.0	4	5	3		5	5	1	8.3
n > 5 mm	4	1	0	6.2	10	1	0		0	0	0	0.0	0	0	0	0.0	0	3	1		1	0	0	0.9
Inter-fractional motion – Auto-match on GTV-Total																								
n	36	36	36		36	36	36		36	36	36		36	36	36		36	36	36		36	36	36	
n > 3 mm	1	1	1	4.6	4	6	2	11.1	0	1	0	0.9	0	0	0	0.0	0	0	1	0.9	2	1	0	2.8
n > 5 mm	1	1	0	1.9	2	1	1	3.7	0	0	0	0.0	0	0	0	0.0	0	0	0	0.0	1	0	0	0.9

FB, free breathing; DIBH, deep inspiration breath hold; VRT, vertical; LNG, longitudinal; LAT, lateral.

Table 8. The mean volume of the CTVs and the overall mean of the percentage deviations between FB and DIBH. Bold values indicate that the overall mean of the percentage deviations are statistically significantly (p ≤ 0.05) negative, i.e. DIBH yields statistically significantly smaller CTV volumes compared to FB in average.

Mean volume	CTV-T (min; max)	CTV-N (min; max)	CTV-Total (min; max)
FB[a] [cm^3]	303 (47; 800)	80 (12; 216)	337 (109; 800)
DIBH[a] [cm^3]	269 (32; 737)	68 (7; 188)	298 (89; 734)
Dev.[b] [%]	**- 14.2 (-34.0; -1.3)**	- 9.0 (-38.2; 55.4)	**- 13.1 (-30.2; -1.3)**

[a.] The mean volume of the CTV-T, CTV-N and CTV-Total, extracted from the treatment planning system Eclipse. [b.] The overall mean of the percentage deviations between FB and DIBH. Negative values indicate that DIBH CTVs are smaller than FB CTVs.

Table 9. The mean of the resulting PTVs in FB and DIBH, including or excluding intra-fractional motion. Additionally, the overall mean of the percentage deviations between FB and DIBH PTVs, and the percentage fraction of DIBH PTVs that were smaller than the FB PTVs for each match methods are presented. Bold values indicate that the overall mean of the percentage deviations are statistically significantly (p ≤ 0.05) negative, i.e. DIBH yields statistically significantly smaller PTV volumes compared to FB in average. The data presented for auto-match on GTV-Total are the results for the 7 patients with separately delineated lymph nodes.

	Auto-match on Spine			Auto-match on GTV-T			Auto-match on GTV-Total		
	PTV-T	PTV-N	PTV-Total	PTV-T	PTV-N	PTV-Total	PTV-T	PTV-N	PTV-Total
Mean volume				**Excluding intra-fractional motion**					
FB [cm^3]	614	216	697	524	212	605	279	200	459
min; max	148;1546	46;531	284;1546	116;1335	45;536	233;1335	115;456	41;499	240;856
DIBH [cm^3]	567	197	643	451	198	530	222	177	392
min; max	120;1482	35;492	258;1482	80;1188	36;498	199;1188	76;387	31;451	224;763
Dev.[a] [%]	**- 9.2**	-4.8	**- 8.3**	**- 15.8**	-3.9	**- 12.8**	**- 21.6**	- 8.0	**- 13.6**
min; max	**-26.3;-0.4**	-23.5;34.8	**-22.9;-0.4**	**-34.5;5.4**	-20.8;34.1	**-31.2;5.4**	**-37.1;-2.1**	-25.8;33.1	**-27.4;0.0**
DIBH < FB[b] [%]	100	85.7	100.0	93.8	71.4	93.8	100	85.7	100
Mean volume				**Including intra-fractional motion**					
FB [cm^3]	645	223	728	558	221	644	296	221	493
min; max	160;1612	48;548	302;1612	129;1428	47;546	247;1428	124;480	47;543	258;909
DIBH [cm^3]	591	226	678	505	217	590	253	204	443
min; max	123;1538	42;550	277;1538	96;1344	41;543	233;1344	92;441	37;508	258;849
Dev.[a] [%]	**- 10.1**	6.9	**- 7.3**	**- 11.2**	2.2	**-8.6**	**- 15.5**	-4.5	**- 9.7**
min; max	**-26.0;-1.2**	-11.6;53.1	**-23.8;-0.5**	**-32.5;3.0**	-12.7;47.0	**-32.5;3.0**	**-29.8;-2.4**	-22.0;37.5	**-21.6;0.0**
DIBH < FB[b] [%]	100	42.9	100	93.8	71.4	93.8	100	85.7	100

[a.] The overall mean of the percentage deviations between FB and DIBH. Negative values indicate that DIBH PTVs are smaller than FB PTVs. [b.] The percentage fraction of DIBH PTVs that are smaller compared to FB PTVs.

9.8   Supplementary material

9.8.1   Treatment delivery

The treatments were delivered in FB using Varian Clinac iX 2300 linear accelerators [21,85] (Varian Medical Systems, Palo Alto, CA) equipped with On-Board Imagers (OBI) capable of performing FB and DIBH CBCT, using version 1.5 of the OBI software. The Varian low-dose thorax CBCT scanning protocol was utilized.

9.8.2   Ethical considerations

The clinical protocol was approved by the Copenhagen Regional Committee on Health Research Ethics (protocol no. H-4-2012-066) and the Danish Data Protection Agency (ID. nr: 2007-58-0015 / HEH.750.24-61). Every patient gave informed consent to the work before inclusion.

9.8.3   Details about the IV contrast administration

The CT injection system was Stelland from MEDRAD.
The IV-contrast we used was Iomeron 300mg I/ml from BRACCO Imaging SpA

For a normal patient, we administered: 50 ml IV for the DIBH scan and 100 ml IV for the 4DCT scan. If the patient weighted < 50 kg, we administered: 35ml IV for the DIBH scan, and 70 ml for the 4DCT scan.

We used a delay time of:

- 60 s for the DIBH scan
- 30 s for the 4DCT scan

We used a contrast flow of:

- 3 ml/s for the DIBH scan

- 2 ml/s for the 4DCT scan

9.8.4   Exclusion/inclusion of CBCT images

FB and DIBH CBCTs were only included in the study if they were acquired during the same treatment session. Thus, additional pre-treatment FB CBCTs acquired other days during the course of treatment were not included. CBCTs revealing large anatomical changes such as creation or disappearance of atelectasis, tumor deformation, shrinkage, and displacement, as well as puncture of the vacuum pillow used for patient fixation, were not included in the analysis. If a patient was re-scanned during the course of treatment only the CBCTs acquired after the re-scans were included in the study to minimize the biases caused by anatomical changes. A total of 166 pre-treatment CBCTs (83 in FB and 83 in DIBH), and 164 post-treatment CBCTs (82 in FB and 82 in DIBH) were acquired and analyzed. However, 119 CBCTs were excluded due to following reasons: anatomical changes (80), poor image quality (3), incompliance with the image protocol (24), automatic match difficulties because of target shrinkage (4), and pneumonia (8). A total of 400 pre-treatment (200 in FB and 200 in DIBH) and 394 post-treatment (197 in FB and 197 in DIBH) automatic registrations on the spine, GTV-T and GTV-Total, and an equal

number of manual verifications on the spine, GTV-T and GTV-N were performed. This resulted in 1012 pre-treatment (506 in FB and 506 in DIBH) and 394 post-treatment shift events for evaluating the three different match methods and the intra-fractional motion.

9.8.5 Details about the image registration

The automatic rigid registration process was performed in three steps, each step with a higher image resolution, improving the efficiency of the algorithm [65]. The registrations were restricted to the field of view of the CBCT scans. Parts of the spinal cord, tumor volume, and malignant lymph nodes reaching beyond this volume of interest were ignored. For visual geometrical verification of the primary tumor and the involved lymph nodes, the pre-defined "lung" HU-window level was used for both the reference CTs and CBCTs. Equivalently, the "abdomen" HU-window level was used for verification of the bony registration.

Although, most of the automatic match settings were predefined by Varian, the observer was allowed to choose what volume of interest (VOI) and which Hounsfield units (HU) within the VOI to use when performing the automatic registrations. For the bony match on the spine, the HU-interval within the VOI was set to [50; 3000] HU. This interval covers not only the cortical bone with high HU-values, but also the soft bone with lower HU-values, around 50 HU. The reason for the 2.5 cm margin around the spinal cord PRV was to include the major part of the vertebra in the bony registration.

For the soft-tissue matches on GTV-T and GTV-Total, the HU-interval was set to [-150; 150] HU to include the major part of the soft-tissue tumor and lymph nodes. The added margin of 1 cm around the GTV-T and GTV-T/IM has been found to yield stable match results according to Rahma et al. [22,113].

9.8.6 The reason why to choose the Un-tagged reconstruction instead of the average (AVG) reconstruction after a 4DCT scan

For a Philips CT scanner, the un-tagged volume will utilize all of the sinogram data to reconstruct the data volume. There is no binning operation. This differs from the AVG dataset in two ways. The 'data averaging' is performed in sinogram space by back-projecting all of the raw data. Furthermore, the AVG volume is an average of the bins that were reconstructed and therefore based on the width and spacing of bins which may not include all of the data collected. Whereas, the un-tagged volume is always a true representation of the time averaged data that was acquired.

9.8.7 Details about the error definition and margin calculations

The anatomical misalignments were expressed in terms of the overall group mean (GM), systematic (Σ) and random (σ) errors, according to van Herk [15]. In the absence of significant biases, the GM will be close to zero. The systematic error (Σ) is a measure of the reproducibility of the setup among patients, and is defined as the standard deviation of the GM. The random error (σ) is a measure for the reproducibility of setup between fractions and is defined as the root mean square of the standard deviations of intra-patient shifts. Treatment execution (random) variations lead to a blurring of the dose distribution, while treatment preparation (systematic) deviations lead to a displacement of the dose

distribution with respect to the CTV [16]. Based on these data, the CTV to PTV margins were calculated according to the Van Herk formalism [15,16]:

$$\text{Margin}_{\text{PTV}} = 2.5 \cdot \Sigma + \beta \cdot \sqrt{\sigma^2 + \sigma_p^2} - \beta \cdot \sigma_p \qquad (9.1)$$

where the parameter β=1.64 assures delivery of 95% of the prescribed dose to 90% of the patient population [17].

Since the spinal cord is a serial OAR, and the treatments were delivered as three dimensional IMRT or RA plans, the PRV margins for the spinal cord were calculated according to McKenzie's formula [18], using the systematic and random components, according to:

$$\text{Margin}_{\text{OAR}} = 2.5 \cdot \Sigma + 0.5 \cdot \sigma \qquad (9.2)$$

To take into account the intra-fractional motion in the margin calculations, all the systematic and all random components were added in quadrature, according to [15,16]:

$$\Sigma = \sqrt{\Sigma_{\text{Inter}}^2 + \Sigma_{\text{Intra}}^2} \qquad (9.3)$$

$$\sigma = \sqrt{\sigma_{\text{Inter}}^2 + \sigma_{\text{Intra}}^2} \qquad (9.4)$$

9.8.8 Statistical analysis

For statistical analysis MATLAB including the Statistics Toolbox version 8.3 (R2013b) (The MathWorks, Natick, MA) was utilized. To evaluate the data several statistical tests were carried out, where the results were considered statistically significant for $p \leq 0.05$. Two-sampled paired t-tests and F-tests were performed to compare the means and the variances of the FB and DIBH data sets. Additionally two-sided Wilcoxon signed rank test were applied to test the medians of the data sets. To compare the match methods against each other in terms of which ones that resulted in the smallest PTVs, balanced one-way ANOVA tests were carried out.

9.8.9 Confounding factors

Potential confounding factors in this study are mainly due to the nature of CBCT imaging. Firstly, the FB CBCT imaging often extends over several respiratory cycles. However, we expect the potential bias to be very small since the FB CBCT images are registered to the time weighted un-tagged reconstruction of a 4DCT scan, which mimics a slow image acquisition, similar to the CBCT. Secondly, the CBCT image extension is spatially limited in the LNG direction. This is more of a problem for locally advanced lung cancer patients than for SBRT patients due to the larger tumor volumes that have the potential to reach beyond this limitation. One solution can be to acquire several CBCTs to cover the whole thorax area, which subsequently could be stitched together to create a long enough 3D image covering the whole thorax area. However this feature is not provided by the manufacturer of the utilized CBCT imaging device at this time. Another confounding factor involving the DIBH imaging is that in most cases it took several DIBH before a

whole CBCT scan was acquired (supplementary Table 12). The beam-off and hold of the CBCT scan acquisition when the patients breathing curve went outside the gating window were controlled manually by the operating radiotherapists (RTT)s. Nonfulfillment of the manually hold of the CBCT acquisition at the time when the breathing curve fails to be within the gating window could yield some motion artifacts during DIBH CBCT imaging. If the CBCT acquisition control unit could receive beam-on information from the respiratory monitoring system, just like the treatment unit, this issue would be minimized. The potential biases are nevertheless expected to be small since no significant image artifacts due to repeated breath-holds during DIBH CBCT imaging were observed in our study.

9.8.10   Clinical practicality

DIBH is more resource intensive for the staff than FB treatment, since each patient needs to be guided throughout all imaging and treatment delivery during the course of treatment. Although DIBH yields the smallest PTVs, the treatment technique introduces more setup uncertainties, resulting in larger CTV to PTV margins compared to FB. The cost of larger uncertainties and the heavier workload for the staff must be weighted against the dosimetric gain for each patient; in terms of saving adjacent healthy OARs and/or enabling possible dose escalation.

Setup verification using GTV-T and GTV-N can be a problem if they are not visible in the same image slices, and the observer needs to scroll between slices in different directions to verify their positions. It is achievable, but very time consuming. Due to the limited time slot on the treatment unit, we advise against performing soft-tissue registration on GTV-Total if the GTV-T and GTV-N are not closely located within an image slice. Soft-tissue auto-match on GTV-T is the preferred match method since the target verification procedure is faster (compared to verification of GTV-Total) and more accurate (compared to the bony registration). Thus, larger CTV to PTV margins should be applied to the CTV-N to ensure the dose coverage and larger PRV margin of the spinal cord to ensure no overdosage of the spinal cord. An additional verification problem may arise if the patient has several involved lymph nodes, and they are located far away from each other. In that case it is difficult to verify the correct lymph node positions. There is also a risk that they may change their relative localization during DIBH. A decision should be taken already at the stage of treatment planning, as to which part of the tumor volume to prioritize during verification, and thereby what setup margins to apply.

Due to the large number of fractions in conventionally fractionated radiotherapy, the cost of daily CBCTs must be weighed against the benefit of increased targeting accuracy and detection of anatomical abnormalities affecting the treatment outcome. Daily CBCT minimizes the risk of missing anatomical changes that might appear and disappear during the course of treatment. These anatomical changes may not just affect the dose distribution, but could also cause tumor displacement or obscure the visibility of the tumor. Møller et al. [26] discovered that for the 163 lung cancer patients analyzed in their study, an adaptive strategy was indicated for 12% as a result of atelectasis, pneumonitis or pleural effusion. This is further supported by our study, where 20% of the totally 449 acquired CBCTs contained anatomical changes, tumor shrinkage or pneumonia.

9.8.11   Future perspectives

In the future, the treatment process is required to be more individually optimized for each patient to obtain the highest treatment outcome possible. Evaluation of both FB and DIBH CT images in order to assess the tumor motion and the potential gain with DIBH prior to treatment planning, together with different margins, can be carried out in order to decide the setup and treatment strategy for the individual patient. The next step could be to evaluate on the treatment plan, instead of volume sizes, by producing many treatment plans for the different treatment strategies (e.g. FB or DIBH treatment plans, match on the tumor or the spine for setup verification, etc.). However, these individualized treatment planning processes are very workload heavy. Nevertheless, if the processes of target and OARs delineation and treatment planning are more automatized, it may be clinically feasible to implement a more individualized treatment. These features are currently not fully integrated in most commercial TPSs, but thorough investigations are carried out [70,114–116].

9.9 Supplementary figures
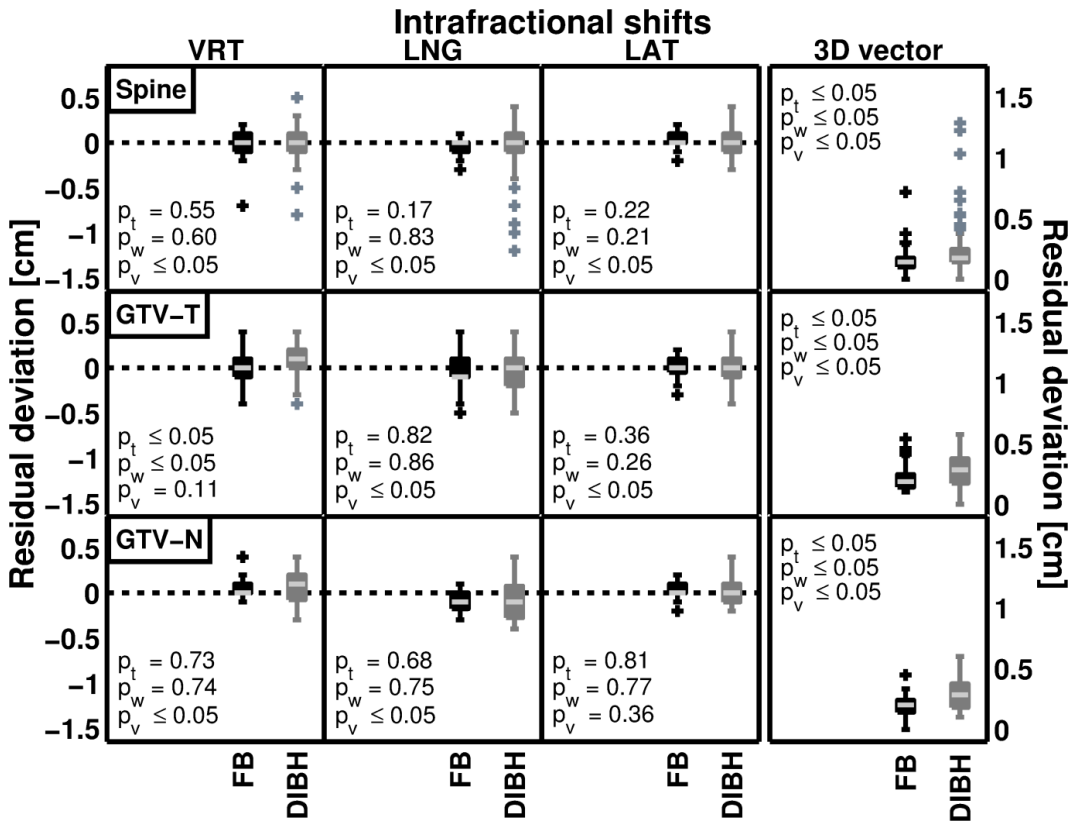
Figure 26. The intra-fractional residual deviations for FB and DIBH in the VRT, LNG, and LAT directions and the corresponding 3D-vector. The first, second and third line of subplots represent the translational shifts between $CBCT_{Before}$ and $CBCT_{After}$ after manual match on the spine, GTV-T, and GTV-N (or lymph node surrogates when the lymph nodes were not visible), respectively. The student's t-test, the Wilcoxon signed rank test and the F-test when investigating the statistically significant differences in mean, median and variance between DIBH and FB are represented by p_t, p_w and p_v, respectively. On each box, the central light gray mark represents the median value. The edges of each box are the 25th and the 75th percentiles, the whiskers correspond to approximately $\pm$ 2.7 SD of the data, and outliers are plotted as crosses individually.
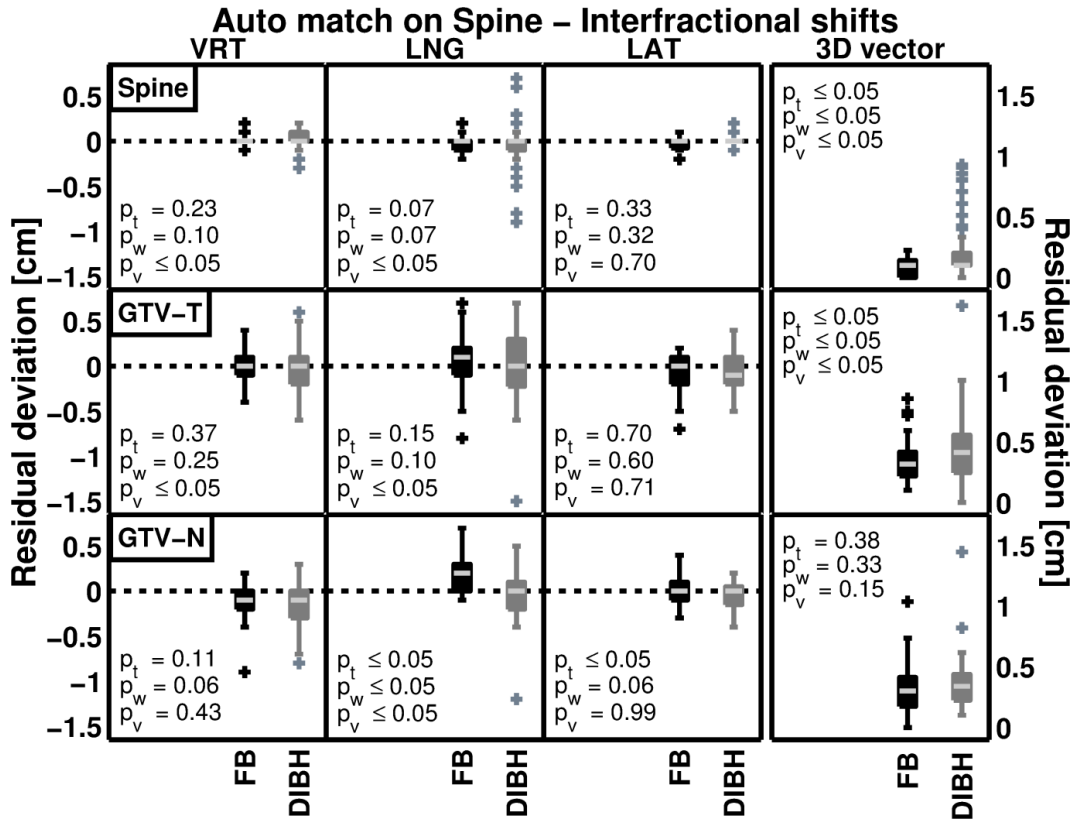
Figure 27. The inter-fractional residual deviations after auto match on the spine for FB and DIBH in the VRT, LNG, and LAT directions, including the corresponding 3D-vectors. The first, second and third line of subplots represent the translational shifts when performing manual match on the spine, GTV-T, and GTV-N (or lymph node surrogates when the lymph nodes were not visible), respectively. Additional figure explanations are described in supplementary Figure 26.
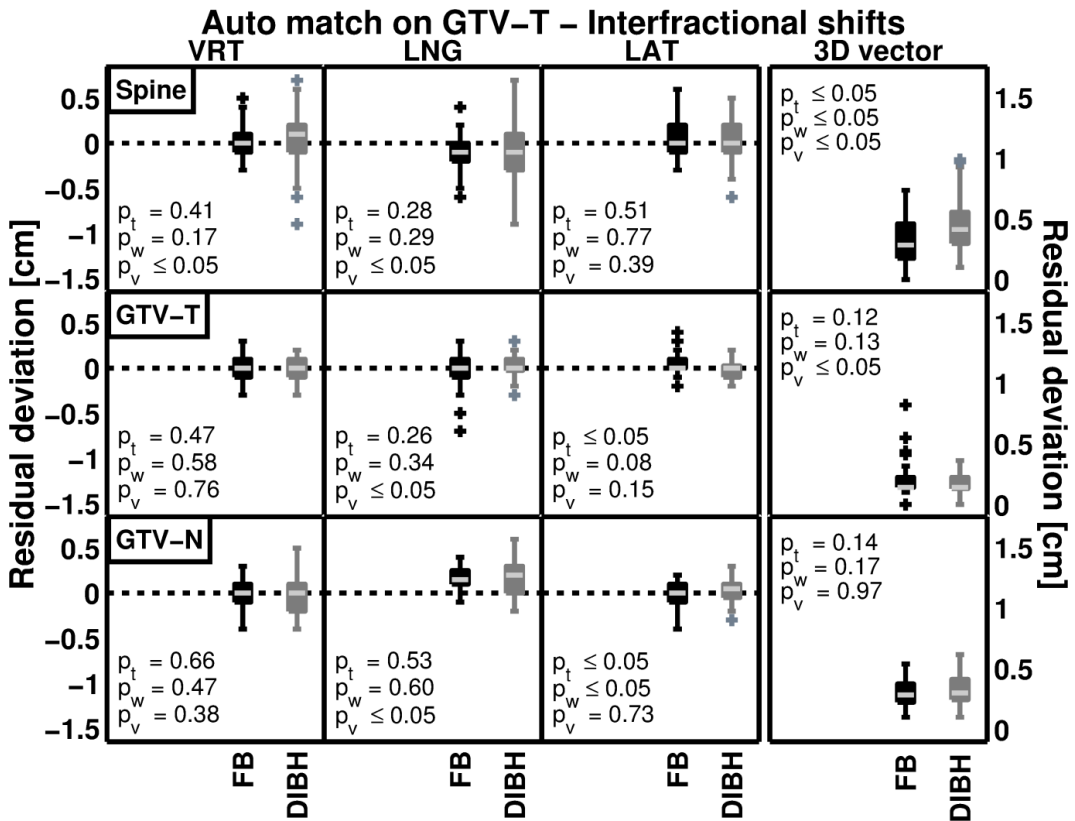
Figure 28. The interfractional residual deviations after auto match on the GTV-T for FB and DIBH in the VRT, LNG, and LAT directions, including the corresponding 3D-vectors. The first, second and third line of subplots represent the translational shifts when performing manual match on the spine, GTV-T, and GTV-N (or lymph node surrogates when the lymph nodes were not visible), respectively. Additional figure explanations are described in supplementary Figure 26.
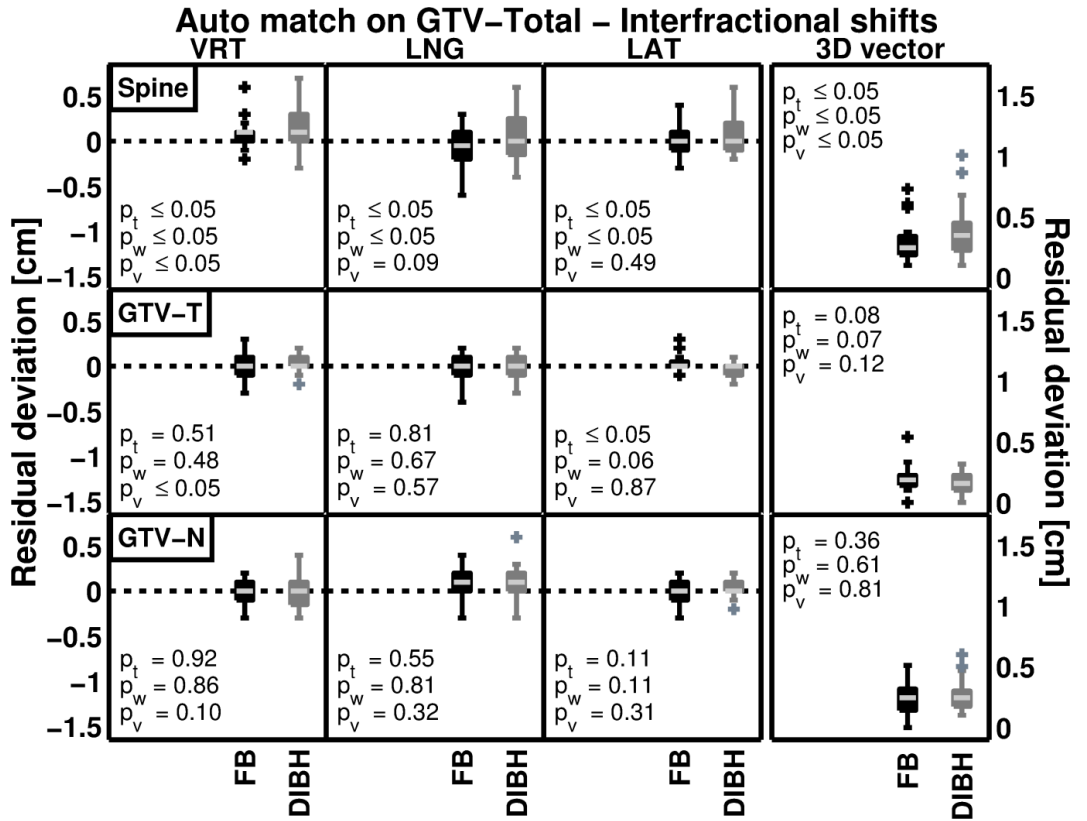
Figure 29. The inter-fractional residual deviations after auto match on the GTV-Total for FB and DIBH in the VRT, LNG, and LAT directions, including the corresponding 3D-vectors. The first, second and third line of subplots represent the translational shifts when performing manual match on the spine, GTV-T, and GTV-N (or lymph node surrogates when the lymph nodes were not visible), respectively. Additional figure explanations are described in supplementary Figure 26.

9.10 Supplementary tables

Table 10. Summary of patient characteristics.

Patient characteristics	Number of patients (%) or median (min;max)
Median Age	62 (48;75)
Gender	
Male	13 (76%)
Female	4 (24%)
Performance Status	
0	16 (94%)
1	1 (6%)
Differentiating grade	
Adenocarcinoma	9 (53%)
Planocellular carcinoma	7 (41%)
Larce cell neuroendocrine carcinoma	1 (6%)
T-stage	
1	1 (6%)
2	4 (24%)
3	6 (35%)
4	6 (35%)
N-stage	
0	2 (12%)
1	3 (18%)
2	8 (47%)
3	4 (24%)
M-stage	
0	17 (100%)
Tumor Location	
Upper lobe	13 (76%)
Middle/lower lobe	4 (24%)
Primary tumor site	
Central	10 (59%)
Peripheral	2 (12%)
Chest wall	4 (24%)
Central/Chest wall	1 (6%)
Mediastinal involvement	
Tumor	1 (6%)
Lymph node	5 (29%)
Tumor and lymph node	9 (53%)
No involvement	2 (12%)

Table 11. The intra- and inter-fractional motion of the spine, GTVT-T and GTV-N for FB and DIBH. Bold style indicates that one breathing technique is statistically significant (p ≤ 0.05) superior to the other breathing technique in terms of the smallest mean, median or standard deviation (SD). Corresponding significance in mean, median and variance for the 3D-vectors are indicated by italic, underline and bold styles, respectively.

	Manual match on Spine [mm]						Manual match on GTV-T [mm]						Manual match on GTV-N [mm]					
	FB			DIBH			FB			DIBH			FB			DIBH		
	VRT	LNG	LAT	VRT	LNG	LAT	VRT	LNG	LAT	VRT	LNG	LAT	VRT	LNG	LAT	VRT	LNG	LAT
Intra-fractional motion - Manual match on Spine, GTV-T, GTV-N, respectively																		
Mean	0.0	-0.2	0.2	-0.2	-0.6	0.0	**0.2**	-0.4	0.2	0.7	-0.3	0.0	0.6	-0.8	0.1	0.7	-0.6	0.0
Median	0.0	0.0	0.0	0.0	0.0	0.0	**0.0**	-1.0	0.0	1.0	0.0	0.0	0.0	-1.0	0.0	1.0	-1.0	0.0
SD	**1.2**	**0.8**	**0.9**	1.6	2.5	1.3	1.4	**1.6**	**1.0**	1.7	2.2	1.3	**1.1**	**1.2**	1.0	1.6	2.3	1.2
|Max shift|	7.0	3.0	2.0	8.0	12.0	4.0	4.0	5.0	3.0	4.0	5.0	4.0	4.0	3.0	2.0	4.0	4.0	4.0
3D-vector (SD)	*<u>1.4 (1.0)</u>*			1.7 (2.3)			*<u>1.9 (1.0)</u>*			2.8 (1.3)			*<u>2.0 (0.8)</u>*			2.8 (1.3)		
|Max 3D-shift|	7.1			12.9			5.4			5.7			4.5			6.0		
GM	-0.1	-0.1	0.1	-0.2	-0.4	0.0	0.3	0.0	0.2	0.7	-0.3	0.0	0.7	-0.6	0.1	0.7	-1.0	0.1
Σ_{Intra}[a]	0.8	0.5	0.5	0.7	1.6	0.6	0.7	1.4	0.6	0.9	1.2	0.8	0.6	0.7	0.5	0.5	1.6	0.7
σ_{Intra}[b]	1.0	0.8	0.9	1.5	1.8	1.2	1.3	1.3	1.1	1.5	1.8	1.1	1.1	1.1	0.9	1.9	1.8	1.0
Inter-fractional motion - Auto match on Spine																		
Mean	0.1	-0.3	-0.2	0.2	-0.8	-0.1	-0.2	0.8	-0.6	-0.4	0.2	-0.7	-1.0	1.7	**-0.1**	-1.7	**-0.4**	-0.6
Median	0.0	0.0	0.0	0.0	0.0	0.0	0.0	1.0	0.0	0.0	0.0	-1.0	-1.0	2.0	0.0	-1.0	**0.0**	0.0
SD	**0.6**	**0.7**	0.6	0.8	2.6	1.3	**1.8**	**2.3**	1.9	2.6	3.8	1.8	1.9	**2.0**	1.5	2.2	3.0	1.5
|Max shift|	2.0	2.0	2.0	3.0	9.0	2.0	4.0	8.0	7.0	6.0	15.0	5.0	9.0	7.0	4.0	8.0	12.0	4.0
3D-vector (SD)	*<u>1.0 (0.7)</u>*			1.0 (2.2)			*<u>3.2 (1.6)</u>*			4.1 (2.5)			3.0 (1.9)			3.4 (2.4)		
|Max 3D-shift|	2.2			9.3			8.5			16.2			10.3			14.4		
GM	0.2	-0.4	-0.1	0.3	-0.8	-0.1	-0.1	0.3	-0.6	-0.5	0.0	-0.7	-1.1	1.5	-0.2	-1.7	-0.2	-0.5
Σ_{Inter}[a]	0.5	0.3	0.4	0.5	1.7	0.5	1.6	2.7	1.7	1.9	2.1	1.5	1.0	1.4	1.2	1.1	1.8	1.3
σ_{Inter}[b]	0.5	0.7	0.6	0.8	2.1	0.5	1.1	1.5	1.1	1.7	3.2	0.9	1.7	1.5	1.3	2.1	2.5	0.9
Margin[c]	1.5	1.1	1.4	1.5	5.2	1.4	7.8	10.9	8.3	8.9	10.3	7.7	6.6	7.5	7.0	7.0	9.0	7.1
Total margin[d]	2.7	1.9	2.1	2.9	7.2	2.5	8.3	11.7	8.6	9.7	11.4	8.3	7.1	8.3	7.8	7.8	10.7	7.7
Inter-fractional motion - Auto match on GTV-T																		
Mean	0.3	-1.1	0.7	0.5	-0.8	0.6	0.1	-0.1	0.3	-0.1	0.2	**0.0**	-0.1	1.6	**-0.2**	-0.2	1.4	0.3
Median	0.0	-1.0	0.0	1.0	-1.0	0.0	0.0	0.0	0.0	0.0	0.0	0.0	0.0	1.5	**0.0**	0.0	2.0	0.5
SD	**1.7**	**2.0**	2.1	2.6	3.3	2.3	1.1	1.6	1.1	1.1	**1.2**	0.9	1.8	**1.4**	1.5	2.1	2.1	1.4
|Max shift|	5.0	6.0	6.0	9.0	9.0	6.0	3.0	7.0	4.0	3.0	3.0	2.0	4.0	4.0	4.0	5.0	6.0	3.0
3D-vector (SD)	*<u>2.8 (1.7)</u>*			4.1 (2.2)			1.4 (1.2)			**1.4 (0.9)**			2.8 (1.2)			3.0 (1.2)		
|Max 3D-shift|	7.4			9.9			8.2			3.6			5.4			6.2		
GM	0.3	-0.9	0.6	0.5	-0.5	0.7	0.0	-0.3	0.1	-0.2	0.2	0.0	-0.3	1.5	-0.3	-0.2	1.7	0.4
Σ_{Inter}[a]	1.5	1.7	1.9	1.9	2.5	2.0	0.8	1.5	0.9	1.0	0.9	0.5	1.4	0.9	1.4	1.5	1.5	1.1
σ_{Inter}[b]	1.3	1.4	1.0	1.7	2.3	1.0	0.9	1.2	0.9	1.0	1.0	0.8	1.3	1.3	1.2	1.6	1.6	1.1
Margin[c]	4.3	4.9	5.2	5.5	7.4	5.4	6.0	7.8	6.2	6.3	6.2	5.1	7.5	6.3	7.5	8.0	8.1	6.6
Total margin[d]	4.8	5.2	5.5	6.1	8.9	5.9	6.7	8.9	6.6	7.5	8.0	6.3	7.9	7.3	8.1	8.6	9.9	7.3
Inter-fractional motion - Auto match on GTV-Total																		
Mean	**0.8**	-0.5	**-0.1**	1.6	0.5	0.7	-0.1	-0.3	**0.2**	0.1	-0.2	*-0.3*	-0.2	1.1	-0.2	-0.2	0.9	0.1
Median	**1.0**	-0.5	**0.0**	1.0	**0.0**	0.0	0.0	0.0	0.0	0.0	0.0	0.0	0.0	1.0	0.0	0.0	1.0	0.0
SD	**1.4**	2.0	1.6	2.2	2.6	1.8	1.4	1.5	0.9	**0.9**	1.3	0.8	1.3	1.6	1.3	1.8	1.8	1.1
|Max shift|	6.0	6.0	4.0	7.0	6.0	6.0	3.0	4.0	3.0	2.0	3.0	2.0	3.0	4.0	3.0	4.0	6.0	2.0
3D-vector (SD)	*<u>2.5 (1.4)</u>*			3.5 (2.1)			1.9 (0.9)			1.6 (0.7)			2.5 (1.1)			2.5 (1.1)		
|Max 3D-shift|	7.3			10.1			5.4			3.2			5.1			6.0		
GM	0.6	-1.0	0.0	1.6	0.4	0.6	0.0	-0.6	0.3	0.0	-0.5	-0.3	-0.4	0.7	-0.1	-0.2	0.9	0.2
Σ_{Inter}[a]	1.1	1.6	1.2	1.2	1.8	1.4	1.1	1.3	0.8	0.6	1.0	0.6	1.0	1.6	0.9	1.4	1.2	0.8
σ_{Inter}[b]	1.1	1.4	1.9	1.9	2.2	1.3	1.1	1.2	0.8	0.8	1.1	0.6	1.0	1.1	1.0	1.2	1.6	0.7
Margin[c]	3.3	4.8	4.0	4.0	5.6	4.2	6.6	7.3	5.9	5.4	6.3	5.3	6.4	7.9	6.1	7.4	7.1	5.8
Total margin[d]	4.0	5.0	4.3	4.7	7.5	4.8	7.3	8.6	6.4	6.9	8.1	6.4	6.9	8.6	7.1	8.1	9.3	6.6

FB, free-breathing; DIBH, deep-inspiration breath-hold; SD, standard deviation; GM, the overall group mean; VRT, vertical; LNG, longitudinal; LAT, lateral. [a] The systematic error component. [b] The random error component. [c] The calculated margins excluding the intra-fractional motion. The PRV margin of the spine is calculated according to [18], and the CTV to PTV margins for GTV-T and GTV-N are calculated according to [15,16], using the penumbra factor $\sigma_p = 0.64$ cm. [d] The calculated margins including the contribution from intra-fractional motion.

Table 12. Time measurements for the different treatment processes. For DIBH, please note the extra DIBH training session (scheduled for 1 h prior the planning CT scan). For the FB 4DCT imaging please note the prolonged processes of CT reconstruction, import and fusion, and GTV delineation.

Process	FB [minutes]				DIBH [minutes]			
	Median	SD	Min	Max	Median	SD	Min	Max
DIBH training session	NaN	NaN	NaN	NaN	51	9.6	38	66
CT scan	10	4.2	4	19	10	4.1	4	24
CT reconstruction	20	14.7	7	63	5	4.2	2	18
CT import and PET fusion [a]	49	16.9	20	90	NaN	NaN	NaN	NaN
Delineation GTV	20	10.3	5	64	9	4.8	2	29
Delineation CTV/PTV	5	5.3	1	27	4	3.2	1	18
Delineation OARs	13	3.4	8	22	15	4.2	7	24
Delineation Total	48	15.3	26	106	36	9.8	23	69
Treatment planning	60	23.6	25	120	60	21.3	25	100
CBCT imaging session [b]	5	1.9	2	13	5	2.2	1	13
DIBH CBCT acquisition [c]	NaN	NaN	NaN	NaN	2.1	1.4	1.1	11.5
Number of breath-holds, [#]	NaN	NaN	NaN	NaN	2	1.6	1	11
First DIBH CBCT session	NaN	NaN	NaN	NaN	11	3.8	5	18

[a.] Estimated time for the corresponding DIBH import and PET fusion process is 10 minutes. [b.] The time to initiate, acquire and save the CBCT images. The presented data do not include the duration data for the first DIBH CBCT acquired, because that session is prolonged due to set-up of reference breath-hold levels. That data is instead presented under "First DIBH CBCT session". [c.] The total beam-on time was about 1 min for both FB and DIBH CBCTs since the same image protocol was applied. The pro-longed time to acquire the DIBH CBCT images was due to the number of breath-holds that were required to complete a full CBCT scan.

10 Paper III

Monte Carlo calculations support organ sparing in Deep-Inspiration Breath-Hold intensity-modulated radiotherapy for locally advanced lung cancer

Paper III is submitted to the scientific journal Radiotherapy & Oncology, and is under review process at the moment. MC simulations were carried out to assess the potential dosimetric benefits of DIBH compared to FB for volumetric-modulated-arc-therapy (VMAT) and IMRT for locally advanced lung cancer. Comparison against a commercial, less accurate, dose calculation algorithm (AAA) was carried out.

Paper III

Monte Carlo calculations support organ sparing in Deep-Inspiration Breath-Hold intensity-modulated radiotherapy for locally advanced lung cancer

Wiviann Ottosson[1,2], Patrik Sibolt[1,2], Christina Larsen[2], Jon A Lykkegaard Andersen[3], Svetlana Borissova[3], Anders Mellemgaard[3], and Claus F Behrens[2]

[1]Center for Nuclear Technologies, Technical University of Denmark, DTU Risø Campus, DK-4000 Roskilde, Denmark
[2]Department of Oncology, Radiotherapy Research Unit, Herlev Hospital, University of Copenhagen, DK-2730 Herlev, Denmark
[3]Department of Oncology, Herlev Hospital, University of Copenhagen, DK-2730 Herlev, Denmark

E-mail: wiot@dtu.dk

Short running title: DIBH radiotherapy for lung cancer patients
Key words: Lung cancer, DIBH, Monte Carlo, Treatment planning, VMAT, IMRT

Abstract

Background and Purpose: Studies indicate that deep-inspiration-breath-hold (DIBH) is advantageous over free-breathing (FB) for locally advanced lung cancer radiotherapy. However, these studies were based on simplified dose calculation algorithms, potentially critical due to the heterogeneous nature of the lung region. Using detailed Monte Carlo (MC) simulations, a comparative study of DIBH vs. FB was therefore designed.

Material and Methods: Eighteen locally advanced lung cancer patients underwent FB and DIBH CT imaging and treatment planning with the Anisotropic-Analytical-Algorithm (AAA) for intensity-modulated radiotherapy or volumetric-modulated-arc-therapy using 66 Gy in 33 fractions. All plans were re-calculated with MC.

Results: Relative to FB, the total lung volume increased 86.8% in DIBH, while the gross tumor volume decreased 14.8%. MC revealed equally under- and over-dosage of the target for FB and DIBH, compared to AAA. For the organs-at-risk (OARs), DIBH reduced the mean heart dose by 25.5% (AAA) vs. 12.6% (MC), the total lung V5Gy/V20Gy by 9.0/20.0% (AAA) vs. 11.6/19.9% (MC).

Conclusions: The MC simulations revealed (i) that DIBH compared with FB can significantly reduce the dose to the OARs even if the treatment planning is carried out with AAA, and (ii) that AAA-based treatment plans resulted in inferior target dose coverage. Target dose deviations were similar for FB and DIBH. Therefore, issue (ii) relates to the treatment planning algorithm rather than treatment technique.

10.1   Introduction

Respiratory motion is a challenge during radiotherapy of non-small-cell lung cancer (NSCLC) patients. Deep-inspiration-breath-hold (DIBH) is a method to diminish the uncertainty of breathing motion during radiotherapy for both lung, breast and Hodgkin lymphoma [101,102,110,117]. During DIBH, the lung is inflated, and the density of the lung parenchyma decreases, while the heart moves toward the back of the thorax, where the shape of the heart is affected of the inflated lungs. For some DIBH cases, the gross tumor volume (GTV) can be displaced away from the radiosensitive spinal cord [110]. DIBH is a treatment method which may enable use of smaller treatment fields due to less tumor motion, consequently reducing dose to the adjacent healthy tissues and organs at risk (OARs).

Lung cancer GTVs are often situated in a region of large tissue heterogeneity where the accuracy of the dose calculation algorithm is critical to a precise evaluation of target dose coverage. Monte Carlo (MC) dose simulations are able to simulate all ionization interactions present in a patient. The disadvantage with MC is the large computation time because of the many interaction histories required. Most commercial dose calculation algorithms utilize approximations to limit the computation time. Many commercial algorithms have issues to correctly account for changes of lateral electron scatter [88–90]. The dose calculation accuracy is thereby affected negatively, and not comparable with MC in heterogeneous geometries. The largest inaccuracies are usually noticed in the transition between materials of different densities. Lateral charged particle disequilibrium will be emphasized during DIBH, since the lung density decreases. The range of secondary electrons will increase resulting in a larger volume of disequilibrium and a broader penumbra at field boundaries [102,103].

The clinical benefit of DIBH for lung cancer patients have previously been evaluated in studies based on simple field technique and simplified calculation algorithms [118–122]. Due to the high amount of heterogeneities present in the lung region, there are limitations to these studies. Still, there are some studies presenting MC simulations [91,102–104,123,124] and measurement data [88,92] for lung treatments. Most of these studies investigate conventional treatment techniques with static fields, and did not investigate the potential benefits of DIBH. However, the MC study by Wang et al. [123] presented a dosimetric evaluation for 5 lung cancer patients treated with intensity modulated radiotherapy (IMRT), where one patient was treated with end-inspiration gating. They did however not assess the potential benefit of DIBH for this more complex treatment technique. This current study, including 18 patients, is the first DIBH MC study designed to obtain accurate assessment of the potential benefits of DIBH compared to free-breathing (FB) for volumetric-modulated-arc-therapy (VMAT) and IMRT for locally advanced lung cancer. For this purpose, VMAT and IMRT treatment plans produced in a convolution-superposition based treatment planning system (TPS) were re-calculated using MC, comparing DIBH with FB.

10.2 Material and methods

10.2.1 Patient data

Eighteen locally advanced NSCLC patients scheduled for curative radiotherapy at Herlev Hospital, between December 2012 and July 2014, were enrolled. The patients were treated in FB with VMAT or IMRT in 33 fractions (fx), receiving a total dose of 66 Gy (2 Gy/fx, 5 fx/week). The treatments were delivered using Varian Clinac iX 2300 linear accelerators [21,85] (Varian Medical Systems, Palo Alto, CA) equipped with On-Board Imagers (OBI) capable of performing FB and DIBH CBCT, using version 1.5 of the OBI software. Table 13 summarizes the patient characteristics.

10.2.2 Ethical considerations

The clinical protocol was approved by the Copenhagen Regional Committee on Health Research Ethics (protocol no. H-4-2012-066) and the Danish Data Protection Agency (ID. nr: 2007-58-0015 / HEH.750.24-61). Every patient gave informed consent prior to inclusion.

10.2.3 Image acquisition

Prior to planning imaging, all patients were introduced during a 30 minute training session to the DIBH procedure by a radiotherapist (RTT). The Varian real-time position management (RPM) system, version 1.7 (Varian Medical Systems), integrated with the CT imaging system, was utilized to monitor the patients' respiration [32]. The patients were audio-visually guided during DIBH by using video goggles to achieve a reproducible inspiration level. During the training session, they were required to hold their breath at least 20 seconds at a reproducible patient-specific amplitude level and a gating window of 2-3 mm width.

All images were acquired in treatment position. The CT image protocol and details about the delineation of anatomical structures have previously been described by Ottosson et al. [21,112]. In brief, each patient was dual-CT scanned in a 16 slice Philips Brilliance CT Big Bore scanner, version 3.5.17001 (Philips Medical Systems, Cleveland, OH) (acquiring a 4-dimensional CT (4DCT) in FB and a normal CT in DIBH). Intra-venous contrast was administered to the patients during both 4DCT and DIBH CT imaging, for better contrast of nodal anatomy in the mediastinum. Each image set included the entire lung volume, starting from the top of the sixth cervical vertebrae. From the FB 4DCT an untagged image reconstruction and a maximum intensity projection (MIP) image set were obtained [21]. Each patient was additionally scanned in a GEMINI TF 16 slice Big Bore PET/CT, version 2.3 (Philips Medical Systems) in order to diminish the delineation un-certainties in the CT.

10.2.4 Definition of target and organs at risk

The image sets were imported and co-registered in the Eclipse TPS, version 10 (Varian Medical Systems). Delineations of anatomical structures were performed according to standard protocol by only one experienced oncologist (JLA or SB) on all image sets for that patient [21]. Contouring of the GTVs was performed in collaboration with an experienced radiologist using information from the co-registered MIP and PET/CT images.

The delineated GTV was subsequently verified and corrected in all breathing phases. Residual structures such as the clinical target volume (CTV), the planning target volume (PTV), medulla, heart, esophagus, lung, healthy lung (the opposing lung from where the primary tumor is located) were additionally delineated solely by the oncologist, whereas CT radiographers semi-automatically delineated the body contour.

10.2.5 *Treatment planning process*

All treatment plans were created using the Anisotropic-Analytical-Algorithm (AAA) dose calculation algorithm in Eclipse by one treatment planner (CL), experienced in lung cancer, in order to avoid inter-observer variability in the treatment planning process. Due to an inferior Hounsfield unit (HU) representation, the FB treatment planning was carried out using the untagged CT reconstruction instead of the MIP image set, which solely was utilized for enhanced target delineation. All treatment plans were designed and optimized for PTV dose coverage and dose reduction to the OARs according to an established dose constraint protocol, as follow; The medulla was not allowed to receive more than 45 Gy ($V_{45Gy} = 0\%$). An absorbed dose of 5 Gy was delivered to less than 60% of the total lung volume ($V_{5Gy\,(Total\,lung)} \leq 60\%$), and to less than 40% of the healthy lung volume ($V_{5Gy\,(Healthy\,lung)} \leq 40\%$). Concurrently, 20 Gy was delivered to less than 35% of the total lung volume ($V_{20Gy} \leq 35\%$), or if that was not possible, the mean dose of the total lung volume was not to exceed 20 Gy (MLD $\leq$ 20 Gy). In a similar way, 50 Gy was delivered to a maximum of 20% of the heart volume ($V_{50Gy} \leq 20\%$), and the mean dose of the heart volume was to be less than 46 Gy (MHD $\leq$ 46 Gy). For the esophagus, 55 Gy was delivered to no more than 30% of the volume ($V_{55Gy} \leq 30\%$), with a maximum dose of 66 Gy ($V_{66Gy} = 0\%$), and the mean dose of the esophagus was to be no more than 34 Gy. In addition to the dose constraints for the OARs there were requirements on the target dose coverage, in order to achieve a clinically acceptable treatment plan. At least 95% of the prescribed dose was to be delivered to 98% of the PTV ($D_{98\%} \geq 95\%$). It is often difficult to comply with the dose coverage constraint because of the heterogeneities in the lung region. Therefore, if the soft-tissue tumor was embedded in lung-tissue, it was acceptable that 98% of the PTV only was covered by 90% of the prescription dose. An overdosage of up to 107% was allowed to 2% of the PTV ($D_{2\%} \leq 107\%$), but the maximum absorbed dose was to be less than 110% ($D_{max} \leq 110\%$). GTV and CTV dose constraints are additionally implemented, where at least 95% of the prescribed dose was to cover 99% of the GTV and CTV, ($D_{99\%} \geq 95\%$).

In this study only 6 MV photon beams were considered, since higher energy photon beams can compromise target coverage due to more pronounced lateral charged particle disequilibrium [83,102–104]. The treatment planner aimed to construct clinically acceptable VMAT plans for all image sets in FB and DIBH. However for three image sets (both FB and DIBH for one patient, and only FB for another patient) it was not achievable and comparative IMRT plans in terms of target dose coverage and preservation of the dose constraints were produced. The VMAT treatment plans were created by partial dual-arcs avoiding initial entrance dose through the healthy lung, medulla and the heart. The IMRT treatment plans were designed in a similar way, consisting of a 5- or 6-field beam arrangement. The beam and arc arrangements between FB and DIBH were for the most parts the same for the same patient. However, some adjustments of beam angle, field weights and apertures were made to achieve clinically acceptable plans.

The measurement-based AAA dose calculation algorithm, utilized in this study for the commercial TPS, has previously been described extensively [88–92]. The AAA algorithm is a three source pencil-beam convolution-superposition model, where the primary and secondary photons and the contamination electrons are individually calculated for each beamlet. The dose contributions from all sources are subsequently superpositioned to the final dose distribution, where the heterogeneity correction only is carried during the super-position phase by a modified Batho heterogeneity correction [88]. The most important approximation of AAA is that the energy deposition is divided into two components, the first component models the photon interactions along the fanline, and the second component models the scatter perpendicular to the fanline as a sum of six radial exponential functions for a discrete number of angular sectors [88–90]. Thus, the two component approximation does not take the divergent scatter of heterogeneities from upper levels correctly into account. The depth and lateral components are anisotropically scaled independently according to the electron density distribution of the medium. Additionally, the approximation of using a discrete number of angular sections for the radial exponential functions cause smoothing of the calculated dose distribution near heterogeneous interfaces [88,89].

10.2.6 Monte Carlo simulations

All treatment plans were subsequently re-calculated using MC, with preserved monitor units and beam configurations, as were used for the commercial AAA algorithm. The MC simulations can provide dose distributions where heterogeneities are more correctly accounted for since the anatomy, including the electron density information, is obtained from each patient's CT image set.

The building and commissioning of a Varian 2300 iX linear accelerator (Varian Medical Systems, Palo Alto, CA, USA) model, as well as the procedure of MC simulation have previously been described by Ottosson et al. [104]. In short, EGSnrc was used as the engine for BEAMnrc, which was utilized to build and commission the MC model [125–127]. The model was tuned to correlate with reference measurements carried out in a homogenous water phantom [104]. The MC simulations of absorbed dose to the patients were carried out by the use of DOSXYZnrc. Voxalized MC phantoms were created via the CTC-ask conversion algorithm using each patient's planning CT and DICOM structure set as input [128]. The voxel sizes were expanded to match the CT scan grid. Backscatter corrections were simulated for each field using the formalism described by Popescu et al.[129]. This correction has further been verified by Sibolt et al. [130]. A set of in-house MATLAB scripts were used to generate input files from each patient's DICOM RP files. These generated input files together with the voxalized phantom and the BEAMnrc-simulated phase space files were used to simulate the absorbed dose to each patient in DOSXYZnrc. The selected number of simulated histories (2×10^8 - 4×10^8 histories) resulted in an estimated statistical uncertainty of about 1% (ranging between 0.57% and 1.23%) in the high dose area. All absorbed doses were reported as dose-to-water, to mimic the reported absorbed doses in the TPS. The procedure described by Siebers et al. [94] to convert MC simulated dose-to-media into dose-to-water was employed. The resulting 3D dose distributions were converted into DICOM RD files using CERR [131] and subsequently imported into the Eclipse TPS to generate dose volume histograms (DVHs).

10.2.7   Data analysis

Dose characteristics and volume data for the GTV, CTV, PTV, total lung, healthy lung, medulla, and esophagus were extracted for FB and DIBH treatment plans calculated with AAA and MC. The conformity index (CI), the lesion coverage fraction (LCF), and the normal tissue overdosage fraction (NTOF) were additionally calculated for the 95% isodose according to Van Esch et al. [78]. These indexes can be utilized to evaluate the quality of the treatment plan in terms of target dose coverage and spread of high dose to adjacent healthy tissue. In brief, the CI_{95} is defined as the 95% isodose volume relative to the size of PTV. The LCF_{95} measures the fraction of PTV that is covered by the 95% isodose volume, i.e. a measure for target underdosage. The $NTOF_{95}$ measures in a similar way the fraction of the 95% isodose volume that is outside the PTV. Thus, NTOF is a method to quantify the relative amount of high dose (i.e. in our case dose over 95% of the prescribed dose) delivered outside of the PTV. Ideal target coverage is characterized by a CI and LCF close to unity, and a NTOF approaching zero. CI assesses only the relative size of the isodose volume without respect to target location. The LCF and NTOF allows for more detailed quality quantification. Patient-specific paired percentage differences between FB and DIBH for the both calculation algorithms were calculated for each patient, and for all investigated dose characteristics and treatment plan quality indexes.

For statistical analysis MATLAB including the Statistics Toolbox version 8.3 (R2013b) (The MathWorks, Natick, MA) was utilized. Wilcoxon signed rank test for non-parametric paired data was carried out to compare the medians of the data sets. The results were considered statistically significant for $p < 0.05$.

10.3   Results

All patients complied with the gating technique and were able to hold their breath within their patient-specific gating window and amplitude level long enough to acquire a full DIBH CT image. The median and range of the gating amplitude levels, breath-hold times to acquire the DIBH CT images, and CT beam-on times to acquire the DIBH CT images were 14.3 mm (10.5; 25.3) mm, 16.4 s (13.3; 19.3) s, and 10 s (9.0; 11.9) s, which resulted in a median duty cycle of 61.1%.

10.3.1   Dose volume histogram

On the left hand side of Figure 30 each patient's cumulative DVH simulated by MC for FB and DIBH is illustrated. Compared to DIBH treatment plans, a larger amount of FB treatment plans did not comply with the applied dose constraints indicated by the black markers in the figure, especially for the total lung and esophagus.

On the right hand side of Figure 30 the median of the MC and corresponding AAA calculated DVHs are presented. The MC simulations reveal considerable under- and over-dosage of the planning target volume compared to AAA. For the OARs, a larger amount of low dose is delivered in the MC simulated treatment plans compared to AAA, especially for the OARs closely situated to the low-density lung-tissue. Hence, this is not observed for the medulla at low doses. On the contrary, the volume of medulla receiving high dose is increased for the MC simulations, where the maximum dose increased by 10% in MC compared to AAA (Figure 30, Table 14).

10.3.2   Organs at risk

The presented volume and DVH data in Table 14 are the median values and ranges or standard deviations (SDs) of the paired data for all 18 patients. The paired volume and dose constraint data of the OARs for each patient are additionally illustrated in Figure 31.

The MC simulations imply that the doses to all the OARs are higher in reality compared to the doses calculated by AAA (Figure 31, Table 14), applicable for both FB and DIBH. Paired statistically significant differences between the AAA and MC algorithms were observed for all dose constraints of the OARs (Table 14). Compared to AAA, the largest increases in delivered mean and maximum doses were observed for the heart. The MHD and maximum heart doses increased in median about 31% and 17%, respectively in FB, and 46% and 48%, respectively in DIBH, for the MC simulated treatment plans, compared to AAA.

In favor of DIBH, statistically significant differences in volume and delivered doses (for both AAA and MC calculations) between FB and DIBH were obtained for all OARs (except the healthy lung and the esophagus) (Table 14, Figure 31). In DIBH, the total lung volume increased substantially for all patients, by a median increment of 86.8% (37.1; 167.5)%. This caused the MLD to reduce in median by 18.1% (4.5; 39.3)% (MC) and 20.4% (2.9; 41.8)% (AAA). DIBH additionally reduced the total lung V_{20Gy} in median by 19.9% (4.7; 43.1)% (MC), which was comparable with the AAA calculations, 20.0% (4.8; 44.3)%. For the V_{5Gy} constraint (which is a measure for the low dose bath in a treatment plan) there was a larger reduction during DIBH for the MC simulations, 11.6% (-11.2; 25.9)%, compared to the AAA calculations, 9.0% (-14.4; 26.4)%. An example of large increment in total lung volume is presented for patient 7 in Figure 32. Various blurry motion image artifacts are clearly observed in the FB image set, especially in the diaphragm area, while the density of the lung parenchyma has been decreased and the tumor edges has become clearer in the DIBH image set.

10.3.3   Target coverage

The paired dose constraint data of the target dose coverage for each patient is illustrated in Figure 33. No statistically significant difference between FB and DIBH data was found in terms of dose coverage constraints of GTV, CTV, and PTV (Table 14, Figure 33) (except for the maximum dose delivered to the PTV, where DIBH resulted in higher maximum dose), applicable for both AAA and MC. Similarly, no statistically significant difference was discovered between FB and DIBH for the treatment plan quality indexes; CI, LCF, and NTOF (except for the LCF (which is a measure of the target underdosage) simulated by MC, where DIBH resulted in about 1% lower LCF, compared to FB).

The MC simulations indicate statistically significant under- and overdosage of the GTVs, CTVs, and PTVs compared to the AAA calculations (Table 14, Figure 33). This was additionally identified by the LCF index, where the MC simulated treatment plans in median were about 1% lower compared to AAA treatment plans, independent of breathing technique (Table 14). The NTOF index (which is a measure for high dose overdosage outside of the PTV) did not indicate any difference in overdosing outside of PTV, neither between FB and DIBH or between AAA and MC treatment plans. The maximum dose and $D_{2\%}$ of the PTV simulated by MC were similar for FB and DIBH, and were in median

about 8% and 4% higher, compared to AAA calculations (Figure 33, Table 14). On the contrary, the MC simulated minimum doses of the PTV were in median 9.1% (3.2; 31.5)% lower in FB, and 12.0% (4.8; 18.8)% lower in DIBH, compared to AAA (Figure 33, Table 14). The $D_{98\%}$ was, regardless of FB or DIBH, about 3.5% lower in median for MC, compared to AAA calculations (Figure 33, Table 14). Similarly, the MC simulated $D_{99\%}$ of the GTV and CTV were about 5% lower for AAA calculated treatment plans, independently of FB or DIBH (Figure 33, Table 14).

10.4   Discussion

Breathing adapted radiotherapy can diminish the challenge of respiratory motion in lung cancer radiotherapy. There exist preconceptions about the impracticability to perform DIBH for lung cancer patients due to comorbidities, such as chronic obstructive pulmonary disease (COPD) or poor pulmonary functionality. However, all 18 locally advanced NSCLC patients enrolled in this study complied with the gating technique, and were able to acquire a full DIBH CT image in one single breath-hold.

This study confirms the dosimetric advantage of DIBH, compared to FB, for locally advanced lung cancer patients by MC simulations of complex IMRT and VMAT treatment plans. However in comparison with AAA, the MC simulations revealed considerable under- and overdosage of the target, and higher doses delivered to the OARs, especially a higher maximum dose to the medulla, heart and esophagus (Table 14).

10.4.1   Comparison with other clinical dose calculation studies

In agreement with the study by Giraud et al. [118], the target dose coverage was found to be identical between FB and DIBH. The Giraud study however, applied smaller CTV-PTV margins for the DIBH treatment plans, while those margins were unaltered in the current study. For DIBH, the increased total lung volume of about 87% in median is in accordance with the study by Rosenzweig et al. [119], while Josipovic et al. [122] reports an average lung volume increase of about 60%. All 18 DIBH treatment plans in the current study were well below the $V_{20\%}$ constraint for the total lung volume and in favor of DIBH (Table 14, Figure 30 - Figure 31). The current study indicates a reduction of about 22% for $V_{20\%}$ during DIBH compared to FB, for both AAA and MC calculations (Table 14, Figure 31). The study by Josipovic et al. [122] found a corresponding reduction in $V_{20\%}$ of about 15% for more simple static field techniques. The study by Tahir et al. [121] evaluated moderate inspiration breath-hold gating against expiration gating by a spirometric system. In favor of inspiration, they found a reduction of only 2.5% for the $V_{20\%}$. Their result is due to the smaller lung volume obtained in moderated inspiration breath-hold, compared to DIBH. The MLD of the current study was reduced by 20.4% (AAA) and 18.1% (MC) for complex treatment plans in DIBH (Table 14). The study by Josipovic et al. [122] found that the MLD only was reduced about 16% for their more simple static treatment technique. In comparison with the current study, where the heart volume decreased about 24% during DIBH (Table 14), no significant reductions of the heart volume were reported by Marchand et al. [120]. They did however utilize a spirometric control for the DIBH procedure and treated with conventional static fields. Giraud et al. [118] found significant benefit of DIBH for the esophagus. This observation was not supported in the current

study, which probably was due to the more complex treatment techniques carried out, compared to their study.

The major benefit with DIBH is the possibility to better spare OARs from radiation, compared to FB. The DIBH procedure is however a more resource intensive treatment technique, in terms of requirement of more personnel, longer simulation and treatment times, extra time slots for patient-specific training sessions, etc. It would therefore be advantageous if patients could be sorted prior to treatment planning, identifying those with potential benefit from DIBH-based treatment. Sorting criteria could include patient size and tumor location, tumor size and proximity to other structures, etc. However, this is out of the scope for this study and the subject of future investigations. Nevertheless, the study by Josipovic et al. [132] identified two NSCLC cases that did not benefit from DIBH, and they decided to treat in FB instead. The first patient had two targets situated close to each other, but they separated during DIBH. This resulted in increased PTV, MLD and $V_{20\%}$. The second patient's setup verification cone beam CT revealed inter-fractional variation of the tumor position, despite good reproducibility of the external surrogate breathing signal. Thus, if clinically implementing DIBH, daily soft-tissue visualization and verification of the tumor position in three dimensions is recommended. Additionally, it is most likely necessary to perform dual-treatment planning, in both FB and DIBH, as a treatment backup if the patients' health gets worse during the course of treatment, where they can no longer proceed with DIBH.

10.4.2   Comparison with other Monte Carlo studies

There are several fundamental differences on how the AAA and MC algorithms calculate absorbed dose in the patients. Some affecting factors of the observed differences between AAA and MC may be; (i) the statistical uncertainty of the MC simulations, and (ii) the conversion from dose-to-media to dose-to-water, (iii) both the AAA and MC models are based on measurements carried out using open fields in homogeneous water setups, (iv) the PTVs are situated in critical build-up and build-down areas where the discrepancies between AAA and MC are anticipated to be the largest.

The dosimetric issues with AAA in heterogeneous volumes are clearly illustrated, especially for the low dose areas of the OARs and for the target dose coverage of the PTV (Figure 30). For the target dose coverage, the dose build-up and build-down is not correctly calculated by the AAA algorithm since the target is embedded in, and/or situated close to low-density lung-tissue.

The optimization processes in Eclipse are carried out in several steps. The inverse planning module does not make use of AAA but uses its own simplified dose calculation algorithm, which is faster but less accurate, compared to AAA [88,133]. The final dose distribution is eventually calculated by a more accurate dose calculation algorithm, e.g. in our case AAA. The study by Mihaylov and Siebers [133] conclude that the optimization convergence error from the inverse optimization process could contribute with up to 5% dose prediction errors if changed to a fully integrated MC optimization process for head-and-neck cases. Our posture is that this error could be even larger for lung cancer cases due to the low-density heterogeneous nature of the lung region. Thus, with a fully integrated MC optimization process the sparing of dose to the OARs could be further improved.

However, it is then important to decide whether or not the prescribed dose and the applied dose constraints should remain unaltered. There is a potential risk if implementing MC for clinical use since all clinical survival data and radiation response data are based on less correct dose calculation algorithms. In that case a thorough MC benchmarking process against a less accurate calculation algorithm needs to be conducted.

It was expected that the target dose coverage for the AAA calculations should not deviate between FB and DIBH, since each treatment plan was designed and optimized to be clinically acceptable in terms of target dose coverage. Thus, did not the median PTV dose decrease as the lung density decreased, contradictory to the study by Aarup et al. [91]. Additionally, compared to FB, there was no statistically significant difference in the number of monitor units delivered in DIBH when an identical dose to the tumor was prescribed. One reason for this could be that the same maximum number of monitor units was utilized as a constraint during the optimization processes for both FB and DIBH treatment plans. Yorke et al. [102] states that there should be expected a discrepancy in target dose coverage between FB and DIBH for the MC simulated treatment plans because of the lower electron densities in the CT images for DIBH. This is not supported in the current study, since no statistically significant discrepancy in target dose coverage between FB and DIBH was observed for the MC simulated treatment plans (Table 14, Figure 30, Figure 33) (except for the maximum dose delivered to the PTV, and the LCF for MC). These findings could be related to the more correct convolution-superposition dose calculation algorithm, i.e. AAA, and the more complex treatment techniques, i.e. IMRT and VMAT, utilized in this study compared to the study by Yorke et al. [102]. The simplified pencil beam based algorithm used in their study to generate treatment plans did not take into account the changes of lateral electron scatter in media other than water. Moreover, the MC algorithm does not distinguish between the lung-tissue in the FB and DIBH images, in terms of different interaction cross-sections.

There was however detected noticeable disagreement between MC and AAA target dose coverage, irrespective of breathing technique (Table 14, Figure 30, Figure 33). In accordance with Yorke et al. [102], the current study identified about 3.5% underdosage of the PTV (i.e. $D_{98\%}$ constraint) for the MC simulated dose, where the dose was reduced near the lung/soft-tissue interface. In contrast, they did not identify any overdosage of the PTV, while the current study found about 4% higher $D_{2\%}$ in median for MC, compared to AAA.

Yorke et al. [102] reports no significant difference between MC and standard treatment planning for the lung and spinal cord. This is in accordance with the current study, except for the larger amount of low dose delivered to the OARs in MC compared to AAA (not applicable for the medulla) (Figure 30). VMAT and IMRT treatment plans are more conform but deliver a larger amount of low dose to the patient volume, compared to conventional static treatment planning [122]. Because of the use of VMAT and IMRT and the known calculation problem of low dose scatter in AAA, the issue of extra low dose delivered to the OARs is emphasized in the current study for the MC simulations. It should moreover be pointed out that the MC uncertainties increase for low doses.

In addition, MC yields a broader penumbra, compared to AAA, in low-density tissue where the ranges of secondary electrons increase. This matter is not correctly accounted for in AAA, where largest discrepancies are found at the interfaces between two media of

various densities. This issue is therefore especially reflected in the lower dose delivered at the edges of the PTV situated closely to the low-density lung-tissue (Figure 30). The matter is additionally reflected in the relative larger volume of the OARs receiving an increased amount of low scattered dose, compared to the AAA calculations (Figure 30). This is especially emphasized for the OARs closely situated to the low-density lung-tissue and air-cavities of esophagus, thus not affecting the medulla. Hanley et al. [134] concluded that the broader penumbra had little clinical effect in DIBH, especially if several treatment fields are used, as for IMRT and VMAT.

10.5   Conclusion

Although the IMRT and VMAT treatment plans are created using a simplified convolution-superposition dose calculation algorithm (i.e. AAA), more accurate MC simulations confirms that DIBH is advantageous over FB for locally advanced NSCLC patients, in terms of reducing undesired dose to the OARs, and still keep the target dose coverage unchanged. However, the MC simulated dose distributions revealed inferior target dose coverage, equally in both FB and DIBH, compared to AAA calculated treatment plans. Consequently, this issue is related to the treatment planning algorithm rather than the utilized breathing technique. The treatment planning may be improved if using a fully integrated MC optimization and dose calculation system. Care should however then be taken if clinically implemented, because all clinical radiation response data are based on old, less accurate dose calculation algorithms.
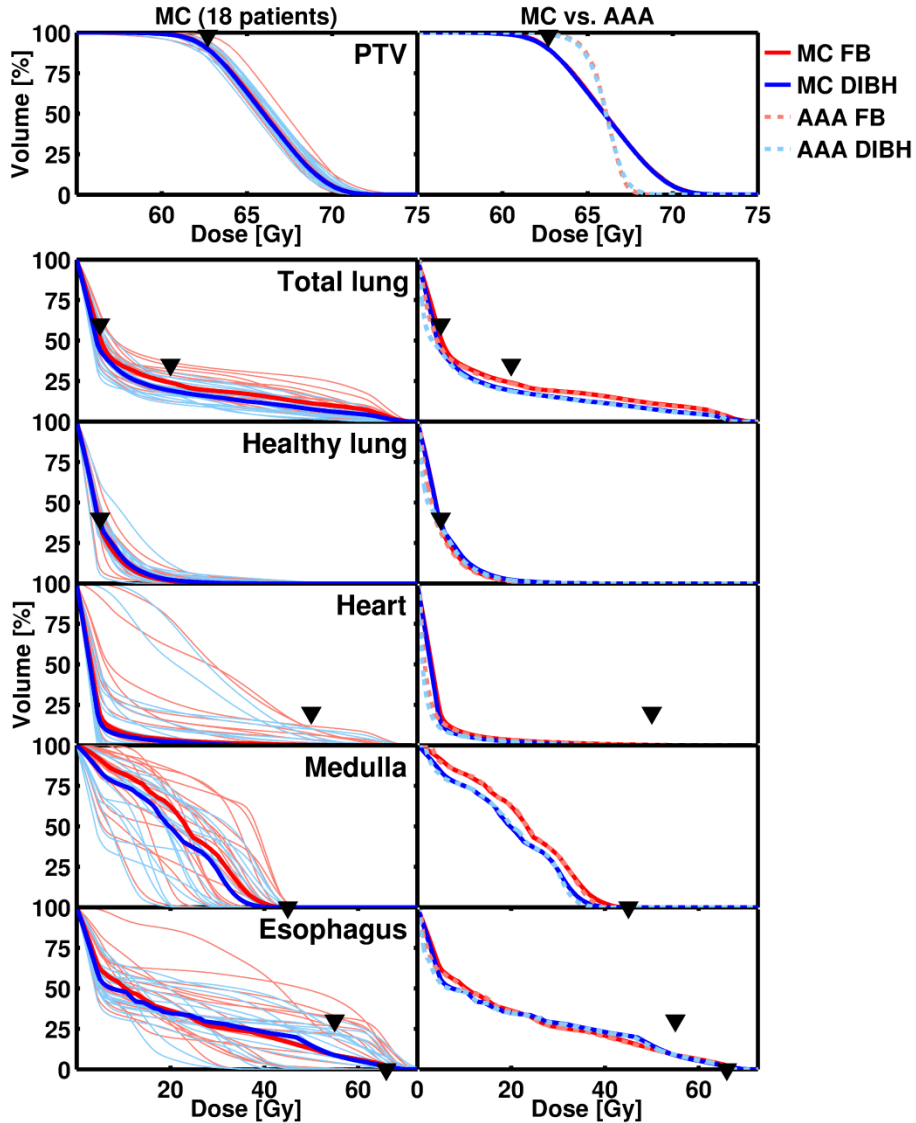
10.6   Figures

Figure 30. The cumulative DVHs for the PTV, total lung, healthy lung, heart, medulla, and esophagus. FB and DIBH are characterized by red and blue colors, respectively. To illustrate the spread of the DVHs for all 18 patients, the DVHs on the left hand side in the figure are only the MC calculated ones. Each thin line represents the MC DVH for one patient, where FB and DIBH DVHs are indicated by light red and light blue colors, respectively. The thick red and blue lines in the figure represent the median MC calculated DVHs of FB and DIBH, respectively. The dashed thick lines depicted in the DVHs on the right hand side in the figure illustrate the corresponding median of the AAA calculated cumulative DVHs. The black markers represent the dose constraint applied for that specific organ during treatment planning. Color version of figure is available online.
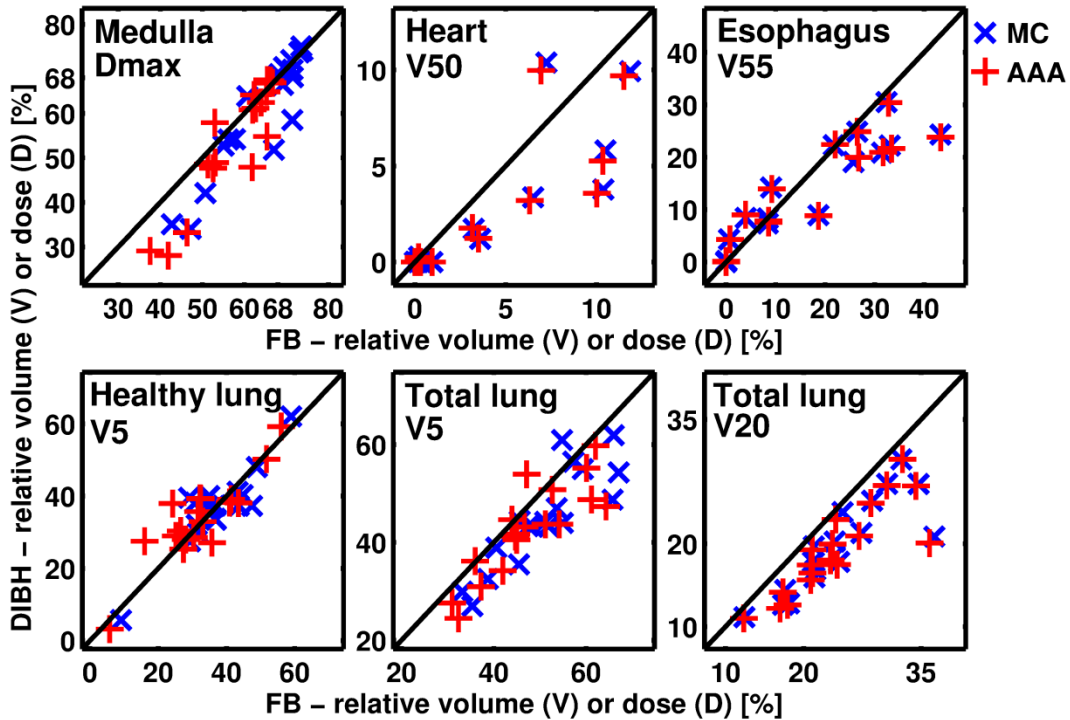
Figure 31. The FB relative to DIBH distributions of the volume and dose constraint for the organs at risk; medulla, heart, esophagus, healthy lung, and total lung for the MC and AAA calculated treatment plans. Each marker represents one patient. If the markers are situated exactly on the black line there is no difference between FB and DIBH doses. DIBH is in favor if the markers are situated below the black line. Correspondingly, FB is in favor if the markers are situated above the black line. A shift between the patients' blue (MC) and red (AAA) markers indicate that there is a calculation difference between the two calculation algorithms. The volume and dose constraints were as follow; Medulla: $D_{max} \leq 45$ Gy = 68.18% (relative dose); Heart: $V_{50Gy} \leq 20\%$ (relative volume); Esophagus: $V_{55Gy} \leq 30\%$; Healthy lung: $V_{5Gy} \leq 40\%$; Total lung: $V_{5Gy} \leq 60\%$ and $V_{20Gy} \leq 35\%$. Markers that are situated at doses higher than these dose constraints are not theoretically clinically acceptable. The MC calculations are considered as golden standard. Color version of figure is available online.
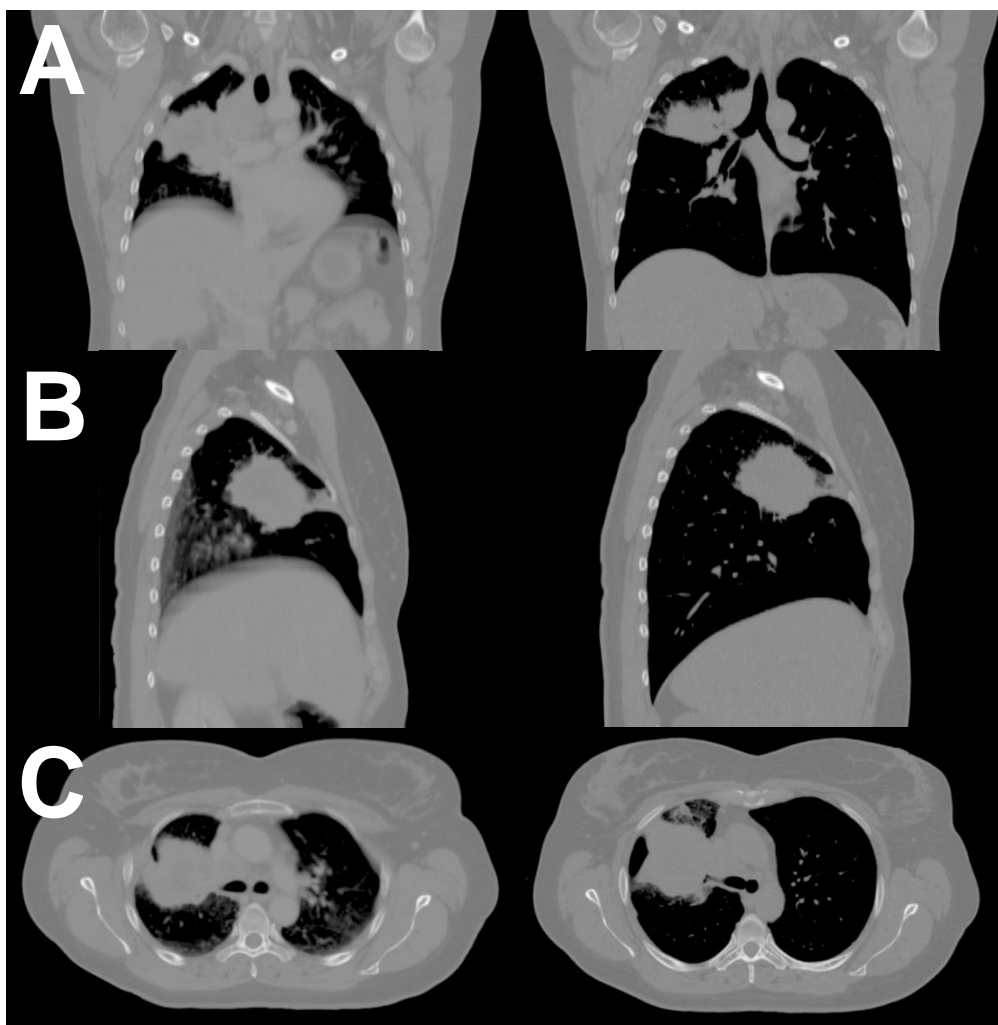
Figure 32. Coronal (A), sagittal (B), and transversal (C) slices of the CT scan for patient number 7. On the left hand side is the FB image set, and on the right hand side is the DIBH image set. For this patient, the total lung volume increased by 167% in DIBH.
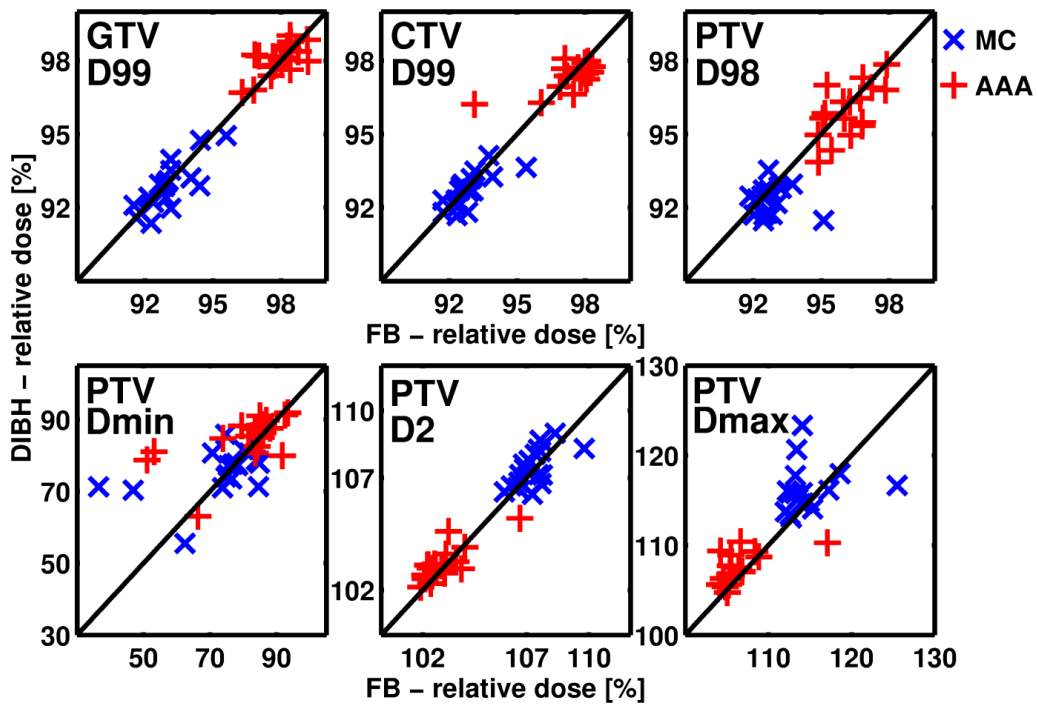
Figure 33. The FB relative to DIBH distributions of the target dose coverage dose constraint of the GTV, CTV, and PTV for the MC and AAA calculated treatment plans. Each marker represents one patient. The dose constraints were as follow; GTV: $D_{99\%} \geq 95\%$ (relative dose); CTV: $D_{99\%} \geq 95\%$; PTV: $D_{98\%} \geq 95\%$; $D_{2\%} \leq 107\%$; $D_{max} \leq 110\%$. Markers that do not fulfill these dose constraints are not theoretically clinically acceptable. Additional figure explanations are described in Figure 31. Color version of figure is available online.

10.7   Tables

Table 13. Summary of patient characteristics.

Patient characteristics	Number of patients (%) or median (min;max)	
Median Age	63	(48;75)
Gender		
Male	12	(67%)
Female	6	(33%)
Performance Status		
0	17	(94%)
1	1	(6%)
Differentiating grade		
Adenocarcinoma	12	(67%)
Planocellular carcinoma	5	(27%)
Large cell neuroendocrine carcinoma	1	(6%)
T-stage		
1	2	(11%)
2	2	(11%)
3	7	(39%)
4	7	(39%)
N-stage		
0	3	(17%)
1	3	(17%)
2	8	(44%)
3	4	(22%)
M-stage		
0	18	(100%)
Tumor Location		
Upper lobe/middle lobe	15	(83%)
Lower lobe	3	(17%)
Primary tumor site		
Central	9	(50%)
Peripheral	3	(17%)
Chest wall	4	(22%)
Central/Chest wall	2	(11%)
Mediastinal involvement		
Tumor	1	(6%)
Lymph node	5	(28%)
Tumor and lymph node	10	(55%)
No involvement	2	(11%)

Table 14. Median dose characteristics for FB and DIBH treatment plans calculated with AAA and MC dose calculation algorithms. Patient-specific paired percentage differences between FB and DIBH for the both calculation algorithms were calculated for each patient, which are presented as the median and standard deviation (SD). Bold style indicates statistically significant paired difference between FB and DIBH for the AAA and MC calculations, respectively. Underline style of the MC calculated median values indicate statistically significant paired difference between MC and corresponding AAA calculations. Statistical testing was performed with paired Wilcoxon signed rank tests with a two tailed significance level of 0.05.

	AAA						MC					
	FB		DIBH		%-Diff.		FB		DIBH		%-Diff.	
Structure	Median (range)		Median (range)		Median (SD)		Median (range)		Median (range)		Median (SD)	
PTV												
volume (cm^3)	557	(185;1377)	501	(145,1349)	**-8.7**	**(5.8)**						
mean dose (Gy)	66.0	(66.0,66.2)	66.0	(66.0, 66.0)	0.0	(0.1)	66.0	(65.5,67.2)	65.9	(65.4,66.6)	-0.1	(0.4)
max dose (%)	105.4	(104.1,117.1)	107.1	(104.7,110.4)	**1.0**	**(5.2)**	113.7	(112.0,125.5)	115.8	(113.1,123.3)	**1.1**	**(3.2)**
min dose (%)	84.6	(51.1,93.4)	85.9	(63.0,91.9)	1.7	(17.9)	76.0	(36.5,84.8)	77.2	(55.5,85.9)	-1.1	(26.2)
D$_{98\%}$ (%)	96.1	(88.6,97.9)	95.7	(91.6,97.8)	-0.2	(1.2)	92.6	(88.5,95.1)	92.4	(89.2,93.5)	-0.3	(1.0)
D$_{2\%}$ (%)	102.6	(101.9,106.8)	103.0	(102.1,105.2)	0.3	(0.6)	107.3	(105.9,109.8)	107.4	(106.3,109.0)	0.4	(0.7)
CI	1.22	(1.05,1.58)	1.19	(1.03,1.59)	-2.0	(9.5)	1.22	(1.03,1.55)	1.18	(1.00,1.57)	-2.9	(10.5)
LCF	0.98	(0.88,1.00)	0.98	(0.91,1.00)	-0.1	(1.5)	0.98	(0.90,1.00)	0.97	(0.89,0.99)	**-1.0**	**(1.8)**
NTOF	0.18	(0.04,0.36)	0.14	(0.04,0.37)	-7.2	(36.1)	0.18	(0.04,0.35)	0.14	(0.03,0.36)	-4.5	(35.0)
CTV												
volume (cm^3)	352	(89,1064)	334	(68,1043)	**-10.2**	**(6.8)**						
D$_{99\%}$ (%)	97.8	(93.1,98.3)	97.5	(96.2,98.1)	-0.2	(1.0)	92.7	(91.7,95.4)	92.7	(91.7,94.1)	0.0	(0.6)
GTV												
volume (cm^3)	212	(29,806)	185	(20,791)	**-14.8**	**(9.5)**						
D$_{99\%}$ (%)	98.1	(96.3,99.2)	98.1	(96.7,99.0)	-0.1	(0.6)	92.9	(91.5,95.6)	92.9	(91.4,94.9)	0.0	(0.7)
Total lung												
volume (cm^3)	3212	(1725,4601)	5918	(3036,8133)	**86.8**	**(31.9)**						
mean dose (Gy)	14.0	(8.2,23.4)	11.6	(7.3,17.2)	**-20.4**	**(9.2)**	14.7	(9.2,23.8)	12.4	(8.4,17.4)	**-18.1**	**(8.3)**
V$_{5Gy}$ (%)	45.8	(31.0,64.3)	43.4	(24.5,59.7)	**-9.0**	**(10.2)**	51.5	(33.1,67.0)	44.0	(27.0,61.9)	**-11.6**	**(9.3)**
V$_{20Gy}$ (%)	23.5	(12.3,36.1)	18.6	(11.0,30.2)	**-20.0**	**(9.8)**	24.0	(12.4,36.7)	19.1	(11.1,30.2)	**-19.9**	**(9.6)**
Healthy lung												
V$_{5Gy}$ (%)	32.0	(5.8,56.1)	34.3	(3.2,59.2)	0.1	(5.8)	36.5	(9.1,59.0)	37.4	(5.7,62.1)	0.0	(4.9)
Medulla												
volume (cm^3)	17	(9,29)	22	(11,31)	**21.4**	**(34.1)**						
max dose (Gy)	41.0	(24.8,44.0)	39.2	(18.5,44.5)	-2.4	(12.1)	45.4	(28.2,48.7)	43.0	(22.5,49.5)	**-3.9**	**(9.8)**
mean dose (Gy)	21.4	(6.4,32.8)	18.1	(6.2,27.2)	**-15.9**	**(14.4)**	21.4	(7.4,33.2)	18.3	(7.1,27.4)	**-16.5**	**(13.3)**
Heart												
volume (cm^3)	765	(501,1137)	563	(386,908)	**-23.7**	**(10.8)**						
mean dose (Gy)	3.4	(0.7,30.9)	2.6	(0.3,29.1)	**25.5**	**(21.2)**	4.4	(2.3,31.0)	3.8	(2.2,29.4)	**-12.6**	**(12.8)**
max dose (Gy)	67.5	(4.1,71.2)	46.9	(1.0,71.8)	**-8.9**	**(67.3)**	70.6	(6.9,77.3)	51.1	(4.7,75.5)	**-10.2**	**(54.6)**
Esophagus												
volume (cm^3)	30	(16,53)	25	(4,51)	1.9	(29.2)						
mean dose (Gy)	18.1	(10.2,39.8)	19.4	(7.1,32.0)	0.0	(20.5)	18.6	(11.0,40.4)	19.8	(7.8,32.4)	0.5	(19.5)
max dose (Gy)	67.2	(35.0,70.4)	67.7	(32.7,71.3)	-0.1	(5.5)	72.2	(39.6,75.7)	72.7	(38.8,75.9)	0.6	(6.3)

AAA, Anisotropic-Analytical-Algorithm; MC, Monte Carlo; FB, free-breathing; DIBH, deep-inspiration breath-hold; %-Diff., percentage difference; PTV, planning target volume; D98% and D2%, percentage dose delivered to 98% and 2% of the PTV, respectively; CI, conformity index; LCF, lesion coverage fraction, NTOF, normal tissue overdosage fraction; CTV, clinical target volume; GTV, gross tumor volume; D99%, percentage dose delivered to CTV and GTV, respectively; V5Gy, V20Gy, V45Gy, V50Gy, V55Gy, percentage of an organ volume receiving at least 5Gy, 20Gy, 45Gy, 50Gy, 55Gy, respectively.

11 Paper IV

Dose verification of radiotherapy for lung cancer by using plastic scintillator dosimetry and a heterogeneous phantom

Paper IV was presented at the 8th International Conference on 3D Radiation Dosimetry (IC3DDose), 4-7 September, 2014 in Ystad, Sweden. The work is published in the Journal of Physics: Conference Series **573** (2015) 012022. An in-house designed thorax phantom is used for scintillator dosimetry in homogeneous and heterogeneous setups, mimicking a lung cancer patient. Clinical relevant treatment plans of different complexities were measured and compared to calculations carried out using a commercial treatment planning system using the AAA algorithm.

Dose verification of radiotherapy for lung cancer by using plastic scintillator dosimetry and a heterogeneous phantom

W Ottosson[1,2], CF Behrens[2], and CE Andersen[1]

[1]Center for Nuclear Technologies, Technical University of Denmark, DTU Risø Campus, DK-4000 Roskilde, Denmark
[2]Department of Oncology, Radiotherapy Research Unit, Herlev Hospital, University of Copenhagen, DK-2730 Herlev, Denmark

E-mail: wiot@dtu.dk

Abstract Bone, air passages, cavities, and lung are elements present in patients, but challenging to properly correct for in treatment planning dose calculations. Plastic scintillator detectors (PSDs) have proven to be well suited for dosimetry in non-reference conditions such as small fields. The objective of this study was to investigate the performance of a commercial treatment planning system (TPS) using a PSD and a specially designed thorax phantom with lung tumor inserts. 10 treatment plans of different complexity and phantom configurations were evaluated. Although the TPS agreed well with the measurements for the least complex tests, deviations of tumor dose > 4% were observed for some cases. This study underpins the dosimetric challenge in TPS calculations for clinically relevant heterogeneous geometries. The scintillator system, together with the special phantom, provides a promising tool for evaluation of complex radiotherapy dose calculations and delivery.

11.1 Introduction

Fiber-coupled organic plastic scintillator detectors (PSDs) feature advantages suitable for complex and dynamic radiation dosimetry in megavoltage photon beams [96–98]. When it comes to heterogeneous setups with lack of charged particle equilibrium (CPE), there are recognized calculation challenges for most commercial treatment planning systems (TPSs). Thus, volumes containing bone, air passages, cavities and lung may deteriorate the TPS dose calculation accuracy [83,93].

The objective of this study was to investigate the performance of a TPS dose calculation algorithm by using a PSD in a heterogeneous setup, analogous to the geometry of a lung cancer patient, while delivering clinical relevant treatment plans of varying complexity.

11.2 Material and methods

11.2.1 Phantom design

A thorax phantom, analogous to a lung cancer patient, was constructed to perform PSD dosimetry in a well-defined heterogeneous geometry. The body of the phantom is made of PMMA, 34 cm in width (W), 23 cm in height (H) and 40 cm in length (L) (Figure 34). It contains three hollow cylinders of L: 50 cm, and a diameter (Ø) of 10 cm. These cylinders can be filled with several inserts of various materials to simulate different homo- and heterogeneous geometries.
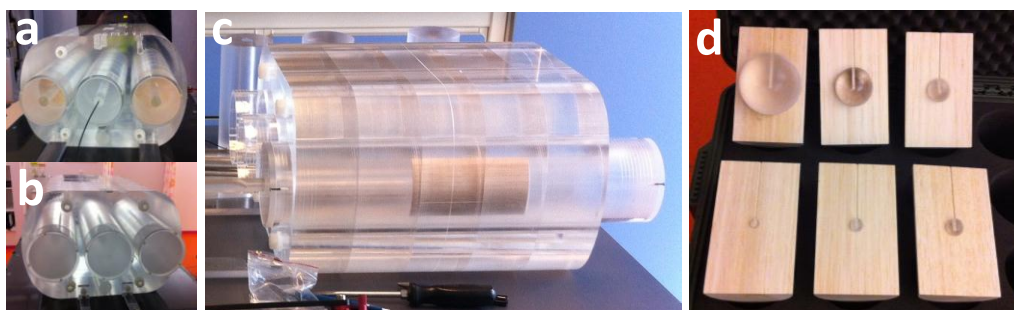

Figure 34. (a) A heterogeneous setup where the two lateral body cylinders are filled with balsa wood inserts. (b) A homogeneous setup, where the whole phantom are filled with PMMA inserts. (c) The heterogeneous setup described in (a) viewed from the side, where the lateral body cylinder containing the lung insert is longitudinal shifted from the central position in the phantom. (d) Balsa wood lung insert with associated tumors, ranging from 1-8 cm in diameter. (Color version of figure is available online.)

The various inserts are made of the copolymer Polyoxymethylene (POM-C), balsa wood, and PMMA representing bone, lung and soft tissue, respectively (Figure 34, Table 15-Table 16). The lung inserts were 15 cm long with a Ø of 9 cm, mimicking a human lung in size. PMMA spheres of various sizes (1-8 cm in diameter) embedded in balsa wood are available to simulate tumors in lung (Figure 34 (d)). In the lower part of the body, two smaller cylindrical holes of Ø: 2 cm and Ø: 3 cm (which also can be altered to Ø: 2 cm) are positioned at different distances from the phantom center, i.e. 6.5 cm and 9.5 cm (Table

16). These holes can, one at a time, be filled with a POM-C rod to simulate the spinal column at different diameters and position from the center of the phantom (Table 16).

11.2.2   Image acquisition and target definition

Four phantom configurations ('Homo.', 'Hetero.', '3 cm tumor' and '5 cm tumor') scanned in a 16 slice Philips Brilliance CT Big Bore, version 3.5.17001 (Philips Medical Systems, Cleveland, OH) using a standard thorax scanning protocol were used in this study (illustrated in Table 16). Table 15 presents the CT image characteristics of the phantom materials of 10 CT series of the phantom compared to corresponding human tissue data for 10 randomly picked lung cancer patients.

Table 15. CT image characteristics of the phantom materials compared to human tissue. Mean HU values and (range) for 10 CT series of the phantom and corresponding tissue data for 10 randomly picked lung cancer patients. Paired t-tests were performed for each tissue type, to check for differences in the mean HU value between the phantom material and the patient tissue data. No significances were found, using $p < 0.05$, i.e. there are good agreement between human tissue and the phantom materials.

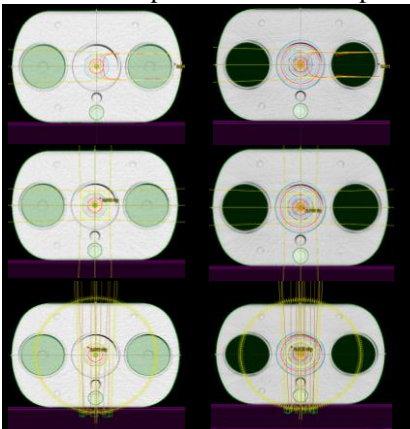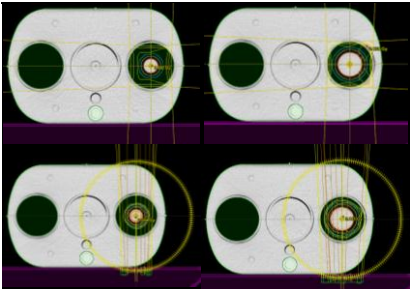| Tissue	Phantom Material		HU[b]	
		Density / [g/cm^3]	Phantom	Patients
Bone	POM-C	1.40	319 (309;327)	313 (210;413)
Lung	Balsa wood	0.10	-913 (-917;-888)	-901 (-977;-770)
Soft tissue	PMMA[a]	1.18	116 (103;123)	118 (84;143)

[a.]Poly(methyl methacrylate)
[b.]Using a standard thorax CT scanning protocol by Philips.

Delineations of the anatomical structures GTV, CTV, PTV, medulla, lung and body were performed on all image sets in the treatment planning system (TPS) Eclipse v. 10 (Varian Medical Systems, Palo Alto, CA, USA). CTVs and PTVs were defined as a 5 mm and 10 mm symmetrical expansion of GTV, respectively.

11.2.3   Experimental setup and calibration conditions

The scintillator used was the BCF-60 (Saint-Gobain Ceramics & Plastics Inc.) with Ø:1 mm and L:2 mm, described by Beierholm et al. [97]. The PSD was calibrated according to the procedure (method C) described by Guillot et al. [100] in a solid water calibration phantom. Measurements were carried out using the ME40 scintillator dosimetry system (DTU Nutech) [98]. The reference dose (100 MU, 10×10 cm^2 field) was measured by a Farmer ionization chamber, type 30011 (PTW, Freiburg, Germany) at a depth of 10 cm in the PMMA phantom QUASAR Multi-Purpose Body Phantom (Modus Medical Devices Inc., London, ON, Canada). Irradiation was delivered by a Varian Clinac iX 2300 linear accelerator (Varian Medical Systems), with a beam energy of 6 MV at a dose rate of 600 MU/min [85]. The accumulated PSD dose for the various treatment plans were compared with corresponding TPS calculated point doses (Table 16).

Table 16. TPS calculated isocentric point doses compared with corresponding PSD measured dose. (Color version of figure is available online).

Isocenter is positioned in the center of the phantom		Fiber dose [Gy]		TPS dose [Gy]		Dose deviation [%]	
Homo. setup	Hetero. setup	Homo.	Hetero.	Homo.	Hetero.	Homo.	Hetero.
		2.001	2.005	2.000	2.000	-0.1	-0.3
Conv.		2.005	2.006	2.000	2.000	-0.3	-0.3
RA		1.976	1.953	1.984	1.965	0.4	0.6
Isocenter is shifted laterally 11 cm		3 cm tumor	5 cm tumor	3 cm tumor	5 cm tumor	3 cm tumor	5 cm tumor
3 cm tumor	5 cm tumor						
Conv.	2.114	2.083	2.000	2.000	-5.4	-4.0	
RA	2.323	2.203	2.268	2.175	-2.4[a]	-1.3	

[a.] The dose deviation per arc was as large as -7.6%.

11.2.4 Treatment plans and delivery

In total, 10 treatment plans of different phantom configurations and isocentric field techniques (single field, 4-field conventional and two-arc Rapid Arc (RA) plans) were created. For each treatment plan the isocenter was positioned in the center of the GTV. For six treatment plans the isocenter was positioned centrally in the phantom. Three of these had a homogenous setup (Figure 34 (b), Table 16), and three of them had a heterogeneous setup (Figure 34 (a), Table 16). For the remaining four treatment plans the isocenter were shifted 11 cm laterally, because the GTVs were situated in the left lung of the phantom (Table 16). Doses were calculated using the AAA algorithm, with a prescribed dose of 2 Gy to the PTV. The RA plans were normalized to the mean dose of the PTV, while the other plans were normalized to the isocenter. All treatment plans satisfied the clinical dose coverage criteria. For the tumors situated in the lung 98% of the PTV volume was covered by minimum 90% of the prescribed dose. For the treatment plans not situated in the lung

the corresponding dose coverage was 95%. The beam energy and dose rate used were 6 MV and 600 MU/min, respectively.

11.3   Results/Discussion

Under calibration conditions the PSDs agreed with the TPS calculations to 0.1%.

Deviations less than 1% were observed between calculated and measured doses when the isocenter was located in the middle of the phantom. For the homogeneous configuration, deviations were in the range of (-0.1%; 0.4%) and for the heterogeneous configuration, deviations were in the range of (-0.3%; 0.6%) (Table 16). The RA plans generally resulted in larger total dose deviation (0.4%; 0.6%) compared with the simple conventional techniques (-0.3%; -0.1%). These low discrepancies, for the centrally positioned point in the phantom, probably illustrate that there is enough distance to adjacent heterogeneities in the phantom to be able to establish CPE. Larger TPS dose deviations (-5.4%; -1.3%) were observed when the isocenter was shifted laterally, since the GTV was situated in the left lung of the phantom. These substantial deviations could potentially be due to lack of sufficient spread of lateral radiation to obtain CPE. Even larger dose deviations (-5.4%; -2.4%) were observed for the smallest tumor size investigated (3 cm in diameter). This small size of tumor is not large enough to re-establish the CPE condition, and this is most likely the reason why the smallest tumor size results in the highest dose deviation. For the laterally shifted phantom configuration, the simple conventional technique resulted in a higher total dose deviation (-5.4%; -4.0%) compared to the more complex RA (-2.4%; -1.3%). The lower dose deviation, when using RA, might be due to the spread of incident radiation over the whole phantom compared to limited incident angles through heterogeneous medium, when using conventional technique.

11.4   Conclusion

Dose deviations of < 1% were observed for isocentric field techniques centered in the middle of the phantom, whereas dose deviations > 4% were observed for some laterally shifted treatment plans. The study confirmed that the smallest tumor size results in the highest dose deviation. The scintillator system and the heterogeneous phantom provide a promising tool for critical evaluations of complex radiotherapy calculations and dose delivery.

12 Paper V

Organic scintillator dosimetry reveals tumor-size dependency in a heterogeneous lung cancer setup for radiotherapy with 6 MV photon beams

Paper V is an unpublished study describing dosimetry issues for different tumor sizes in heterogeneous setups. For this purpose, an in-house designed thoracic-like phantom was used for scintillator dosimetry, mimicking a lung cancer patient with lung tumors of different tumor sizes. Clinical relevant treatment plans of different complexities were measured and compared to calculations carried out using a commercial AAA dose calculation algorithm.

Organic scintillator dosimetry reveals tumor size dependency in a heterogeneous lung cancer setup for radiotherapy with 6 MV photon beams

W Ottosson[1,2], P Sibolt[1,2], CF Behrens[2], and CE Andersen[1]

[1]Center for Nuclear Technologies, Technical University of Denmark, DTU Risø Campus, DK-4000 Roskilde, Denmark
[2]Department of Oncology, Radiotherapy Research Unit, Herlev Hospital, University of Copenhagen, DK-2730 Herlev, Denmark

E-mail: wiot@dtu.dk

Abstract

Purpose: Radiotherapy for lung cancer generally has a poor prognosis. Motion during imaging and treatment is a major challenge, but also other factors may contribute to the poor prognosis. One such factor is the ability of current treatment planning systems to accurately compute absorbed dose to tumors in the thorax region where large heterogeneities are present. The current study was designed to experimentally address the question: What is the agreement between actual delivered dose and computed dose using the Anisotropic-Analytical-Algorithm (AAA) in Eclipse treatment planning system for a thoracic-like geometry with tumors of different sizes? This is an important question given the widespread use of AAA and the changes in tumor sizes both over the course of treatment, and from patient-to-patient.

Material and Methods: To perform measurements under well-defined conditions, a thoracic-like phantom was designed. The phantom made of PMMA can be filled with inserts of various materials, including simulated lung tumors made of PMMA spheres (ranging from 1-8 cm in diameter) which are embedded in low-density balsa wood that simulates lung-tissue. 14 different phantom setups underwent CT scanning, structure delineation, and treatment planning. 56 isocentric treatments of different complexity and phantom configurations were calculated using AAA. To perform accurate dosimetry under these non-reference conditions, point measurements were carried out using water-equivalent, organic plastic scintillator detectors (PSDs). Dose differences between measurements and AAA calculations were calculated.

Results: Considerable tumor-size dependence was observed. For tumor sizes ≤ 2 cm, the dose deviations between AAA calculations and PSD measurements were 7.4±1.8% (median ± 1SD). For larger tumor sizes (3-8 cm in diameter) corresponding dose deviations were 4.2±1.4%. For the most homogeneous setup, the dose deviations were insignificant (0.3±0.6%). The results were essentially independent of treatment technique.

Conclusions: This study suggests a systematic tumor-size dependent dose calculation error for treatment planning on small tumor sizes in heterogeneous setups. This may originate from imperfections in the AAA algorithm. The largest dose deviations were observed for the smallest tumor sizes. Although, it is well known that AAA has issues in heterogeneous regions, we are not aware of any previous experimental study demonstrating a similar systematic tumor-size effect. The effect is large enough to potentially have implications for lung cancer treatment planning.

12.1 Introduction

Lung cancer gross tumor volumes (GTVs) are often situated in regions of large tissue heterogeneities. Most commercial treatment planning systems (TPSs) have recognized calculation issues in these regions due to the absence of charged particle equilibrium (CPE) and because of difficulties to correctly account for changes of lateral electron scatter [88–91,93]. The largest inaccuracies are usually in the transition between materials of different densities. Additionally, for lung cancer treatments, tumor volume shrinkage during radiotherapy is well known [27,36,105–107]. Adaptive radiotherapy is one solution to correct for tumor shrinkage and other anatomical changes during the course of treatment. For cases where the tumor decreases, the treatment fields can be adapted accordingly, i.e. the field sizes can be decreased in order to spare adjacent healthy tissue from radiation. The TPS calculation issues increase when the tumor and field sizes decrease due to simultaneous decrease of CPE.

The advantages of using fiber-coupled organic plastic scintillator detectors (PSD) for complex and dynamic radiotherapy dosimetry in megavoltage photon beams have previously been presented in studies based on homogeneous setups in either water or solid water phantoms [95–98]. Additionally, benchmarking against Monte Carlo simulations have shown good agreement with measurements, and a recent study by Francescon even concluded the Exradin W1 PSD (Standard Imaging, Middleton, WI, USA) to be the only detector of those investigated that could reproduce the Monte Carlo simulated data in water with high accuracy [97,99]. PSDs are particularly well suited for complex dose verifications due to their water-equivalency, and small size for high spatial resolution and minimum perturbation of the radiation fields. Alanine and thermoluminescent dosimeters (TLDs) are also highly water equivalent, but they do not provide real-time output, which is a significant drawback in studies involving many treatments and complex phantom setups.

In order to explore the heterogeneous TPS calculation issues further, a heterogeneous thoracic-like phantom was constructed for PSD dosimetry. Several tumor inserts of different sizes (ranging from 1-8 cm in diameter) were embedded in low-density balsa wood representing lung tissue to simulate the change of tumor size during the course of a lung cancer treatment. This current study is the first experimental study designed to obtain accurate assessments of the dose delivered in different heterogeneous setups, mimicking a lung cancer patient with varying tumor sizes embedded in low-density media. For this purpose, PSD measurements for a range of various phantom setups, simulating different tumor sizes, and using different complex isocentric treatment techniques were carried out.

12.2 Material and methods

12.2.1 Phantom design

The phantom design has previously been described by Ottosson et al. [108]. In brief, a thoracic-like phantom, analogous to the thorax of a lung cancer patient, has been constructed to carry out PSD dosimetry in well-defined heterogeneous geometries. The body of the phantom was made of Poly(methyl methacrylate) (PMMA), containing three hollow cylinders, which all can be filled with several inserts of various materials to simulate different homo- and heterogeneous geometries. The various inserts were made of

the copolymer Polyoxymethylene (POM-C), balsa wood, and PMMA representing bone, lung and soft tissue, respectively. PMMA spheres of various sizes (ranging from 1-8 cm in diameter), embedded in low-density balsa wood were used to simulate soft-tissue tumors situated in low-density lung-tissue.

12.2.2 Image acquisition, target definition and treatment planning

Prior to treatment planning, fourteen phantom configurations were scanned in a 16 slice Philips Brilliance CT Big Bore, version 3.5.17001 (Philips Medical Systems, Cleveland, OH) using a standard thorax scanning protocol. The fillings of the two lateral cylinders were altered between PMMA and balsawood, representing a Soft-tissue-Tumor-Soft-tissue (STS) setup or Lung-Tumor-Lung (LTL) setup, respectively (Figure 35). The central cylinder was either filled with one of the tumor inserts with the diameters: (1, 1.5, 2, 3, 5, 8) cm embedded in balsa wood, or a PMMA cylinder with the diameter of 9 cm. In our previous study we found good agreement between human tissue and the phantom materials in terms of Hounsfield unit representation of the various materials [108].

Delineations of the anatomical structures were carried out according to the Ottosson [108] study in the TPS Eclipse v. 10 (Varian Medical Systems, Palo Alto, CA, USA). The clinical target volumes (CTVs) and planning target volumes (PTVs) were defined as a 5 mm and 10 mm symmetrical expansion of the GTV, respectively.

Treatment planning and dose calculation was carried out in Eclipse using the Anisotropic-Analytical-Algorithm (AAA). For each image set, four different isocentric treatment plans of various complexities were carried out (Figure 35), resulting in 56 different treatment plans according to Figure 35; (a.) a single-field technique with an entry angle of 90 degrees. (b.) a four-field conventional box technique. (c.) a five-field intensity-modulated radiotherapy technique (IMRT), and (d.) a dual-arc volumetric-modulated-arc technique (VMAT). The beam directions were preserved for each type of treatment plan for all tumor sizes investigated. The isocenters of all treatment plans were positioned at the center of the GTV, situated in the center of the phantom. For the IMRT and VMAT treatment plans a mean dose of 2 Gy was prescribed to the PTV, while the single-field and 4-field techniques were normalized to give 2 Gy at the isocenter (Figure 35). All treatment plans, except the single-field technique, satisfied the clinical dose coverage criteria. For the tumors situated in the lung, 98% of the PTV was covered by a minimum of 90% of the prescribed dose.
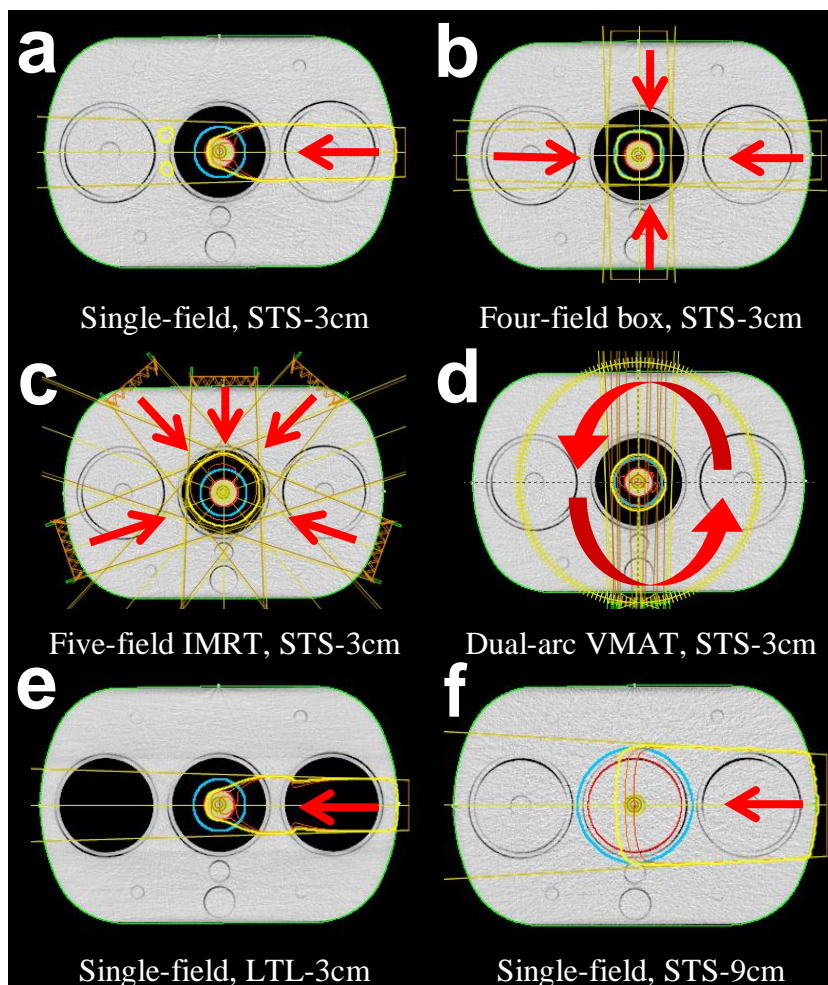
Figure 35. Schematic illustration of the different treatment techniques and some phantom setups. STS and LTL describes the fillings of the body cylinders. (a.-d.) illustrates a 3 cm tumor insert situated in the central cylinder of the phantom, where the two lateral cylinders were filled with PMMA, (i.e. a STS-3cm setup). Four different treatment techniques were carried out: (a.) a single-field technique, (b.) a four-field conventional box technique (c.) a five-field IMRT, and (d.) a dual-arc VMAT. (e.) illustrates the single-field technique when the lateral cylinders where changed into balsa wood, (i.e. a LTL-3cm setup). (f.) is an example of when all the body cylinders were filled with PMMA, and the GTV was represented by a tumor diameter size of 9 cm, without any adjacent low-density media (i.e. a STS-9cm setup, a full homogeneous setup). The GTV, PTV and body of the phantom were delineated in red, blue (with a thicker line width) and green colors, respectively. The 90%, 95% and 100% isodose curves were colored yellow (with a thicker line width), light orange, and dark orange, respectively. Red arrows indicate the beam directions for the various treatment techniques.

12.2.3   Experimental setup and calibration conditions

All measurements were carried out utilizing the BCF-60 scintillator (Saint-Gobain Ceramics & Plastics Inc.) with a diameter of 1 mm and a length of 2 mm, further described

by Beierholm et al. [97]. The PSD was calibrated according to the procedure (method C) described by Guillot et al. [100] in a solid water calibration phantom. Measurements were carried out using the ME40 scintillator dosimetry system (DTU Nutech) [98]. The reference dose (100 MU, 10×10 cm^2 field size, 90 cm source-to-surface distance) was measured by both the scintillator and a Farmer ionization chamber, type 30011 (PTW, Freiburg, Germany) at a depth of 11.5 cm in the solid water phantom. To determine the dosimetric correction factor between the solid water phantom and the in-house developed PMMA phantom, corresponding measurements were carried out in the PMMA phantom (using a homogeneous setup, i.e. STS-9, Figure 35f). The depth of 11.5 cm agreed with the center position in the PMMA phantom. Irradiation was delivered by a Varian Clinac iX 2300 linear accelerator (Varian Medical Systems), with a beam energy of 6 MV at a dose rate of 600 MU/min [85]. The calibration dose was normalized to the corresponding calculated dose in Eclipse to eliminate the daily output variation of the linear accelerator.

Prior to irradiation of the different tumor inserts, the PMMA phantom was positioned based on image guidance by cone-beam CT (CBCT) images of the phantom setup, acquired at the treatment unit. The CBCT images were registered and matched to the planning CT, where focus was to match the tumor inserts to achieve the correct phantom position. For the measurements, the PSD was positioned at the isocenter (i.e. in the center of the tumors) centrally situated in the PMMA phantom. Measurements were carried out in two sessions. During the first session, the size of the tumor insert gradually decreased, starting with the largest tumor insert, while the tumor size gradually increased, starting with the smallest tumor insert during the second measurement session. The measured PSD dose for the various treatment plans were compared with corresponding AAA calculated point doses.

12.2.4 Data analysis and statistical testing

Measured percentage dose deviations relative to the AAA calculations were assessed. A three-way ANOVA-test was performed to determine the statistical significance of the dose deviations in regard to the treatment techniques, tumor sizes and phantom setups. Bonferroni adjustment for the three comparison groups was carried out to compensate for multiple comparisons. The results were considered statistically significant after adjustment for $p \leq 0.05$.

12.3   Results

The mean and one standard deviation (1 SD) of the dosimetric correction factor between the solid water calibration phantom and the PMMA phantom measured with the ionization chamber was 0.9983 (0.0013).

The AAA calculated and PSD measured isocenter doses for the IMRT treatments were statistically significantly higher compared to the other treatment techniques (not presented). The PSD measurements indicate that the doses in the center of the tumors were in median about $4.7 \pm 2.8\%$ ($\pm$ 1SD) higher in reality compared to the doses calculated by AAA, irrespectively of treatment techniques, sizes of tumor inserts, or what lateral phantom configuration utilized (Figure 36).
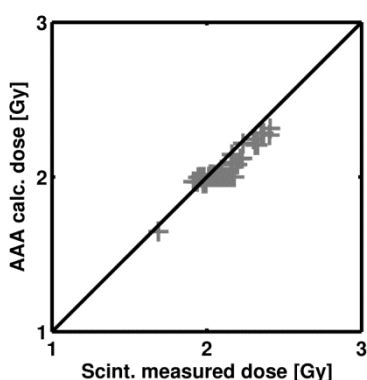
Figure 36. The AAA calculated dose relative to the scintillator measured dose. If the markers are situated exactly on the black line there is no difference between the doses. AAA calculates a lower dose compared to the scintillator measurements if the markers are situated below the black line.

For the dose deviations, no statistically significant differences were found among the treatment techniques, irrespective if the lateral cylinders were filled with balsa wood or PMMA (Figure 37a). However, compared to the LTL setups, there were observed tendencies (not statistical significant) that the medians of the dose deviations were higher for the STS setups, in both respect to the treatment techniques (Figure 37a) and tumor size (Figure 37b). Considerable tumor-size dependence was observed irrespectively of treatment technique or lateral phantom setup. Dose deviations between AAA calculations and measurements were 7.4±1.8% in median for tumor sizes ≤ 2 cm, with a clear increase in dose deviations for decreasing tumor sizes. The smallest tumor size (1 cm) irradiated by a single-field treatment plan resulted in the largest dose deviation (11.5%). For larger tumor sizes (3-8 cm in diameter) corresponding dose deviations were 4.2±1.4% in median. For the most homogeneous setup, where the central cylinder was filled with PMMA (i.e. STS-9cm and LTL-9cm), the dose deviations were 0.3±0.6% in median. For the LTL setups, no trend was observed for the tumor sizes ranging from 3-8 cm. For the same tumor sizes, a small decreasing trend was found for the STS setups when increasing the tumor size.

When removing the effect from treatment technique and tumor-size dependency, it was found that STS setups were statistically significantly higher compared to LTL setups (not presented). Similarly, if removing the effect of the lateral phantom setups and the tumor-size dependency, the percentage dose deviations for the conventional and the single-field treatment techniques were statistically significantly higher compared to the rest of the treatment techniques (not presented).
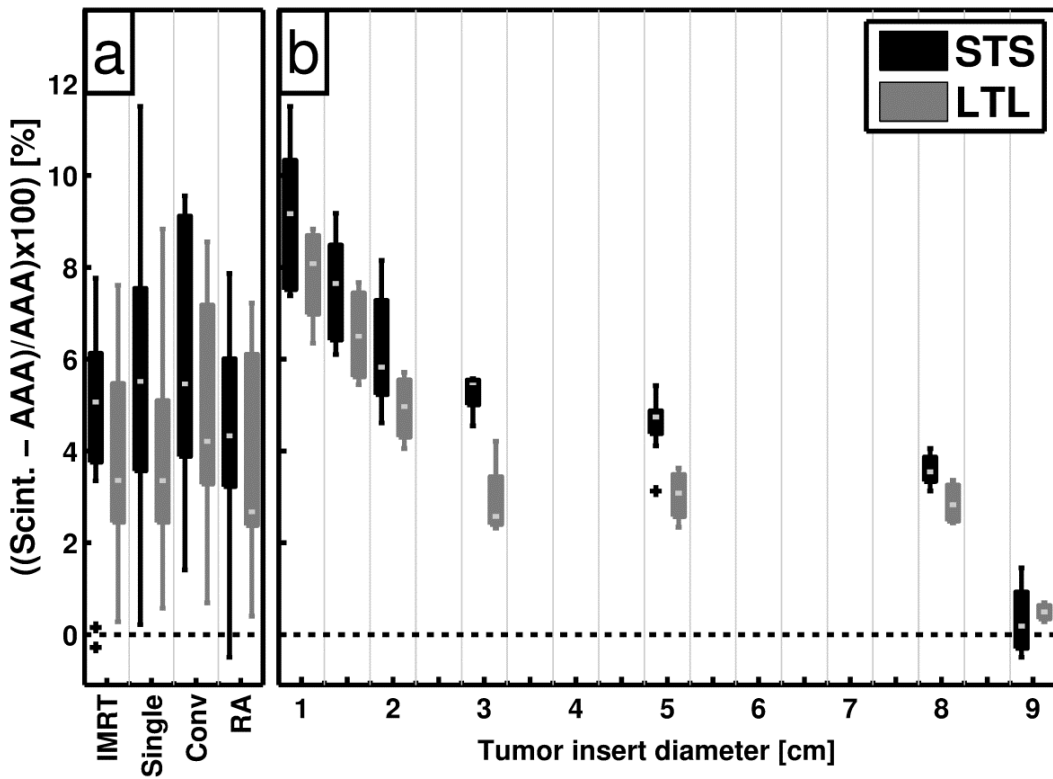
Figure 37. The measured percentage dose deviation relative to the AAA calculations stratified by (a.) treatment technique or, (b.) the tumor size for the STS and LTL phantom setups. The black dotted line is equal to zero dose deviation. The black boxes represent the data when the two lateral cylinders were filled with PMMA, (i.e. STS setups). The gray boxes represent likewise the data when the two lateral cylinders were filled with balsa wood, (i.e. LTL setups). On each box, the central light gray mark represents the median value. The edges of each box are the 25th and the 75th percentiles, the whiskers correspond to approximately ± 2.7 SD of the data, and outliers are plotted as crosses individually.

12.4   Discussion

This study illustrates the dosimetric issues with the AAA dose calculation algorithm when it comes to small tumor sizes embedded in low-density media, which is clinically relevant for lung cancer treatments. Interestingly, the STS setups resulted in higher dose deviations in median, compared to the LTL setups, irrespectively of treatment technique and tumor size. The dose deviation of 0.3±0.6% for STS-9cm and LTL-9cm setups in the current study is comparable with the results presented in our previous study [108], where we found dose deviations of -0.2±0.4% for centrally positioned PSDs in STS-9cm and LTL-9cm setups. For the tumor inserts, the major difference between this study, and the previous, was the location of the tumor inserts in the phantom. In the previous study, the tumors were located in the lateral cylinder, while they were located in the central cylinder in the current study. The reason to have the tumor inserts located in the central cylinder in the current study, although this does not mimic the geometry of a lung cancer patient, was to

minimize the potential influences of the phantom body curvature and beam distribution around the phantom. These features could have potential influence on the tumor-size dependency, which would be hard to interpret. However, already in our previous study, an indication for tumor-size dependency was observed between the 3 and 5 cm tumor sizes investigated [108]. For the 3 cm tumor, the dose deviations were -5.4% and -2.4%, for the four-field conventional and VMAT treatment plans, respectively. For the 5 cm tumor, the dose deviations were -4.0% and -1.3%, respectively. Similar differences between the 3 and 5 cm tumor sizes were found in the STS setup in the current study (Figure 37b). However, no such difference between the 3 and 5 cm tumors was observed for the more heterogeneous LTL setup. The insignificant dose deviations for the most homogeneous setups, in this and the previous study, indicate that the distance from the measurement point to adjacent heterogeneities in the phantom was large enough to establish CPE. Similar to the prior study, the conventional treatment plans in this study resulted in higher dose deviations compared to more complex plans. One reason for this observation could be the fact that the more complex treatment plans (IMRT and VMAT) have several beam entries around the body of the phantom, and not just directly through the low-density material of the phantom. Thus, the larger dose deviation for the simplest field techniques could potentially be due to lack of sufficient spread of lateral radiation, required in order to obtain CPE. Irrespectively of tumor setup or treatment technique, the smallest tumor sizes resulted in the largest dose deviations. The results presented in the current study clearly indicate that there exists a considerable tumor-size dependency irrespectively of tumor setup or treatment technique, especially for small tumor sizes ≤ 2 cm. Consolidating MC simulations will be of great value for further establishment of these observed dose deviations.

12.4.1 Confounding factors

A potential confounding factor in the current study could be the size of the calculation grid utilized in Eclipse, which was $0.25 \times 0.25 \times 0.25$ cm^3. This could be further improved down to a grid size of $0.1 \times 0.1 \times 0.1$ cm^3. Moreover, the CT scan of the phantom was based on a clinical thorax scanning protocol with a CT image slice spacing of 2 mm. Since the length of the PSD utilized in the current study was 2 mm, correct positioning of the detector at sub-mm precision is crucial and could be an issue. Phantom positioning prior to irradiation was carried out by CBCT image guidance. Since the phantom did not include any motion, the confounding factor for the phantom setup procedure is anticipated to be small. Although, PMMA and balsawood were found to be HU-equivalent to human tissue [108], there could be some deviation from the CT calibration curve since they are not tissue-equivalent materials in terms of anatomical compositions. This potential bias is expected to be small, but requires supplementary investigations.

12.5   Conclusion

This study demonstrates systematic tumor-size dependent dose errors when using the AAA dose calculation algorithm for treatment planning, which is emphasized for small tumor sizes. This considerable tumor-size dependency may originate from imperfections in the AAA algorithm for small tumor sizes in heterogeneous setups. The largest dose deviations were observed for the smallest tumors. Conventional field techniques resulted in higher dose deviations compared to more complex treatment techniques, such as IMRT and

VMAT. Compared to the LTL setups, the STS setups resulted overall in higher dose deviations. The scintillator system and the heterogeneous phantom provide a promising tool for critical evaluation of complex radiotherapy calculations and dose delivery. Although it is well known that AAA results in erroneous treatment plans in heterogeneous regions, we are not aware of any previous experimental study demonstrating similar systematic tumor size effect. The effect is large enough to potentially have implications for lung cancer treatment planning

Conflict of interest statement

The authors declare no conflict of interest.

Acknowledgment

13 Bibliography

[1]   The Association of the Nordic Cancer Registries. NORDCAN database, http://www-dep.iarc.fr/NORDCAN/english/frame.asp, (accessed: February 27, 2015).

[2]   Statens Serum Institut. Tal og Analyse: Cancerregisteret 2013, http://www.ssi.dk/~/media/Indhold/DK - dansk/Sundhedsdata og it/NSF/Registre og kliniske databaser/Registre/Cancerregisteret 2013.pdf, (accessed: February 27, 2015).

[3]   Ferlay J, Soerjomataram I, Ervik M, Dikshit R, Eser S, Mathers C, et al. GLOBOCAN 2012 v1.0, Cancer Incidence and Mortality Worldwide: IARC CancerBase No. 11. Lyon, France, 2013, http://globocan.iarc.fr, (accessed: February 26, 2015).

[4]   Engholm G, Ferlay J, Christensen N, Bray F, Gjerstorff ML, Klint A, et al. NORDCAN--a Nordic tool for cancer information, planning, quality control and research. Acta Oncol, 2010;49:725–36.

[5]   Dansk Lunge Cancer Gruppe. DOLG - Årsrapport 2013, 2014, http://www.lungecancer.dk/documents/2C44EF04-F99D-4239-91D8-33522ECFBE70.pdf, (accessed: February 27, 2015).

[6]   Marshall HM, Leong SC, Bowman R V, Yang IA, Fong KM. The science behind the 7th edition Tumour, Node, Metastasis staging system for lung cancer. Respirology, 2012;17:247–60.

[7]   Armstrong J, Raben A, Zelefsky M, Burt M, Leibel S, Burman C, et al. Promising survival with three-dimensional conformal radiation therapy for non-small cell lung cancer. Radiother Oncol, 1997;44:17–22.

[8]   Rengan R, Rosenzweig KE, Venkatraman E, Koutcher LA, Fox JL, Nayak R, et al. Improved local control with higher doses of radiation in large volume stage III non small cell lung cancer. Int J Radiat Oncol Biol Phys, 2004;60:741–7.

[9]   Marks LB, Bentzen SM, Deasy JO, Kong F-MS, Bradley JD, Vogelius IS, et al. Radiation dose-volume effects in the lung. Int J Radiat Oncol Biol Phys, 2010;76:S70–6.

[10]   Graham M V, Purdy JA, Emami B, Harms W, Bosch W, Lockett MA, et al. Clinical dose-volume histogram analysis for pneumonitis after 3D treatment for non-small cell lung cancer (NSCLC). Int J Radiat Oncol Biol Phys, 1999;45:323–9.

[11]   The Danish Lung Cancer Group (DOLG). DOLG 's Radioterapigruppes Rekommandationer for Udførelse af STRÅLEBEHANDLING VED LUNGE KRÆFT. Denmark, 2014, http://www.dolg.dk/pdf/rekommandationer.pdf, (accessed: February 26, 2015).

[12]   Persson GF, Nygaard DE, Brink C, Jahn JW, Munck af Rosenschöld P, Specht L, et al. Deviations in delineated GTV caused by artefacts in 4DCT. Radiother Oncol, 2010;96:61–6.

[13]   Fredberg Persson G, Nygaard DE, Munk af Rosenschöld P, Richter Vogelius I, Josipovic M, Specht L, et al. Artifacts in conventional computed tomography (CT)

and free breathing four-dimensional CT induce uncertainty in gross tumor volume determination. Int J Radiat Oncol Biol Phys, 2011;80:1573–80.

[14] International commission on radiation units and measurements. ICRU Report 83: Prescribing, recording, and reporting photon-beam intensity-modulated radiation therapy (IMRT). Oxford, 2010.

[15] Van Herk M. Errors and margins in radiotherapy. Semin Radiat Oncol, 2004;14:52–64.

[16] Van Herk M, Remeijer P, Rasch C, Lebesque JV. The probability of correct target dosage: dose-population histograms for deriving treatment margins in radiotherapy. Int J Radiat Oncol Biol Phys, 2000;47:1121–35.

[17] Sonke J-J, Rossi M, Wolthaus J, van Herk M, Damen E, Belderbos J. Frameless stereotactic body radiotherapy for lung cancer using four-dimensional cone beam CT guidance. Int J Radiat Oncol Biol Phys, 2009;74:567–74.

[18] McKenzie A, van Herk M, Mijnheer B. Margins for geometric uncertainty around organs at risk in radiotherapy. Radiother Oncol, 2002;62:299–307.

[19] Juhler Nøttrup T, Korreman SS, Pedersen AN, Aarup LR, Nyström H, Olsen M, et al. Intra- and interfraction breathing variations during curative radiotherapy for lung cancer. Radiother Oncol, 2007;84:40–8.

[20] Korreman SS, Juhler-Nøttrup T, Boyer AL. Respiratory gated beam delivery cannot facilitate margin reduction, unless combined with respiratory correlated image guidance. Radiother Oncol, 2008;86:61–8.

[21] Ottosson W, Baker M, Hedman M, Behrens CF, Sjöström D. Evaluation of setup accuracy for NSCLC patients; studying the impact of different types of cone-beam CT matches based on whole thorax, columna vertebralis, and GTV. Acta Oncol, 2010;49:1184–91.

[22] Rahma F, Sibolt P, Ottosson W, Behrens CF, Sjöstrom D. Evaluation of soft-tissue match methods for utilization in CBCT guided adaptive radiotherapy of lung cancer patients – clinical benefits, limitations and margin determination. Lund University, 2014.

[23] Nielsen TB, Hansen VN, Westberg J, Hansen O, Brink C. A dual centre study of setup accuracy for thoracic patients based on Cone-Beam CT data. Radiother Oncol, 2012;102:281–6.

[24] Juhler-Nøttrup T, Korreman SS, Pedersen AN, Persson GF, Aarup LR, Nyström H, et al. Interfractional changes in tumour volume and position during entire radiotherapy courses for lung cancer with respiratory gating and image guidance. Acta Oncol, 2008;47:1406–13.

[25] Schmidt ML, Hoffmann L, Kandi M, Møller DS, Poulsen PR. Dosimetric impact of respiratory motion, interfraction baseline shifts, and anatomical changes in radiotherapy of non-small cell lung cancer. Acta Oncol, 2013;52:1490–6.

[26] Møller DS, Khalil AA, Knap MM, Hoffmann L. Adaptive radiotherapy of lung cancer patients with pleural effusion or atelectasis. Radiother Oncol, 2014;110:517–22.

[27] Kataria T, Gupta D, Bisht SS, Karthikeyan N, Goyal S, Pushpan L, et al. Adaptive radiotherapy in lung cancer: dosimetric benefits and clinical outcome. Br J Radiol, 2014;87:20130643.

[28] Persson GF, Nygaard DE, Hollensen C, Munk af Rosenschöld P, Mouritsen LS, Due AK, et al. Interobserver delineation variation in lung tumour stereotactic body radiotherapy. Br J Radiol, 2012;85:6–10.

[29] Boda-Heggemann J, Fleckenstein J, Lohr F, Wertz H, Nachit M, Blessing M, et al. Multiple breath-hold CBCT for online image guided radiotherapy of lung tumors: simulation with a dynamic phantom and first patient data. Radiother Oncol, 2011;98:309–16.

[30] Kincaid RE, Yorke ED, Goodman KA, Rimner A, Wu AJ, Mageras GS. Investigation of gated cone-beam CT to reduce respiratory motion blurring. Med Phys, 2013;40:041717.

[31] Ford EC, Mageras GS, Yorke E, Ling CC. Respiration-correlated spiral CT: A method of measuring respiratory-induced anatomic motion for radiation treatment planning. Med Phys, 2003;30:88–97.

[32] Vedam SS, Keall PJ, Kini VR, Mostafavi H, Shukla HP, Mohan R. Acquiring a four-dimensional computed tomography dataset using an external respiratory signal. Phys Med Biol, 2003;48:45–62.

[33] Keall PJ, Mageras GS, Balter JM, Emery RS, Forster KM, Jiang SB, et al. The management of respiratory motion in radiation oncology report of AAPM Task Group 76. Med Phys, 2006;33:3874.

[34] Rietzel E, Liu AK, Chen GTY, Choi NC. Maximum-Intensity Volumes for Fast Contouring of Lung Tumors Including Respiratory Motion in 4DCT Planning. Int J Radiat Oncol Biol Phys, 2008;71:1245–52.

[35] Abdelnour AF, Nehmeh SA, Pan T, Humm JL, Vernon P, Schöder H, et al. Phase and amplitude binning for 4D-CT imaging. Phys Med Biol, 2007;52:3515–29.

[36] Sonke J-J, Belderbos J. Adaptive radiotherapy for lung cancer. Semin Radiat Oncol, 2010;20:94–106.

[37] Ezhil M, Vedam S, Balter P, Choi B, Mirkovic D, Starkschall G, et al. Determination of patient-specific internal gross tumor volumes for lung cancer using four-dimensional computed tomography. Radiat Oncol, 2009;4:4.

[38] Muirhead R, McNee SG, Featherstone C, Moore K, Muscat S. Use of Maximum Intensity Projections (MIPs) for target outlining in 4DCT radiotherapy planning. J Thorac Oncol, 2008;3:1433–8.

[39] Liu HH, Balter P, Tutt T, Choi B, Zhang J, Wang C, et al. Assessing Respiration-Induced Tumor Motion and Internal Target Volume Using Four-Dimensional Computed Tomography for Radiotherapy of Lung Cancer. Int J Radiat Oncol Biol Phys, 2007;68:531–40.

[40] Underberg RWM, Lagerwaard FJ, Slotman BJ, Cuijpers JP, Senan S. Use of maximum intensity projections (MIP) for target volume generation in 4DCT scans for lung cancer. Int J Radiat Oncol Biol Phys, 2005;63:253–60.

[41] Lu W, Neuner GA, George R, Wang Z, Sasor S, Huang X, et al. Audio-visual biofeedback does not improve the reliability of target delineation using maximum intensity projection in 4-dimensional computed tomography radiation therapy planning. Int J Radiat Oncol Biol Phys, 2014;88:229–35.

[42] Wolthaus JWH, Schneider C, Sonke J-J, van Herk M, Belderbos JSA, Rossi MMG, et al. Mid-ventilation CT scan construction from four-dimensional respiration-

correlated CT scans for radiotherapy planning of lung cancer patients. Int J Radiat Oncol Biol Phys, 2006;65:1560–71.

[43] Saito T, Sakamoto T, Oya N. Comparison of gating around end-expiration and end-inspiration in radiotherapy for lung cancer. Radiother Oncol, 2009;93:430–5.

[44] Berson AM, Emery R, Rodriguez L, Richards GM, Ng T, Sanghavi S, et al. Clinical experience using respiratory gated radiation therapy: Comparison of free-breathing and breath-hold techniques. Int J Radiat Oncol Biol Phys, 2004;60:419–26.

[45] Kini VR, Vedam SS, Keall PJ, Patil S, Chen C, Mohan R. Patient training in respiratory-gated radiotherapy. Med Dosim, 2003;28:7–11.

[46] Yorke E, Rosenzweig KE, Wagman R, Mageras GS. Interfractional anatomic variation in patients treated with respiration-gated radiotherapy. J Appl Clin Med Phys, 2005;6:19–32.

[47] Wong JW, Sharpe MB, Jaffray DA, Kini VR, Robertson JM, Stromberg JS, et al. The use of active breathing control (ABC) to reduce margin for breathing motion. Int J Radiat Oncol Biol Phys, 1999;44:911–9.

[48] Sonke J-J, Lebesque J, van Herk M. Variability of four-dimensional computed tomography patient models. Int J Radiat Oncol Biol Phys, 2008;70:590–8.

[49] Mampuya WA, Nakamura M, Matsuo Y, Ueki N, Iizuka Y, Fujimoto T, et al. Interfraction variation in lung tumor position with abdominal compression during stereotactic body radiotherapy. Med Phys, 2013;40:091718.

[50] Bissonnette JP, Franks KN, Purdie TG, Moseley DJ, Sonke J-J, Jaffray DA, et al. Quantifying Interfraction and Intrafraction Tumor Motion in Lung Stereotactic Body Radiotherapy Using Respiration-Correlated Cone Beam Computed Tomography. Int J Radiat Oncol Biol Phys, 2009;75:688–95.

[51] Cho B, Poulsen PR, Sloutsky A, Sawant A, Keall PJ. First Demonstration of Combined kV/MV Image-Guided Real-Time Dynamic Multileaf-Collimator Target Tracking. Int J Radiat Oncol Biol Phys, 2009;74:859–67.

[52] Depuydt T, Poels K, Verellen D, Engels B, Collen C, Buleteanu M, et al. Treating patients with real-time tumor tracking using the Vero gimbaled linac system: Implementation and first review. Radiother Oncol, 2013;112:343–51.

[53] Verellen D, Depuydt T, Gevaert T, Linthout N, Tournel K, Duchateau M, et al. Gating and tracking, 4D in thoracic tumours. Cancer/Radiothérapie, 2010;14:446–54.

[54] Gopalakrishna K. CyberKnife: A new paradigm in radiotherapy. J Med Phys, 2010;2:63–4.

[55] Cho B, Poulsen PR, Sawant A, Ruan D, Keall PJ. Real-time target position estimation using stereoscopic kilovoltage/megavoltage imaging and external respiratory monitoring for dynamic multileaf collimator tracking. Int J Radiat Oncol Biol Phys, 2011;79:269–78.

[56] Poulsen PR, Fledelius W, Cho B, Keall P. Image-based dynamic multileaf collimator tracking of moving targets during intensity-modulated arc therapy. Int J Radiat Oncol Biol Phys, 2012;83:e265–71.

[57] Poulsen PR, Cho B, Sawant A, Ruan D, Keall PJ. Detailed analysis of latencies in image-based dynamic MLC tracking. Med Phys, 2010;37:4998–5005.

[58] Sawant A, Venkat R, Srivastava V, Carlson D, Povzner S, Cattell H, et al. Management of three-dimensional intrafraction motion through real-time DMLC tracking. Med Phys, 2008;35:2050–61.

[59] Poulsen PR, Carl J, Nielsen J, Nielsen MS, Thomsen JB, Jensen HK, et al. Megavoltage image-based dynamic multileaf collimator tracking of a NiTi stent in porcine lungs on a linear accelerator. Int J Radiat Oncol Biol Phys, 2012;82:321–7.

[60] Yip S, Rottmann J, Berbeco R. The impact of cine EPID image acquisition frame rate on markerless soft-tissue tracking. Med Phys, 2014;41:061702.

[61] Rottmann J, Keall P, Berbeco R. Markerless EPID image guided dynamic multi-leaf collimator tracking for lung tumors. Phys Med Biol, 2013;58:4195–204.

[62] Cho BCJ, Bezjak A, Dawson LA. Image guidance in non-small cell lung cancer. Semin Radiat Oncol, 2010;20:164–70.

[63] Purdie TG, Bissonnette J-P, Franks K, Bezjak A, Payne D, Sie F, et al. Cone-beam computed tomography for on-line image guidance of lung stereotactic radiotherapy: localization, verification, and intrafraction tumor position. Int J Radiat Oncol Biol Phys, 2007;68:243–52.

[64] Yeung AR, Li JG, Shi W, Newlin HE, Chvetsov A, Liu C, et al. Tumor localization using cone-beam CT reduces setup margins in conventionally fractionated radiotherapy for lung tumors. Int J Radiat Oncol Biol Phys, 2009;74:1100–7.

[65] Grams MP, Brown LC, Brinkmann DH, Pafundi DH, Mundy DW, Garces YI, et al. Analysis of automatic match results for cone-beam computed tomography localization of conventionally fractionated lung tumors. Pract Radiat Oncol, 2014;4:35–42.

[66] Guckenberger M, Meyer J, Wilbert J, Baier K, Mueller G, Wulf J, et al. Cone-beam CT based image-guidance for extracranial stereotactic radiotherapy of intrapulmonary tumors. Acta Oncol, 2006;45:897–906.

[67] Grau C, Muren LP, Høyer M, Lindegaard J, Overgaard J. Image-guided adaptive radiotherapy - integration of biology and technology to improve clinical outcome. Acta Oncol, 2008;47:1182–5.

[68] Steenbakkers RJHM, Duppen JC, Fitton I, Deurloo KEI, Zijp LJ, Comans EFI, et al. Reduction of observer variation using matched CT-PET for lung cancer delineation: a three-dimensional analysis. Int J Radiat Oncol Biol Phys, 2006;64:435–48.

[69] Edmund JM, Kjer HM, van Leemput K, Hansen RH, Andersen JAL, Andreasen D. A voxel-based investigation for MRI-only radiotherapy of the brain using ultra short echo times. Phys Med Biol, 2014;59:7501–19.

[70] Sharp G, Fritscher KD, Pekar V, Peroni M, Shusharina N, Veeraraghavan H, et al. Vision 20/20: perspectives on automated image segmentation for radiotherapy. Med Phys, 2014;41:050902.

[71] Wang H, Dong L, O'Daniel J, Mohan R, Garden AS, Ang KK, et al. Validation of an accelerated "demons" algorithm for deformable image registration in radiation therapy. Phys Med Biol, 2005;50:2887–905.

[72] Van Leemput K, Larsen R. 02505 Course Note - Medical Image Analysis. Kongens Lyngby,Technical University of Denmark, DTU Informatics, 2012, http://www2.imm.dtu.dk/courses/02505/.

[73] Gao J, Chai P, Yun M-K, Liu S-Q, Shan B-C, Wei L. Respiratory motion correction with an improved demons algorithm for PET images. Chinese Phys C, 2012;36:1025–30.

[74] Thirion JP. Fast Non-Rigid Matching of 3D Medical Images apport, 1995.

[75] Thirion JP. Image matching as a diffusion process: an analogy with Maxwell's demons. Med Image Anal, 1998;2:243–60.

[76] Hanna GG, Hounsell AR, O'Sullivan JM. Geometrical analysis of radiotherapy target volume delineation: a systematic review of reported comparison methods. Clin Oncol, 2010;22:515–25.

[77] Dice LR. Measures of the amount of ecologic association between species. Ecology, 1945;26:297–302.

[78] Van Esch A, Huyskens DP, Behrens CF, Samsoe E, Sjolin M, Bjelkengren U, et al. Implementing RapidArc into clinical routine: A comprehensive program from machine QA to TPS validation and patient QA. Med Phys, 2011;38:5146–66.

[79] MedCalc Software. ROC curve, http://www.medcalc.org/manual/roc-curves.php, (accessed: March 5, 2015).

[80] Veiga C, Lourenço AM, Mouinuddin S, van Herk M, Modat M, Ourselin S, et al. Toward adaptive radiotherapy for head and neck patients: Uncertainties in dose warping due to the choice of deformable registration algorithm. Med Phys, 2015;42:760–9.

[81] Ge Y, O'Brien RT, Shieh C-C, Booth JT, Keall PJ. Toward the development of intrafraction tumor deformation tracking using a dynamic multi-leaf collimator. Med Phys, 2014;41:061703.

[82] Attix FH. Introduction to radiological physics and radiation dosimetry. Weinheim. WILEY-VCH Verlag GmbH & Co. KGaA, 2004.

[83] Papanikolaou N, Battista JJ, Boyer AL, Kappas C, Klein E, Mackie TR, et al. AAPM Report no. 85: Tissue inhomogeneity corrections for mega voltage photon beams. Madison, WI, USA, 2004, https://www.aapm.org/pubs/reports/rpt_85.pdf.

[84] Podgorsak EB. Radiation Oncology Physics: A Handbook for Teachers and Students. IAEA, Vienna, 2005.

[85] Sjöström D, Bjelkengren U, Ottosson W, Behrens CF. A beam-matching concept for medical linear accelerators. Acta Oncol, 2009;48:192–200.

[86] IAEA. TRS-398: Absorbed Dose Determination in External Beam Radiotherapy: An International Code of Practice for Dosimetry Based on Standards of Absorbed Dose to Water.

[87] Wong JW, Purdy JA. On methods of inhomogeneity corrections for photon transport. Med Phys, 1995;17:807–14.

[88] Van Esch A, Tillikainen L, Pyykkonen J, Tenhunen M, Helminen H, Siljamäki S, et al. Testing of the analytical anisotropic algorithm for photon dose calculation. Med Phys, 2006;33:4130–48.

[89] Tillikainen L, Helminen H, Torsti T, Siljamäki S, Alakuijala J, Pyyry J, et al. A 3D pencil-beam-based superposition algorithm for photon dose calculation in heterogeneous media. Phys Med Biol, 2008;53:3821–39.

[90] Robinson D. Inhomogeneity correction and the analytic anisotropic algorithm. J Appl Clin Med Phys, 2008;9:112–22.

[91]   Aarup LR, Nahum AE, Zacharatou C, Juhler-Nøttrup T, Knöös T, Nyström H, et al. The effect of different lung densities on the accuracy of various radiotherapy dose calculation methods: implications for tumour coverage. Radiother Oncol, 2009;91:405–14.

[92]   Rønde HS, Hoffmann L. Validation of Varian's AAA algorithm with focus on lung treatments. Acta Oncol, 2009;48:209–15.

[93]   Knöös T, Wieslander E, Cozzi L, Brink C, Fogliata A, Albers D, et al. Comparison of dose calculation algorithms for treatment planning in external photon beam therapy for clinical situations. Phys Med Biol, 2006;51:5785–807.

[94]   Siebers JV, Keall PJ, Nahum AE, Mohan R. Converting absorbed dose to medium to absorbed dose to water for Monte Carlo based photon beam dose calculations. Phys Med Biol, 2000;45:983–95.

[95]   Beddar AS, Mackie TR, Attix FH. Water-equivalent plastic scintillation detectors for high-energy beam dosimetry: I. Physical characteristics and theoretical considerations. Phys Med Biol, 1992;37:1883–900.

[96]   Beddar AS, Mackie TR, Attix FH. Water-equivalent plastic scintillation detectors for high-energy beam dosimetry: II. Properties and measurements. Phys Med Biol, 1992;37:1901–13.

[97]   Beierholm AR, Ottosson RO, Lindvold LR, Behrens CF, Andersen CE. Characterizing a pulse-resolved dosimetry system for complex radiotherapy beams using organic scintillators. Phys Med Biol, 2011;56:3033–45.

[98]   Beierholm AR, Behrens CF, Hoffmann L, Andersen CE. Acquiring beam data for a flattening-filter free linear accelerator using organic scintillators. Radiat Meas, 2013;56:290–3.

[99]   Francescon P, Beddar S, Satariano N, Das IJ. Variation of kQclin,Qmsrfclin,fmsr for the small-field dosimetric parameters percentage depth dose, tissue-maximum ratio, and off-axis ratio. Med Phys, 2014;41:101708.

[100]   Guillot M, Gingras L, Archambault L, Beddar S, Beaulieu L. Spectral method for the correction of the Cerenkov light effect in plastic scintillation detectors: A comparison study of calibration procedures and validation in Cerenkov light-dominated situations. Med Phys, 2011;38:2140–50.

[101]   Baker M, Vallentin S, Andersen K, Ottosson W, Sjöström D. Evaluation of cardiopulmonary and ladca dose in left-sided breast cancer patients by utilizing the deep inspiration breath holding technique. In: Heshmati A, Dilani A, Baban SMJ, editors. Perspect. Kurdistan's Econ. Soc. Transit. Vol. II, Newcastle upon Tyne. Cambridge Scholars Publishing, 2013, p. 154–70.

[102]   Yorke ED, Wang L, Rosenzweig KE, Mah D, Paoli J-B, Chui C-S. Evaluation of deep inspiration breath-hold lung treatment plans with Monte Carlo dose calculation. Int J Radiat Oncol, 2002;53:1058–70.

[103]   Wang L, Yorke E, Desobry G, Chui C-S. Dosimetric advantage of using 6 MV over 15 MV photons in conformal therapy of lung cancer: Monte Carlo studies in patient geometries. J Appl Clin Med Phys, 2002;3:51–9.

[104]   Ottosson RO, Karlsson A, Behrens CF. Pareto front analysis of 6 and 15 MV dynamic IMRT for lung cancer using pencil beam, AAA and Monte Carlo. Phys Med Biol, 2010;55:4521–33.

[105] Knap MM, Hoffmann L, Nordsmark M, Vestergaard A. Daily cone-beam computed tomography used to determine tumour shrinkage and localisation in lung cancer patients. Acta Oncol, 2010;49:1077–84.

[106] Guckenberger M, Wilbert J, Richter A, Baier K, Flentje M. Potential of adaptive radiotherapy to escalate the radiation dose in combined radiochemotherapy for locally advanced non-small cell lung cancer. Int J Radiat Oncol Biol Phys, 2011;79:901–8.

[107] Woodford C, Yartsev S, Dar AR, Bauman G, van Dyk J. Adaptive radiotherapy planning on decreasing gross tumor volumes as seen on megavoltage computed tomography images. Int J Radiat Oncol Biol Phys, 2007;69:1316–22.

[108] Ottosson W, Behrens CF, Andersen CE. Dose verification of radiotherapy for lung cancer by using plastic scintillator dosimetry and a heterogeneous phantom. J Phys Conf Ser, 2015;573:012022.

[109] Barnes EA, Murray BR, Robinson DM, Underwood LJ, Hanson J, Roa WHY. Dosimetric evaluation of lung tumor immobilization using breath hold at deep inspiration. Int J Radiat Oncol Biol Phys, 2001;50:1091–8.

[110] Mageras GS, Yorke E. Deep inspiration breath hold and respiratory gating strategies for reducing organ motion in radiation treatment. Semin Radiat Oncol, 2004;14:65–75.

[111] Peng Y, Vedam S, Chang JY, Gao S, Sadagopan R, Bues M, et al. Implementation of feedback-guided voluntary breath-hold gating for cone beam CT-based stereotactic body radiotherapy. Int J Radiat Oncol Biol Phys, 2011;80:909–17.

[112] Ottosson W, Lykkegaard Andersen JA, Borrisova S, Mellemgaard A, Behrens CF. Deformable image registration for geometrical evaluation of DIBH radiotherapy treatment of lung cancer patients. J Phys Conf Ser, 2014;489:012077.

[113] Rahma F, Ottosson W, Behrens CF, Sjöström D, Sibolt P. Soft-tissue matching methods for lung cancer radiotherapy - benefits, limitations and margin determination. Phys Medica, 2014;30:e93–4.

[114] Craft DL, Hong TS, Shih HA, Bortfeld TR. Improved planning time and plan quality through multicriteria optimization for intensity-modulated radiotherapy. Int J Radiat Oncol Biol Phys, 2012;82:e83–90.

[115] Voet PWJ, Dirkx MLP, Breedveld S, Fransen D, Levendag PC, Heijmen BJM. Toward fully automated multicriterial plan generation: A prospective clinical study. Int J Radiat Oncol Biol Phys, 2013;85:866–72.

[116] Zarepisheh M, Long T, Li N, Tian Z, Romeijn HE, Jia X, et al. A DVH-guided IMRT optimization algorithm for automatic treatment planning and adaptive radiotherapy replanning. Med Phys, 2014;41:061711.

[117] Petersen PM, Aznar MC, Berthelsen AK, Loft A, Schut DA, Maraldo M, et al. Prospective phase II trial of image-guided radiotherapy in Hodgkin lymphoma: Benefit of deep inspiration breath-hold. Acta Oncol, 2014:1–7.

[118] Giraud P, Morvan E, Claude L. Respiratory gating techniques for optimization of lung cancer radiotherapy. J Thorac Oncol, 2011;6:2058–68.

[119] Rosenzweig K, Hanley J, Mah D. The deep inspiration breath-hold technique in the treatment of inoperable non–small-cell lung cancer. Int J Radiat Oncol, 2000;48:81–7.

[120] Marchand V, Zefkili S, Desrousseaux J, Simon L, Dauphinot C, Giraud P. Dosimetric comparison of free-breathing and deep inspiration breath-hold radiotherapy for lung cancer. Strahlenther Onkol, 2012;188:582–9.

[121] Tahir BA, Bragg CM, Lawless SE, Hatton MQF, Ireland RH. Dosimetric evaluation of inspiration and expiration breath-hold for intensity-modulated radiotherapy planning of non-small cell lung cancer. Phys Med Biol, 2010;55:N191–9.

[122] Josipovic M, Persson GF, Håkansson K, Damkjær SMS, Bangsgaard JP, Westman G, et al. Deep inspiration breath hold radiotherapy for locally advanced lung cancer: comparison of different treatment techniques on target coverage, lung dose and treatment delivery time. Acta Oncol, 2013;52:1582–6.

[123] Wang L, Yorke E, Chui C-S. Monte Carlo evaluation of 6 MV intensity modulated radiotherapy plans for head and neck and lung treatments. Med Phys, 2002;29:2705–17.

[124] Ding GX, Duggan DM, Lu B, Hallahan DE, Cmelak A, Malcolm A, et al. Impact of inhomogeneity corrections on dose coverage in the treatment of lung cancer using stereotactic body radiation therapy. Med Phys, 2007;34:2985–94.

[125] Kawrakow I. Accurate condensed history Monte Carlo simulation of electron transport. I. EGSnrc, the new EGS4 version. Med Phys, 2000;27:485–98.

[126] Kawrakow I. Accurate condensed history Monte Carlo simulation of electron transport. II. Application to ion chamber response simulations. Med Phys, 2000;27:499–513.

[127] Rogers DWO, Faddegon BA, Ding GX, Ma C-M, We J. BEAM: A Monte Carlo code to simulate radiotherapy treatment units. Med Phys, 1995;22:503–24.

[128] Ottosson RO, Behrens CF. CTC-ask: a new algorithm for conversion of CT numbers to tissue parameters for Monte Carlo dose calculations applying DICOM RS knowledge. Phys Med Biol, 2011;56:N263–74.

[129] Popescu IA, Shaw CP, Zavgorodni SF, Beckham WA. Absolute dose calculations for Monte Carlo simulations of radiotherapy beams. Phys Med Biol, 2005;50:3375–92.

[130] Sibolt P, Cronholm RO, Beierholm AR, Behrens CF. Measurements of the relative backscatter contribution to the monitor chamber for modern medical linear accelerators; a multi-center study. Radiat Meas, 2015;72:75–80.

[131] Deasy JO, Blanco AI, Clark VH. CERR: A computational environment for radiotherapy research. Med Phys, 2003;30:979–85.

[132] Josipovic M, Aznar MC, Persson GF. Deep inspiration breath hold radiotherapy of lung cancer: The good, the bad and the ugly case. Acta Oncol, 2014;53:1446–8.

[133] Mihaylov IB, Siebers J V. Evaluation of dose prediction errors and optimization convergence errors of deliverable-based head-and-neck IMRT plans computed with a superposition/convolution dose algorithm. Med Phys, 2008;35:3722–7.

[134] Hanley J, Debois MM, Mah D. Deep inspiration breath-hold technique for lung tumors: the potential value of target immobilization and reduced lung density in dose escalation. Int J Radiat Oncol Biol Phys, 1999;45:603–11.

[135] Sundhedsstyrelsen. Tal og Analyse: Cancerregisteret 2010. 2010, http://sundhedsstyrelsen.dk/publ/Publ2011/DAF/Cancer/Cancerregisteret2010.pdf, (accessed: January 15, 2011).

Bibliography

[136] Dansk Lunge Cancer Gruppe. DOLG - Årsrapport 2009. 2010,
       www.lungecancer.dk.

[137] Perez C, Bauer M, Edelstein S. Impact of tumor control on survival in carcinoma of
       the lung treated with irradiation. J Radiat, 1986.
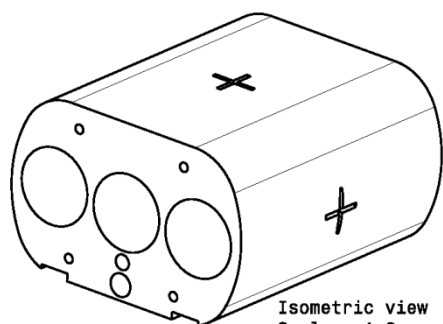
Appendices

14 Appendix A: Phantom design

14.1 2D phantom blueprints

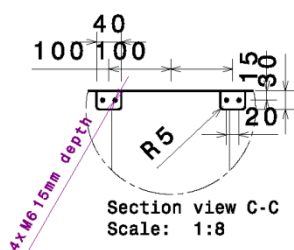This section describes the design of the phantom in detail.

- Main Body
- Body Cylinder
- Tumor
- Lung insert

14.2 3D phantom

- Cross-sections
- Cross-sections in a rotated viewing angle
- Dissected phantom

Isometric view
Scale: 1:6

Main Body

Section view A-A
Scale: 1:6

Section view C-C
Scale: 1:8

The body phantom consist of 4
blocks of PMMA, each with a
width of 100 mm. The blocks
are assebled by 4 ø12 mm rods
(2 on the left and right at
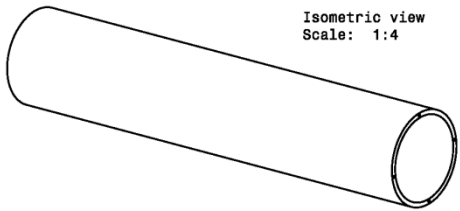the top of the body, and the
other 2 similarly at the
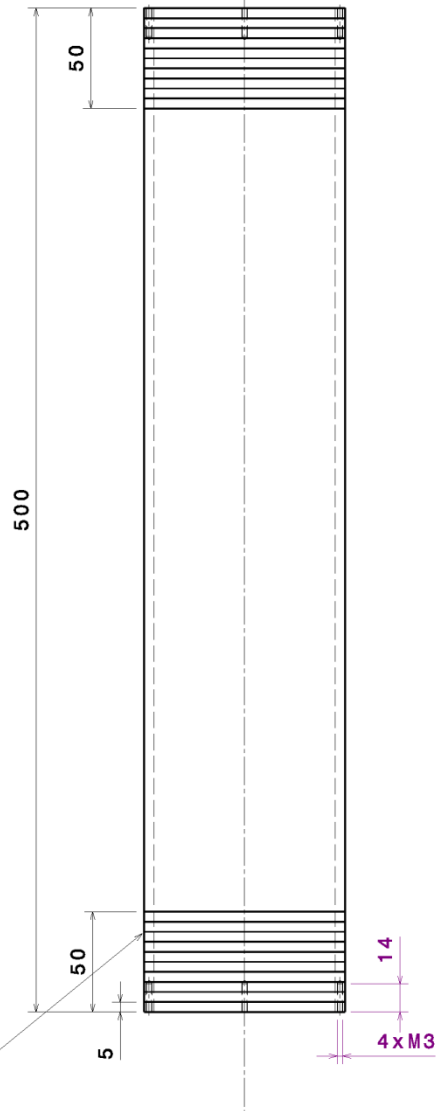bottom of the body).
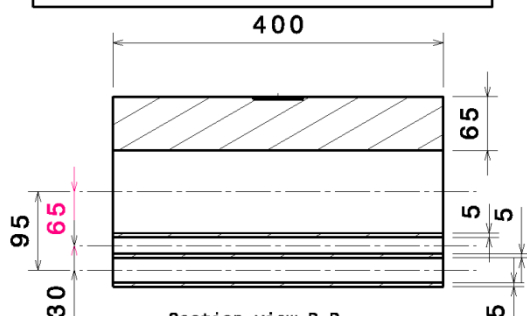
Section view B-B
Scale: 1:6
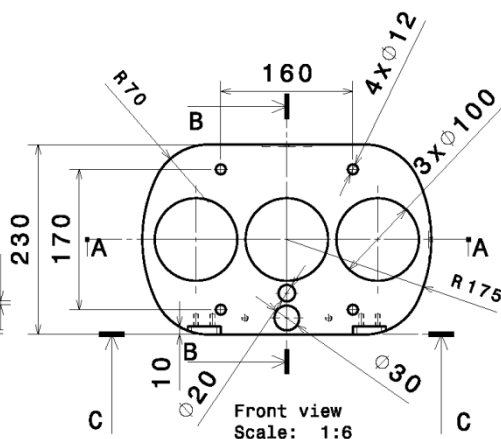
Front view
Scale: 1:6

The ø30 hole at the bottom of the phantom is
to be fitted the "outer" medulla insert.
Similarly, the ø20 hole is to be fitted the
"inner" medulla insert.

Isometric view
Scale: 1:4

Body Cylinders

⌀100

⌀90

47.5

Front view
Scale: 1:2

Left view
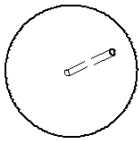Scale: 1:2

50

500

50

5

14

4 x M3
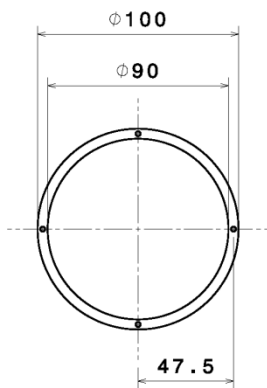
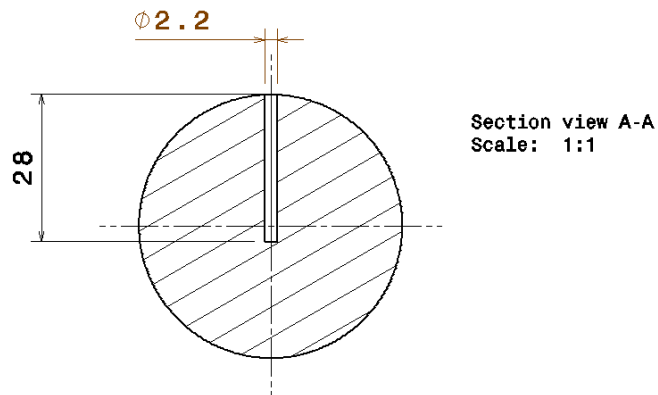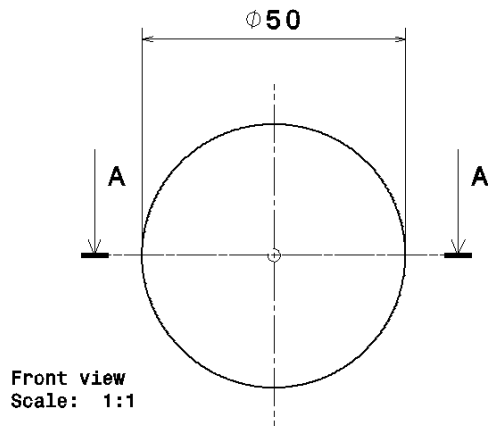10 Grooves of 0,2 mm depth
at both ends

3 hollow PMMA movable cylinders to be
fitted within the body

v

Appendix A: Phantom design – 2D blueprints
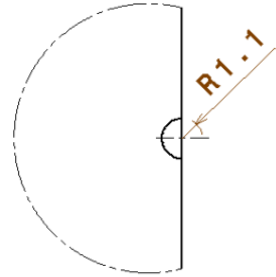
Isometric view
Scale: 1:2

Tumor
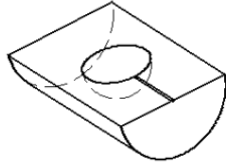
⌀50

A   A

Front view
Scale: 1:1

⌀2.2

28

Section view A-A
Scale: 1:1

6 tumors in PMMA are to be made with a
diameter of 10, 15, 20, 30, 50 and 80 mm.

Lung insert

Isometric view
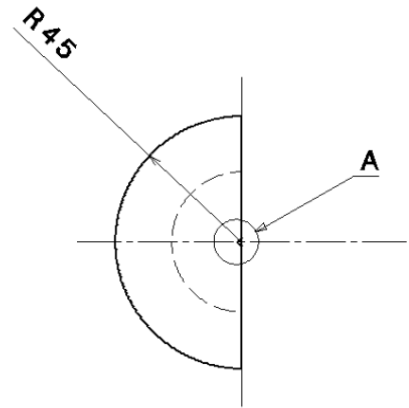**Scale: 1:4**

Detail A
Scale: 3:1

R1.1

R25

75

R45

A
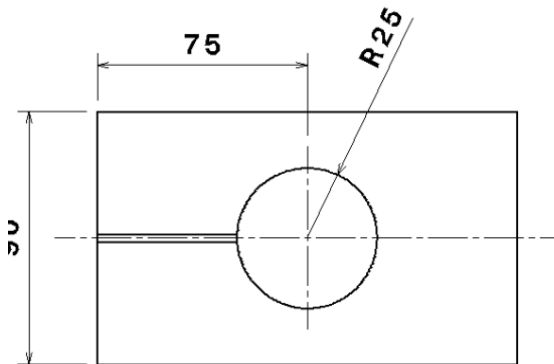
Front view
Scale: 1:2

Left view
Scale: 1:2

2 halves in balsa wood are to be made that fit
each tumor. The outer diameter must match the body
cylinders' inner diameter.

14.3   Cross-sections
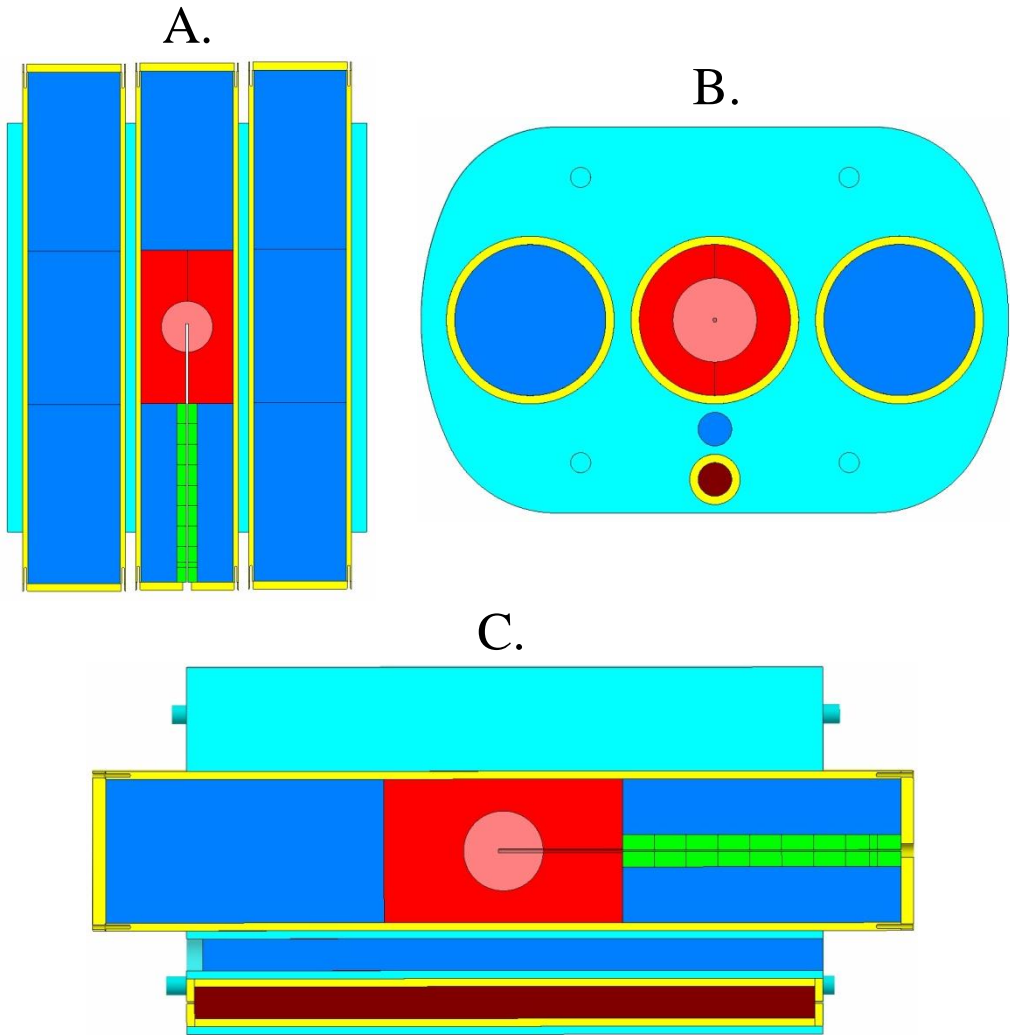
Figure 38. (A.) Coronal, (B.) translational, and (C.) sagittal cross-sections of the phantom. In this particular setup the colors mean the following: Light blue is the phantom body made of PMMA. Dark blue is the PMMA inserts. The yellow color represents the hollow PMMA cylinders with their lids on at the ends. The red central cylinder is made of balsa wood. Where a 5 cm PMMA tumor (pink) is situated in the center. The green plugs are in this case made out of PMMA. The maroon color is a 2 cm delrin rod used to simulate the spine.

14.4 Rotated cross-sections

A.

B.

C.
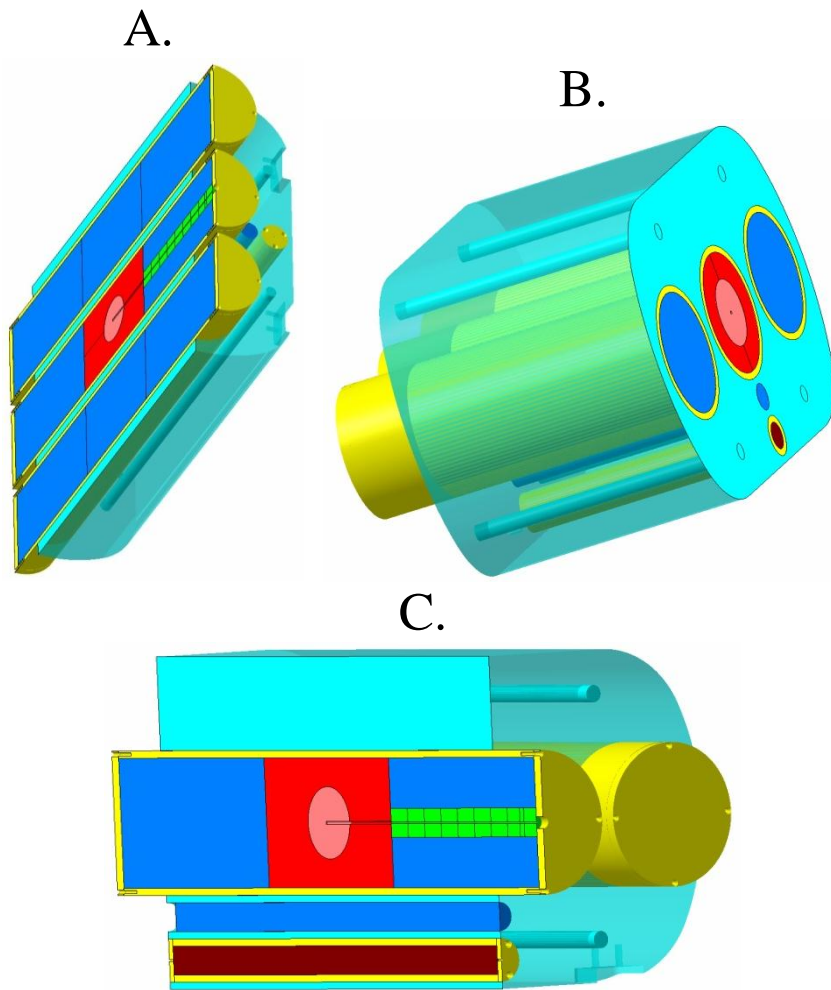
Figure 39. (A.) Coronal, (B.) translational, and (C.) sagittal cross-sections of the phantom in a rotated viewing angle. Additional figure explanations are described in Figure 38.

14.5 Dissection of the full phantom setup

A.   B.   C.   D.   E.
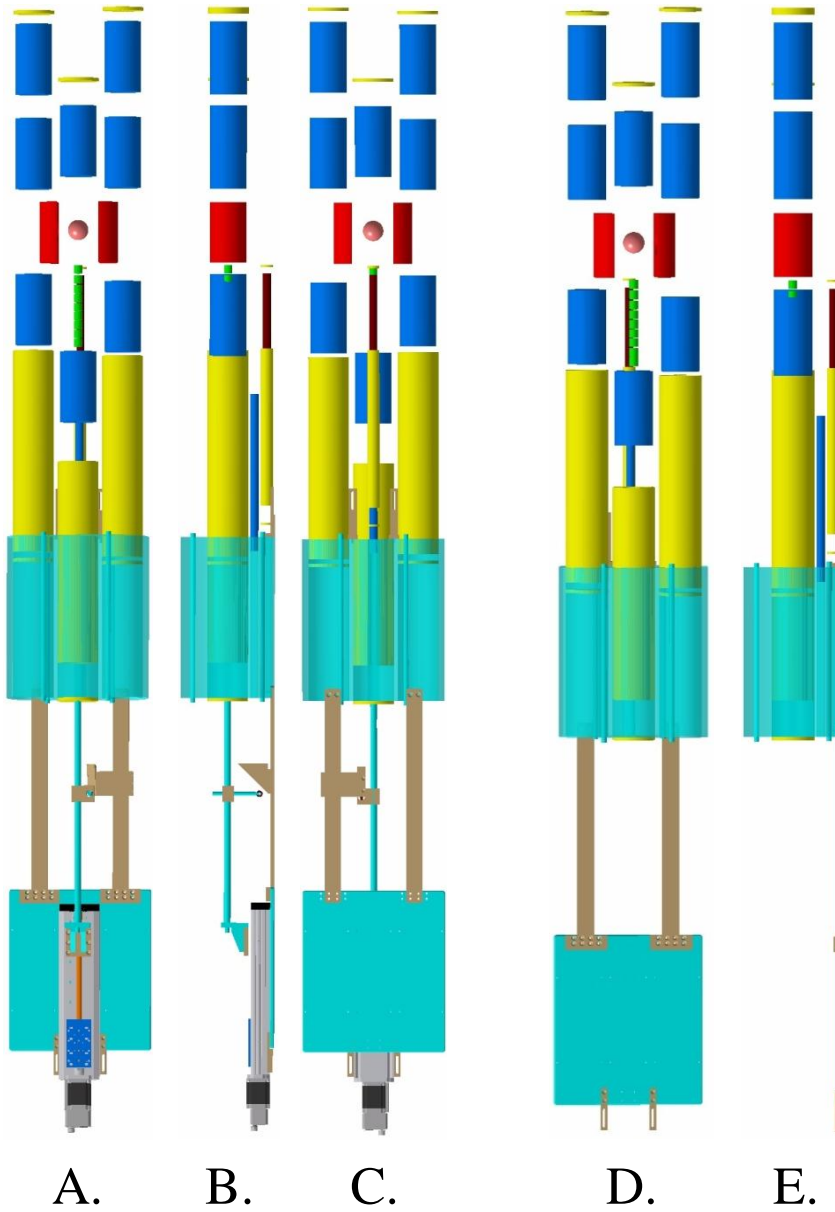
Figure 40. Different views of the phantom setup with (A-C) and without (D-E) the optional linear actuator and motion measurement device attached. Frontal view (A and E), Side-view (B and E), and view from below (C). Additional figure explanations are described in Figure 38.

14.6 Rotated view of the full phantom setup
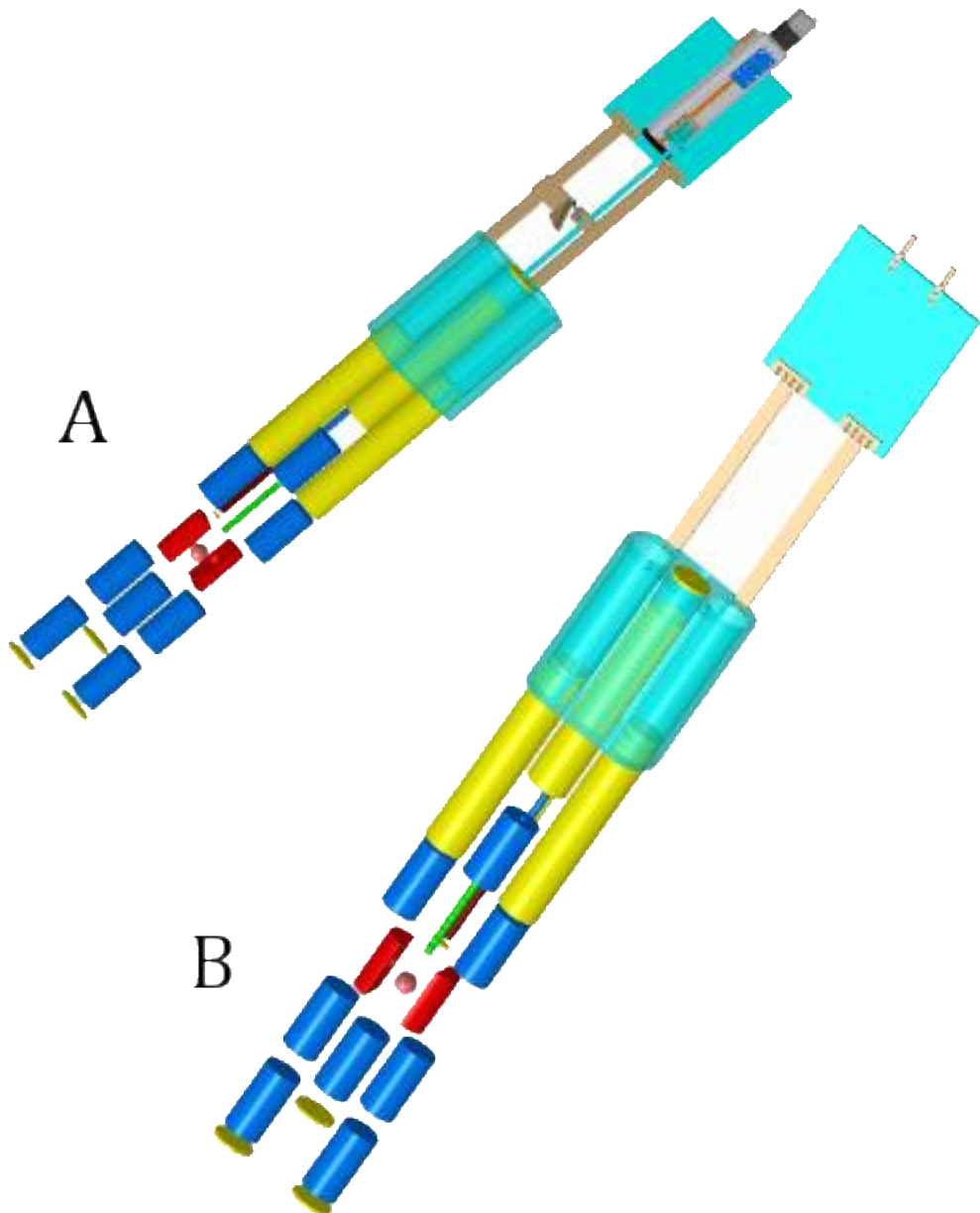
Figure 41. Rotated viewing angle of the dissection phantom setups in Figure 40, with (A) and without (B) the optional linear actuator and motion measurement device. Additional figure explanations are described in Figure 38.

15 Appendix B: Chemical analysis

This section describes the results from the chemical analysis of delrin and balsa wood carried out by BELAB AB and ALS Scandinavia AB.

- CHNO analysis of balsa wood
- Elemental analysis of balsa wood
- CHNO of delrin
- Elemental analysis of delrin
- Uncertainty data

15.1 CHNO analysis of balsa wood

BELAB AB

ANALYSCERTIFIKAT
Certificate of analysis

Sida 1/1

Provnr:	141819
Rapportdatum:	2014-07-10
Ankomstdatum:	2014-07-07

Provmärke: ALS, bränsle
Provtyp: Bränsle
ID.nummer: 975335
Märkt:

Kundnr 1042

ALS Scandinavia AB

Aurorum 10
977 75 Luleå
Sverige

Godkänd av
Albin Klint

Kundreferens
Martina Krekula

Beställningsnr
L1416586

Analys		Enhet	Notering	Laboratorium	Norm
Kol (C) torrt	48.7	% ts		Belab	SS-EN 15104:2011/15407:2011
Väte (H) torrt	6.0	% ts		Belab	SS-EN 15104:2011/15407:2011
Kväve (N) torrt	0.10	% ts		Belab	SS-EN 15104:2011/15407:2011
Syre (O) torrt	43.3	% ts		Belab	Beräknad

Mätosäkerhet, se BILAGA TILL ANALYSRAPPORT.
Lev.tillst = Leveranstillstånd, tp = torrt prov, ∗ = vatten inkluderat, # = Ej ackrediterat
Denna rapport får endast återges i sin helhet, om inte utfärdande laboratorium i förväg skriftligen godkänt annat.

BELAB
Bränsle&Energilaboratoriet AB
Exportgatan 20
602 28 NORRKÖPING

Tel: 011-157370
Fax: 011-160740
Mobil: 070-2428740

www.belab.nu
mail@belab.nu
556608-0783

15.2 Elemental analysis of balsa wood

Registrerad   **2014-06-24 10:02**
Utfärdad   **2014-07-11**

Technical University of Denmark
Wiviann Ottosson
Center for Nuclear Technologie
Fredriksborgvej 399 Build 201
DK-4000 Roskilde
Denmark

Projekt   **Projnr:59515, Uppdragsnr:E-2**

Analys: MF5

Er beteckning	Balsaträ					
Labnummer	U10975335					
Parameter	**Resultat**	**Mätosäkerhet (±)**	**Enhet**	**Metod**	**Utf**	**Sign**
BELAB	**Attached**			1	1	SH
TS*	94.6		%	2	W	TJ
Aska 550°C*	1.7		% TS	3	W	TJ
Si*	17.6		mg/kg TS	3	S	SVS
Al*	7.78		mg/kg TS	3	S	SVS
Ca*	1820		mg/kg TS	3	S	SVS
Fe*	<10		mg/kg TS	3	S	SVS
K*	6360		mg/kg TS	3	S	SVS
Mg*	356		mg/kg TS	3	S	SVS
Mn*	2.71		mg/kg TS	3	S	SVS
Na*	7.94		mg/kg TS	3	S	SVS
P*	236		mg/kg TS	3	S	SVS
Ti*	2.28		mg/kg TS	3	S	SVS
As	<0.1		mg/kg TS	3	H	ENMU
Ba*	15.4		mg/kg TS	3	S	SVS
Be*	0.0112		mg/kg TS	3	S	SVS
Cd	0.113	0.022	mg/kg TS	3	H	ENMU
Co	0.0393	0.0145	mg/kg TS	3	H	ENMU
Cr*	0.481		mg/kg TS	3	S	SVS
Cu	3.75	0.71	mg/kg TS	3	H	ENMU
Hg	<0.02		mg/kg TS	3	H	ENMU
Mo*	0.0914		mg/kg TS	3	S	SVS
Nb*	<0.08		mg/kg TS	3	S	SVS
Ni	0.150	0.056	mg/kg TS	3	H	ENMU
Pb	2.19	0.44	mg/kg TS	3	H	ENMU
S*	104		mg/kg TS	3	S	ENMU
Sc*	<0.02		mg/kg TS	3	S	SVS
Sn*	<0.03		mg/kg TS	3	S	ENMU
Sr*	21.9		mg/kg TS	3	S	SVS
V*	<0.03		mg/kg TS	3	S	SVS
W*	0.132		mg/kg TS	3	S	SVS
Y*	0.207		mg/kg TS	3	S	SVS
Zn	5.83	1.42	mg/kg TS	3	H	ENMU
Zr*	0.0721		mg/kg TS	3	S	SVS

Elemental analysis of balsa wood, details

Rapport

Sida 2 (2)

L1416586

4ZKN1FIGS1

	Metod
1	Analys enligt se bifogad rapport från Underleverantör.
2	Analys enligt TS enligt SS 02 81 13-1.
3	Vid analys av As, Cd, Cu, Co, Hg, Ni, Pb, B, S, Se och Zn gäller: Analysprov har torkats vid 50°C och elementhalterna har TS-korrigerats till 105°C. Upplösning har skett i mikrovågsugn i slutna teflonbehållare med salpetersyra / väteperoxid. För övriga grundämnen gäller: 0.1 g torkat prov smälts med 0.4 g LiBO₂ och upplöses i HNO₃. Analys har skett enligt EPA –metoder (modifierade) 200.7 (ICP-AES) och 200.8 (ICP-SMS).

	Godkännare
ENMU	Enrico Muth
SH	Sofie Hannu
SVS	Svetlana Senioukh
TJ	Thea Johansson

	Utf¹
H	ICP-SFMS
S	ICP-SFMS
W	Våtkemi
1	För analysen svarar BELAB, Exportgatan 20, 602 28 Norrköping, som är av det svenska ackrediteringsorganet SWEDAC ackrediterat laboratorium (Reg.nr. 1820).

* efter parameternamn indikerar icke ackrediterad analys.

Mätosäkerheten anges som en utvidgad osäkerhet (enligt definitionen i "Guide to the Expression of Uncertainty in Measurement", ISO, Geneva, Switzerland 1993) beräknad med täckningsfaktor lika med 2 vilket ger en konfidensnivå på ungefär 95%.

Mätosäkerhet från underleverantör anges oftast som en utvidgad osäkerhet beräknad med täckningsfaktor 2. För ytterligare information kontakta laboratoriet.

Denna rapport får endast återges i sin helhet, om inte utfärdande laboratorium i förväg skriftligen godkänt annat.
Resultaten gäller endast det identifierade, mottagna och provade materialet.
Beträffande laboratoriets ansvar i samband med uppdrag, se aktuell produktkatalog eller vår webbplats www.alsglobal.se

Den digitalt signerade PDF filen representerar orginalrapporten. Alla utskrifter från denna är att betrakta som kopior.

¹ Utförande teknisk enhet (inom ALS Scandinavia) eller anlitat laboratorium (underleverantör).

15.3   CHNO analysis of delrin

BELAB AB

ANALYSCERTIFIKAT
Certificate of analysis

Sida   1/1

Provnr:	**141840**
Rapportdatum:	2014-07-14
Ankomstdatum:	2014-07-09

Provmärke: ALS, Plast_
Provtyp: Plast
ID.nummer: 975852
Märkt:

Kundnr   1042

ALS Scandinavia AB

Aurorum 10
977 75   Luleå
Sverige

Godkänd av   Kundreferens   Beställningsnr
Albin Klint   Martina Krekula   L1416751

Analys		Enhet	Notering	Laboratorium	Norm
Askhalt, 550°C	<0.3	% ts		Belab	SS-EN 14775:2009/15403:2011
Kol (C) torrt	40.7	% ts		Belab	SS-EN 15104:2011/15407:2011
Väte (H) torrt	6.9	% ts		Belab	SS-EN 15104:2011/15407:2011
Kväve (N) torrt	<0.10	% ts		Belab	SS-EN 15104:2011/15407:2011
Syre (O) torrt	52.3	% ts		Belab	Beräknad

Mätosäkerhet, se BILAGA TILL ANALYSRAPPORT.
Lev.tillst = Leveranstillstånd, tp = torrt prov, • = vatten inkluderat, # = Ej ackrediterat
Denna rapport får endast återges i sin helhet, om inte utfärdande laboratorium i förväg skriftligen godkänt annat.

BELAB
Bränsle&Energilaboratoriet AB
Exportgatan 20
602 28 NORRKÖPING

Tel: 011-157370
Fax: 011-160740
Mobil: 070-2428740

www.belab.nu
mail@belab.nu
556608-0783

15.4 Elemental analysis of delrin

Rapport

Sida 1 (2)

L1416750

5CGBKE57QT

2030
ISO/IEC 17025

Registrerad	**2014-06-25 13:27**	**Technical University of Denmark**
Utfärdad	**2014-07-15**	**Wiviann Ottosson**

Center for Nuclear Technologie
Fredriksborgvej 399 Build 201
DK-4000 Roskilde
Denmark

Projekt   **Projnr:59515, Uppdragsnr:E-2**

Analys: I4A-OP

Er beteckning	**Plastmaterial, POM-C**				
Labnummer	U10975852				
Parameter	**Resultat**	**Enhet**	**Metod**	**Utf**	**Sign**
BELAB	Bifogad		1	1	ELEN
As	<0.7	mg/kg	2	H	SVS
Ca	<400	mg/kg	2	H	SVS
Cd	<0.05	mg/kg	2	H	SVS
Co	<0.05	mg/kg	2	H	SVS
Cr	<0.3	mg/kg	2	H	SVS
Cu	<0.9	mg/kg	2	H	SVS
Hg	<0.09	mg/kg	2	H	SVS
Mn	<0.4	mg/kg	2	H	SVS
Ni	<0.4	mg/kg	2	H	SVS
Pb	<0.4	mg/kg	2	H	SVS
S*	<20	mg/kg	2	S	SVS
Zn	<2	mg/kg	2	H	SVS

Elemental analysis of delrin, details

Rapport

L1416750

2030
ISO/IEC 17025

5CGBKE57QT

	Metod
1	Analys enligt se bifogad rapport från Underleverantör.
2	Analys av plastmaterial enligt paket I-4a. Observera att om det finns element tillsatta som härdare i plastmaterial kan detta resultera i ett ofullständigt utbyte. För mer information kontakta laboratoriet. Uppslutning har skett med koncentrerad salpetersyra i slutna teflonkärl i mikrovågsugn. Analys har skett enligt EPA –metoder (modifierade) 200.7 (ICP-AES) och 200.8 (ICP-SFMS).

	Godkännare
ELEN	Elina Engström
SVS	Svetlana Senioukh

	Utf[1]
H	ICP-SFMS
S	ICP-SFMS
1	För analysen svarar BELAB, Exportgatan 20, 602 28 Norrköping, som är av det svenska ackrediteringsorganet SWEDAC ackrediterat laboratorium (Reg.nr. 1820).

* efter parameternamn indikerar icke ackrediterad analys.

Mätosäkerheten anges som en utvidgad osäkerhet (enligt definitionen i "Guide to the Expression of Uncertainty in Measurement", ISO, Geneva, Switzerland 1993) beräknad med täckningsfaktor lika med 2 vilket ger en konfidensnivå på ungefär 95%.

Mätosäkerhet från underleverantör anges oftast som en utvidgad osäkerhet beräknad med täckningsfaktor 2. För ytterligare information kontakta laboratoriet.

---

[1] Utförande teknisk enhet (inom ALS Scandinavia) eller anlitat laboratorium (underleverantör).

15.5   CHNO analysis, uncertainty data

BELAB AB.

BILAGA TILL ANALYSRAPPORT

Metodförteckning för ackrediterade kemiska analyser med angivande av mätosäkerhet samt mätområde.

Aska (6:8)				
Analys-variabel	Metod	Mätprincip	Mät-osäkerhet	Mät-område
Oförbränt	SS 187187, utg. 1	LECO TGA 701	0,5 %* 7 %**	0,5-7 % 7-99,9 %
Askans smältförlopp	SIS-CEN TS 15404:2007	Rörugn	4 %**	850- 1500 °C
Kol	SS-EN 15407:2011	LECO Truspec CHN	0,10 %* 3 %**	0,1-5 % 5-90 %
Väte	SS-EN 15407:2011	LECO Truspec CHN	0,10 %* 10 %**	0,1-1 % 1-90 %
Kväve	SS-EN 15407:2011	LECO Truspec CHN	0,10 %* 10 %**	0,1-1 % 1-90 %
Fukt, total	SS-EN 15414:2011		1 %* 6 %**	1-10 % 10-90 %
Svavel	SS-EN 15408:2011	LECO SC-144DR	0,012 %* 0,05 %* 8 %**	0,012-0,06 % 0,06-0,65 % 0,65-12 %
Klor	SS-EN 15408:2011	Dionex, ICS-90	0,04 %* 0,10 %* 34 %**	0,04-0,10 % 0,1-0,3 % 0,3-5 %
Organisk kol, totalt, TOC	SS-EN 13137 mod.	LECO TGA 701 LECO SC-144DR	0,4 %* 20 %**	1-2 % 2-20 %
Värmevärde Kalorimetriskt Effektivt	SS-EN 15400:2011	LECO AC 350, AC 600	500 J/g*	5-50 MJ/Kg

* = ABS, absolut mätosäkerhet (k = 2, ger vid normalfördelning ett intervall som innehåller ca: 95% av fördelningens värden)
** = RSD, relativ standardosäkerhet (k = 2, ger vid normalfördelning ett intervall som innehåller ca: 95% av fördelningens värden)
Analysresultatet gäller insänt prov.

Mineralanalyserna utförs av ALS Scandinavia AB, Ackrediterat av SWEDAC (Regnr 1087).
Cesiumanalyserna utförs av Gammadata. Ackrediterat av SWEDAC (Regnr 1489).

Analyser märkta med # är inte ackrediterade. Laborationer ackrediteras av Styrelsen för ackreditering och teknisk kontroll
(SWEDAC) enligt svensk lag. Den ackrediterade verksamheten vid laboratorierna uppfyller kraven i SS-EN ISO/IEC 17 025
(2005). Denna rapport får endast återges i sin helhet, om inte utfärdande laboratorium i förväg skriftligen godkänt annat.

16 Appendix C: Clinical protocol (in Danish)

This section describes the LuCaRa protocol details.

- Clinical DIBH-LuCaRa protocol (in Danish)
- Layman resumé (in Danish)
- Information for participants
- Approval by the Institutional Reviewing Board

Evaluering af DIBH gating til patienter med lokal-avanceret lungecancer planlagt til kurativ stråleterapi

DIBH-LuCaRa

Herlev Universitets Hospital

Version 9, 03-12-2012

Appendix C: Clinical protocol (in Danish)

Indehold

Evaluering af DIBH gating for patienter med lokal-avanceret lungecancer planlagde til kurativ stråleterapi

(DIBH-LuCaRa)

Medlemmer af projektgruppen fra Onkologisk afd.:

Projektansvarlig: Hospitalsfysiker, M.Sc., Ph.d.-studerende, Wiviann Ottosson

Klinisk ansvarlige: Overlæge Ph.d. Anders Mellemgaard, Afdelingslæge Jon Lykkegaard Andersen og afdelingslæge Svetlana Borissova.

Ansvarlig radiograf: Henriette Klitgaard Mortensen

1. Resumé

Formål:

Det overordnede formål er at udvikle en metode til en mere præcis og effektiv strålebehandling baseret på Deep-Inspiration-Breath-Hold (DIBH) gating teknik til patienter med lokal-avanceret lungekræft.

Hypotese:

Ved at øge præcisionen i billeddannelsen til planlægningen af strålebehandling, og i selve strålebehandlingen, er det muligt at levere højere stråledosis til tumoren, mens dosis til normalvævet vil bibeholdes eller eventuelt mindskes.

Patienter:

I studiet inkluderes 40 patienter med inoperabel lokal-avanceret lungekræft.

Metode:

Inden start af strålebehandling øver patienterne sig sammen med personale fra Stråleterapien i at holde vejret ved dyb indånding, ifølge DIBH gating teknikken. I forbindelse med planlægning, og ugentlig strålebehandling, foretages supplerende DIBH billeddannelse til det standardmæssige strålebehandlingsforløb. Størrelsen af behandlings-volumen, og dosimetri forhold planlagt ved henholdsvis konventionel 4DCT i fri vejrtrækning og DIBH CT vil blive sammenlignet. Selve strålebehandlingen vil ske i henhold til nuværende praksis på Herlev Universitets Hospital. De foretagne billed-undersøgelser vil bruges til beregning af populationsbaseret margins omkring tumor med henblik på intra- og inter-fraktionelle tumorbevægelser. Billedundersøgelserne vil også bruges til beregning af den teoretiske strålebehandling som kunne være givet, hvis planen adapteredes i henhold til tumorregression og anatomiske ændringer henover behandlings-forløbet, både i fri vejrtrækning og i DIBH.

Etiske overvejelser:

På grund af de ekstra billedundersøgelser i forbindelse med studiet vil patienterne blive udsat for ekstra stråledosis mod behandlingsområdet, dvs. brystkassen. I forhold til nuværende behandlingsprocedure på Herlev Universitets Hospital, hvor CBCT-skanninger udføres ugentligt, vil patienterne udsættes for en total ekstra stråledosis på *63-66 mSv* (afhængigt af antallet behandlingsdage). – I forhold til standardprocedure på de centre i Danmark (fx Aarhus og Odense) som rutinemæssigt laver daglige CBCT-skanninger til patientpositionering før strålebehandling, medfører protokollen kun en ekstra total stråledosis på ***16.5 - 27 mSv***. Selve strålebehandlingen giver en langt større terapeutisk stråledosis (45 Gy / 60 Gy/ 66 Gy, 2Gy/fraktion – hvor 66 Gy med fotonbestråling svarer til ca. 66 000 mSv [organvægtningfaktor = 1, og strålevægtningfaktor = 1]). Gennemsnitsalderen for disse patienter er 70år, og tidsrammen for udvikling af stokastiske stråleskader er 10 – 20 år. Den øgede risiko for komplikationer, og fremkaldelse af sekundær kræft på baggrund af de ekstra skanninger, skønnes således at være meget begrænset. For denne patientgruppe er risikoen for at dø af anden årsag (fx deres lungecancer eller tobaks-relaterede sygdomme) langt højere.

Perspektiv:

På længere sigt forventes det at resultaterne fra projektet bidrager til at forbedre strålebehandlingen af lokal-avanceret lungekræft i Danmark. Vi håber at kunne udvikle metoder til at bedre kunne tilpasse behandlingen til den enkelte patient. Ved at gøre strålebehandlingen mere præcis kan man øge tumorkontrol uden samtidig at øge bivirkningerne. En øget dosis til denne patientgruppe som tit har store lungetumorer vil sandsynligvis betyde en forbedring af deres prognose.

2. Indledning

Lungecancer er den næst-hyppigeste kræftsygdom i Danmark, med ca. 4200 nye tilfælde i 2009 [135], hvor ca.34% af patienterne med lungecancer henvises til strålebehandling [136]. Dødeligheden blandt patienter med lungecancer er højere end ved de fleste andre former for cancer, og 5 års overlevelsen er kun 10% [136]. Der er et presserende behov for forbedring af strålebehandling til patienter med lungekræft. Meget tyder på, at den dosis man i dag anvender ved behandling af lokal-avanceret lungekræft, er for lille og dette forhold afspejles i 5 års overlevelsen. Tidligere studier har vist at lokal tumorkontrol er associeret med overlevelsen [137] og at bedre tumorkontrol kan opnås ved at øge stråledosis [8,137]. Dog kan levering af høj dosis bl.a. inducere lungetoksicitet [9,10], og dosis til tumoren begrænses af den maksimalt tolererede dosis til omkringliggende normale risikoorganer. Strålebehandling til lungetumorer er vanskeligt, fordi tumoren bevæger sig med vejrtrækningen. Ved planlægning af stråleterapi tillægges margener omkring tumoren for at tage højde for de usikkerheder der er på grund af subklinisk tumorvæv, respiration, andre organ bevægelser, og lejringsusikkerheder af patienten ved behandling. De ekstra margener resulterer i at et større område omkring tumoren medbestråles hvilket øger risikoen for toksicitet i tilstødende normalt væv. DIBH gating er en teknik, som potentielt kan forbedre strålebehandlingen af patientgruppen. Ved DIBH gating vejledes patienterne i at holde vejret tæt på deres maksimale inspiration i den korte tid (15-30 sekunder) strålebehandling og billeddannelse varer. Dette fører til en dæmpning af tumorens

bevægelse og en udvidelse af lungevævet. Ved at bruge DIBH gated stråleterapi kan det bestrålede volumen omkring tumoren reduceres, og således skånes normalt lungevæv og omkringliggende risikoorganer bedre for stråling. Dette kan gøre det muligt at øge stråledosis uden at give for meget dosis til risikoorganerne. Med hensyn til at skåne lunge, er lav lungedensitet ved dyb indånding en fordel [43]. Mere grundige undersøgelser er nødvendigt for at studere den praktiske fremgangsmåde, og på sigt den kliniske gevinst af at tilbyde DIBH gating til patienter med lokal-avanceret lungecancer.

3. Forsøgets formål

Det overordnede formål er at undersøge muligheden for at indføre DIBH gating som en ny behandlingsforløb for patienter med lokal-avanceret lungecancer. Deltagere i studiet vil få lavet 2 planlægningsscanninger. Den ene anvendes til den konventionelle behandling og den anden (DIBH) bruges i forsøgssammenhæng for at vurdere om man kan opnå en forbedret teoretisk stråleplan for den pågældende patient. Med baggrundsviden om stråledoser og stråletoksicitet kan man vurdere om den teoretiske DIBH behandling vil føre til en bedre behandling med hensyn til tumorkontrol og bivirkninger. Under behandlingsforløbet (midtvejs og i slutningen) vil patienten desuden få lavet de samme typer af CT-skanninger igen. Disse ekstra skanninger skal bruges til at evaluere tumorvariationen henover behandlingsforløbet og den dosimetriske påvirkning af behandlingsplanen, samt reproducerbarheden af patientens respirationsmønster. Selve den strålebehandling som patienterne får, vil ikke påvirkes af forsøget men vil foregå fuldstændigt svarende til afdelingens sædvanlige praksis.

4. Problemstillinger

- Undersøgelse af muligheden for at foretage DIBH gated billeddannelse og strålebehandling til patienter med lokal-avanceret lungecancer.

- Karakterisering af tumors lokalisation, form og bevægelse ved planlægningen af strålebehandling, og henover behandlingsforløbet, med og uden instruktioner til at holde vejret ifølge DIBH gating teknikken.

- Vurdering af margener for behandlingsfelter, baseret på populationsviden om tumorvariationer baseret på fri vejrtrækning og DIBH.

- Undersøgelse af den dosimetriske fordel ved at bruge DIBH gating teknikken i forhold til fri vejrtrækning ved planlægning af strålebehandling, med henblik på billeddannelse, forskellige feltteknikker, avancerede beregnings algoritmer, og brug af forskellige behandlingsenergier.

- Studere den teoretiske mulighed for dosiseskalering til tumorområdet, uden at give mere dosis til omkringliggende normale væv.

- Studere dosimetriske ændringer forårsaget af tumors variationer henover behandlingsforløbet.

5. Baggrund

CT-skanning er en røntgenundersøgelse, der giver billedinformation om patientens geometri og vævstype (bløddele, knogle, lunge etc.) i tre dimensioner (3D), og som anvendes ved planlægning af strålebehandling. På grund af bevægelse kan billedartefakter dannes som kan påvirke planlægningen af stråleterapi. På Herlev Universitets Hospital foretages der derfor for alle kurativt intenderet lungecancer-patienter en 4DCT-skanning i forbindelse med deres planlægning af strålebehandling for at kunne måle lungetumorens bevægelse under vejrtrækning (den 4 dimension er tiden). På grund af bevægelsen må strålebehandlingsfelterne udvides så meget at tumoren er indenfor strålefelterne under hele behandlingsforløbet. De udvidede strålefelterne medfører desværre at mere af det raske lungevæv, hjerte, spiserør, lever og rygmarv medbestråles, hvilket kan give flere strålings-inducerede bivirkninger.

Der er for nylig indført en ny behandlingsteknik ved behandling af brystcancer patienter, nemlig DIBH gating. Ved DIBH gating holder patienterne vejret ved dyb indånding under både billedoptagelse og strålebehandling. På den måde mindskes både brystkassens og dermed tumorens bevægelse, og mængden af billedartefakter som kan påvirke planlægningen af strålebehandling. Således mindskes størrelsen af behandlings-felterne.

Desværre ved vi ikke hvor stor behandlingsmæssig fordel der er ved at anvende DIBH gated strålebehandling til patienter med lokal-avanceret lungecancer som tilbydes kurativ intenderet strålebehandling. Første trin i en nærmere vurdering af værdien af DIBH er denne undersøgelse som ser på det praktiske forløb og den teoretiske fordel.

6. Patienter

I forsøget inkluderes, efter informeret samtykke, 40 patienter med lokal-avanceret lungecancer stadie II-III, henvist til kurativ strålebehandling på Herlev Universitets Hospital.

6.1. Styrkeberegning

Parret t-test vil blive brugt til at vurdere den statistiske signifikans af fund. Baggrunds-variable vil blive beskrevet med deskriptiv statistik.

Udefra en formodning om at det definerede tumorområde inklusive tumorbevægelse, dvs. Internal Target Volume (ITV), kan reduceres med 30%, og med $\alpha = 0.05$ og en styrke på 80% skal 40 patienter indgå i studiet for at opnå en tilstrækkelig statistisk styrke til at påvise en reduktion i størrelsen af ITV i forbindelse med DIBH.

6.2. Inklusionskriterier

- Alder > 18 år
- Alle patienter henvist til kurativ strålebehandling, uanset histologi og uanset frak-tionering
- Skal kunne forstå mundtlig og skriftlig information på dansk
- Underskrevet informeret samtykke erklæring og patientinformation

6.3. Eksklusionskriterier

- Graviditet

7. Information af patienter

Informationssamtaler forestås af lægerne i lungecancer gruppen på Onkologisk afdeling. Patienten gøres opmærksom på, at det kan være hensigtsmæssigt at følges med en pårørende eller anden bisidder til samtalen. Det vil være hensigtsmæssigt at samtalen finder sted en dag patienten skal møde frem på hospitalet til information om den forestående strålebehandling. Samtalen planlægges således at den informerende part er nøje bekendt med patientens sygehistorie og undersøgelses- og behandlingsplan i øvrigt. Samtalen skal foregå roligt og uforstyrret i et samtalerum på afdelingen. Patienterne bliver informeret om forsøgets baggrund, formål, deltagerantal, ind- og udgangskriterier, tidsforløb, praktiske gennemførelse, ulemper og fordele for patienten, samt fremtidige perspektiver. Der oplyses endvidere om økonomiske forhold, patientrettigheder, fortrolighed vedrørende patientoplysninger og efterfølgende information om projektets resultater. Patienten opfordres til at deltage i projektet, men det fremhæves at dette er frivilligt, og at beslutningen ikke påvirker patientens behandling i øvrigt. Det sikres at patienten har forstået informationen. Der udleveres skriftlig patientinformation, og det fortrykte tillæg "Forsøgspersonens rettigheder i et sundhedsvidenskabeligt forsknings-projekt". Patienten gives betænkningstid, og mulighed for yderligere samtale.

8. Metode

Der er tale om et prospektivt metodeudviklingsstudie med henblik på at kunne tilbyde patienter med lokal-avanceret lungecancer et mere effektivt strålebehandlingsforløb. I de følgende afsnit beskrives de anvendte metoder.

8.1. Åndedrætsinstruktion og monitorering

Undersøgelserne kræver ingen forberedelse. Ca. 1 time før CT-skanningerne vil patienten møde op i Stråleterapien ved Herlev Universitets Hospital, hvor patienten vil øve sig i at holde vejret ved dyb indånding ifølge DIBH gating teknikken. Patienten vil øve sig sammen med erfarent personale fra Stråleterapien, hvor patienten vil blive guidet til at hold vejret på det niveau ved dybt indånding (ca. 70-80% af maksimal indånding) som passer patienten bedst, ved visuel guidning med hjælp af computerbriller. På brystkassen påsættes infrarøde markører. Brystkassens bevægelser ved vejrtrækning i det anteriore - posteriore plan registreres via et infrarødt kamera monteret på lejret (ved CT-skanning) eller på væggen (ved Mould og behandling). Signaloptagelserne er en visuel læsbar kurve med tid og bevægeudsving som akser. Øvelser foregår indtil patienten klarer at opnå en re-producerbar amplitude og holde vejret stabilt på det niveau (indenfor 2 mm) i mindst 15 sekunder. Alle DIBH billeddannelser i studiet vil blive foretaget under visuel åndedræts-instruktion til patienten ved brug af computerbriller. Åndedrætsmonitoreringssystemer som afdelingen har til rådighed er RPM™ fra Varian Medical Systems.

8.2. Billeddannelse

Efter DIBH-øvelsen går patienten videre til rutinemæssig 4DCT-skanning, hvor patienten vil blive lejret af to medarbejdere fra Stråleterapien. Det sikres at patienten ligger på samme måde ved den efterfølgende DIBH-skanning som ved 4DCT-skanningen, der bliver brugt til planlægning af strålebehandlingen. Patienten vil blive lejret og fikseret i behandlingsposition. Der er overvågning af patienten hele tiden under optagelsen af billeder, og patienterne kan altid kontakte skannerpersonalet undervejs i undersøgelsen. Alle CT-skanningerne foretages i en Philips BigBore CT-skanner, som står i Stråleterapien, og der vil altid være en læge i nærheden under CT-skanning. Der vil først blive foretaget en DIBH-skanning, som tager ca. 15 sekunder, og derefter 4DCT-skanningen i fri vejrtrækning, som tager ca. 1 minut. Der vil efter sædvanlige retningslinjer blive givet kontrast til 4D og DIBH CT-skanningerne. Der bliver booket ca. 1 time til CT-skanning for hver patient for at give tid til generel CT-information, omklædning, lejring på lejret og CT-skanning (4DCT og DIBH). Tidspunktet for CT-skanningerne og DIBH øvelsen vil blive planlagt i samråd med patienten, således at de passer bedst mulig i forhold til patientens behandling. Fordelen er at DIBH-skanningen foretages når patienten alligevel er mødt op til den rutinemæssige 4DCT-skanning ved planlægning af sin strålebehandling. Patienten vil desuden få lavet ekstra 4D og DIBH CT-skanninger midtvejs og i slutningen af sit behandlingsforløb, hvor der er booket ca. 1 time ekstra til CT-skanning udover behandlingstiden de dage.

- 4DCT foretages ved optagelse af mange billedsnit gennem hele patienten ved langsom fremføring af lejret. Under CT-skanningen trækker patienten vejret frit, og bagefter sorteres billederne automatisk efter hvornår i åndedrætscyklus de er taget. Man får således typisk 10 skanninger der repræsenterende hver sin fase i åndedrættet. Herudfra kan man vurdere tumors bevægelse.

- DIBH foretages ved at der kun er optagelse af billedsnit når patienten holder vejret i den ved Mould forudbestemte vejrtrækningsamplitude (indenfor 2 mm).

I forbindelse med patientens strålebehandling vil patienten rutinemæssigt foretage daglig billedvejledt lejring inden start af strålebehandling ved brug af to dimensionale (2D) ortogonale kV røntgenbilleder, samt ugentligt 3D røntgenbilleder ved brug af Cone Beam CT (CBCT). Dette er for at sikre at patienten er lejret på samme måde ifølge den position som er forudbestemt ved planlægningen af strålebehandling, og for at sikre at tumoren er indenfor behandlingsområdet. I det her forsøg vil patienten udover de rutinemæssige daglige/ugentlige røntgenbilleder ved opstilling, også foretage supplerende ugentlige DIBH CBCT (både før og efter behandling), hvor patienten er positioneret i behandlingsposition på lejret. De billeder (hvor patienten holder vejret) vil efterfølgende sammenlignes med de tilsvarende billeder (hvor patienten trækker vejret normalt) som patienten foretager dagligt for positionering inden strålebehandling, for at evaluere DIBH gating teknikken gennem hele behandlingsforløbet. Der er booket 40 minutter ekstra ved behandling til DIBH billeddannelse de ugentlige dage hvor DIBH billeddannelse er aktuelt, hvilket resulterer i en total behandlingstid på ca. 1 time.

Efterfølgende vil de forskellige typerne af billeddannelse (4DCT, DIBH, og 3D opstillingsbilleder) registreres/fusioneres sammen med match på patientens knogle-

strukturer. Det skal gøres for at det skal være muligt at evaluere og sammenligne skanningerne med henblik på position, form og størrelse af tumor, og andre organer i brystkasseregionen under behandlingsforløbet, samt evaluering og sammenligning af beregnet dosisfordelinger.

8.3. Strålebehandling

Alle patienter vil behandles på Herlev Universitets Hospital ifølge gældende standard behandlingsplaner i fri vejrtrækning (hvor behandlingsplanen er baseret på 4DCT-skanningen), dvs. strålebehandlingen er ikke afhængig af om patienten klarer at udføre DIBH gating eller ikke. Foretagne DIBH-billeddannelser bruges til teoretisk evaluering af de eventuelle behandlingsmæssige fordele ved at basere strålebehandlingen på DIBH gating teknikken.

Tumorindtegning og planlægning af strålebehandling vil blive udført, både på 4DCT- og DIBH CT-skanningerne (foretagne ved planlægning, midtvejs og i slutningen af behandlingsforløbet). Behandlingsplaner og tumordefinition baseret på DIBH i forhold til planlægning i normal vejrtrækning (sædvanlig 4DCT-skanning) kan sammenlignes gennem hele behandlingsforløbet. Skanningerne vil blive brugt til flere typer af avancerede dosisberegninger for sammenligninger, fx; undersøgelse af forskellige feltteknikker, avancerede beregningsalgoritmer, og brug af forskellige behandlingsenergier. Der vil også blive undersøgt om det teoretisk ville være muligt at give højre dosis til tumoren, uden at give mere dosis til de omkringliggende normale væv, ved brug af DIBH sammenlignet med 4DCT.

I forbindelse med at man vurderer patienter som egnet til kurativt intenderet strålebehandling vil patienter, som opfylder inklusionskriterierne blive inviteret til at deltage i projektet, og informeret om formålet. Herefter vil de blive bedt om deres samtykke til denne. Giver patienterne ikke deres samtykke, vil deres behandling forløbe uden: DIBH-træning, supplerende DIBH CT-skanning ved planlægningen, supplerende ugentlig DIBH billeddannelse ved selve strålebehandlingen, samt ekstra CT-skanninger midtvejs og i slutningen af behandlingsforløbet.

9. Etiske overvejelser

Der er ikke nogen ekstra risici ved DIBH-skanningen i forhold til den rutinemæssige 4DCT-skanning. Dog, i forhold til den aktuelle behandlingsstandard, vil den enkelte patient i studiet få en større stråledosis; samtidig vil det for patienten betyde en potentiel gevinst med ekstra kvalitetskontrol, med mulighed for intervention og re-dosisplanlægning af behandlingsplanen. Vurdering af billedundersøgelserne vil gøres midtvejs, og hvis det skulle vise sig at være nødvendigt for en god strålebehandling, vil den dosisplan, der er beregnet ud fra den ekstra 4DCT-skanning foretaget midtvejs i behandlingsforløbet, bruges til fortsat behandling.

Så snart der er udviklet en metode som resulterer i en teoretisk mere præcis og effektiv strålebehandling med bedre sygdomskontrol og færre bivirkninger baseret på DIBH gating teknik, vil denne metode blive benyttet ved behandlingen af patienter med lokal-avanceret lungetumorer stadie II-III. Studiet udføres i henhold til Helsinki deklarationens betingelser. Alle data opbevares i henhold til tilladelse fra Datatilsynet.

9.1. Udelukkelse fra og afbrydelse af forsøg

Det er frivilligt at deltage i forsøget. Patienterne kan når som helst og uden at give en grund trække sit samtykke tilbage, uden at det vil få konsekvens for deres videre strålebehandling.

Desuden vil forsøget afbrydes for den enkelte patient hvis vi finder ud af ved DIBH-øvelsen at det er alt for hårdt for patienten at holde vejret i mindst ca. 15 sekunder. Forsøget vil yderligere kunne afbrydes såfremt CT-skanneren eller gating-udstyret (udstyr for registrering af patientens vejrtrækning, samt computerbriller) går i stykker og ikke kan repareres indenfor kort tid når patienten er mødt op til planlægning af sin strålebehandling.

9.2. Stråledosis

I forbindelse med studiet vil patienterne blive udsat for ekstra stråledosis, fortrinsvis i behandlingsområdet på grund af de ekstra billedoptagelser. Ved planlægningen af stråleterapi CT-skannes patienterne to gange (DIBH og 4DCT). Patienten vil midtvejs og i slutningen af behandlingsforløbet få gentaget disse scanninger. Hvad angår effektiv dosis til patienten så bidrager DIBH CT-skanningen med ca. *5 mSv* svarende til en tredjedel af dosis fra 4DCT-skanningen, som er omkring *15 mSv*. Den ekstra dosis fra DIBH CT-skanningen svarer til lidt over den naturlige årlige baggrundsdosis i Danmark som er 3 mSv/år.

For at opnå en så præcis strålebehandling af lungecancer som muligt, foretages det rutinemæssigt på Herlev Universitets Hospital Cone Beam CT scanninger af patienterne. På grund af kapacitetsproblemer på Herlev Hospital udføres der i dag kun ugentlig CBCT-skanninger for positionering før strålehandling. Dog, indenfor en snar fremtid kommer også lungepatienterne standardmæssigt i Herlev gennemgå daglig CBCT-skanninger. Ugentlige CBCT-skanninger er allerede indført som standardprocedure på andre centre i Danmark, (fx i Aarhus og Odense), hvilket alene giver patienten en dosis på *49.5 mSv*. Patienterne som indgår i projektet vil under sit behandlingsforløb (som er mellem 6-7 uger) ugentligt (for at kunne evaluere den *inter*-fraktionelle [dvs. mellem behandlinger] tumorbevægelse) foretage to ekstra DIBH CBCT-skanninger mens de er placeret på lejret i behandlingsposition, både føre og efter sin behandling (for at kunne evaluere den *intra*-fraktionelle [dvs. under en enkel behandling] tumorbevægelse). CBCT-skanningerne svarer til en dosis på *1.5 mSv/billede*, dvs. de får en total ekstra effektiv dosis på ca. *15 / 18 / 21 mSv* i behandlingsområdet, afhængigt af om patienten behandles i 5 (45 Gy), 6 (60 Gy) eller 7 uger (66 Gy). I forhold til nuværende behandlingsprocedure på Herlev Hospital, hvor CBCT-skanninger udføres ugentligt, vil patienterne udsættes for en total ekstra stråledosis på ***60-66 mSv*** svarende til ca. 20-22 års baggrundsstråling. I den raske befolkning vil denne ekstra stråledosis øge risikoen for at inducere en uhelbredelig cancersygdom med ca. 0.3%, fra den generelle risiko på 25% til 25.3%. Sammenholdt med

den langt større stråledosis patienterne modtager i terapeutisk øjemed (45 / 60 / 66 Gy, 2 Gy/fraktion – hvor 66 Gy med fotonbestråling svarer til ca. 66 000 mSv), er den ekstra stråledosis som patienten modtager i forbindelse med projektet lille, og holdes under tærsklen for deterministiske skader, men der er en lille øget risiko for stokastiske skader (fx en ny uhelbredelig cancersygdom, en såkaldt stråleinduceret sekundær cancer). I forhold til standardprocedure på de centre i Danmark som rutinemæssigt laver daglige CBCT-skanninger til patientpositionering før strålebehandling, medfører protokollen kun en ekstra total stråledosis på *16.5-27 mSv.* Denne patientgruppe har i flere undersøgelser vist sig at have en begrænset langtidsoverlevelse, hvor 5 års overlevelsen kun er 10% [136]. Dette skyldes kræftsygdommen, men også den comorbiditet, for eksempel hjertekar-sygdomme og rygerlunger, der er årsagen til at disse patienter ikke primært kan opereres. De lungecancer-patienter som kommer til strålebehandling har en gennemsnitsalder på ca. 70 år, og tidsrammen for udvikling af stokastiske stråleskader er 10 – 20 år. Derfor konkluderer vi, at for denne patientgruppe er risikoen for at dø af anden årsag (fx deres lungecancer eller tobaksrelaterede sygdomme) end eventuelt en strålingsinduceret sekundær cancer på baggrund af de ekstra skanninger, langt højere.

Table 17. Forsøgsforløb og ekstra stråledosis.

Standardbehandling	Forsøg	Ekstra tid	Ekstra stråledosis
PET/CT	Informations samtale	15 min	
4DCT	DIBH-øvelse + DIBH CT	60 min	5 mSv
NSCLC 60: ~ 2. 7. 12. 17. 22. 30 behandling NSCLC 66: ~ 2. 7. 12. 17. 22. 27. 33. behandling SCLC 45: ~ 2. 7. 12. 17. 22 behandling	2 x DIBH CBCT (før og efter behandling)	40 min	3 mSv/skanningsdag (1.5 mSv/CBCT)
~ 17. behandling	4DCT + DIBH CT	60 min	15 mSv + 5 mSv
~ 22. /~30./ ~ 33. behandling ved 45 Gy / 60 Gy / 66 Gy dosering	4DCT + DIBH CT	60 min	15 mSv + 5 mSv

Total ekstra dosis hvis patienten deltager i forsøget ifølge:

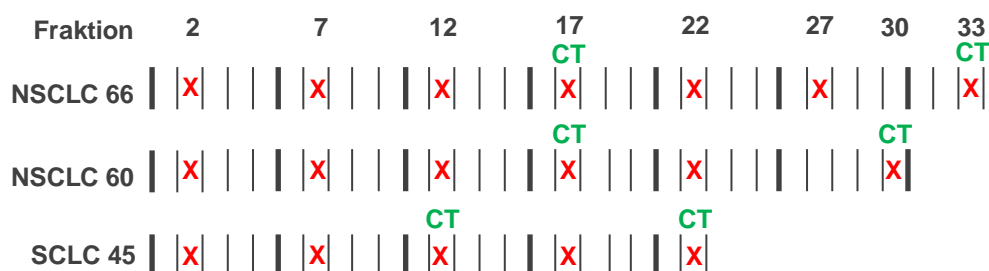|	Herlev procedure (rutine-mæssigt *ugentlige* CBCT)	Standard procedure på de centre som rutinemæssigt laver *daglige* CBCT
45 Gy dosering	**55 mSv**	**27 mSv**
60 Gy dosering	**63 mSv**	**18 mSv**
66 Gy dosering	**66 mSv**	**16.5 mSv**

Figure 42. Skema over hvornår i behandlingsforløbet patienterne skal DIBH CBCT skannes, før og efter behandling (rød kryds), samt og re-CT skannes (grøn CT).

10. Perspektiv

Det er vores håb, at vi ved denne undersøgelse kan vise at en strålebehandling af lokal-avanceret lungecancer baseret på DIBH-skanning er muligt, og resulterer i en stråle-behandling tilsvarende, eller bedre end, en behandling baseret på 4DCT-skanning. Forhåbentlig bliver definition af lungetumorerne mere præcise, da tumor- og organ-bevægelsen mindskes ved at holde vejret ved billedoptagelsen. Forsøget er først og fremmest en for-studie for at undersøge de eventuelle behandlingsmæssige fordele ved at basere strålebehandlingen på DIBH teknikken. På længere sigt forventes det at resultaterne fra projektet bidrager til at forbedre strålebehandlingen af lokal-avanceret lungecancer i Danmark. Vi håber at kunne udvikle metoder til bedre at kunne tilpasse behandlingen til den enkelte patient. Ved at gøre strålebehandlingen mere præcis kan man øge tumorkontrol uden samtidig at øge bivirkningerne.

11. Tidsplan

Patienterne forventes inkluderet i perioden 1. september 2012 – 30. august 2014. Databearbejdning vil foregå sideløbende og i det efterfølgende år.

12. Økonomi

Der gives ikke honorar til medvirkende patienter. Det er ph.d.-studerende hospitalsfysiker Wiviann Ottosson som taget initiativ til dette projekt. Der er ikke nogle firmafinansieret fondsstøtte i forbindelse med projektet. Teknisk udstyr og lokaler stilles til rådighed af Stråleterapien ved Herlev Universitets Hospital.

13. Publikation

Resultaterne af forsøget, negative såvel som positive, samt inkonklusive resultater vil blive offentliggjort og fremlagt på faglige konferenser i ind- og udland, og eventuelt publiceret i internationale anerkendte tidsskrifter indenfor området med Wiviann Ottosson som 1. forfatter.

14. Forsøgsansvarlige

Hospitalsfysiker, M. Sc., Ph.d.-studerende, Wiviann Ottosson
Onkologisk Afdeling R, 51AA, Herlev Hospital
Tlf.: 3868 94 21, e-mail: wivott01@heh.regionh.dk

Overlæge Ph.d. Anders Mellemgaard, 38 682 891, Afdelingslæge Jon Lykkegaard
Andersen 38 681 081, Afdelingslæge Svetlana Borissova 38 689 096, Radiograf Henriette
Klitgaard Mortensen 3868 9230

16.1 Layman resumé (in Danish)

Evaluering af DIBH gating til patienter med lokal-avanceret lungecancer planlagt til kurativ stråleterapi (DIBH-LuCaRa)

Lungecancer er den næst-hyppigste kræftsygdom i Danmark, med ca. 4200 nye tilfælde i 2009. Dødeligheden blandt patienter med lungecancer er højere end ved de fleste andre former for cancer, og 5 års overlevelsen er kun 10%. Der er et stort behov for forbedring af strålebehandling til patienter med lungekræft. Problemet med strålebehandling er at man rammer det omgivende normale væv, som kun tåler en vis dosis stråler. Strålebehandling til lungetumorer er også vanskeligt, fordi tumoren bevæger sig med vejrtrækningen. Dette medfører at man giver strålebehandling mod et større område omkring tumoren for at være sikker på at ramme.

Ved DIBH gating vejledes patienterne i at holde vejret efter en dyb indånding den korte tid (15-30 sekunder) skanning eller strålebehandling varer. Dette fører til en dæmpning af tumorens bevægelse og en udvidelse af lungevævet. Ved at bruge DIBH gated stråleterapi kan det bestrålede område omkring tumoren reduceres, og således skånes normalt lungevæv og omkringliggende organer mere for stråling. Mere grundige undersøgelser er nødvendigt for at studere den praktiske fremgangsmåde, og på sigt den kliniske gevinst af at tilbyde DIBH gating til patienter med lokal-avanceret lungecancer.

Under forsøget vil patienterne få den sædvanlige strålebehandling, hvor patienten trækker vejret normalt ved planlægnings CT skanning, daglige opstillingsbilleder før strålebehandling, samt under selve strålebehandlingen. Udover dette vil der blive lavet ekstra CT skanning ved planlægning og 2 gange under strålebehandlingen, samt ugentlige opstillingsbilleder med DIBH gating før og efter behandling.

Ved at sammenligne den bestråling der bliver givet med den normale fremgangs måde, med den teoretiske behandling man kunne have givet med DIBH gating kan man vurdere om det vil være muligt at give en mere optimeret behandling. En bedre behandling vil være en behandling som muliggør større dosis mod tumor og mindre dosis mod det normale væv i omgivelserne. I forsøget vil man for det første se om det rent praktisk er muligt at lade patienterne holde vejret samtidigt med CT skanning og strålebehandling. Dernæst vil man vurdere om det er muligt at mindske størrelsen af det område der rammes af strålebehandlingen og om det dermed vil være muligt at øge dosis mod tumoren.

Da behandlingen gives helt efter sædvanlig praksis vil patienter som deltager i forsøget ikke umiddelbart få fordel af deltagelse. Vi håber at fremtidige patienter kan få en mere effektiv og mindre skadelig behandling hvis DIBH gating viser sig at virke. Dog, i forhold til den aktuelle behandlingsstandard på Herlev Hospital, vil den enkelte patient i studiet få en større stråledosis mod brystkassen i forbindelse med de ekstra røntgenbilleder patienten vil blive udsat for, svarende til *60-66 mSv* (afhængigt af antallet behandlingsdage). Samtidig vil det for patienten betyde en potentiel gevinst med ekstra kvalitetskontrol, med mulighed for intervention og re-dosisplanlægning af behandlingsplanen. I forhold til standardprocedure på de centre i Danmark som rutinemæssigt laver daglige CBCT-skanninger til patientpositionering før strålebehandling, medfører protokollen kun en ekstra total stråledosis på *16.5-27 mSv*. Sammenholdt med den langt større stråledosis patienterne modtager i terapeutisk øjemed, er den ekstra dosis som patienten modtager i

forbindelse med projektet lille og holdes under tærsklen for deterministiske skader, men der er en lille øget risiko for stokastiske skader. Risikoen for denne patientgruppe at dø af anden årsag (fx deres lungecancer eller tobaksrelaterede sygdomme) end eventuelt en strålingsinduceret sekundær cancer på baggrund af de ekstra skanninger, skønnes være langt højere. Ulempen for patienten hvis de deltager i forsøget er, at de skal regne med at det tager ekstra tid de dage hvor de får lavet ekstra røntgenbilleder.

Alle patienter ældre end 18 år med lungecancer som planlægges til strålebehandling med helbredende sigte, kan deltage i forsøget. De skal kunne forstå mundtlig og skriftlig information på dansk. Gravide vil blive ekskluderede. Patienter vil blive inviteret til protokollen mens behandlingen planlægges i Onkologisk ambulatorium, og det vil være personalet i stråleterapien som giver instruktion i at holde vejret under skanning, og behandlingsforløb. Det planlægges at 40 patienter indgår i forsøget.

Der gives ikke honorar til medvirkende patienter. Der er ikke nogle firmafinansieret fondsstøtte i forbindelse med projektet. Teknisk udstyr og lokaler stilles til rådighed af Stråleterapien ved Herlev Universitets Hospital.

Resultaterne fra undersøgelsen, negative såvel som positive, samt inkonklusive resultater vil blive offentliggjort og fremlagt på faglige konferenser i ind- og udland, og eventuelt publiceret i internationale anerkendte tidsskrifter indenfor området.

16.2 Information for participants (in Danish)

Deltagerinformation om deltagelse i et videnskabeligt forsøg

Evaluering af DIBH gating til patienter med lokal-avanceret lungecancer planlagt til kurativ stråleterapi

Vi henvender os til dig for at spørge, om du vil deltage i et videnskabeligt forsknings-projekt.

Før du beslutter, om du vil deltage i forsøget, skal du fuldt ud forstå, hvad forsøget går ud på, og hvorfor vi gennemfører forsøget. Vi vil derfor bede dig om at læse denne deltagerinformation grundigt.

Du vil blive inviteret til en samtale om forsøget, hvor denne deltagerinformation vil blive uddybet, og hvor du kan stille de spørgsmål, du har om forsøget. Du er velkommen til at tage et familiemedlem, en ven eller en bekendt med til samtalen.

Hvis du beslutter dig for at deltage i forsøget, vil vi bede dig om at underskrive en samtykkeerklæring. Husk, at du har ret til betænkningstid, før du beslutter, om du vil underskrive samtykkeerklæringen.

Samtykket omfatter adgang til videregivelse og behandling af nødvendige oplysninger om dit helbredsforhold, øvrige private forhold, og andre fortrolige oplysninger, som led i kvalitetskontrol af forsøget og eventuel monitorering.

Det er frivilligt at deltage i forsøget. Du kan når som helst og uden at give en grund trække dit samtykke tilbage.

Baggrund for forsøget:

Strålebehandling til lunge tumorer er vanskeligt, fordi tumoren bevæger sig med vejrtrækningen. CT-skanning er en røntgenundersøgelse, der rutinemæssigt anvendes til billeddannelse af sygdomme i kroppen. På grund af tumor bevægelse i forbindelse med vejrtrækningen kan det være svært at se den præcise placering af lungetumoren på en CT-skanning. Man må derfor normalt udvide det områder der gives stråler mod, for at sikre at tumor bliver ramt selvom den bevæger sig med vejrtrækningen. Det udvidede strålefelt medfører desværre at mere af det raske lungevæv, hjerte, lever og rygmarv medbestråles, hvilket kan give flere bivirkninger. For at mindske dette problem udføres der, i forbindelse med planlægningen af din stråleterapi, rutinemæssigt en vejrtrækningstilpasset CT-skanning (4DCT) for at kunne måle lungetumorens bevægelse under vejrtrækning.

Vi undersøger nu om strålebehandlingen kan blive mere præcis hvis den der får behandlingen kan holde vejret ved dyb indånding (Deep-Inspiration Breath-Hold = DIBH) i den korte tid strålebehandlingen og billeddannelsen varer (ca. 15-30 sekunder). Vi forventer at man ved at holde vejret kortvarigt kan mindske tumorens bevægelse, og dermed problemet at se den præcise lokalisation af tumoren på en CT-skanning. Hvis det lykkes vil man kunne mindske størrelsen af de områder der skal have stråler, og dermed mindske bivirkningerne ved behandlingen.

Formålet med forsøget:

Formålet med forsøget er at undersøge om det er teknisk muligt at lave planlægnings CT-skanning hvis patienten holder vejret i ca. 20-30 sekunder. Vi kan så sammenligne den rutine-CT-skanning vi normal laver for at planlægge strålebehandling, med en samtidig CT-skanning hvor man har holdt vejret kortvarigt (DIBH). Vi sammenligner så den behandling der bliver givet med den normale teknik med den behandling man teoretisk kunne have givet hvis man havde holdt vejret under skanning og stråleterapi. Målet er at udvikle en metode til mere præcis strålebehandling

Hvad indebærer undersøgelsen?

Selve den strålebehandling der er planlagt til dig vil blive gennemført fuldstændigt som vanligt.

Forsøget går ud på at du derudover får lavet en ekstra CT-skanning ved planlægningen af din strålebehandling hvor du holder vejret kortvarigt mens skanningen foretages (DIBH). I forbindelse med strålebehandlingen vil vi hver uge lave kontrolbilleder for at sikre at strålebehandlingen rammer korrekt. Ved disse kontrolbilleder vil vi bede dig holde vejret kortvarigt, så vi kan foretage DIBH billeder både før og efter behandling. Du vil desuden få lavet ekstra CT-skanninger midtvejs og ved afslutningen af dit behandlingsforløb (hvor du både trækker vejret normalt og hvor du holder vejret kortvarigt ifølge DIBH). Du skal regne med at det tager ekstra tid de dage hvor du får lavet ekstra skanninger hvis du deltager i forsøget. Det tager ca. en time mere end vanligt ved selve planlægningsskanningen. Denne time går til vejrtrækningsøvelser før planlægnings-skanningen, og så selve den ekstra skanning. Vejrtrækningsøvelserne foregår under vejledning af personalet. Det tager ca. 60 min udover din behandlingstid de dage hvor vi foretager de ekstra kontrolskanninger (midtvejs og i slutningen af dit behandlingsforløb). Der vil blive givet kontrast både til den almindelige skanning, og til den ekstra medmindre du er allergisk overfor kontrast. De ugentlige dage hvor du for lavet ekstra DIBH kontrolbilleder før og efter behandling må du regne med at det tager ca. 40 min mere end vanligt, hvilket resulterer i en total behandlingstid på ca. 1 time. Forsøget påvirker ikke den behandling du skal have, og kræver ikke ekstra fremmøder eller ekstra undersøgelser. Deltagelse kræver ikke forberedelse.

Der skal i alt indgå 40 patienter i forsøget.

Mulig nytte af forsøget:

Det er vores håb, at vi ved denne sammenlignende undersøgelse kan vise at en stråle-behandling af lungecancer baseret på DIBH-billeddannelse er muligt, og resulterer i en strålebehandling som er bedre end den teknik vi bruger i dag. Forhåbentlig kan DIBH hjælpe til at give en mere præcis lokalisation af de områder der skal have stråler.

Forsøget er første trin i udviklingen af denne nye teknik og skal primært afklare om det er realistisk at bruge DIBH i forbindelse med planlægning af strålebehandling af lunge-cancer.

Bivirkninger og ulemper ved at deltage i forsøget:

Der er ikke nogen ekstra risici ved DIBH-skanningen i forhold til den rutinemæssige CT-skanning. Øvelse i at holde vejret ifølge DIBH teknikken samt selve de ekstra DIBH-skanninger tager tid. Det betyder at du vil bruge mere tid ved planlægningen af din strålebehandling og ved behandlingerne.

På grund af de ekstra skanninger i forbindelse med studiet vil du blive udsat for ekstra stråledosis mod brystkassen, svarende til ca. 22 gange den naturlige årlige baggrunds bestråling i Danmark (3 mSv/år). Selve strålebehandlingen giver en langt større stråledosis. Den totale ekstra stråledosis (ca. 66 mSv) på baggrund af de ekstra skanninger svarer til ca. 0.3% øgning af risikoen at inducere en uhelbredelig cancersygdom, fra den generelle risiko på 25% til 25.3%.

Der kan være risici ved forsøget, som vi endnu ikke kender. Vi beder dig derfor om at fortælle, hvis du oplever problemer med dit helbred, mens forsøget står på. Hvis vi opdager bivirkninger, som vi ikke allerede har fortalt dig om, vil du naturligvis blive orienteret med det samme, og du vil skulle tage stilling til, om du ønsker at fortsætte i forsøget.

Deltagelse og afbrydelse af forsøg:

Det er frivilligt at deltage i forsøget. Du kan når som helst og uden at give en grund trække dit samtykke tilbage, uden at det vil få konsekvens for din videre behandling.

Forsøget vil afbrydes hvis vi finder ud af ved DIBH-øvelsen at det er vanskeligt at holde vejret i mindst 15 sekunder.

Oplysninger om økonomiske forhold:

Der gives ikke honorar til medvirkende patienter. Det er ph.d.-studerende hospitalsfysiker Wiviann Ottosson som taget initiativ til dette projekt. Hendes studier er finansieret af Center for Nukleare Teknologier (Nutech) ved Danmarks Tekniske Universitet (DTU) samt Stråleterapien på Herlev Universitets Hospital. Der er ikke nogle firmafinansieret fondsstøtte i forbindelse med projektet. Teknisk udstyr og lokaler stilles til rådighed af Stråleterapien ved Herlev Universitets Hospital.

Adgang til forsøgsresultater:

Resultaterne fra undersøgelsen, negative såvel som positive, samt inkonklusive resultater vil blive offentliggjort og fremlagt på faglige konferenser i ind- og udland, og publiceret i internationale tidsskrifter indenfor området.

Forsøgsansvarlige for projektet er:

Hospitalsfysiker, M. Sc., Ph.d.-studerende, Wiviann Ottosson
Onkologisk Afdeling R, 51AA, Herlev Hospital
Tlf.: 3868 94 21, e-mail: wivott01@heh.regionh.dk

Overlæge Ph.d. Anders Mellemgaard, 38 682 891, Afdelingslæge Jon Lykkegaard Andersen 38 681 081, Afdelingslæge Svetlana Borissova 38 689 096, Radiograf Henriette Klitgaard Mortensen 3868 9230
Som også gerne besvarer spørgsmål om forsøget.

Rettigheder:

Som deltager i et biomedicinsk forskningsprojekt har du ifølge Sundhedsloven visse rettigheder. Vi vil gerne opfordre dig til at læse om dem i den vedlagte publikation fra den centrale videnskabsetiske komite: "Forsøgspersoners rettigheder i et sundhedsvidenskabeligt forskningsprojekt".

Forsøget er godkendt af den videnskabsetiske komite for Region Hovedstaden med journalnummeret: H-4-2012-066. Såfremt du ønsker at deltage, bedes du venligst underskrive samtykkeerklæringen på næste side.

Vi håber, at du med denne information har fået tilstrækkeligt indblik i, hvad det vil sige at deltage i forsøget, og at du føler dig rustet til at tage beslutningen om din eventuelle deltagelse. Hvis du har spørgsmål om projektet som det øvrige personale du kommer i kontakt med ikke kan besvare, er du velkommen til at kontakte ovenstående projektansvarlige person.

16.3   Approval by the Institutional Reviewing Board

The clinical protocol was approved by the Copenhagen Regional Committee on Health Research Ethics (protocol no. H-4-2012-066) and the Danish Data Protection Agency (ID. nr.: 2007-58-0015 / HEH.750.24-61). Every patient gave informed consent to the work before inclusion.